Darstellung und Charakterisierung neuer Übergangsmetallkomplex-substituierter Polyoxoniobate mit makrozyklischen Aminmolekülen:

Untersuchungen zum Einfluss der Syntheseparameter auf die Kristallisation sowie zur Abgabe und Aufnahme von Kristallwassermolekülen

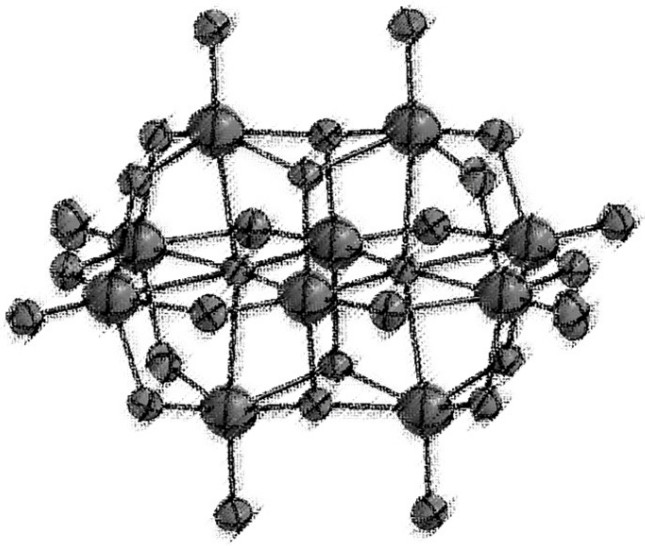

Dissertation

zur Erlangung des Doktorgrades

der Mathematisch-Naturwissenschaftlichen Fakultät

der Christian-Albrechts-Universität zu Kiel

vorgelegt von

Joanna Dopta

Kiel 2018

Erster Gutachter:	Prof. Dr. Wolfgang Bensch
Zweiter Gutachter:	Prof. Dr. Norbert Stock
Tag der mündlichen Prüfung:	29.11.2018

Die vorliegende Dissertation wurde unter Anleitung von

Prof. Dr. Wolfgang Bensch

in der Zeit von

2013 bis 2018

am Institut für Anorganische Chemie

der Christian-Albrechts-Universität zu Kiel

angefertigt.

„Moleküle sind magisch“

Jean und Len Alchimiste Werbekampagne 2018

Kurzzusammenfassung

Die Ziele der Arbeiten waren die Synthese und Charakterisierung neuer Polyoxoniobate (PONbs) mit Übergangsmetallkomplexen, welche makrozyklische Aminmoleküle als Liganden enthalten, und die Untersuchung des Einflusses der Reaktionsparameter auf die Produktbildung.

PONbs sind Anionen mit hoher negativer Ladung, welche meistens in stark basischen Lösungen hergestellt werden und daher werden ladungskompensierende Kationen benötigt, welche im alkalischen pH-Bereich stabil sind. Übergangsmetall (ÜM)-Komplexe mit makrozyklischen Aminmolekülen als Liganden sind ideale Kandidaten, da diese eine hohe Stabilität im alkalischen Milieu aufweisen und das ÜM-Kation meistens nicht koordinativ absättigen, was die Ausbildung von Bindungen zwischen dem anionischen Cluster und dem ÜM-Komplex ermöglicht.

Mit Cu^{2+} konnten zwei neue PONbs unterschiedlicher Clustergeometrie hergestellt und charakterisiert werden: $K_5[Cu(H_2O)_2(cyclam)]_{1.5}\{[Cu(cyclam)][Cu(H_2O)(cyclam)]_2\mathbf{HSiNb_{18}O_{54}}\}(NO_3)\cdot 30H_2O$ und $\{[Cu(cyclam)(H_2O)]_2[Cu(cyclam)][\mathbf{Nb_{10}O_{28}}]\}_n\cdot 9nH_2O$ (cyclam = 1,4,8,11-Tetraazacyclotetradekan). Die beiden Verbindungen wurden durch Variation des pH-Wertes bei sonst identischen Reaktionsbedingungen erhalten. Durch die Anwendung dynamischer hydrothermaler Bedingungen, d.h. durch kontinuierliches Rühren des Gemisches, konnte die Reaktionszeit von Tagen oder sogar Wochen auf weniger als 1 Stunde reduziert werden. Untersuchungen der thermischen Stabilität belegen, dass das Kristallwasser ohne signifikante Änderung der Kristallinität entfernt werden kann, wie die Ergebnisse von Röntgenbeugungsexperimenten nachweisen konnten. Nach Zugabe von Wasser zu den dehydratisierten Proben wird das Ausgangsmaterial wieder gebildet. Bei höheren Zersetzungstemperaturen wird ein nanokristallines Produkt erhalten, welches bisher noch nicht eindeutig identifiziert werden konnte.

Bei Verwendung von $Ti(O^iPr)_4$ wird ein weiteres Dekaniobat, $[Cu(cyclam)(H_2O)_2]\{[Cu(cyclam)]_2[\mathbf{Nb_{10}O_{28}}]\}\cdot 27H_2O$, erhalten. Die Verbindung verliert bereits Kristallwassermoleküle nach Isolierung aus der Mutterlauge. Die partielle Dehydratisierung führt zu einer strukturellen Phasenumwandlung. Die Wassermoleküle können durch Behandlung mit Wasser wieder eingelagert werden, so dass die Ausgangsstruktur erhalten wird. Mit Synchrotron-Röntgenpulverbeugung und Totalstreumethoden wurde der Prozess der Dehydratisierung untersucht. Aus den Totalstreudaten wurde die Paarverteilungsfunktion (PDF) berechnet und es konnte ein sehr

präzises Histogramm der interatomaren Abstände in der Probe ermittelt werden, welches sich bei der wasserreichen und wasserarmen Phase unterscheidet.

Mit Ni^{2+}-Kationen konnten vier Titanoniobate synthetisiert werden, welche in der PONb-Chemie recht selten sind. Die violetten Kristalle von $[Ni(cyclam)]_4[\mathbf{Ti_2Nb_8O_{28}}]\}_n \cdot \sim 28nH_2O$ und gelbe Kristalle von $K[Ni(cyclam)]_3[\mathbf{TiNb_9O_{28}}] \cdot nH_2O$ (n = 10-18) wurden durch Variation der Titanquelle erhalten. Die erste Verbindung enthält Ni^{2+}-Kationen in oktaedrischer Umgebung und wurde mit $Ti(O^iPr)_4$ synthetisiert, während die anderen Verbindungen mit quadratisch-planar koordinierten Ni^{2+}-Kationen mit $K_2TiO(C_2O_4)_2 \cdot 2H_2O$ oder mit $Ti(O^iPr)_4$ unter Zugabe von Oxalat-Anionen aus der gleichen Reaktionsmischung hergestellt werden konnten.

Abstract

The aims of this work were the hydrothermal synthesis and characterization of novel polyoxoniobates (PONbs), the evaluation of the synthesis parameters onto product formation, and the optimization of the synthesis conditions.

PONbs are anions with high negative charges synthesized mostly in strong basic media, and thus charge compensation by cations is required which are stable in this pH range. Transition metal (TM) complexes with macrocyclic amine molecules are ideal because of their high stability and their vacant coordination sites that enable bond formation between the anionic cluster and the TM complex, and therefore, cyclam (cyclam = 1,4,8,11-tetraazacyclotetradecane) was chosen as ligand.

With Cu^{2+}, two novel PONbs with different geometries, $K_5[Cu(H_2O)_2(cyclam)]_{1.5}\{[Cu(cyclam)][Cu(H_2O)(cyclam)]_2\mathbf{HSiNb_{18}O_{54}}\}(NO_3)\cdot 30H_2O$ and $\{[Cu(cyclam)(H_2O)]_2[Cu(cyclam)][\mathbf{Nb_{10}O_{28}}]\}_n\cdot 9nH_2O$ were synthesized from the same reaction mixture just by adjusting the pH value. Moreover, by applying hydrothermal stirring conditions, the reaction time was significantly reduced to less than 1 h and high yields were obtained. Investigation of the stabilities revealed a reversible dehydration/rehydration for the decaniobate and the formation of a nanosized material at higher decomposition temperatures.

After adding $Ti(O^iPr)_4$ to the reaction slurry, a second decaniobate containing compound was isolated, $[Cu(cyclam)(H_2O)_2]\{[Cu(cyclam)]_2[\mathbf{Nb_{10}O_{28}}]\}\cdot 27H_2O$. This compound loses crystal H_2O molecules upon removing from the mother liquor, yielding a new compound with a different crystal structure. The H_2O molecules are reintegrated when the sample is treated with water. The water loss process was investigated *via* synchrotron X-ray powder diffraction and X-ray total scattering. Evaluation of the total scattering data yields the pair distribution function (PDF) and revealed a precise histogram of the interatomic distances in the structures, being different for the water-rich and water-poor phase.

The replacement of Cu^{2+} by Ni^{2+} cations yielded four titanoniobate containing compounds, which are quite rare in PONb chemistry. Violet crystals of $[Ni(cyclam)]_4[\mathbf{Ti_2Nb_8O_{28}}]\}_n\cdot\sim 28nH_2O$ and yellow crystals of $K[Ni(cyclam)]_3[\mathbf{TiNb_9O_{28}}]\cdot nH_2O$ (n = 10-18) were obtained by varying the titanium source. The first compound with Ni^{2+} cations in octahedral environment was synthesized with $Ti(O^iPr)_4$, while the latter compounds with square-planar coordinated Ni^{2+} cations were prepared with $K_2TiO(C_2O_4)_2\cdot 2H_2O$ or $Ti(O^iPr)_4$ with addition of oxalate anions from the same reaction mixture.

Inhaltsverzeichnis

1. Einleitung

1.1 Polyoxoniobate (PONbs)

POMs sind negativ geladene Ionen, welche aus {MO*x*}-Polyedern aufgebaut sind (*x* = 4-7; M = V, Nb, Ta, Mo, W) und sich durch Kondensationsreaktionen bilden. POMs der Gruppen V und VI mit überwiegend MO_6-Oktaedern als primärer Baueinheit weisen ähnliche strukturelle Merkmale auf: kurze terminale M=O Bindungen und aufgrund der starken pπ-dπ-Orbitalüberlappung lange zu den kurzen Bindungen *trans*-ständige M-O-Einfachbindungen. Zusätzlich weisen POMs einige Gemeinsamkeiten bei der Verknüpfung der MO_6-Oktaeder in den Clustern in den Festkörperstrukturen auf.[1]

Allerdings ist das Verhältnis von Ladung-zu-Radius bei den POMs der 5. Gruppe wesentlich größer als bei den Gruppe 6–POMs (Beispiel: $[SiW_{12}O_{40}]^{4-}$/$[SiNb_{12}O_{40}]^{16-}$) und folglich ist die Ladungsdichte mit 0.075 zu 0.30 höher. Generell nimmt mit höherer Ladungsdichte die Stabilität der Polyoxoanionen bei höheren pH-Werten zu. Daher werden POMs mit Mo und W eher im sauren Bereich erhalten, während sich POVs, PONbs und POTas im alkalischen Milieu bilden. Wie bereits kurz erwähnt stellen verzerrte MO_6-Oktaeder die fundamentale Baueinheit dar, was auf Grund ähnlicher Ionenradien[2] (Nb^{5+}:0.64 Å; Ta^{5+}:0.64 Å; Mo^{6+}:0.59 Å; W^{6+}:0.60 Å) erwartet werden kann, und deren Verknüpfung führt zu ähnlichen Clustergeometrien.[3]

Bis auf wenige Ausnahmen (Vgl. Kap. 1.2) ist Nb^{5+} in PONbs oktaedrisch koordiniert. Die bei den PONbs am häufigsten vorkommenden Clustergeometrien werden in dem Lindqvist-Anion $[Nb_6O_{19}]^{8-}$ (Isopolyoxoniobat) und Keggin-Anion $[MNb_{12}O_{40}]^{x-}$ (Heteropolyoxoniobat, M = Haupt- oder Nebengruppenelement), beobachtet (Abb. 1).

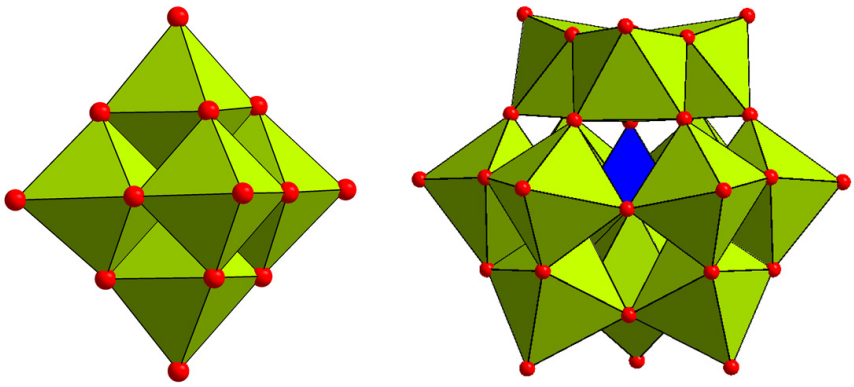

Abb. 1: Polyederdarstellung der am häufigsten vorkommenden PONb-Clustergeometrien; links: $[Nb_6O_{19}]^{8-}$, rechts: $[MNb_{12}O_{40}]^{x-}$.

Verglichen mit ihren leichteren Homologen, den Polyoxovanadaten (POVs), welche eine vielfältige Redoxchemie aufweisen, sind PONbs und Polyoxotantalate (POTas) elektrochemisch inert und kommen in wässrigen Lösungen immer in der Oxidationsstufe +V vor.[4] Die chemische Ähnlichkeit zwischen den beiden schwereren Homologen Niob und Tantal ist wesentlich stärker als zwischen Vanadium und Niob, was auf die Lanthanoidenkontraktion zurückzuführen ist. Diese äußert sich z.B. darin, dass die gemeinsamen Clusteranionen, die Hexametallate $\{Nb_6O_{19}\}$ und $\{Ta_6O_{19}\}$, trotz stark unterschiedlicher Molmassen annähernd den gleichen Radius aufweisen.[4]

Trotz ähnlicher Größe und Ladungsdichte gibt es auch Unterschiede zwischen PONbs und POTas, welche auf das Vorhandensein leerer f-Orbitale zurückgeführt werden.[5] Protonierte $\{H_xNb_6O_{19}\}$-Spezies sind im alkalischen Medium stabiler als Tantalate und dreifach protonierte $\{Ta_6O_{19}\}$-Anionen erfordern Bedingungen, bei denen der Cluster dissoziiert.[6] Das bedeutet gleichzeitig auch, dass Niobate basischer als Tantalate sind und damit die stärksten Basen unter den POMs darstellen. Dieses wurde durch die Bestimmung der pK_a-Werte für die Gleichgewichte $[HNb_6O_{19}]^{7-}/[Nb_6O_{19}]^{8-}$ und $[HTa_6O_{19}]^{7-}/[Ta_6O_{19}]^{8-}$ herausgefunden.[4][6] Zwar ist der Löslichkeitstrend der beiden Anionen in Wasser identisch (Cs-Salze sind besser löslich als K-Salze), jedoch assoziieren die Alkalimetallionen bei PONbs direkt an das Anion, während die Tantalatanionen durch eine Solvathülle von den Kationen getrennt sind. Vermutlich ist aus diesem Grund noch nie eine andere POTa-Geometrie in H_2O als die von $\{Ta_6O_{19}\}$ beobachtet worden, was darauf schließen lässt, dass die Verwendung anderer Lösungsmittel vermutlich zu neuen Clustergeometrien führen kann.[7]

1.2 Entwicklung und Meilensteine der Polyoxoniobat-Chemie

Bis zum Beginn der 90er Jahre war die Chemie der PONbs beschränkt auf das Lindqvist-Anion $[Nb_6O_{19}]^{8-}$ und einige Cluster gleicher Geometrie wie $[M(Nb_6O_{19})_2]^{12-}$ ($M = Mn^{IV}, Ni^{IV}$) oder $[M(en)Nb_6O_{19}]^{5-}$ (en = Ethylendiamin, M = Co^{III}, Cr^{III}; allerdings keine Einkristallstrukturdaten) und einem einzigen Bericht über das Dekaniobat-Anion $[Nb_{10}O_{28}]^{6-}$ (Abb. 2a).[1][8][9] Die Reaktion des $\{Nb_6O_{19}\}$-Clusters mit Seltenerdoxiden führte zum Einbau von isolierten $[Ln_3O(OH)_3(OH_2)_3]^{4+}$ ($Ln = Eu^{3+}$, Er^{3+}, Lu^{3+})–Kationen in eine Polyoxoniobat-Struktur, wobei die Geometrie des PONb-Anions erhalten blieb.[10][11][12] Erst zu Beginn der 2000er Jahre wurde die Chemie der PONbs um das erste Heteropolyoxoniobat vom Keggin-Typ erweitert.[13] Anzumerken ist hierbei, dass durchaus auch schon früher POWs mit Nb^{5+}

bekannt waren, diese allerdings durch das geringe Nb:W-Verhältnis zu den POWs gezählt werden.[14][15][16][17] Parallel dazu wurden die ersten Titanoniobate entdeckt (Vgl. Kap.1.4.4).

2011 wurde zum ersten Mal ein zweites POM-Übergangsmetall in einen PONb–Keggin-Cluster integriert.[18] Die neuen Anionen $[VNb_{12}O_{40}(VO)_2]^{9-/11-}$ konnten mit $[Cu(en)_2(H_2O)x]^{2+}$ (x = 0-1) und/oder $[Cu(2,2´\text{-bipy})_2]^{2+}$-Kationen (2,2´-bipy = 2,2´-Bipyridin) stabilisiert und kristallisiert werden. In den Verbindungen liegen Vanadium-Kationen entweder ausschließlich als V^V oder gemischtvalent als $V^{IV/V}$ vor. Das lösliche TMA-Salz (TMA = Tetramethylammonium) dieses Anions wurde in Lösung untersucht und der Cluster ist im pH-Bereich von 6.5 - 9.0 stabil.[19] Im Laufe der letzten Jahre konnten Keggin-PONbs u.a. aufgrund ihrer hohen Stabilität mit zahlreichen Elementen synthetisiert und charakterisiert werden (Vgl. Kap. 1.4.1).

Der erste höher kondensierte Cluster stellt das $[Nb_{24}O_{72}]^{24-}$-Anion dar (Abb. 2c), welches drei $[Nb_7O_{22}]^{9-}$-Einheiten beinhaltet, die über $\{NbO_6\}$-Oktaeder verknüpft sind. Bemerkenswert an den drei Verbindungen mit diesem Clustertyp, welche im gleichen Jahr von zwei Arbeitsgruppen veröffentlicht wurden, war die Tatsache, dass zum ersten Mal $[Cu(en)_2]^{2+}$-Übergangsmetallkomplexe als ladungskompensierende Spezies eingesetzt wurden, während bisher überwiegend Alkalimetallkationen verwendet wurden. Eine Annahme ist, dass die Kupfer-Amin-Kationen mit geringerer Ladungsdichte die Bildung größerer PONb-Anionen begünstigen.[20][21]

Kurze Zeit später wurde zum ersten Mal ein in der POM-Chemie seltener, pentagonal-bipyramidaler $\{NbO_7\}$-Polyeder beschrieben, der Bestandteil der Strukturen der noch größeren PONb-Anionen $[HNb_{27}O_{76}]^{16-}$ und $[H_{10}Nb_{31}O_{93}(CO_3)]^{23-}$ ist (Abb. 2d), und Alkalimetallionen agierten als Gegenionen.[22]

Eine Besonderheit stellt die 2010 publizierte Verbindung $K_{12}Na[H_{23}Nb^{IV}O_8Cu_{24}(Nb_7O_{22})_8]$ dar, in der eine bis dahin in der PONb-Chemie noch nie beobachtete tetragonal-antiprismatische $\{Nb^{IV}O_8\}$-Baueinheit gefunden wurde.[23] Dies war der erste und gleichzeitig der letzte Bericht über ein PONb mit Nb^{4+}-Spezies.

Eine weitere Steigerung der Anzahl an Nb-Zentren liegt in dem $\{Nb_{32}O_{96}\}$-Cluster vor: vier $[Nb_7O_{22}]^{9-}$ -Baueinheiten sind über $\{NbO_6\}$-Oktaeder über gemeinsame Ecken zum finalen Cluster verknüpft.[24] 48 Nb^V-Zentren liegen in dem $[Nb_{48}V_8(OH)_{30}O_{130}]^{18-}$-Cluster (Abb. 2f) vor, in dem interessanterweise die zu $[Nb_7O_{22}]^{9-}$ analoge $[VNb_6O_{22}]^{10-}$-Einheit beobachtet wird.[25] Die Baugruppe $\{MNb_6O_{22}\}$ scheint kein Exot zu sein (Vgl. Kap. 1.4.3) und die

Bildung von PONb-Clustern zu begünstigen, wie z.B. das $[H_4Ni_{10}(H_2O)_8Nb_{32}O_{102}]^{20-}$-Anion belegt, in dessen Struktur $[NiNb_6O_{22}]^{12-}$-Anionen vorliegen.[26]

Ein spektakuläres Beispiel stellt der erste Fe^{III}-substituierte PONb-Cluster, $[Fe_3Nb_{25}O_{76}]^{18-}$ (Abb. 2g), dar, in dem sowohl pentagonal-bipyramidale $\{NbO_7\}$ als auch quadratisch-pyramidale $\{NbO_5\}$-Einheiten vorhanden sind.[27]

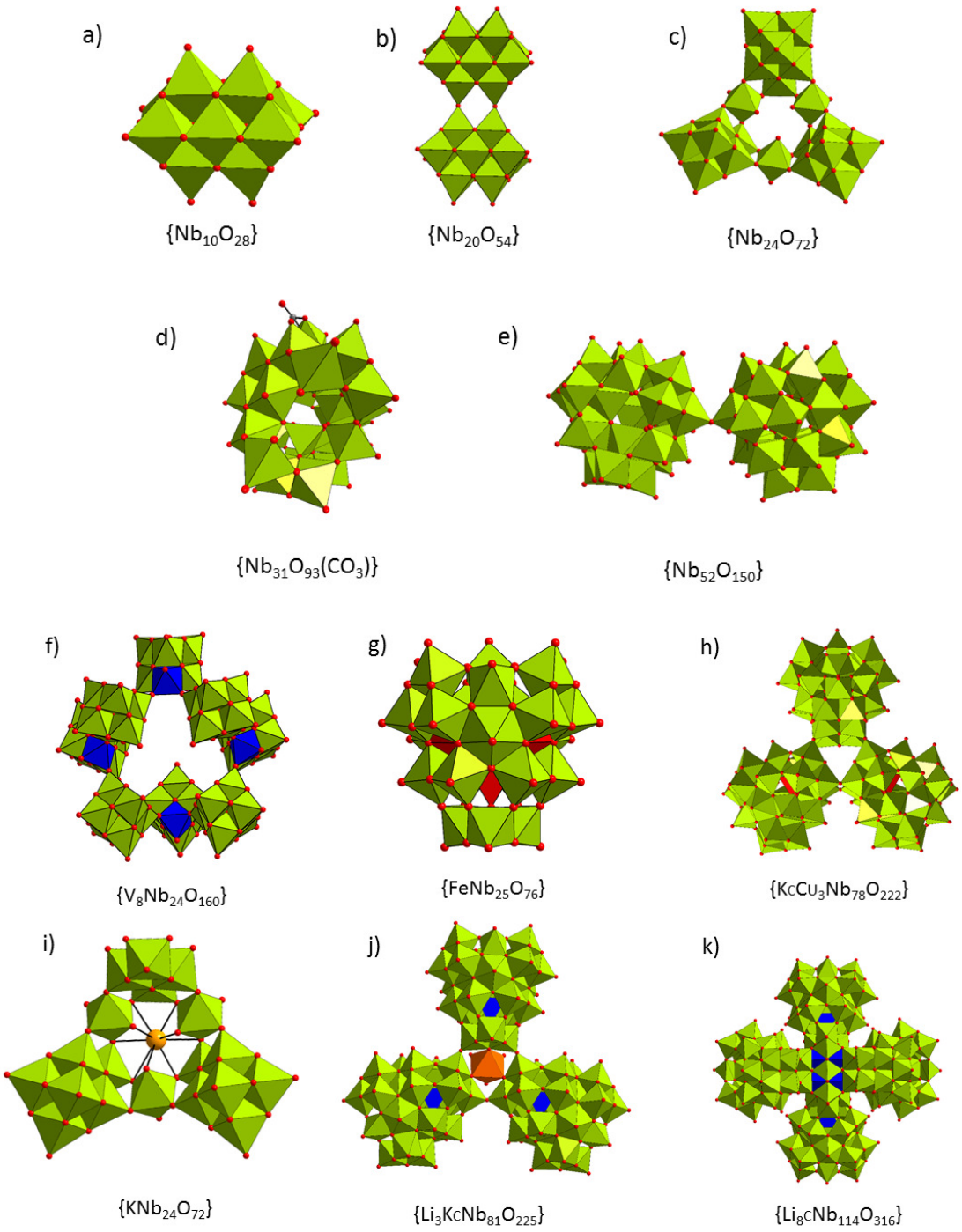

Abb. 2: Ausgewählte Isopolyoxoniobate und Heteropolyoxoniobate mit integrierten Übergangsmetall- oder eingeschlossenen Alkalimetallkationen. [1,28,20–22,29,25,27,30]

Mit Seltenerdionen wurden in den letzten Jahren Verbindungen mit dem $\{LnW_{12}O_{36}(H_2O)_{24}(Nb_6O_{19})_{12}\}$-Cluster (Ln = Y, La, Pr, Nd, Sm, Eu, Gd, Tb, Dy, Ho, Er und Yb) hergestellt und charakterisiert.[31] Der $\{Nb_{24}O_{72}\}$-Cluster konnte über $\{Eu(H_2O)_3Ox\}$-Einheiten (x = 4,5) zu einem formalen Dimer mit der Formel $\{Eu_3(H_2O)_9Nb_{48}O_{138}(H_2O)_6\}$ verbunden werden.[32] Da Seltenerdionen oft hohe Koordinationszahlen bevorzugen, sind diese für die Integration in PONb-Strukturen bestens geeignet, wenn auch auf synthetische Tricks zurückgegriffen werden muss (Vgl. Kap. 1.3).

PONbs beeindruckender Clustergröße mit eingeschlossenen Li^+, K^+ und Cu^{2+}-Kationen wurden erst kürzlich beschrieben und ein Prototyp ist z.B. $\{Li_8{\subset}Nb_{114}O_{316}\}$ mit 114 Nb-Zentren (Abb. 2k).[29]

Der Weltrekord in Bezug auf die Anzahl an Nb-Zentren wurde kürzlich aufgestellt: der $\{Nb_{288}O_{768}(OH)_{48}(CO_3)_{12}\}$-Cluster stellt das größte PONb-Anion dar und ist der Cluster mit der zweithöchsten Anzahl an Metallzentren in POMs[33] (nur in $\{Mo_{368}\}$ liegen mehr Metallzentren vor[34]). $\{Nb_{288}O_{768}(OH)_{48}(CO_3)_{12}\}$ weist *C*6-Symmetrie auf und hat eine Ausdehnung von 4.3 x 3.6 nm (Vgl. $\{Mo_{368}\}$ ca. 5.4 x 3.7 nm), kann also als Nanokapsel angesehen werden.

Dieser kurze Ritt durch die Historie der PONbs belegt, dass diese in den letzten Jahren aus dem Dornröschenschlaf geweckt wurden und aus dem Schatten ihrer berühmten ‚Verwandten' treten.

1.3 Synthese von Polyoxoniobaten und synthetische Herausforderungen

Für die Synthese von POVs, POMos oder POWs können wasserlösliche Oxoanionen eingesetzt werden wie z.B. $[VO_4]^-$ $[VO_4]^{3-}$, $[MoO_4]^{2-}$ oder $[WO_4]^{2-}$. Verbindungen mit analogen monomeren Einheiten sind in der Nb- und Ta-Chemie nicht bekannt, was vermutlich am Ionenradius von Nb^{5+}/Ta^{5+} und der geringeren Ladungsdichte im Vergleich zu V^{5+} und Mo^{6+}/W^{6+} liegt.[1] Das schwerlösliche Nb_2O_5 lässt sich nur durch Aufschluss in alkalischer Schmelze oder in stark basischen Lösungen auflösen, und unter solchen Bedingungen werden ausschließlich Anionen mit Lindqvist-Geometrie $\{Nb_6O_{19}\}$ gebildet.[13] Einige PONbs konnten mit Nb-Alkoxiden hergestellt werden.[35][36] Da die Alkoxide recht feuchtigkeitsempfindlich sind und Synthesen in organischen Lösungsmitteln erfordern, scheinen diese wenig geeignet zu sein. Auch Niobsäure $Nb_2O_5{\cdot}xH_2O$ wurde bei der Synthese verwendet und in den letzten Jahren hat sich das lösliche Hexaniobat als viel versprechend erwiesen. Verbindungen dieses Anions erzeugen in H_2O einen basischen pH-Wert und sind

relativ leicht herstellbar. Allerdings ist das Hexaniobat-Anion unter moderaten Bedingungen stabil, so dass hydrothermale Bedingungen notwendig sind, um andere Clustergeometrien wie z.B. ein PONb-Anion vom Keggin-Typ zu erhalten.[13]

Die Mehrzahl der der PONbs wurde in einem engen pH-Wert-Bereich im alkalischen Medium synthetisiert, was den PONb-Chemiker vor einige Herausforderungen stellt. Viele ÜM- und auch Seltenerdionen fallen in diesem pH-Wertbereich als Hydroxide bzw. Oxo/Hydroxo-Verbindungen aus, was oft durch Einsatz komplexierender Reagenzien wie Aminmolekülen oder Mineralisatoren verhindert werden kann. So sind PONb-Verbindungen mit ÜM-Komplexen als Ladungskompensatoren mit den meisten gängigen Aminen wie Ethylendiamin, Diaminopropan, 1,10-Phenanthrolin oder 2,2´-Bipyridin bekannt.

Bei den Seltenerd-PONbs wurde zunächst EDTA als Ligand (EDTA = Ethylendiamintetraacetat) verwendet.[10][11][12] In folgenden Arbeiten wurden die Reaktionsmischungen komplexer, und immer wurden Carbonsäuren oder deren Salze von Zitronensäure, Essigsäure, Nikotinsäure etc. zugegeben, welche möglicherweise die Fällung der Seltenerdhydroxide verhindern.[31][37]

Zum Einfluss der Syntheseparameter auf die Geometrie der Cluster gibt es wenige Untersuchungen. Beispielsweise wurde berichtet, dass die beiden PONb-Anionen $[VNb_{12}O_{40}\{NbO(CO_3)\}_2]^{13-}$ und $[V_xNb_{24}O_{76}]^{n-}$ (x = 3,4; n = 12,17) aus identischen Reaktionsgemischen kristallisieren, je nachdem ob das Kalium- oder das Natriumsalz der Hexaniobats als Edukt verwendet wird.[38]

Nicht nur die Edukte, sondern auch die Reaktionstemperatur kann die Produktbildung beeinflussen. So wird bei Einsatz identischer Reaktanten und Einwaageverhältnisse bei 140 °C $[Co(1,2\text{-dap})_2]_4[HPV_6Nb_{10}O_{44}]\cdot 17H_2O$ erhalten und bei 160 °C kristallisiert $[Co(1,2\text{-dap})_2]_5[PV_6Nb_{12}O_{46}](OH)_7\cdot 15H_2O$ (1,2-dyp = 1,2-Diaminopropan).[39]

Nicht selten kommt es vor, dass Ionen oder molekulare Bausteine in PONb-Strukturen gefunden wurden, welche unabsichtlich generiert wurden. Bei der Synthese von $K_{14}Na[GaNb_{18}O_{54}]\cdot 31\ H_2O$ wurde kein Na^+ eingesetzt, sondern dieses stammt vermutlich aus verunreinigtem Nb_2O_5 und bei der Herstellung von $K_{19}Na_4[H_{10}Nb_{31}O_{93}(CO_3)]\cdot 35H_2O$ gelang CO_2 aus der Umgebungsluft in die Reaktionsmischung und es wurde CO_3^{2-} in der basischen Lösung gebildet.[22]

Die Reaktionsgemische, aus denen vielkernige PONb-Spezies kristallisieren, sind meist recht komplex und oft werden Substanzen zugesetzt, welche nicht in die Struktur integriert werden. Daher stellt sich die Frage, welche Rolle diese „Additive“ bei der Bildung der Produkte

spielen. Vor kurzer Zeit wurden Untersuchungen durchgeführt, um die Bildungsmechanismen von Nb-Riesenclustern aufzuklären. Die Ergebnisse zeigten, dass sich in Lösungen von $\{Nb_{10}O_{28}\}$-Clustern verschieden große Aggregate wie z.B. das $[Nb_{24}O_{72}]^{24-}$-Anion in Abhängigkeit vom anwesenden Alkalimetallions bilden.[40] Alkalimetallionen spielen, wie schon für $\{Nb_6O_{19}\}$-Cluster nachgewiesen (Vgl. Kap. 1.4.2), eine sehr wichtige Rolle z.B. für das Löslichkeitsverhalten und die Assoziation verschiedener Spezies der PONbs. Zusätzlich werden Alkalimetallionen oft in Vakanzen der Riesencluster gefunden (Vgl. Kap. 1.4), und so ist es nicht verwunderlich, aber sehr aufschlussreich, dass eine Abhängigkeit der Bildung der Produkte vom eingesetzten Alkalimetallion nachgewiesen werden konnte. Trotz erster Informationen über die Bildung von PONbs bleiben viele Fragen bezüglich der Mechanismen und des Einflusses verschiedener Syntheseparameter auf die Bildung von PONbs offen, so dass erheblicher Forschungsbedarf besteht.

1.4 Polyoxoniobatcluster-Geometrien und deren Modifizierung

1.4.1 Keggin-Anionen

Bei den Heteropolyoxoniobaten sind Keggin-Anionen mit der allg. Summenformel $\{XM_{12}O_{40}\}$ und deren Derivate am häufigsten vertreten. M ist das POM-Metallion, welches oktaedrisch von Sauerstoff umgeben ist. Jeweils drei dieser Oktaeder sind kantenverknüpft und bilden eine sog. Triade. Vier dieser Triaden sind über Ecken verknüpft und umgeben ein tetraedrisch koordiniertes Kation X. Durch die Vielzahl der Kationen, welche mit Sauerstoff Tetraeder bilden, sind auch viele unterschiedliche PONb-Keggin-Ionen bekannt (Tab.1). X umfasst $[SiO_4]^{4-}$, $[GeO_4]^{4-}$, $[PO_4]^{3-}$, $[AsO_4]^{3-}$ und $[VO_4]^{3-}$ (Tab. 1). Zudem können auch die $\{NbO_6\}$ Oktaeder durch andere oktaedrische Baueinheiten ersetzt werden, wie z.B. durch $\{VO_6\}$ oder $\{WO_6\}$. Durch die Anordnung der eckenverknüpften Triaden ergeben sich Vakanzen, wodurch sich die Oberfläche der hoch negativ geladenen Clusteranionen weiter modifizieren lässt. Diese Vakanzen können paarweise durch zwei bis sechs quadratisch pyramidale $\{V^{IV/V}O_5\}$ Einheiten oder verzerrt trigonale $\{Sb^{III}O_4\}$ Einheiten besetzt sein, wobei letztere maximal zweimal je Clusteranion vorhanden sind, da sonst vermutlich die Verzerrung zu groß würde. Ein seltener Fall ist die chemische Modifizierung durch verzerrt quadratisch-pyramidale $\{Nb^{V}O_5\}$ Einheiten, welche in der Verbindung $Rb_{13}[GeNb_{13}O_{41}]\cdot 23H_2O$ vorliegen.[41]

Die hohe negative Ladung des Anions kann durch Integration von Heteroatomen erniedrigt werden, was die Stabilität erhöhen kann.

Interessanterweise können solche Cluster ineinander umgewandelt werden. Ausgehend von einem $[PNb_{12}O_{40}]^{15-}$ Anion lässt sich durch eine hydrothermale Reaktion in Anwesenheit von Sb_2O_3 ein $[PSb_2Nb_{12}O_{40}]^{9-}$-Anion herstellen. Durch Erhitzen einer TBA-Lösung von $[PNb_{14}O_{42}]^{9-}$ bzw. $[P(NbO)_2Nb_{12}O_{40}]^{9-}$ können die Nb=O Einheiten entfernt werden [42].

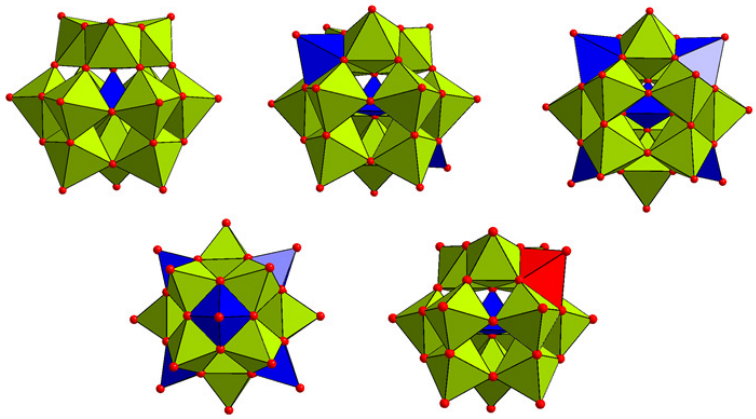

Abb. 3: Schematische Darstellung unterschiedlicher Modifizierungen der Keggin-Ionen; grün: $\{NbO_6\}$, blau: $\{SiO_4\}$; rot: $\{NbO_5\}$.

Tab. 1: Übersicht über verschieden substituierte PONbs vom Keggin-Typ.

X=0
$K_{12}[Ti_2O_2][SiNb_{12}O_{40}]\cdot16H_2O$ [13]
$Na_{12}[Ti_2O_2][SiNb_{12}O_{40}]\cdot xH_2O$ [43]
$Na_{10}[Nb_2O_2][SiNb_{12}O_{40}]\cdot xH_2O$ [43]
$Na_{10}[Nb_2O_2][GeNb_{12}O_{40}]\cdot xH_2O$ [43]
$Na_{12}[Ti_2O_2][GeNb_{12}O_{40}]\cdot xH_2O$ [43]
$TMA_{10}[H_5PNb_{12}O_{42}]\cdot30.5H_2O$ [42]
$K_8H_2(Nb_2O_2)[SiNb_{12}O_{40}]\cdot20H_2O$ [44]
$Na_{16}[SiNb_{12}O_{40}]\cdot4H_2O$ [45]
$Na_{16}[GeNb_{12}O_{40}]\cdot4H_2O$ [45]
$Li_{13}K[SiNb_{12}(OH)_2O_{38}]\cdot17H_2O$ [46]
$K_{10-x}[H_xGeNb_{12}O_{40}][Nb_2O_2]\cdot11H_2O$ x =1-1.5 [47]
$[Cu^ICu^{II}{}_3(\mu_3\text{-}OH)(H_2O)_6(trz)_3]_2(PW_9Nb_3O_{40})\cdot13H_2O$ [48]
$[Cu^ICu^{II}{}_3(\mu_3\text{-}OH)(H_2O)_4(Htrz)(trz)_3]_2(PW_9Nb_3O_{40})\cdot13H_2O$ [48]
$Cs_{14.9}H_{5.1}[Nb_4O_6(\alpha\text{-}Nb_3SiW_9O_{40})_4]$ [49]
X=1
$Rb_{13}[GeNb_{13}O_{41}]\cdot23H_2O$ [41]
$Cs_{10.6}[H_{2.4}GeNb_{13}O_{41}]\cdot27H_2O$ [41]
$Cs_{18}H_6[(NbOH)SiNb_{12}O_{40}]_2\cdot38H_2O$ [41]
X=2
$[Cu(en)_2]_{3.5}[Cu(en)_2(H_2O)]\{[VNb_{12}O_{40}(VO)_2][Cu(en)_2]\}\cdot17H_2O$ [18]
$[Cu(en)_2]_{0.5}[Cu(en)_2(H_2O)]_2\{[VNb_{12}O_{40}(VO)_2][Cu(en)_2][Cu(2,2'bipy)_2]\}\cdot7H_2O$ [18]
$(TMA)_9[PV_2Nb_{12}O_{42}]\cdot19H_2O$ [50]
$(TMA)_9[V_3Nb_{12}O_{42}]\cdot18H_2O$ [19]
$\{Cu(en)_2\}_6\{GeNb_{12}V^{IV}{}_2O_{42}\}\cdot20H_2O$ [51]
$\{Cu(en)_2\}_3K_2Na_4\{GeNb_{12}V^{IV}{}_2O_{42}\}\cdot23H_2O$ [51]
$\{Cu(en)_2\}_6\{SiNb_{12}V^{IV}{}_2O_{42}\}\cdot18H_2O$ [51]

$\{Cu(en)_2\}_3K_2Na_4\{SiNb_{12}V^{IV}_2O_{42}\}\cdot 19H_2O$[51]
$[Cu(en)_2(H_2O)_2]_4[H_2SiSb_2Nb_{12}O_{40}]\cdot 18H_2O$[52]
$[Cu(en)_2(H_2O)_2]_4[H_2GeSb_2Nb_{12}O_{40}]\cdot 18H_2O$[52]
$[Cu(en)_2(H_2O)_2]_4[HPSb_2Nb_{12}O_{40}]\cdot 18H_2O$[52]
$[Cu(en)_2(H_2O)_2]_4[HAsSb_2Nb_{12}O_{40}]\cdot 18H_2O$[52]
$[Cu(en)_2(H_2O)_2]_4[HVSb_2Nb_{12}O_{40}]\cdot 18H_2O$[52]
$[Cu(en)_2]_3[Cu(en)_2(H_2O)]_4\{[Cu(en)_2]_2[HSiSb_2Nb_{12}O_{40}]_2\}\cdot 18H_2O$[52]
$[Cu(en)_2]_3[Cu(en)_2(H_2O)]_4\{[Cu(en)_2]_2[HGeSb_2Nb_{12}O_{40}]_2\}\cdot 18H_2O$[52]
$[Cu(en)_2]\{[Cu(en)_2]_3[SiSb_2Nb_{12}O_{39}]\}\cdot 11H_2O$[52]
$[Cu(en)_2]\{[Cu(en)_2]_3[GeSb_2Nb_{12}O_{39}]\}\cdot 11H_2O$[52]
$TMA_9[PSb_2Nb_{12}O_{40}]\cdot 28H_2O$[42]
$[Cu(en)_2][Cu(en)_2(H_2O)_2][Cu(en)_2(H_2O)]_2\{H_4SiNb_{12}V_2O_{42}\}\cdot 7H_2O$[53]
$[Cu(en)_2]_4[Cu(en)_2(H_2O)_2][PV^{IV}V^{V}Nb_{12}O_{42}](OH)_2\cdot 11H_2O$[54]
$[Co(en)_3]_2[Co(en)_2(H_2O)_2]_{0.5}[H_{2.5}PV^{IV}V^{V}Nb_{12}O_{42}]\cdot 20H_2O$[54]
$[Na(H_2en)_5][VNb_{14}O_{42}(NO_3)_2]\cdot 12H_2O$[55]
$[K_7Na_4][VNb_{14}O_{42}(NO_3)_2]\cdot 31H_2O$[55]
$TMA_9[PNb_{14}O_{42}]\cdot 26H_2O$[42]
$Na_9H_4[VNb_{12}O_{40}\{NbO(CO_3)\}_2]\cdot 37H_2O$[38]
X=4
$[Co(1,2\text{-dap})_2]_4[HPV_6Nb_{10}O_{44}]\cdot 17H_2O$[39]
$[Cu(trien)]_4[VNb_{12}(VO)_4O_{40}][OH]\cdot 10H_2O$[56]
$[Cu(1,2\text{-dap})_2]_4[AsNb_{12}O_{40}(VO)_4]\cdot(OH)\cdot 7H_2O$[57]
$Na_2\{[Cu(en)_2(H_2O)]_4[PNb_{12}O_{40}(V^{IV}O)_{2.5}]\}\cdot 13H_2O$[58]
$[Cu(en)_2(H_2O)][Cu(en)_2]_4\{AsNb_9V_7O_{44}\}\cdot 8H_2O$[59]
$[Cu(en)_2(H_2O)][Cu(en)_2]_4H\{AsNb_8V_8O_{44}\}\cdot 11H_2O$[59]
X=6
$[Cu(en)_2]_4[PNb_{12}O_{40}(VO)_6]\cdot(OH)_5\cdot 8H_2O$[60]
$[Cu(1,2\text{-dap})_2]_4[PNb_{12}O_{40}(VO)_6]\cdot(OH)_5\cdot 6H_2O$[60]
$[Co(1,2\text{-dap})_2]_5[PV_6Nb_{12}O_{46}](OH)_7\cdot 15H_2O$[39]
$[Cu(trien)]_4[VNb_{12}(VO)_6O_{40}][OH]_5\cdot 5H_2O$[56]
$[Co(1,2\text{-dap})_3]_4[PNb_{12}O_{40}(V^{IV}O)_6][OH]_5\cdot 20H_2O$[61]
X=8
$(H_2en)Na_2[Zn(en)_2(Hen)\}\{Zn(en)_2(H_2O)\}_2\{PNb_8V^{IV}_8O_{44}\}]\cdot 11H_2O$[58]
$\{Ni(en)_3\}_5H\{V^{V}Nb_8V^{IV}_8O_{44}\}\cdot 9H_2O$[58]
$Na\{Cu(en)_2\}_3\{[Cu(en)_2]_2[PNb_8V^{IV}_8O_{44}]\}\cdot 11H_2O$[58]

1.4.2 Hexaniobate

Während der Doktorarbeit wurde ein vorgefertigtes Hexaniobat als Edukt für die Synthese neuer PONbs verwendet.

Die Struktur des $[Nb_6O_{19}]^{8-}$-Anions wurde 1953 von I. Lindqvist aufgeklärt [62] und war gleichzeitig auch das erste PONb-Anion, welches überhaupt isoliert und charakterisiert werden konnte.

IR- und Raman-Studien belegten, dass das Anion auch in Lösung intakt bleibt und in basischen Lösungen bei pH 8-14 die dominante Spezies ist.[63][64][65] Wird der pH-Wert der Hexaniobat-Lösung gesenkt, so treten protonierte Spezies auf: $[HNb_6O_{19}]^{7-}$ ($pK_{a1} \approx$ 12-13),

$[H_2Nb_6O_{19}]^{6-}$ ($pK_{a2} \approx$ 10-11) und $[H_3Nb_6O_{19}]^{5-}$ ($pK_{a3} \approx$ 9-10).[66][67] Außerdem kristallisieren hexaniobathaltige Verbindungen bereits bei T < 100 °C, während bei Hetero-PONbs hydrothermale Bedingungen Voraussetzung sind.[13][68]

Für die Synthese von PONbs haben sich die Alkalisalze des Hexaniobats als besonders viel versprechend erwiesen und hauptsächlich wird das Kaliumsalz $K_7HNb_6O_{19}$ eingesetzt. Obwohl Hexaniobate schon seit mehr als 50 Jahren bekannt sind, sind sie aufgrund ihrer besonderen Eigenschaften immer noch interessant für die PONb-Forschung. Die Festkörperstrukturen der Alkali-Hexaniobate weisen interessante Trends auf. Die meisten Salze kristallisieren mit einer hohen Anzahl Kristallwassermolekülen (9 - 16 H_2O pro Formeleinheit) aus. Je größer der Radius des das Alkalimetall-Ions ist, desto größer ist die Anzahl der Bindungen zu Cluster-Sauerstoffatomen. So ist im Cs-Salz jedes $[Nb_6O_{19}]^{8-}$ Anion von acht Cs^+-Kationen umgeben, während im Na-Salz im Schnitt nur zwei Na^+-Kationen eine Bindung zum PONb-Anion ausbilden. Generell wird bei gemischten Salzen beobachtet, dass je kleiner das Kation ist, desto eher bevorzugen die H_2O Moleküle die Ausbildung von Wasserstoffbrückenbindungen zu O^{2-}-Clusteranionen. Diese Wechselwirkungen korrelieren auch mit dem Protonierungsgrad des Clusters; so wurden protonierte Spezies in Lithium-Salzen noch nie beobachtet, während mono- und diprotonierte Lindqvist-Anionen bei Salzen der schwereren Homologen von Li häufig sind. Zusätzlich hängt der Protonierungsgrad von der Temperatur ab, da die Protonierungsreaktion exotherm ist und folglich bei höheren Temperaturen nichtprotonierte Spezies beobachtet werden.[1][7][69][70]

Das assoziative Verhalten von Alkalimetallionen und $\{Nb_6O_{19}\}$ im Festkörper lässt sich noch gut verstehen, da größere und weniger hydratisierte Ionen wie Cs^+ stärker assoziieren als kleinere. Ungewöhnlich jedoch ist deren Löslichkeit, welche von Li^+ zu Cs^+ zunimmt. Da die Cs^+-Ionen durch die schwächere Hydrathülle stärker assoziieren, würde man erwarten, dass diese schlechter löslich sind. Dies wird für die anderen POMs auch beobachtet.[71] Durch SAXS-Untersuchungen (Small Angle X-Ray Scattering) konnte bestätigt werden, dass die K-, Rb- und Cs-Salze des Hexaniobats auch in (basischer) Lösung als „neutrale“ Spezies vorliegen.[7] Somit gibt es keine signifikanten attraktiven Wechselwirkungen zwischen den molekularen Baueinheiten und die Ionen bleiben in Lösung. Dieses ungewöhnliche Lösungsverhalten tritt bei POMs mit höherer Ladungsdichte eher auf.[72]

Obwohl beide Ionen schon lange Zeit bekannt sind, konnten erst kürzlich die Absorptionen der Hexaniobat (und -tantalat) Anionen im UV-Bereich gründlicher untersucht und erklärt werden. So wurde festgestellt, dass die Absorbanz mit steigendem pH-Wert (und geringerem

Protonierungsgrad) zunimmt. Zudem konnte der Extinktionskoeffizient bestimmt werden, so dass der Niob-Gehalt von Lösungen nun mit einfachen UV-Vis-spektroskopischen Methoden bestimmt werden kann. Dies wurde für andere Nb^{5+}-Salze bestätigt, die im basischen Milieu das Hexaniobat-Anion bilden, welches anschließend detektiert werden kann.[69]

Mit NMR-Techniken kann der Protonierungsgrad der Nb-Lindqvist-Spezies eindeutig festgestellt werden und die Ergebnisse einer Bond Valence Sum-Analyse[73][74], welche normalerweise angewendet wird, wird dadurch unterstützt.[75]

Obwohl also das Nb-Lindqvist-Anion schon seit mehr als einem halben Jahrhundert bekannt ist, ist es immer noch Gegenstand aktueller PONb-Forschung.

1.4.3 Decaniobate: pH-Stabilität und Reaktivität

In Lösung konnte mittels Raman-Spektroskopie nachgewiesen werden, dass das Dekaniobat-Anion in Lösung zwischen pH 5.5 und 9.9 die dominante Spezies ist und bei pH ~ 11 vollständig zum $[Nb_6O_{19}]^{8-}$ Anion dissoziiert, welches am basischen Ende der pH-Skala auch die einzige Spezies in Lösung darstellt. Wird der pH-Existenzbereich unterschritten, so kommt es zur Fällung von $Nb_2O_5 \cdot xH_2O$, der sog. Niobsäure.[76] Dazwischen liegen unterhalb von pH = 6.5 einfach protonierte Spezies vor.[77] Oberhalb von pH ≥ 7.5 beginnt die Dissoziation und deren Rate erhöht sich mit höherem pH-Wert.[77] Die Dissoziation zum Hexaniobat ist bei 293 K zumindest zum Teil reversibel und kann durch Temperaturerhöhung beschleunigt werden.[78] Während der Konversion von Deka- zu Hexaniobat konnte ein Heptaniobat-Anion $[Nb_7O_{22}]^{9-}$ als reaktives Intermediat nachgewiesen werden[78], und findet sich auch als strukturelle Baueinheit in PONb-Clustern, wie z.B. im $[Nb_{24}O_{72}]^{24-}$ Anion.[20][21][24] So konnte auch ein Mechanismus zur baseninduzierten Dissoziation vorgeschlagen werden (Abb.4).

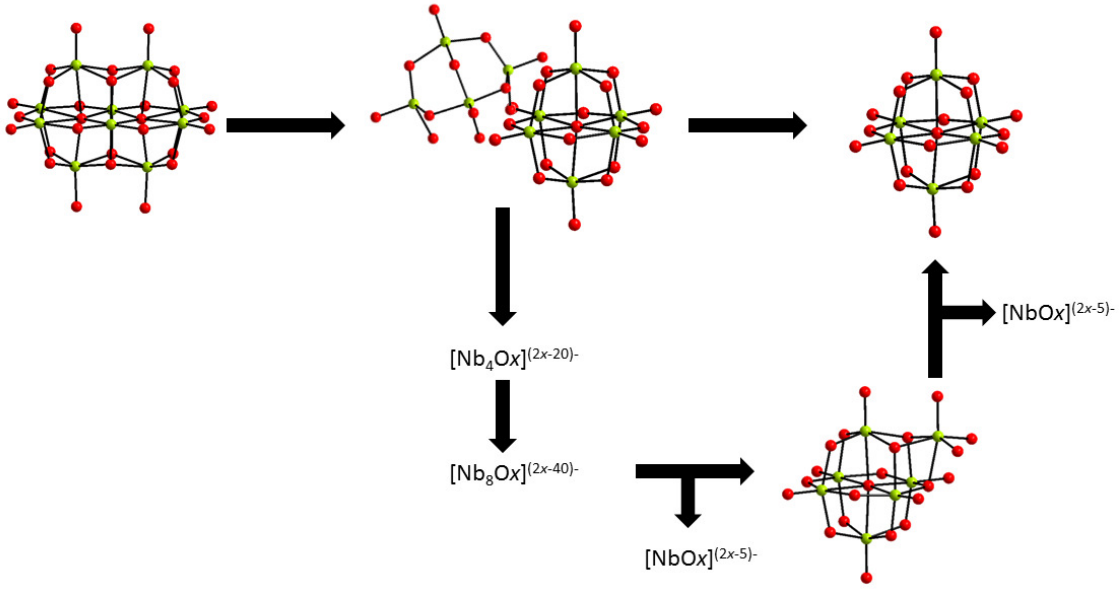

Abb. 4: Vorgeschlagener Mechanismus für die baseninduzierte Dissoziation des Dekaniobat-Anions in Hexa- und Heptaniobatanionen. Gezeichnet nach Ref. [77].

Zunächst kommt es zur Abspaltung eines Tetramers an den μ_3-verbrückenden O^{2-}-Anionen, wobei ein Abspaltungsprodukt das $[Nb_6O_{19}]^{8-}$-Anion ist. Die abgespaltenen Tetramere kondensieren sofort und bilden das Heptaniobat-Anion $[Nb_7O_{22}]^{9-}$ (Abb.5).[77]

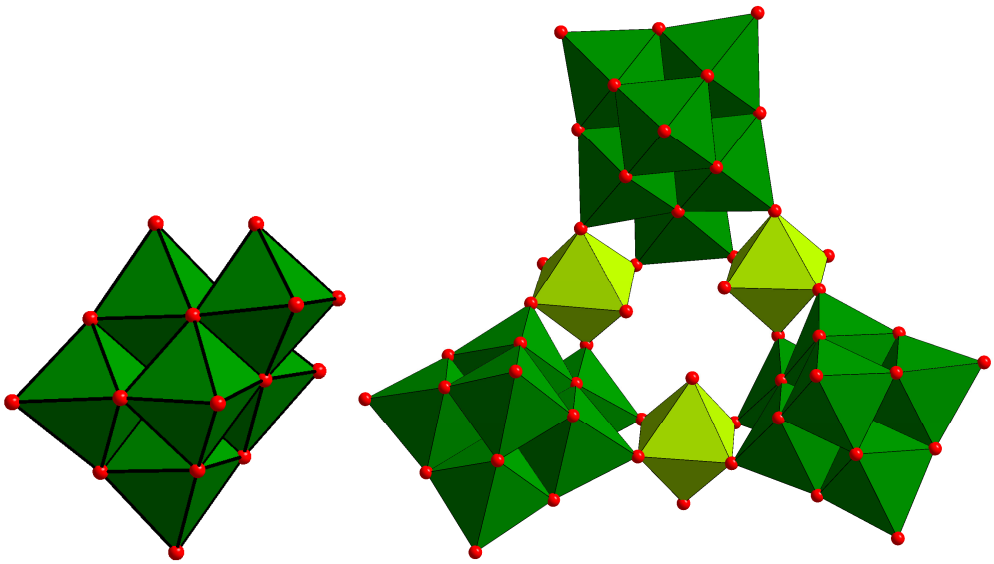

Abb.5: Polyederdarstellung der Heptaniobat-Einheit (links), welche auch als Strukturbaustein in größeren PONb-Clustern beobachtet wird, hier gezeigt für das $[Nb_{24}O_{72}]^{24-}$-Anion.[20]

Bei der Reaktion kommt es vermutlich zunächst zu einem nucleophilen Angriff eines OH^--Anions auf eines der „inneren“ Nb^{5+}-Kationen. Durch diese Wechselwirkung kommt es zur Verschiebung dieser Kationen aus der Clustermitte und die Bindung zum μ_3-verbrückenden O^{2-}-Anion wird gebrochen. Die Koordinationssphäre des nun koordinativ nicht mehr

abgesättigten Nb^{5+}-Kations wird mit H_2O-Molekülen aufgefüllt. Diese können nun durch Protonierung der übrigen O^{2-} Anionen diese labilisieren und das Molekül zerfällt.[79]

Das Icosaniobat-Anion $[Nb_{20}O_{54}]^{8-}$ kann aus $[Nb_{10}O_{28}]^{6-}$ durch Ansäuern in Tetrahydrofuran oder CH_3CN als TBA^+-Salz erhalten werden.[28][80] Bei dem Anion handelt sich um ein Dimer des Decaniobates, bei dem zwei $\{Nb_{10}O_{28}\}$-Cluster über die ehemals terminalen O^{2-}-Anionen verknüpft sind, welche die größte Basizität aufweisen.[77] Dabei verlieren O^{2-}-Anionen ihren Doppelbindungscharakter. Durch die Abwesenheit des *trans*-Effekts kommt es zur Verkürzung der entsprechenden gegenüberliegenden Nb-O-Bindung.[28]

Trotz intensiver Forschung ist die Anzahl der bekannten Verbindungen mit dem $[Nb_{10}O_{28}]^{6-}$-Anion recht limitiert. Die erste Verbindung mit TMA^+- bzw. Na^+-Kationen als ladungskompensierende Spezies war aufgrund der Zersetzung des hydrolyseempfindlichen Edukts $Nb(OEt)_5$ recht schwer zu reproduzieren[35][36], was später mit $Nb_2O_5 \cdot xH_2O$ unter hydrothermalen Bedingungen besser gelang[81] und das Anion auch mit TBA^+ erhalten werden konnte.[80] Die ersten anorganisch-organischen Hybridverbindungen konnten mit $K_7HNb_6O_{19} \cdot 13H_2O$ und $[Zn(2,2´\text{-bipy})_2]^{2+}$- bzw. $[Co(2,2´\text{-bipy})_2]^{2+}$-Kationen synthetisiert werden.[82] Bei höherer Reaktionstemperatur konnte auch $[Ni(2,2´\text{-bipy})_x]^{2+}$ (x = 2,3) integriert werden und schließlich mit 1,10-Phenanthrolin ein weiteres aromatisches Amin in $[ÜM(1,10\text{-phen})_x][Nb_{10}O_{28}] \cdot 8H_2O$ (ÜM = Ni^{2+}, Co^{2+}, Zn^{2+}; x = 2,3).[83] Es ist erstaunlich, dass - bis auf die in dieser Arbeit vorgestellten- keine Verbindungen des Dekaniobat-Anions mit Kupfer-Amin-Komplexen bekannt sind, obwohl sich diese generell sehr gut zur Ladungskompensation eignen und auch sehr viele Beispiele bekannt sind.

Kürzlich konnte gezeigt werden, dass Dekaniobat-Anionen in wässriger Lösung in Gegenwart von Alkalimetallionen zur Dissoziation neigen, wobei dieser Effekt bei Cs^+ am stärksten ist und bei TMA^+-Kationen nicht beobachtet wird.[40] Dies ist zum einen auf die leichte Erhöhung des pH-Werts zurückzuführen, denn dieser Effekt ist in gepufferten Lösungen nicht zu beobachten. Zusätzlich ist die Stabilität des Dekaniobat-Anions auch von der Konzentration des Alkalimetall-Ions abhängig, welche mit höheren Alkalimetallion-Konzentrationen abnimmt. Allerdings dissoziieren die Cluster nicht zum Lindqvist-Ion, sondern bilden größere Aggregate wie z.B. $[Nb_{24}O_{72}]^{24-}$ oder deren Dimere oder Tetramere und es gibt Hinweise darauf, dass die Größe der Aggregate mit der Größe des Alkalimetallions ansteigt. Diese Aggregate beinhalten das $[Nb_7O_{22}]^{9-}$ Anion, welches bereits zuvor als reaktives Intermediat bei der Dissoziation vom Deka- zum Hexaniobat postuliert wurde.[78]

1.4.4 Titanoniobate

Das erste Titanoniobat $Na_8[Ti_2Nb_8O_{28}]\cdot 34H_2O$ wurde aus $Nb_2O_5\cdot xH_2O$, $Ti(O^iPr)_4$ und NaOH-Lösung hydrothermal hergestellt[36]. Zwar konnte Ti^{4+} schon vorher in eine PONb-Struktur integriert werden, allerdings agieren in der Struktur $[Ti_2O_2]^{4+}$ Einheiten nur als verbrückende Baugruppen zwischen den Clustern, so dass diese nicht zu Titanoniobaten gezählt werden.[13][43] Das $[Ti_2Nb_8O_{28}]^{8-}$-Anion lässt sich formal aus dem $\{Nb_{10}O_{28}\}$-Cluster ableiten, in dem die beiden zentralen Nb^V-Positionen durch Ti^{IV} substituiert sind (Abb.7). Obwohl die oktaedrische Koordination für beide Kationen günstig ist, beobachtet man keine Fehlordnung, sondern eine Ausordnung der Kationen. Interessanterweise gilt das nicht nur für Ti-PONbs, sondern auch für einige Schichtperowskite, in denen zumindest eine partielle Ausordnung beobachtet wird; dort befinden sich die $\{NbO_6\}$ Oktaeder eher in den äußeren Slab Sites, während die $\{TiO_6\}$ Oktaeder Plätze geringerer Verzerrung bevorzugen.[36] Auch in dem „Super-Lindqvist"-Clusteranion $[Ti_{12}Nb_6O_{44}]^{10-}$ (Abb. 6) befinden sich die $\{TiO_6\}$ Oktaeder im Zentrum des Clusters und weisen keine terminalen Ti=O-Bindungen auf.[84] Zur Stabilität von $\{Ti_2Nb_8O_{28}\}$ wurden Kraftfeldrechnungen durchgeführt, in denen jedes mögliche Isomer berücksichtigt wurde. Die Ergebnisse belegen, dass die Stabilität mit abnehmender Länge der Nb/Ti-μ_6-O-Bindung zunimmt. Diese Bindung ist am kürzesten, wenn beide Ti^{4+}-Kationen die inneren Positionen besetzen. Da Nb^{5+} größer ist als Ti^{4+}, ist bei dieser Anordnung der Oktaeder die Abstoßung geringer und somit diese Geometrie energetisch am günstigsten.[36]

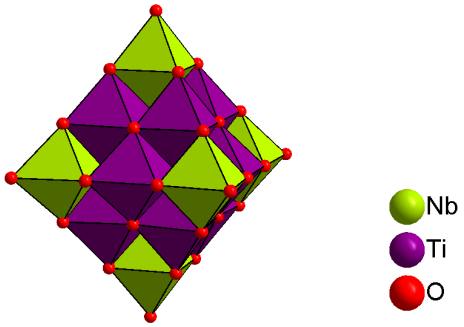

Abb. 6: Struktur des $\{Ti_{12}Nb_6O_{44}\}$-Clusters.

Durch die Synthese des $[TiNb_9O_{28}]^{7-}$-Anions wurde die systematische Reihe der Ti-PONbs vervollständigt und es war möglich, den Einfluss der Substitution auf die Stabilität zu untersuchen. Auch in dieser Struktur besetzt Ti^{IV} die zentralen Positionen, allerdings gemischtbesetzt mit Nb^V.[85]

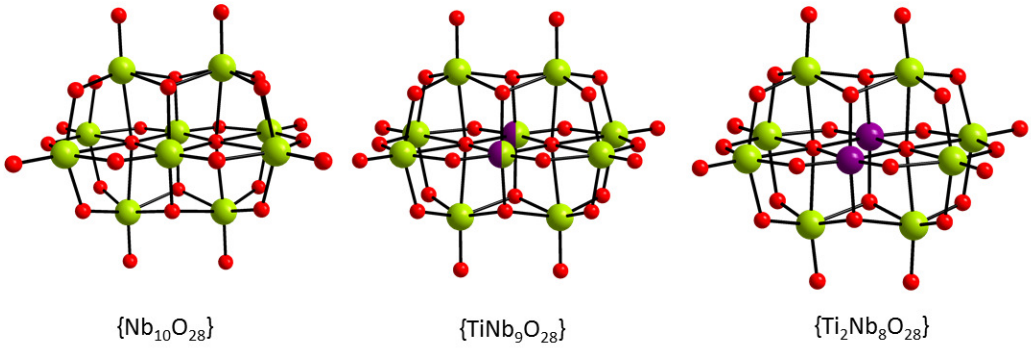

Abb. 7. Der $\{Nb_{10}O_{28}\}$ -Cluster und die durch Substitution erhaltenen Titanoniobate.

Stabilitätsuntersuchungen mit Hilfe von ^{17}O-NMR ergaben aufschlussreiche Ergebnisse. Die Dissoziation des $[Ti_2Nb_8O_{28}]^{8-}$-Anions kann über die Intensität des Signals für die μ_6-verbrückenden O^{2-}-Anionen verfolgt werden. Die Untersuchungen belegten, dass der baseninduzierte Dissoziationspfad von $\{Nb_{10}O_{28}\}$ zu $\{Nb_6O_{19}\}$für das $[Ti_2Nb_8O_{28}]^{8-}$-Anion nicht existiert, d.h. auch im stark alkalischen Milieu wird keine Dissoziation beobachtet. Da in diesem Pfad die Dissoziation von den μ_3-verbrückenden O^{2-}-Anionen hervorgerufen wird, führt die Substitution von Nb^{5+} durch Ti^{4+} dazu, dass die formale Ladung an diesem O^{2-}-Anion abnimmt und der nucleophile Angriff, der die baseninduzierte Dissoziation von $\{Nb_{10}O_{28}\}$ zu $\{Nb_6O_{19}\}$ einleitet[79], unterdrückt wird. Dafür verringert sich leicht die Stabilität der Verbindung bei sauren pH-Werten, so dass bei pH ≤ 5.5 ein amorphes Gel gebildet wird ($\{Nb_{10}O_{28}\}$ detektierbar bis pH 5).[86] Da das $[TiNb_9O_{28}]^{7-}$ -Anion unsymmetrisch substituiert ist und ein μ_3-verbrückendes O^{2-}-Anion durch die Bindung zum Nb^{5+}-Kation weiterhin labil ist, beobachtet man hier wie bei $\{Nb_{10}O_{28}\}$ die Dissoziation zum $\{Nb_6O_{19}\}$-Cluster bei höheren pH-Werten.[86] Allerdings kommt es erst oberhalb von pH = 12 zur Dissoziation ($\{Nb_{10}O_{28}\}$: ab 7.5 langsame Dissoziation) und das Molekül zersetzt sich auch erst unterhalb von pH = 5. Somit kann die Stabilität durch Substitution maßgeblich beeinflusst werden, je nachdem in welchem pH-Bereich z.B. für eine mögliche Anwendung das Anion stabil sein soll.

Analog zu $\{Nb_{10}O_{28}\}$ und $\{Nb_6O_{19}\}$ können Titanoniobat-Cluster in Lösung protoniert vorliegen, sodass die pK_s-Werte bestimmt werden konnten. So nimmt die Säurestärke mit der Substitution von $\{H_xNb_{10}O_{28}\}$ über $\{H_xTiNb_9O_{28}\}$ bis zum $\{H_xTi_2Nb_8O_{28}\}$ ab.[86]

Zusätzlich konnten im Rahmen der ^{17}O-NMR-Untersuchungen neue μ_6-O-Signale bei pH ≤ 7.5 für $\{Ti_2Nb_8O_{28}\}$ und bei pH ≤ 6.0 für $\{TiNb_9O_{28}\}$ detektiert werden, welche im Verhältnis zum μ_6-Signal der beiden bekannten Anionen zu höheren Feldern verschoben sind und auf das Vorhandensein neuer, noch unbekannter Niobat-Spezies hindeuten.[79] Die Titanoniobat-

Chemie ist bisher nur auf die Dekaniobat- und die „Super“-Lindqvist-Geometrie beschränkt und es gibt nur ein Beispiel eines ÜM-substituierten $\{Ti_2Nb_8O_{28}\}$-Clusters[87], so dass mit Sicherheit neue Clustergeometrien erhalten werden können.

1.5 Eigenschaften und mögliche Anwendungen von PONbs

Obwohl auf dem Gebiet der PONbs erst seit etwa 20 Jahren intensiver geforscht wird, gibt es zahlreiche interessante Anwendungen, welche in Tabelle 2 zusammengefasst sind.

Wie alle POMs weisen auch PONbs sehr gute katalytische Eigenschaften auf. Durch deren hohe Basizität eignen sich diese gut für basische Katalyse, wie z.B. bei der Knoevenagel-Kondensation zur Knüpfung von C-C-Doppelbindungen aus CH-aziden Verbindungen und Carbonylen.[88] Im ersten Schritt muss mithilfe eines (basischen) Katalysators die CH-azide Verbindung durch einen Katalysator deprotoniert werden. Für diese Reaktion wurde das $[Nb_{10}O_{28}]^{6-}$-Anion eingesetzt, welches zwar niedrige Ausbeuten der Kupplungsprodukte ergeben hat, doch gegenüber den gängigen Basen entscheidende Vorteile hat. So können auch weniger azide Verbindungen leicht deprotoniert werden. Es gibt zwar auch andere dafür geeignete Katalysatoren ähnlicher Basenstärke, jedoch zersetzen sich diese oft bereits bei geringen Spuren von H_2O und CO_2, so dass sich PONbs wesentlich besser dafür eignen.[89]

PONb-Keggin-Ionen sind im Festkörper häufig durch kationische Einheiten wie $[Nb_2O_2]^{6+}$ oder $[Ti_2O_2]^{4+}$ zu Ketten verknüpft. Zwischen dieses Ketten können sich locker gebundene Alkalimetallkationen und Wassermoleküle einlagern, die z.B. gegen Sr^{2+}-Kationen ausgetauscht werden können. Da flüssige radioaktive Abfälle stark alkalisch sind, bietet die hohe Stabilität der PONbs in diesem pH-Bereich erneut entscheidende Vorteile zur Entfernung von radioaktivem Sr.[90]

Im medizinischen und pharmakologischen Bereich sind POMs generell interessant, da diese antivirale und antitumorale Wirkung zeigen und dabei eine geringe Toxizität aufweisen.[91]

Auch einige Keggin-PONbs wiesen vielversprechende Antitumoreigenschaften auf, beispielsweise gegen Magenkrebszellen und zeigten sogar Selektivität zwischen Tumor- und gesunden Blutzellen.[58]

Tabelle 2: Übersicht über Polyoxoniobate und verschiedene Anwendungen.

Cluster	Anwendung	Lit.
$\{Ni(en)_3\}_5H\{V^{V}Nb_8V^{IV}{}_8O_{44}\}\cdot 9H_2O$ $(H_2en)Na_2[Zn(en)_2(Hen)\}\{Zn(en)_2(H_2O)\}_2\{PNb_8V^{IV}{}_8O_{44}\}]\cdot 11H_2O$ $Na\{Cu(en)_2\}_3\{[Cu(en)_2]_2PNb_8V^{IV}{}_8O_{44}\}\cdot 11H_2O$ $Na_2\{[Cu(en)_2(H_2O)]_4[PNb_{12}O_{40}(V^{IV}O)_{2.5}]\}\cdot 13H_2O$ $K_3Na_2[\{Cu(H_2O)(phen)]_2\}\{CuNb_{11}O_{35}H_4\}\cdot 22H_2O$ $K_4Na[\{Cu(H_2O)(2,2'\text{-bipy})]_2\}\{CuNb_{11}O_{35}H_4\}\cdot 25H_2O$ $\{Cu(en)_2\}_6\{GeNb_{12}V^{IV}{}_2O_{42}\}\cdot 20H_2O$ $\{Cu(en)_2\}_3K_2Na_4\{GeNb_{12}V^{IV}{}_2O_{42}\}\cdot 23H_2O$ $\{Cu(en)_2\}_6\{SiNb_{12}V^{IV}{}_2O_{42}\}\cdot 18H_2O$ $\{Cu(en)_2\}_3K_2Na_4\{SiNb_{12}V^{IV}{}_2O_{42}\}\cdot 19H_2O$	**Antitumor-Aktivität**	[58] [92] [51]
$\{PNb_{12}(VO)_6O_{40}\}$ $\{As_2Nb_4(O_2)_4O_{14}H_{1.5}\}$ $KNa_2[H_{21}Nb_{24}O_{72}]\cdot 38H_2O$ $K_2Na_2[H_{28}Nb_{32}O_{96}]\cdot 80H_2O$ $K_{12}[H_{21}Nb_{24}O_{72}]_4\cdot 107H_2O$ $Na_4[Cu(en)_2(H_2O)_2]_5[Na_6Ge_8Nb_{32}O_{108}H_8(OH)_4]\cdot 41H_2O$ $Na_{12}K_8[Co_{14}(OH)_{16}(H_2O)_8Nb_{36}O_{106}]\cdot 71H_2O$ $K_{10}[Nb_2O_2(H_2O)_2][SiNb_{12}O_{40}]\cdot 12H_2O$ $[Cu(en)_2]_{11}K_4Na_2[KNb_{24}O_{72}H_9]_2\cdot 120H_2O$ $TMA_5[H_2TeNb_5O_{19}]\cdot 20H_2O$ $(TMA)_6[H_2Cr^{III}Nb_9O_{28}]\cdot 14H_2O$ $(TMA)_8[Mn^{III}Nb_9O_{28}]\cdot 29H_2O$ $(TMA)_7[H_2Co^{III}Nb_9O_{28}]\cdot 25H_2O$ $[Na(H_2en)_5][VNb_{14}O_{42}(NO_3)_2]\cdot 12H_2O$ $[K_7Na_4][VNb_{14}O_{42}(NO_3)_2]\cdot 31H_2O$ $[Co(1,2\text{-dap})_2]_4[HPV_6Nb_{10}O_{44}]\cdot 17H_2O$ $[Co(1,2\text{-dap})_2]_5[PV_6Nb_{12}O_{46}](OH)_7\cdot 15H_2O$ $K_{10}[(Nb_6O_{19})Cr^{III}(H_2O)_2]_2\cdot 28H_2O$ $K_5[H_2AgNb_6O_{19}]\cdot 11H_2O$ $Na_{18}[V_8Nb_{48}(OH)_{30}O_{130}]\cdot 33H_2O$ CdS-$[Nb_6O_{19}]$-Nanokomposit	**Photokat. H_2-Entwicklung**	[60] [93] [24] [94] [95] [96] [30] [97] [98] [55] [39] [99] [100] [25] [101]
$\{Nb_{10}V_4O_{40}(OH)_2\}$ $\{PNb_{12}(VO)_6O_{40}\}$ $\{(GeOH)_2Ge_2Nb_{16}O_{54}\}$ $\{K(GeOH)_2Ge_2Nb_{16}H_3O_{54}\}$ $[Ni(2,2'\text{-bipy})_2]_3[Nb_{10}O_{28}]\cdot 2H_2O$ $[M(phen)_3]\{[Ni(phen)_2]_2[Nb_{10}O_{28}]\}\cdot 8H_2O$ (M=Ni, Co, Zn) $[Cu(en)_2]_2\{[Cu(1,10\text{-phen})][Cu(1,10\text{-phen})(H_2O)]Nb_6O_{19}\}\cdot 10.5H_2O$ $[Cu(en)_2]_2\{[Cu(2,2'\text{-bipy})][Cu(2,2'\text{-bipy})(H_2O)]Nb_6O_{19}\}\cdot 9H_2O$ $[Cu(en)_2][Cu(en)_2(H_2O)_2]_3[Ti_2Nb_8O_{28}]\cdot 8H_2O$ $Na_6K_{10}[Cu(en)_2]_4[Ln_{12}W_{12}O_{36}(H_2O)_{24}(H_3Nb_6O_{19})_{12}]\cdot 15en\cdot 18H_2O$ $(CN_3H_6)_7K_3H_{17}\{Eu_3(H_2O)_9Nb_{48}O_{138}(H_2O)_6\}\cdot 40H_2O$ $K_7H[Nb_6O_{19}]$ $K_6[Nb_{10}O_{28}]$ $K_8[Ti_2Nb_8O_{28}]$ $[K_{14}H_2Si_4Nb_{16}O_{56}]$	**Lumineszenz**	[102] [60] [103] [83] [104] [87] [31] [32] [105]
$[Na(H_2en)_5][VNb_{14}O_{42}(NO_3)_2]\cdot 12H_2O$ $[K_7Na_4][VNb_{14}O_{42}(NO_3)_2]\cdot 31H_2O$ $[Cu(1,2\text{-dap})_2]_4[AsNb_{12}O_{40}(VO)_4]\cdot(OH)\cdot 7H_2O$ $[\{Co^{II}(1,2\text{-dap})_3]_4[PNb_{12}O_{40}\}(V^{IV}O)_6][OH]_5\cdot 20H_2O$	**Wasseradsorption**	[55] [57] [61]

$Cs_2K_{10}[Nb_6O_{19}\{Pt(OH)_2\}]_2 \cdot 13H_2O$ $K_7H[Nb_6O_{19}]$ $K_6[Nb_{10}O_{28}]$ $K_8[Ti_2Nb_8O_{28}]$ $[K_{14}H_2Si_4Nb_{16}O_{56}]$ $Na_4[trans\text{-}\{Cp^*Ir\}_2Nb_6O_{19}] \cdot 22H_2O$	**Elektrokatalytische Wasserspaltung**	[106] [105] [107]
$[Cu(en)_2(H_2O)][Cu(en)_2]_4\{AsNb_9V_7O_{44}\} \cdot 8H_2O$ $[Cu(en)_2(H_2O)][Cu(en)_2]_4H\{AsNb_8V_8O_{44}\} \cdot 11H_2O$ $K_6H_3[Nb_2K(H_2O)_4(A\text{-}\alpha\text{-}SiW_9O_{34})_2] \cdot 23H_2O$ $K_4[\{Cu(en)_2(H_2O)\}_4\{Cu(en)_2\}\{H_2Te_2Nb_{24}O_{72}\}] \cdot 8H_2O$ $[Na_6(H_2O)_{13}][Li(H_2O)_2][H(Nb_6O_{19})]$ CdS-$[Nb_6O_{19}]$-Nanokomposit	**Photokatalytische Farbstoffdegradation**	[59] [108] [109] [110] [101]
$TMA_5[HNb_4P_2O_{14}(O_2)_4] \cdot 9H_2O$ $TMA_3[H_7Nb_6P_4O_{24}(O_2)_6] \cdot 7H_2O$ $[(CH_3)_4N]_5[H_3Nb_6O_{19}] \cdot 20H_2O$	**Abscheidung dünner Filme**	[111] [54]
$H[Cu(en)_2(H_2O)]_8[Cu(en)_2(H_2O)_2]_2\{K_4[Cu(en)_2]_2$ $[Cu(en)_2(GeNb_{18}O_{54})]_2\}[Nb_3W_3O_{19}] \cdot 32H_2O$	**Protonenleitung**	[112]
$[Cu(en)_2]_4[Cu(en)_2(H_2O)_2][P^{IV}V^{V}Nb_{12}O_{42}](OH)_2 \cdot 11H_2O$ $[Co(en)_3]_2[Co(en)_2(H_2O)_2]_{0.5}[H_{2.5}P^{IV}V^{V}Nb_{12}O_{42}] \cdot 20H_2O$	**Oxidation von Alkanen**	[113]
$Na_8\{Ni[Ni(en)_2Nb_{10}O_{32}\} \cdot 28H_2O$	**Epoxidierung von Alkoholen**	[114]
$H_2Li_5Na_5K_5[Cu(en)_2]_7[Nb_{47}O_{128}(OH)_6(CO_3)_2] \cdot 20H_2O$ $Li_8[Nb_6O_{19}]$ $K_8[Nb_6O_{19}]$ $Cs_8[Nb_6O_{19}]$ $K_{12}[Ti_2O_2][GeNb_{12}O_{40}] \cdot 19H_2O$	**Zersetzung von Kampfstoffen**	[33] [115] [116]
$Na_{12}[Ti_2O_2][GeNb_{12}O_{40}] \cdot xH_2O$ $Na_{12}[Ti_2O_2][SiNb_{12}O_{40}] \cdot xH_2O$ $Na_{10}[Nb_2O_2][SiNb_{12}O_{40}] \cdot xH_2O$ $Na_{10}[Nb_2O_2][GeNb_{12}O_{40}] \cdot xH_2O$	**Selektiver Ionenaustausch von Na+ gegen Cd^{2+}, Sr^{2+}, U^{4+} und NpO_2^+**	[90]
$(TMA)_6[Nb_{10}O_{28}] \cdot 6H_2O$	**Basische Katalysatoren für Knoevenagel und Claisen-Schmidt-Kondensation**	[89]
C_3N_4-$[Nb_6O_{19}]$-Nanokomposit	**Adsorption von Farbstoffen**	[117]
$(TMA)_6[Nb_{10}O_{28}]$	**Enzyminhibition**	[118] [119]

Einige Keggin-PONbs wiesen vielversprechende Antitumoreigenschaften auf, beispielsweise gegen Magenkrebszellen und zeigten sogar Selektivität zwischen Tumor- und gesunden Blutzellen.[58]

1.6 Besondere Eigenschaften von Komplexen mit makrozyklischen Aminmolekülen

Bei ÜM-Komplex-substituierten PONbs kommen Kupfer-Amin-Komplexe am häufigsten vor. Dies wird oft auf die flexible Koordinationsgeometrie des Cu^{2+}-Kations durch den Jahn-Teller-Effekt zurückgeführt. Werden ein-, zwei- oder dreizähnige Liganden verwendet, so können annähernd sphärische, koordinativ abgesättigte Cu-Komplexe wie z.B. $[Cu(2,2´\text{-bipy})_3]^{2+}$ gebildet werden. Durch die ebenfalls annähernd sphärische Geometrie der POM-

Anionen entstehen Hohlräume, welche mit Lösungsmittel-Molekülen oder Kationen besetzt werden.[120] Der Einsatz von solchen Cu-Komplexen erschwert eine Ausordnung der Bausteine und erhöht somit die Wahrscheinlichkeit von Fehlordnungen in POM-Festkörperstrukturen. Dieses kann verhindert werden, indem durch die Wahl des komplexierenden Aminmoleküls die Koordinationssphäre nicht abgesättigt wird und folglich freie Koordinationsstellen vorhanden sind, über welche eine Wechselwirkung mit den O^{2-}-Anionen der POM-Cluster möglich ist. In der vorliegenden Arbeit ist dies durch den Einsatz eines tetradentaten makrozyklischen Aminmoleküls 1,4,8,11-Tetraazacyclotetradekan (cyclam) (Abb. 8) nicht nur mit Cu^{2+}, sondern auch mit Ni^{2+} als Zentralion gelungen.

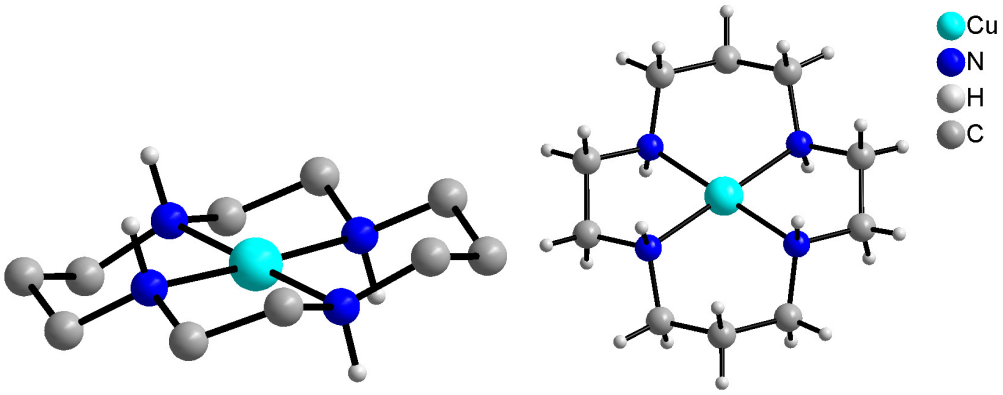

Abb. 8 : Der $[Cu(cyclam)]^{2+}$-Komplex. Das häufigste Diastereomer, das *trans*-III-Isomer ist dargestellt.

Über die Synthese von Cyclam wurde zum ersten Mal von J. v. Alphen 1937 berichtet[121] und der Kurzname entstand durch die Abkürzung für „**cycl**ic tetra**am**ine“. Es existieren fünf mögliche Diastereomere der *cis*- und der *trans*-Form, von denen das *trans*-III- bzw. R,R,S,S-Diastereomer am häufigsten beobachtet wird (Abb.8, rechts).[122] Wie sich später herausstellte, enthielt das Produkt von v. Alphens Synthese, die auf der Umsetzung von 1,3-Dibromopropan und 1,2-Bis(2´-aminoethyl)propan in Gegenwart von Natrium basierte, nur geringe Mengen des Zielmoleküls.[123] Die alternativ dazu vorgeschlagene Syntheseroute lieferte zwar ein phasenreines Produkt, doch mit einer wesentlich zeitaufwändigeren Methode. Die absoluten Ausbeuten sind gering, da die Synthese in stark verdünnten Lösungen durchgeführt werden muss, um Polymerisationsreaktionen zu vermeiden.[124] Eine sehr effektive und günstige Methode basiert auf dem Einsatz eines Ni^{2+} Komplexes mit N,N´-Bis(3-aminopropyl)ethylendiamin als Ligand, welcher als Templat agiert. Die Zyklisierung dieses linearen Liganden erfolgt mithilfe von Glyoxal über eine Schiff´sche Base, deren Doppelbindungen anschließend hydriert werden. Das Produkt ist der $[Ni(cyclam)]^{2+}$-Komplex, aus welchem das Ni^{2+}-Kation mit kochender NaCN-Lösung entfernt werden kann.[125]

Schon früh wurde die besondere Stabilität von Cyclam im Vergleich zu anderen makrozyklischen Aminen festgestellt. Cyclam ist die einzige Verbindung der mindestens 12-gliedrigen makrozyklischen Tetraamine, welche nicht hygroskopisch und bei Raumtemperatur flüssig ist, sondern in Form farbloser Nadeln als Feststoff kristallisiert und erst bei T > 180 °C schmilzt.[123] Durch Aufklärung von Kristallstrukturen konnte die besondere Stabilität durch die Ausbildung intramolekularer Wasserstoffbrücken zwischen den freien Elektronenpaaren der Stickstoffatome und den N-H- Protonen erklärt werden.[124]

Auch die Bildungsenthalpien verschiedengliedriger Makrozyklen erreichen ein Minimum bei den 14-gliedrigen Ringen, was sich u.a. durch die Geometrie des Moleküls erklären lässt. Das Viereck, welches über die vier Stickstoffatome aufgespannt ist, ist sehr symmetrisch mit nahezu 90° Winkeln, was eine Orbitalüberlappung des einsamen Elektronenpaars der Stickstoffatome mit dem leeren d_{x2-y2} Orbital eines Übergangsmetallkations begünstigt und zur Ausbildung außergewöhnlich stabiler Komplexe führt. Anzumerken ist, dass dieser Vorteil nur beim Cyclam und nicht z.B. beim Isocyclam (C2 und C3-Ketten sind jeweils benachbart) auftritt, was sich auch in den Komplexstabilitäten widerspiegelt. Komplexe mit Cyclam sind sowohl kinetisch als auch thermodynamisch stabil und zersetzen sich weder in stark basischen noch in sauren Lösungen.

Erwähnenswert ist noch, dass durch Komplexierung mit Cyclam auch d-Metallionen in ungewöhnlichen Oxidationsstufen stabilisiert werden können, wie z.B. Cu^{3+}, Ag^{2+}, Ag^{3+} und Hg^{3+}. Für die Stabilisierung dieser Oxidationsstufen ist es keine hinreichende Bedingung, ein cyclisches Molekül einzusetzen, und es lassen sich wieder die höchsten Stabilitäten bei dem 14-gliedrigen Molekül cyclam feststellen.[124]

1.7 Ziel und Motivation

Die Chemie der PONbs ist, wie oben diskutiert, recht gut entwickelt. Im Vergleich zu Polyoxometallaten mit Mo, W oder V ist die strukturelle Vielfalt deutlich geringer und die Bildung von PONbs ist deutlich weniger gut verstanden als für andere POMs. Die Ziele der vorliegenden Arbeit waren die Synthese und Charakterisierung neuer Isopolyoxo- und Heteropolyoxoniobate unter Verwendung des Precursors $K_7HNb_6O_{19}$. Als ladungskompensierende Spezies sollten Komplexe makrozyklischer Aminmoleküle verwendet werden, da diese eine außergewöhnlich hohe Stabilität aufweisen und vakante Stellen für mögliche Bindungsbildung mit den anionischen PONbs aufweisen.

Die Synthese neuer PONbs ist sehr herausfordernd, da deren Bildung von sehr vielen voneinander abhängigen Reaktionsparametern abhängt und deren Einfluss auf die Produktbildung nur wenig verstanden ist. Im Gegensatz zu anderen POMs stehen nur wenige Edukte zur Verfügung, welche bereits einen PONb-Cluster enthalten. Da $\{Nb_6O_{19}\}$ in wässrigen Lösungen bei Raumtemperatur thermodynamisch am stabilsten ist, können Cluster mit anderen Zusammensetzungen nur hydrothermal synthetisiert werden. Diese Synthesemethode muss als explorativ angesehen werden, da eine Produktvorhersage nicht möglich ist. Oft sind die Ausbeuten gering und es werden Produktgemische erhalten. Dies kann weitgehend vermieden werden, wenn die Reaktionsmischung während des Heizens gerührt wird, was als „dynamische“ Synthese bezeichnet wird. Allerdings muss immer überprüft werden, ob die unter statischen Bedingungen hergestellten Verbindungen auch unter dynamischen Bedingungen zugänglich sind. Viele Verbindungen enthalten größere Mengen an Kristallwasser und daher war die Untersuchung, ob diese reversibel entfernt und wieder aufgenommen werden kann, ein wesentlicher Bestandteil der experimentellen Arbeiten. Durch die gezielte Entfernung des Kristallwassers können eventuell neue Verbindungen erhalten werden, welche mit den gängigen Synthesetechniken nicht zugänglich sind.

2. Experimentalteil

2.1 Verwendete Chemikalien

In Tab. 3 sind die in der Doktorarbeit verwendeten Chemikalien aufgeführt.

Tab. 3: Übersicht über Reinheit und Hersteller der verwendeten Chemikalien.

Name	Summenformel	Reinheit	Hersteller
1,4,8,11-Tetraazacyclotetradekan	$C_{10}H_{24}N_4$	>98 %	Alfa Aesar
Ethanol	C_2H_5OH	99.9 %	Walter-CMP
Kalium-bis(oxalato)oxotitanat(IV)-Monohydrat	$K_2TiO(C_2O_4)_2 \cdot H_2O$	90 %	Sigma-Aldrich
Kaliumhydroxid Plättchen	KOH	85 %	Abcr
Kaliumhydroxid 1M	KOH		Merck
Kupfer(II)nitrat-Trihydrat	$Cu(NO_3)_2 \cdot 3H_2O$	>99 %	Merck
Kupfer(II)sulfat-Pentahydrat	$CuSO_4 \cdot 5H_2O$	99 %	Gruessing
Natriumhydrogencarbonat	$NaHCO_3$	99 %	Gruessing
Nickel(II)nitrat-Hexahydrat	$Ni(NO_3)_2 \cdot 6H_2O$	>99 %	Merck
Salzsäure	HCl	37 %	VWR
Niob(V)oxid	Nb_2O_5	99.5 %	Abcr
Tetraisopropylorthotitanat	$Ti(O^iPr)_4$	>98 %	Merck

2.2 Verwendete Charakterisierungsmethoden und Geräte

Die Charakterisierung der Reaktionsprodukte erfolgte mit Hilfe der Röntgenpulverdiffraktometrie, Einkristallstrukturanalyse, Elektronenmikroskopie gekoppelt mit energiedispersiver Röntgenanalyse (EDX), thermischen Analysemethoden (Thermogravimetrie gekoppelt mit Differenzthermoanalyse, DTA-TG), Elementaranalyse sowie spektroskopischen Methoden (IR- und UV/Vis-Spektroskopie). Einzelne Proben wurden zusätzlich mit Differenzial-Thermoanalyse (DSC) und H_2O-Sorptionsmessungen untersucht.

Hier soll auf die Funktionsprinzipien der analytischen Methoden nicht weiter eingegangen werden, da es sich dabei um gängige Methoden der anorganischen Chemie handelt. Die verwendeten Geräte sind in Tabelle 4 aufgeführt.

Tab. 4: Übersicht über verwendete Geräte.

Methode	Gerät, Hersteller	Gerätemerkmale
Pulverdiffraktometrie	Stadi-P, Stoe	Cu-Kα_1 (λ=1.5406 Å) Transmissionsgeometrie Ge-Monochromator Mythen 1K-Detektor
IR-Spektroskopie	1.Vertex70 FT-IR-Spektrometer, Bruker 2.Alpha-P ATR-IR-Spektrometer, Bruker	1. RT-DLaTGS-Detektor Platinum-ATR-Einheit mit Diamantkristall Auflösung: 3 cm^{-1} 2. Auflösung: 4 cm^{-1} 4000-375 cm^{-1}
Diffuse Reflektanz	Cary 5 UV-Vis Zweikanal- Spektrometer, Carian Techtron Pty.	2000-20 cm-1; Referenz: $BaSO_4$ Auflösung: 3 cm^{-1}
Differenz-Thermoanalyse gekoppelt mit Thermogravimetrie (DTA-TG)	Sta 409 CD, Netzsch	Heizrate: 4K/min N_2-Fluss (75 mL/min) Pt-Pt/Rh Thermoelement
Differenzialthermoanalyse (DSC)	DSC Star System, Mettler-Toledo AG	N_2- und Luftatmosphäre

Einkristallstrukturanalyse	IPDS-2, Stoe	Mo Kα (λ=1.5406 Å) T =170 K
Elementaranalyse	1. Ario MICRO cube Elementaranalysator, Elementar 2. CHNS-O-Elemenaranalysator Euro EA 3000 Series, Euro Vector	1. Pyrolyse bei T= 1200 °C, 2. Pyrolyse bei 1050 °C Detektion mittels GC mit Wärmeleitfähigkeitsdetektor
Energiedispersive Röntgenanalyse und Rasterelektronenmikroskopie (EDX/SEM)	ESEM XL30, Philips	200 000fache Vergrößerung
Wassersorption	Belsorp$_{max}$, BEL JAPAN INC.	T = 303 K

2.3 Synthesetechniken

Die im Rahmen der Doktorarbeit synthetisierten Verbindungen wurden unter hydrothermalen Bedingungen hergestellt. Für einige Synthesen wurden Teflonbehälter (V = 33 mL) als schwimmender Einsatz in Stahlautoklaven verwendet, meistens jedoch wurden die Synthesen in DURAN©-Glasröhrchen (V = 11 mL) mit PTFE-Dichtungen und PBT-Deckeln (T_{max} = 180 °C) durchgeführt. Die festen Edukte wurden in das Reaktionsgefäß eingewogen, anschließend dest. H_2O und andere flüssige Edukte dazugegeben, gut durchmischt und anschließend ggf. der pH-Wert der Lösung mit 1 M KOH oder 1 M HCl eingestellt. Das Tempern erfolgte zum Teil statisch für 24 - 120 h oder mit Rühren durch Verwendung eines Magnetheizrührers für 15 min - 24 h. Die Abkühlung der Reaktionsgefäße unter statischen Bedingungen wurde unkontrolliert durchgeführt. Die Glasröhrchen bei dynamischen Synthesen wurden im Eisbad abgeschreckt. Die festen Produkte wurden entweder mithilfe eines Glasfiltertiegels oder Schwarzbandfilterpapers abfiltriert, mit dest. H_2O gewaschen und an Luft getrocknet. Die Mutterlaugen der dynamischen Synthesen wurden in Schnappdeckelgläser (V = 5 mL) überführt und das Lösungsmittel an Luft langsam verdampft.

Der Vorteil dynamischer Synthesen besteht darin, dass die Reaktanten im Reaktionsmedium homogen verteilt werden und die Synthesezeiten von mehreren Tagen auf Stunden verkürzt werden. Zusätzlich kann die Ausbeute eines Produkts durch die kontinuierliche Durchmischung signifikant verbessert werden. Allerdings können keine Einkristalle erhalten werden, sondern polykristalline Pulver. Falls jedoch das Löslichkeitsprodukt während der Reaktion nicht überschritten wird oder sich in der Lösung noch gelöste Produkte befinden, können durch langsames Verdampfen des Lösungsmittels Einkristalle erhalten werden. Es ist jedoch anzumerken, dass Produkte, welche durch Synthesen unter statischen Bedingungen erhalten werden, nicht zwingend auch dynamisch hergestellt werden können und umgekehrt.

Wie bereits erwähnt ist die Auswahl der Edukte zur Synthese von PONbs limitiert. Niobhaltige Alkoxide zersetzen sich schnell an Luft und erschweren die Reproduzierbarkeit (Vgl. Kap. 1.3). Niob(V)-Oxid und die Hydrate mit der allgemeinen Formel $Nb_2O_5 \cdot xH_2O$ sind äußerst schwer löslich und reaktionsträge. Daher wurde als Niob-Quelle $K_7HNb_6O_{19} \cdot 13H_2O$ als Precursor verwendet. Dieses lässt sich schnell und einfach in hohen Ausbeuten synthetisieren, ist leicht in Wasser löslich und generiert den für die Synthese von PONbs geeigneten pH-Wert von ~12.

Die Darstellung des Precursors $K_7HNb_6O_{19}\cdot 13H_2O$ erfolgte nach einer Vorschrift von Shum *et al*. [126] 26 g (0.4 mol) KOH Plättchen wurden in einem Nickel-Tiegel geschmolzen und 13.3 g (0.05 mol) Nb_2O_5 portionsweise dazugegeben. Die Schmelze wurde für 30 min über der blauen Bunsenbrennerflamme erhitzt und in 100 mL bidest. H_2O gelöst. Feste Bestandteile wie nicht umgesetztes Nb_2O_5 wurden abfiltriert und das Filtrat auf die Hälfte des Volumens eingeengt. Nach dem Auskristallisieren über Nacht wurden farblose Nadeln erhalten, welche mit einer 50/50 Wasser/Ethanol-Mischung gewaschen wurden. Die Ausbeute betrug etwa 14 g (62 %).

3. Veröffentlichungen

3.1 Der Einfluss ausgewählter Reaktionsparameter auf die Bildung [Cu(cyclam)]$^{2+}$-substituierter PONbs und deren thermische Zersetzung

Zusammenfassung der Publikation „Controlling Fast Nucleation and Crystallization of Two New Polyoxoniobates“

Die Reaktion von *in-situ* erzeugten [Cu(cyclam)]$^{2+}$-Kationen mit $K_7HNb_6O_{19}\cdot 13H_2O$ unter hydrothermalen Bedingungen führte in Abhängigkeit vom pH-Wert zur Kristallisation von zwei Verbindungen mit unterschiedlichen Clustergeometrien: $K_5[Cu(H_2O)_2(cyclam)]_{1.5}\{[Cu(cyclam)][Cu(H_2O)(cyclam)]_2\mathbf{HSiNb_{18}O_{54}}\}\cdot 30H_2O$ bei pH > 10.3 und $\{[Cu(cyclam)(H_2O)]_2[Cu(cyclam)][\mathbf{Nb_{10}O_{28}}]\}_n\cdot 9nH_2O$ bei pH < 10.3. In den Strukturen beider Verbindungen sind die Cu^{2+}-Kationen kovalent an die PONb-Anionen gebunden. Durch Rühren des Reaktionsgemisches während der Reaktion konnten die beiden Verbindungen phasenrein und in sehr kurzer Zeit (30 min) erhalten werden. Die Kristallwassermoleküle der Verbindung mit dem $[Nb_{10}O_{28}]^{6-}$-Anion konnten thermisch bis T = 200 °C entfernt werden, wobei eine strukturelle Phasenumwandlung beobachtet wird. Der Verlauf der H_2O-Sorptionskurve der bei 200 °C behandelten Probe deutet ebenfalls auf eine Phasenumwandlung hin. Wird diese Verbindung an Luft bei 600 °C zersetzt, wird die Bildung eines unbekannten nanokristallinen Materials beobachtet.

Reprinted with permission of *Cryst. Growth Des.* **2018**, *7*, 4130-4139. DOI: 10.1021/acs.cgd.8b00548.

CRYSTAL GROWTH & DESIGN

Article

Cite This: Cryst. Growth Des. 2018, 18, 4130−4139

pubs.acs.org/crystal

Controlling Fast Nucleation and Crystallization of Two New Polyoxoniobates

Joanna Dopta, Dana-Céline Krause, Christian Näther, and Wolfgang Bensch*

Institut für Anorganische Chemie, Christian-Albrechts-Universität Kiel, Max-Eyth-Straße 2, D-24118 Kiel, Germany

Supporting Information

ABSTRACT: Applying identical amounts of starting materials allowed the solvothermal preparation of two new polyoxoniobates by controlling the pH value of the reaction mixture. Stirring the slurries afforded crystallization of $K_5[Cu(H_2O)_2(cyclam)]_{1.5}\{[Cu(cyclam)][Cu(H_2O)(cyclam)]_2HSiNb_{18}O_{54}\}(NO_3)\cdot 30H_2O$ (**I**) and $\{[Cu(cyclam)(H_2O)]_2[Cu(cyclam)][Nb_{10}O_{28}]\}_n\cdot 9nH_2O$ (**II**) within short reaction times and in high yields. While compound **I** crystallizes from the mother liquor at room temperature after hydrothermal treatment at pH values >10.3, compound **II** is isolated at pH < 10.3 by filtration, i.e., **II** is formed at the reaction conditions applied. Time-dependent experiments demonstrate that under stirring, pure samples of both compounds can be obtained within 30 min. Syntheses without stirring the educt mixtures leads to very low yields of **I** and crystallization of **II** in comparable yields afforded about 20 h reaction time. In the structure of **I**, the rare $[SiNb_{18}O_{54}]^{14-}$ anion is found, which is surrounded by $[Cu(cyclam)]^{2+}$ complexes and K^+ cations. The water molecules form a very unusual hydrogen bonding pattern which may be classified as a L4(2)4(4)5(4)10(4)16(6)42(14) water cluster. Compound **II** features the decaniobate anion $[Nb_{10}O_{28}]^{6-}$, is obtained after short reaction time in high yields and exhibits a reversible release/uptake of crystal water molecules.

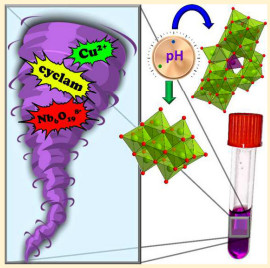

INTRODUCTION

High nuclearity polyoxometalates (POMs) with cluster shells of different shape, charge, and functionality form an outstanding class of materials with enormous structural varieties and applications in various fields like medicine and catalysis.[1−12] While high-nuclearity POM clusters based on Mo or W crystallize in a wide pH range between approximately 0 and 8.5,[13−20] the product formation among group V POMs is more sensitive to changes of pH value.[21−24] In contrast to molybdates and tungstates, where a great variety of precursors like, e.g., $[MoO_4]^{2-}$, $[WO_4]^{2-}$, $\{Mo_7O_{24}\}$, $\{PW_{12}O_{40}\}$, or $\{P_2W_{18}O_{64}\}$ is available, the number of suitable starting materials containing prebuilt cluster shells in the field of polyoxovanadates (POVs) and polyoxoniobates (PONbs) is limited. The usage of heteroatom containing POVs as synthons was recently identified as a promising approach for the generation of new POVs,[23,25] but such preformed compounds do not exist in the field of PONbs.[24,26,27]

The niobium sources for preparation of PONbs are scarce: Nb_2O_5 is practically insoluble in common solvents and only reacts in alkaline melts to form a hexaniobate anion, while niobium alkoxide precursors like, e.g., $Nb(OC_2H_5)_5$ are sensitive to air and moisture.[24,28] The resulting hydrolysis product $Nb_2O_5\cdot xH_2O$[29] can be dissolved in alkali or TMA^+ (tetramethylammonium) hydroxide solutions.[30] Among others, several Keggin ion derivatives like, e.g., $\{XNb_{12}O_{40-44}\}$ (X = Si,[31−34] Ge,[32,33] PV_2,[35] V_3[36] PSb_2,[37] PNb_2[37]) as well as Lindqvist type PONbs $\{H_xNb_6O_{19}\}$[38−41] (x = 0−4) could be crystallized using $Nb_2O_5\cdot xH_2O$ as niobium source.

One of the first PONb cluster geometries different from the prominent Lindqvist ion was the decaniobate anion $[Nb_{10}O_{28}]^{8-}$ (abbreviated as $\{Nb_{10}O_{28}\}$) composed of ten edge-sharing NbO_6 octahedra, which crystallized from an alkaline methanolic solution of niobium ethoxide ($Nb(OC_2H_5)_5$) after 24 h.[42] Due to the low stability of the alkoxide precursor, the syntheses were difficult to be reproduced,[28] but this can be enhanced by employing directly $Nb_2O_5\cdot xH_2O$.[29] The first TM amine complex (TM = transition metal) expanded $\{Nb_{10}O_{28}\}$ cluster was synthesized under hydrothermal conditions applying $K_7HNb_6O_{19}\cdot 13H_2O$.[43] Charge balance was achieved by *in situ* generated $[TM(2,2'\text{-bipy})_2]^{2+}$ complexes (2,2′-bipy = 2,2′-bipyridine; TM = Co^{2+}, Zn^{2+}), which connect the anions via O-TM-O bridges into zigzag chains. With a similar synthesis protocol but at elevated temperatures, two decaniobate compounds of different dimensionalities (0D, 1D) were obtained containing $[Ni(2,2'\text{-bipy})_x]^{2+}$ (x = 2, 3) complexes. In addition, decaniobates were also reported containing $[TM(1,10\text{-phen})_x]^{2+}$ complexes (TM = Ni^{2+}, Co^{2+}, Zn^{2+}; x = 2,3; 1,10-phen = 1,10-phenanthroline).[44]

Hydrothermal treatment of $[Nb_6O_{19}]^{8-}$ salts can also provide an avenue to cluster geometries which are unprecedented in PONb chemistry. In the presence of sodium metasilicate a new cluster geometry was prepared featuring the

Received: April 12, 2018
Revised: May 16, 2018
Published: June 8, 2018

DOI: 10.1021/acs.cgd.8b00548
Cryst. Growth Des. 2018, 18, 4130−4139

C-shaped $[SiNb_{18}O_{54}]^{14-}$ polyanion consisting of two full and two "half" hexaniobate subunits which encapsulate a $[SiO_4]^{4-}$ tetrahedron.[45] The $[SiNb_{18}O_{54}]^{14-}$ polyanion (abbreviated as $\{SiNb_{18}O_{54}\}$) could be isolated by a combination of hydrothermal and solvent diffusion methods. The latter was crucial for the formation of solid products, since clear solutions were obtained after hydrothermal treatments and solvent evaporation led only to gel-like phases. During further solvothermal syntheses, the first $\{SiNb_{18}O_{54}\}$ based inorganic−organic hybrid sample with composition $[Cu(en)_2]_3\{[Cu(en)_2][H_6SiNb_{18}O_{54}]\}\cdot 22H_2O$ (en = ethylenediamine) was synthesized.[46] The polyanion could be also prepared with other main group elements as heteroatoms. Recently, the hydrothermal reaction between $\{Nb_6O_{19}\}$ and a monolacunary $\{GeW_{11}O_{39}\}$ Keggin-type ion led to the formation of $H[Cu(en)_2(H_2O)]_8[Cu(en)_2(H_2O)_2]_2\{K_4[Cu(en)_2]_2[Cu(en)_2(GeNb_{18}O_{54})]_2\}[Nb_3W_3O_{19}]\cdot 32H_2O$, which represents a very interesting structure containing both C-shaped $\{GeNb_{18}O_{54}\}$ and Lindqvist $\{Nb_3W_3O_{19}\}$ moieties.[47]

Although the solvothermal approach is powerful for synthesizing new and fascinating materials, the products cannot be predicted.[48] Most compounds were obtained by a trial-and-error method varying systematically different reaction parameters. Because of their chemical inertness and porous surface which benefits the growth of single crystals, Teflon lined steel autoclaves are widely used. However the usage of this experimental setup prevents visual control of the reaction progress and the reaction slurry cannot be stirred generating concentration gradients often leading to inhomogeneous products.

Applying dynamic hydrothermal conditions in glass tubes the two new compounds $K_5[Cu(H_2O)_2(cyclam)]_{1.5}\{[Cu(cyclam)][Cu(H_2O)(cyclam)]_2HSiNb_{18}O_{54}\}(NO_3)\cdot 30H_2O$ (**I**) and $\{[Cu(cyclam)(H_2O)]_2[Cu(cyclam)][Nb_{10}O_{28}]\}_n\cdot 9nH_2O$ (cyclam = 1,4,8,11-tetraazacyclotetradecane) (**II**) were prepared under identical conditions by adjusting the pH value. The structures are unique because a macrocyclic amine molecule could be successfully integrated in the PONb structure. Compound **I** is a rare example of an organic−inorganic hybrid based on the $[SiNb_{18}O_{54}]^{14-}$ anion and crystallizes after a short reaction time. In addition, compared to other known decaniobates, compound **II** could be obtained reproducibly in high yields within a very short reaction time of only 30 min. Compound **II** can be reversibly dehydrated and rehydrated without significantly affecting the crystallinity. Herein, we report the syntheses and characterizations of the two new compounds featuring two different PONb cores.

EXPERIMENTAL SECTION

Characterization Techniques. X-ray diffraction patterns (XRDP) were recorded with Cu $K\alpha_1$ radiation (λ = 1.540 598 Å, Ge monochromator) on a STOE Stadi-P diffractometer with a Ge monochromator and a Mythen 1K detector. A Bruker Alpha-P IR spectrometer was used for measuring MIR spectra in a range of 4000−400 cm^{-1}. UV/vis diffuse reflectance spectra were collected on an UV/vis two-channel spectrometer Cary 5 from Carian Techtron Pty., Darmstadt, using $BaSO_4$ as white standard. Optical electronic properties were evaluated applying the Kubelka−Munk method.[49] CHN analyses were done with a EURO EA elemental analyzer (EURO VEKTOR). DTA-TG curves were measured under air or nitrogen atmosphere on a Netzsch STA 409 CD with a heating rate of 4 K min^{-1}. DSC curves were recorded on a DSC Star System with STARe Excellence software (Mettler-Toledo AG) under air and nitrogen atmosphere. The calibration of the instruments was done using standard reference materials. Water sorption measurements were performed using a $Belsorp_{max}$ instrument (BEL JAPAN INC.) at 303 K. To remove the crystal water molecules the samples were treated in two different ways prior to the measurements: one sample was placed in an ampule which was evacuated for 12 h at room temperature; the second sample was heated to 200 °C in N_2 atmosphere. Energy dispersive X-ray analyses (EDX) were done on a Philips Environmental Scanning Electron Microscope ESEM XL30 with an EDX detector. For structure determination the intensity data collection for both compounds was performed at 170 K with a STOE Imaging Plate Diffraction System (IPDS-2) with Mo K_α radiation (λ = 0.71073 Å). The structures were solved with SHELXT-97[50] and refined against F^2 using SHELXL-2014.[51] For both compounds, a numerical absorption correction was performed ($T_{min/max}$: 0.5409/0.7507 for **I** and 0.6261/0.7543 for **II**). All non-hydrogen atoms except some water O atoms in **II** were refined anisotropically. The C−H and N−H H atoms were positioned with idealized geometry and refined isotropically with $U_{iso}(H)$ = 1.2 U_{eq}(C,N) using a riding model. In compound **I**, the water H atoms were not located but considered in the calculation of the molecular formula and the molecular weight. In total, 35 H_2O molecules were found. 32 of the oxygen positions are fully occupied, two are half occupied (O96, O98), and two further water O atoms are disordered with an occupancy of 80:20 (O76) and 70:30 (O97). The O−H H atoms in **II** were located in difference Fourier maps, and their bond lengths were set to ideal values and finally they were refined isotropically with $U_{iso}(H)$ = 1.5 U_{eq}(O) using a riding model. After the structure refinement of **II**, some additional residual electron density peaks were observed in the difference Fourier map that indicate the presence of water molecules. Because no reasonable structure model was found, the data were corrected for disordered solvents using the Squeeze option in Platon.[52] The residual number of electrons collected during the Squeeze procedure is 188, corresponding to 5 water molecules per formula unit. The solvent accessible free space calculated with Platon yields ~558 $Å^3$.

CCDC-1835027 (**I**) and CCDC-1835028 (**II**) contain the supplementary crystallographic data for this paper. These data can be obtained free charge from the Cambridge Crystallographic Data Centre via http://www.ccdc.cam.ac.uk/data_request/cif.

Syntheses. General: All chemicals except $K_7HNb_6O_{19}\cdot 13H_2O$ were purchased (Nb_2O_5: abcr, 99.5% Nb; $Cu(NO_3)_2\cdot 3H_2O$: Merck, >99%, 1,4,8,11-tetraazacyclotetradecane: Alfa Aesar, >98%, KOH, 85%: abcr, HCl, 37%: VWR) and were used without further purification. $K_7HNb_6O_{19}\cdot 13H_2O$ was synthesized applying a literature method.[53] The pH was adjusted with aqueous solutions of 1 M KOH or 1 M HCl. Unless otherwise mentioned, the reactions were carried out under hydrothermal conditions with stirring of the slurries (magnetic stirrer) in DURAN glass tubes with an inner volume of 11 mL. To interrupt the reaction, the mixtures were quenched in ice-cold water after distinct time intervals of 30 min, 1 h, 2 h, etc. Subsequently, the solutions were filtered, transferred into straight glass tubes and the solvent was left to evaporate at room temperature. For comparison, some reactions were carried out without stirring in Teflon-lined steel autoclaves (inner volume: 30 mL) and the resulting solids were washed with water after separation by filtration.

$K_5[Cu(H_2O)_2(cyclam)]_{1.5}\{[Cu(cyclam)][Cu(H_2O)(cyclam)]_2HSiNb_{18}O_{54}\}(NO_3)\cdot 30H_2O$ (I). 0.2 mmol $K_7HNb_6O_{19}\cdot 13H_2O$, 0.4 mmol $Cu(NO_3)_2\cdot 3H_2O$, and 0.4 mmol 1,4,8,11-tetraazacyclotetradecane (cyclam) were dispersed in 3 mL H_2O (pH = 12.3). The reaction mixture was kept under stirring at T = 130 °C for 3 h. The clear violet solution was transferred into a glass tube and after slow evaporation of the mother liquor violet block shaped crystals were obtained. Yield: 26 mg (6.4% based on Nb). $C_{90}H_{358}N_{38}K_{10}Cu_9Si_2Nb_{36}O_{184}$: calcd. in %: C 11.65, H 3.89, N 5.73; found C 11.48, H 3.47, N 5.33.

$\{[Cu(cyclam)(H_2O)]_2[Cu(cyclam)][Nb_{10}O_{28}]\}_n\cdot 9nH_2O$ (II). *Method 1*: The same synthetic procedure was performed as for **I** but the pH was adjusted with 1 M aqueous HCl to <10.4. During the reaction, a violet powder was formed. The microcrystalline solid product was recovered by filtration and was identified by PXRD as

DOI: 10.1021/acs.cgd.8b00548
Cryst. Growth Des. 2018, 18, 4130−4139

compound **II**. Yield: 72 mg at pH = 10.3 (26% based on Nb). *Method 2:* Identical mixtures as in *method 1* were reacted in a Teflon-lined steel autoclave with an inner volume of 30 mL under static hydrothermal conditions. After 20 h at 130 °C, violet needles of **II** suitable for single crystal structure analysis were obtained. Yield: 120 mg (44% based on Nb). $Cu_3C_{30}H_{94}N_{12}Nb_{10}O_{39}$: calcd. in %: C 15.22, H 4.00, N 7.10; found C 15.24, H 3.96, N 7.05.

RESULTS AND DISCUSSION

Synthetic Aspects. To the best of our knowledge, all literature-known PONbs synthesized via the hydrothermal route were obtained in Teflon-lined autoclaves. An interesting question is whether these materials crystallize before cooling the reactor and whether any intermediates are formed.[24,48] Beyond the lack of visual control, there are good reasons to replace the Teflon liners as containers for hydrothermal syntheses. Due to the porous surface, Teflon can take up small ions or molecules, which are difficult to remove and which may be released during the synthesis, impeding the reproducibility of the experiments. This is a disadvantage in particular for the preparation of PONbs, because their formation is very sensitive to changes of the reaction conditions.[54] Due to the possibility of visual control during the reaction, we used glass reactors, and indeed, we observed the formation of one of the compounds presented here already during solvothermal treatment.

Stirring the reaction mixture ("dynamic" conditions) leads to a homogeneous distribution of dissolved species and often phase pure products are formed. Under static conditions, single crystals are often obtained despite the unwanted concentration gradient in the slurry. We want to note that products of a dynamic reaction are not necessarily identical with those obtained from identical reaction mixtures without stirring.[55]

We applied $K_7HNb_6O_{19}{\cdot}13H_2O$ which is soluble in water and generates a pH value beneficial for formation of PONbs (pH ≈ 12). The *in situ* generated $[Cu(cyclam)]^{2+}$ complex cation was used because of the high stability[56] and the two vacant coordination sites which may lead to bond formation to O^{2-} anions of the PONb cluster.

For the synthesis of **I**, $K_7HNb_6O_{19}{\cdot}13H_2O$, $Cu(NO)_3{\cdot}3H_2O$ and cyclam were dissolved in water yielding a clear solution (Scheme 1) with a pH of ∼12.3. After 3 h, the solution was filtered, whereby no solid products were obtained. Slow evaporation of the mother liquor at room temperature to approximately 0.5 mL yielded $K_5[Cu(H_2O)_2(cyclam)]_{1.5}\{[Cu(cyclam)][Cu(H_2O)(cyclam)]_2HSiNb_{18}O_{54}\}(NO_3){\cdot}30H_2O$ (**I**) as violet block-shaped single crystals. Phase purity was confirmed by XRDP (Figure S1).

Time dependent syntheses demonstrated that the yield increased with extension of the reaction time. Even after 30 min of reaction time, enough material crystallized from the mother liquor for XRDP characterization demonstrating phase purity of the product. The maximum yield could be obtained after 14 h (∼43%). In further experiments, the influence of the pH value onto product formation was investigated applying dynamic conditions. Prior to heating, the pH value of the reaction slurry was set between 8.3 and 10.3, whereby the formation of light violet colored precipitates was observed. By reacting the mixtures at 130 °C, the new compound $\{[Cu(cyclam)(H_2O)]_2[Cu(cyclam)][Nb_{10}O_{28}]\}_n{\cdot}9nH_2O$ (**II**) was obtained as microcrystalline violet powder. In contrast to **I**, the formation of **II** could be optically observed during the reaction and the solid product that was recovered directly after

Scheme 1. Schematic Representation of the Syntheses of Compounds I and II

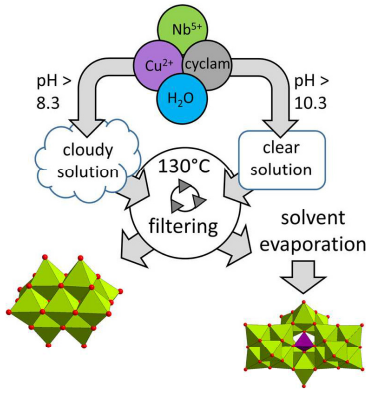

filtration was identified as **II** by XRDP (Figure S2). Evaporation of the mother liquor at room temperature did not afford further crystalline products. The yield was ∼70% (pH = 8.7) after 30 min of reaction time, while no significant increase of the yield could be observed by extending the time (after 3 h: 77%). If the slurry is not stirred, the yield of **II** is reduced to ∼2% based on Nb after 30 min. This observation indicates that stirring achieves a more homogeneous distribution of the reactants in solution. Interestingly, the yield of **II** decreases with increasing pH (∼48% at pH = 9.5; ∼26% at pH = 10.3 for a reaction time of 3 h). This is in full accordance with reaction dynamics studies of aqueous solutions of $[Nb_{10}O_{28}]^{6-}$, where ^{17}O NMR experiments in combination with ESI-MS revealed an increasing dissociation rate of decaniobate ions forming hexaniobate anions with increasing pH.[57]

Single crystal structure determination and EDX analysis of **I** clearly evidenced the presence of Si^{4+} ions, although no silicon source was employed in the reaction slurry. Hence, it must be assumed that alkaline pH leads to dissolution of silica from the glass tube. By repeating the synthesis in a Teflon-lined steel autoclave employing sodium metasilicate ($Na_2SiO_3{\cdot}3H_2O$) for 24 h at the same pH value of 12.3 without altering the remaining reaction parameters, compound **I** could also be obtained but in a very low yield. Therefore, we assume that the slow release of the silica species in the glass vessel benefits the crystallization of **I**. The incorporation of ions not supplied in the reaction slurry is not unprecedented and examples are $K_{14}NaGaNb_{18}O_{54}]{\cdot}31H_2O$[58] or in $K_{14}Na_6[II_4Ni_{10}(II_2O)_8Nb_{32}O_{102}]{\cdot}73II_2O$,[59] which were synthesized without Na^+ cation supply, or $K_{19}Na_4[H_{10}Nb_{31}O_{93}(CO_3)]{\cdot}35H_2O$, which was formed by uptake of CO_2 from the atmosphere.[54]

The study presented here validates the charge-density rule, which states that PONbs with higher charge densities are stable in a more alkaline pH regime.[24,58] The charge density is defined as the ratio between the charge of the anion and the number of non-hydrogen atoms.

According to this, **I** has a charge density of (13/73) = 0.178 and **II** (6/38) = 0.16. Because compound **I** was obtained at higher pH value, the system presented here follows this rule.

DOI: 10.1021/acs.cgd.8b00548
Cryst. Growth Des. 2018, 18, 4130−4139

Further prominent examples for the rule is the presence of $[Nb_6O_{19}]^{8-}$ at higher and $[Nb_{10}O_{28}]^{6-}$ at lower pH values (charge-densities: 0.32 and 0.16, respectively).[27,57]

Crystal Structures. $K_5[Cu(H_2O)_2(cyclam)]_{1.5}\{[Cu(cyclam)][Cu(H_2O)(cyclam)]_2HSiNb_{18}O_{54}\}(NO_3)\cdot 30H_2O$ (**I**) crystallizes in the triclinic space group *P*1 with one formula unit per unit cell with all atoms except one Cu^{2+} cation being located on general positions. Details of structure determination and refinement results are summarized in Table S1. The central structural motif consists of a $\{HSiNb_{18}O_{54}\}$ PONb cluster with three Cu^{2+} centered complexes attached covalently via terminal O atoms. The cluster shell (Figure 1) contains two

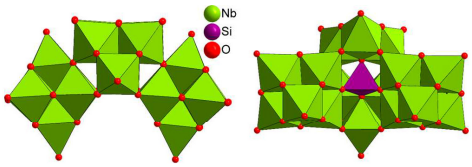

Figure 1. Different views on $\{HSiNb_{18}O_{54}\}$ PONb cluster; Green: NbO_6 octahedra; purple: SiO_4 tetrahedra. Attached Cu^{2+} centered complexes are not displayed.

Lindqvist $\{Nb_6O_{19}\}$ structural units, two "half" Lindqvist groups $\{Nb_3O_{19}\}$ and a SiO_4 tetrahedron, which is connected by corner-sharing. Alternatively, the $\{Nb_3O_{19}\}$ triads and the SiO_4 tetrahedron may be viewed as a $\{SiNb_3O_{26}\}$ Keggin fragment, connected to two Lindqvist units via corner sharing.

In the $\{HSiNb_{18}O_{54}\}$ cluster, five different types of oxygen atoms can be identified: terminal Nb=O_t, Nb-μ_2-O, Si/Nb-μ_3-O, Si/Nb-μ_4-O, and Nb-μ_6-O bridging atoms. The corresponding bond lengths are 1.739(5)−1.770(5) Å, 1.811(5)−2.076(5) Å, 1.639(4)−2.235(4) Å, 1.626(4)−2.491(4) Å, and 2.209(4)−2.546(4) Å, respectively (Table S2) and match well with values reported for $\{SiNb_{18}O_{54}\}$ containing compounds.[45,46]

Bond valence sum calculations (BVS) yield an oxidation state of +5 for Nb with values ranging from 5.11 to 5.27 (average: 5.13, Table S3). The value for Si of 4.73 indicates an "over bonded" Si^{4+} ion, but the Si−O distances of 1.626(4)−1.650(4) Å are in good agreement with those reported for other Si-PONbs.[31,60] Charge balance requires that the anion is monoprotonated. BVS calculations (Table S3) for O^{2-} anions provided values of 1.34−1.72 (average: 1.60) for terminal, 1.68−2.16 (average: 1.88) for μ_2-O, and 1.93−2.09 (average: 1.99) for μ_3-O atoms, suggesting that most likely the proton is either located on O14 (BVS: 1.35) or delocalized over terminal O atoms.

The five crystallographically independent Cu^{2+} cations in the structure of **I** are coordinated by cyclam molecules and O atoms (Figure 2).

Two Cu^{2+} cations (Cu1/Cu3) are in an octahedral environment of four N atoms of the ligand, one O atom of a H_2O molecule, and one terminal O atom of the cluster anion (Figure 2a,b). Cu4 has bonds to the N atoms of one cyclam molecule and a terminal O atom of the anion yielding a distorted square pyramidal environment (Figure 2c), while Cu2 and Cu5 are surrounded by one cyclam ligand and two H_2O molecules generating distorted octahedra (Figure 2d,e). Cu4 has an O^{2-} anion of an adjacent cluster anion at 3.031(6) Å, but this distance is longer than the sum of the van der Waals radii (2.92 Å[61]). The Cu−N bond lengths for all complexes scatter between 1.995(8) and 2.034(6) Å with N−Cu−N cis-angles between 85.1(3)° and 94.9(3)° and trans-angles of 173.8(3)−180.0° (Table S4), in agreement with reported values.[62−65] The Cu−Ow (w = water) bonds are in the range of 2.451(8)−2.648(6) Å and the latter is slightly longer than those reported for isolated copper cyclam complexes with aqua ligands with distances up to 2.531(2) Å.[63,65−69] The Cu−O bonds to terminal O^{2-} anions of the cluster are between

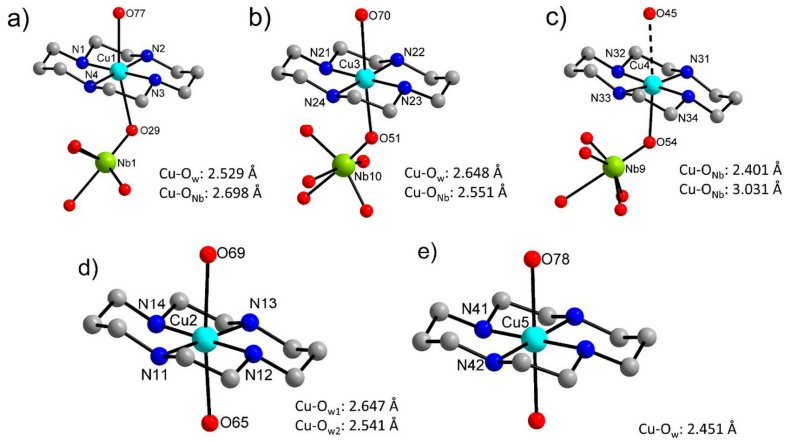

Figure 2. a−e. View of the different coordination environments of the Cu^{2+} cations in the $[Cu(cyclam)]^{2+}$ complexes in **I** (O_W: water oxygen atoms, O_{Nb}: terminal cluster oxygen atoms). H atoms are omitted for clarity. Besides the N atoms of the cyclam ligands in the equatorial plane, the octahedra are completed either by O atoms of water molecules (O_W) or both water O atoms and terminal O atoms of the cluster (O_{Nb}). The long Cu−O distance is shown in dashed lines.

DOI: 10.1021/acs.cgd.8b00548
Cryst. Growth Des. 2018, 18, 4130−4139

2.401(6) and 2.698(4) Å. Such bond lengths were also observed in $[\{Cu(cyclam)\}(VO_3)_2]\cdot 5H_2O$.[70] Along [010] a chain-like arrangement is observed with alternating short and long Cu−O distances (Figure 3). Overall, each anion is

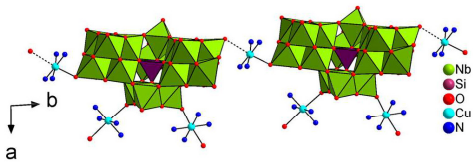

Figure 3. View of $\{HSiNb_{18}O_{54}\}$ clusters decorated by $[Cu(cyclam)(H_2O)]^{2+}$ and $[Cu(cyclam]^{2+}$ cations in the structure of **I**. Dotted line: long Cu−O distances (Cu(4)−O(45): 3.031(6) Å). Green polyhedra: NbO_6; purple polyhedra: SiO_4. Water O atoms, K^+ cations, and NO_3^- anions, as well as C and H atoms, are not displayed for the sake of clarity.

decorated by three Cu^{2+} centered complexes and the remaining two $[Cu(cyclam)(H_2O)]^{2+}$ molecules are located between the chain-like arrangement (Figures S3 and S4).

Four of the five unique K^+ cations are located between two $\{HSiNb_{18}O_{54}\}$ clusters and one (K4) is found in the pocket of the cluster anion (Figure 4).

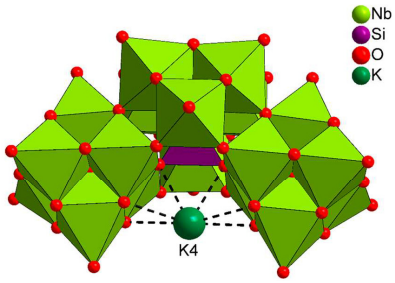

Figure 4. View of the $[HSiNb_{18}O_{54}]^{13-}$ anionic unit in **I**. The location of the K4 ion is displayed.

Each potassium ion is surrounded by water molecules and cluster O^{2-} anions and have coordination numbers (CN) of 5 (K3), 6 (K4), 7 (K1, K2), and 8 (K5) with average K−O bond lengths of 2.812−2.881 Å using a cutoff of 3.03 Å for the interionic distances. We note that the sum of ionic radii is 2.72−2.89 Å,[71] depending on the CN. K3 is located in the plane of four O^{2-} anions, which is electrostatically not satisfiying. Therefore, K−O distances up to 3.15 Å were considered, which leads to an increase of the CN to 6 (K3), 8 (K1, K2, K5), and 9 (K4), respectively (Table S5, Figure S5a). Such long K−O separations up to ∼3.2 Å are not unusual and were already reported for $KOH\cdot 4H_2O$[72] or in $K_{14}H[K@Si_4Nb_{16}O_{56}]\cdot 26H_2O$.[73]

The polyhedra around the K^+ cations are irregular and they share edges and corners, e.g., the polyhedron around K3 shares corners with those around K1 and K5 (Figure S5b). The KO_x polyhedra adopt a one-dimensional arrangement between the cluster anions along [010] (Figure S6).

Because the H atoms of the 35 H_2O molecules could not be located, O···O distances up to the sum of the van der Waals radii (3.04 Å) were considered as possible donor−acceptor distances for O−H···O bonds. The O···O distances range from 2.616 to 2.987 Å (Table S6), and a complex pattern is generated in the *bc* plane containing H_2O bonded to Cu^{2+} cations and proposed H_2O molecules surrounding K^+ cations. As mentioned above, some H_2O are disordered, and for the sake of clarity these molecules are not considered. Following the notation of Infantes et al.,[74,75] the water network can be denoted as L4(2)4(4)5(4)10(4)16(6)42(14); i.e., there are four-membered rings which are surrounded by two or four other rings, five-membered rings sharing H_2O molecules of four other rings, etc. (Figure S7). In the 16-membered rings, the $[Cu(cyclam)(H_2O)_2]^{2+}$ cations are located, while each cavity in the 42-membered rings is occupied by two $\{HSiNb_{18}O_{54}\}$ clusters along [100] (Figure 5). The view

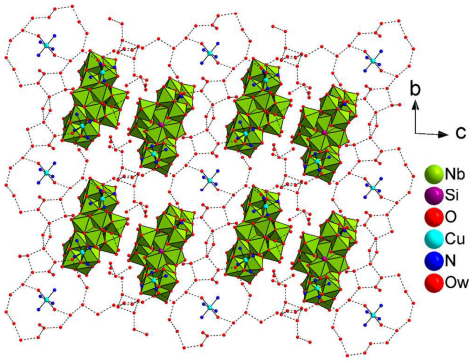

Figure 5. View of the arrangement of the layered L4(2)4(4)5(4)-10(4)16(6)42(14) water motif along [100] with the $\{SiNb_{18}O_{54}\}$ clusters located in the 42-membered rings in the structure of **I**. Green polyhedra: NbO_6; purple polyhedra: SiO_4; some atoms are omitted.

along [010] reveals that those rings are arranged in a wave-like manner with the anions being located between the rings (Figure S8). Some of the water molecules form 4-membered discrete water clusters that would be denoted as D3 and D4, respectively.

The compound $\{[Cu(cyclam)(H_2O)]_2[Cu(cyclam)][Nb_{10}O_{28}]\}_n\cdot 9nH_2O$ (**II**) crystallizes in the monoclinic space group *C*2/*c* (Table S1). All unique atoms except Cu2 are located on general positions. The two crystallographically independent Cu^{2+} cations are in a distorted octahedral coordination geometry with four N donors of the cyclam ligand in the equatorial plane and two O^{2-} anions in axial positions. The orientation of the N−H protons of the cyclam molecules around both Cu1 and Cu2 yields the trans-III (S,S,R,R) configuration[56,76,77] (Figure 6).

All Nb centers are in an octahedral environment of O^{2-} anions and the NbO_6 octahedra are connected via edge-sharing to form the $\{Nb_{10}O_{28}\}$ decaniobate ion (Figure 7). The geometry may be described as a rectangle generated by six edge-sharing NbO_6 octahedra which is capped by four NbO_6 units. The O^{2-} anions can be grouped according to the number of bridging metal atom centers: Nb−O_t, Nb-μ_2-O, Nb-μ_3-O, and Nb-μ_6-O with bond lengths 1.738(3)−1.753(3) Å,

DOI: 10.1021/acs.cgd.8b00548
Cryst. Growth Des. 2018, 18, 4130−4139

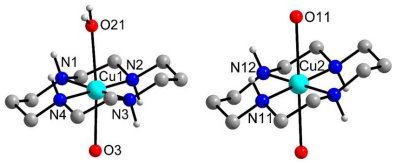

Figure 6. View of of the coordination environments around the two crystallographically independent Cu^{2+} cations in **II**. Only selected atoms are labeled. Ligand H atoms omitted.

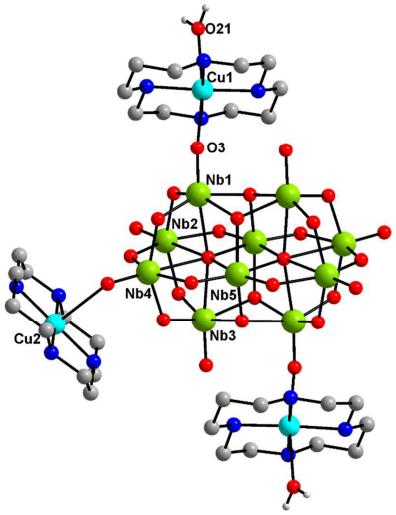

Figure 7. View of the decaniobate anion in **II**, decorated by three Cu^{2+} centered complexes. Only selected atoms are displayed and only a few atoms are labeled.

1.916(3)−2.097(3) Å, 2.009(3)−2.138(3) Å, and 2.225(2)−2.545(2) Å, respectively (Table S7), agreeing with data reported for other decaniobate compounds.[42−44,78] The O−Nb−O angles scatter from 73.2(1)° to 164.3(1)° (Table S8) reflecting a pronounced distortion of the NbO_6 octahedra. BVS calculations confirm the oxidation state of +5 for all Nb centers (average: 5.05, Table S3).

The $[Nb_{10}O_{28}]^{6-}$ anion is decorated by two $[Cu(cyclam)(H_2O)]^{2+}$ molecules via Nb−O_t−Cu bonds (Figure 7) involving ions which are the most basic sites of the decaniobate anion.[57]

The corresponding Cu1−O3 and Cu2−O11 distances are 2.469(3) Å and 2.721(4) Å, respectively, connecting the $\{Nb_{10}O_{28}\}$ anions into a chain directed along [100] (Figure 8).

The Cu−O_w bond of 2.594(5) Å is only slightly longer than those reported for $[Cu(cyclam)]^{2+}$ complexes containing compounds.[63,65−69] The Cu−N bonds are between 2.005(3) and 2.030(4) Å with N−Cu−N angles of 85.6(2)° and 94.6(2)° (Table S9), in good accordance with data reported in the literature.[63,64,68,69] Concerning the N/O−Cu−N/O angles, the $[Cu(cyclam)(H_2O)]^{2+}$ complex is more distorted (81.2(2)−172.1(1)°) than the other one (85.5(1)−180°). A possible reason is the involvement of the H_2O molecule in intramolecular H bonding interaction (N−H···O: 3.038(6) Å; ∠(NHO) = 111.6°) and O−H···O interactions with O_t atoms of neighboring clusters (Figure S9) (O−H···O: 2.746(5) Å; ∠(OHO) = 167.7°). Hydrogen bonds between the H_2O ligand and terminal O atoms of the $[Nb_{10}O_{28}]^{6-}$ anion connect the clusters along the *c* axis (Figure 9).

Strong hydrogen bonds (Table S10) are found between the N−H atoms of the cyclam ligands and the terminal and μ_2-bridging O atoms of the decaniobate anion (N−H···O distances: 2.949(4)−3.049(4) Å; ∠(NHO) = 145.9−168.4°). Furthermore, C−H atoms of cyclam and terminal as well as bridging (μ_2-, μ_3-O) cluster O^{2-} anions (C−H···O distances: 3.241(6)−3.480(6) Å; ∠(CHO) = 123.6−158.3°) are also involved in H bonding interactions. The crystal water molecules exhibit relatively strong H bonding interactions with terminal and μ_2-bridging cluster O^{2-} anions (O−H···O distances: 2.798(4)−3.217(5) Å; ∠(OHO) = 139.1−175.4°)

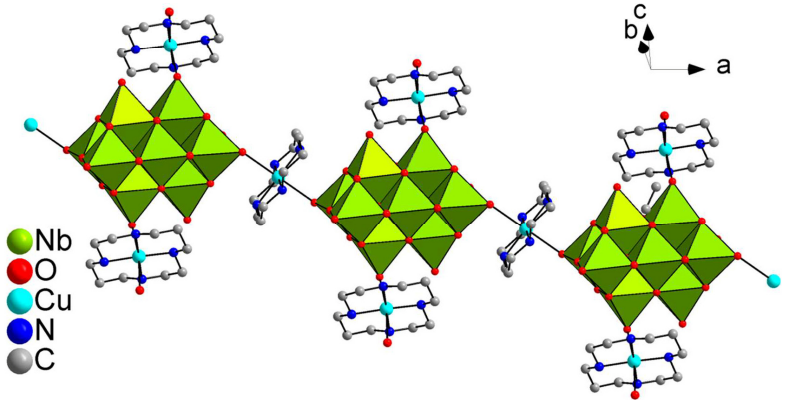

Figure 8. View of the chain generated through long Cu−O bonds in the structure of **II**. H atoms and crystal water molecules are omitted for clarity. Green polyhedra: NbO_6 units.

DOI: 10.1021/acs.cgd.8b00548
Cryst. Growth Des. 2018, 18, 4130−4139

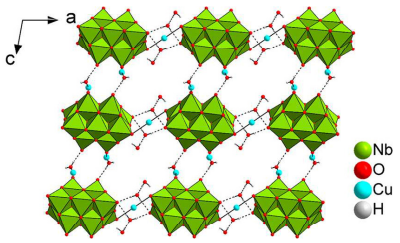

Figure 9. View of the arrangement of crystal water molecules in compound **II** and their involvement in hydrogen bonds (shown as dashed lines). Green polyhedra: NbO_6; organic ligands are omitted for clarity.

and weaker interactions with the C−H H atoms of the cyclam molecule ((C−H···O distances: 3.258(6)−3.579(7) Å; ∠(CHO) = 125.8−169.9°). The two unique H_2O molecules form a cluster which can be denoted as D2 (D = discrete) following the nomenclature of Infantes et al.[74,75] This D2 unit interacts with O^{2-} of the cluster anions via O−H···H bonds leading to a R4 motif (R = ring).

Optical Properties in the UV−vis Region. To evaluate the electronic transitions from UV−vis data, the Kubelka−Munk relation was applied (Figures S10 and S11). For **I**, the broad absorption at 519 nm (2.39 eV) arises from Cu^{2+} d−d transitions $E_g \rightarrow {}^2T_{2g}$,[79−82] while for **II**, the same transition occurs at 521 nm (2.38 eV). Both transitions correspond to the absorption of green light, in good accordance to the violet color of the compounds. The strong absorption located at about 326 nm (3.8 eV) for both compounds is most probably a charge transfer band.

Thermal Investigations. The thermal properties of both compounds were investigated in air and nitrogen atmosphere. Regardless of the atmosphere, compound **I** decomposes in not well-resolved steps (Figures S12 and S13). When heated in air, the first mass loss of about 15%, which is accompanied by an endothermic event (T_p = 104 °C), matches well with the emission of 35 water molecules (calc. 14.9%). Starting at ∼200 °C and up to 650 °C, further decomposition with a mass loss of about 20% is observed, which may be explained by the emission of cyclam molecules (calc. 19.5%). The reflections in the XRDP of the sample obtained at 500 °C could be assigned to Cu and CuO (Figure S14a). We want to note that in the XRDP of several decomposition samples, modulated backgrounds are observed indicating the presence of X-ray amorphous material. After heating to 1000 °C, a dark green residue is formed and most of the reflections in the XRDP could be assigned to $CuNb_2O_6$, $K_{5.75}Nb_{10.85}O_{30}$, and SiO_2 (Figure S14b). After heating the sample to 1000 °C in N_2, the TG curve above 200 °C is less steep compared to decomposition in air (Figure S15). The residue recovered at 600 °C showed only reflections of CuO in the XRDP (Figure S16a). The XRPD of the black powder formed at 1000 °C (Figure S16b) exhibits a large number of reflections and an unambiguous assignment to known compounds is difficult, but most of them could be assigned to $K_xNb_yO_{30}$ ($x \sim 6$, $y \sim 10.8$), Cu, NbO_2, and SiO_2.

In the TG curve of **II** measured in air, a well resolved mass loss up to ∼200 °C with an endothermic event at T_p = 129 °C occurs which can be assigned to the loss of crystal water molecules (Figure S17). During structure refinement, six H_2O molecules could be located. As mentioned above (see Experimental Section), five additional water molecules may occupy void spaces, giving rise to 11 H_2O molecules per formula unit. This is in full agreement with the first mass loss of 8.4% (calc. 8.4%). The following decomposition reaction from 200−500 °C (Δm = 23.2%) is accompanied by three exothermic signals at T_p = 300, 349, and 365 °C, as well as a broad shoulder around 400 °C, which is better resolved in the DSC curve (Figure S18) with T_p = 396 °C. The mass loss between 200 and 600 °C of 26% is in good agreement with removal of three cyclam molecules (calc. 25.2%).When the decomposition is stopped at ∼520 °C, an olive green solid containing ∼1% residual C and N is obtained. The XRDP (Figure S19a) revealed a modulated background and only two very weak reflections were observed, which may be assigned to CuO. The light green solid isolated after heating to 600 °C does not contain any residual C or N. The reflections in the powder pattern could not be assigned to any known copper or niobium or mixed oxides (Figure S19b). Furthermore, the material seems to be nanocrystalline in nature. Further investigations concerning the composition and properties are under way. After heating to 1000 °C, the XRDP of the light green residue shows mainly reflections of $Nb_{12}O_{29}$ and $CuNb_2O_6$ (Figure S19c).

The TG curve collected in N_2 atmosphere exhibits only two mass steps until ∼600 °C (Figures S20 and S21). The black residue at 600 °C contains elemental Cu (Figure S22a), in contrast to the experiment carried out in air where an unidentified material was obtained. The decomposition is not complete at 1000 °C and the sample still contains residual C (∼5%) and N (∼1.3%). Most reflections in the XRDP can be assigned to Cu and NbO_2 (Figure S22b).

In contrast to **I**, a pronounced plateau is observed after removal of H_2O. In a further experiment, decomposition was stopped at 200 °C and the residue was investigated with XRDP. The material exhibits a good crystallinity after dehydration and the powder pattern clearly differs from the simulated pattern of **II** (Figure S23). After stirring the dehydrated sample for 2 h in water and drying on air, the powder pattern matches well with the simulated pattern of **II**, indicating that the material is fully recovered (Figure S24).

The water adsorption properties of **II** were investigated with water vapor sorption measurements using samples treated in different ways (see Experimental Section). The sorption isotherm of the sample dehydrated at room temperature by evacuation shows a water uptake of only ∼7 of the 11 crystal water molecules at a partial pressure p/p_0 = 0.9 (Figure 10). For the sample heated at 200 °C the uptake of 7 H_2O molecules is already reached at p/p_0 = 0.7 and a higher partial pressure is required for adsorption of all 11 molecules. The different behavior of the two samples can be traced back to the crystal structures: evacuation does not significantly change the crystal structure while heat treatment at 200 °C leads to formation of a new compound with a different crystal structure (Figure S29).

■ CONCLUSION

We demonstrated that control of the pH value is an important synthetic parameter for the directed preparation of new polyoxoniobates. In addition, the pH value significantly influences the yield of the compounds and also stirring the reaction slurry is required for formation of phase pure

DOI: 10.1021/acs.cgd.8b00548
Cryst. Growth Des. 2018, 18, 4130−4139

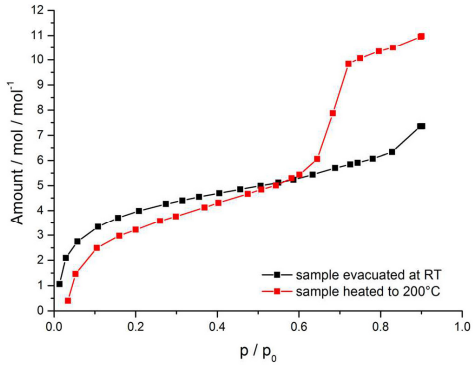

Figure 10. Water sorption isotherms of samples of compound **II** evacuated at room temperature (black) and heated to 200 °C (red).

products. The rare $\{SiNb_{18}O_{54}\}$ cluster in the structure of **I** is covalently expanded by Cu^{2+}centered complexes. Crystal lattice water molecules form a complex network through H bonding interactions. In the structure of **II** decaniobate anions are connected into a chain via Cu−O_t bonds of [Cu(cyclam)]$^{2+}$ cations along [100]. Compound **I** is decomposed upon heating in several not well resolved steps, and depending on the atmosphere and final temperature, different compounds are formed. The TG curve of **II** shows a distinct plateau due to removal of crystal water molecules. The XRDP evidence that the dehydrated material exhibits good crystallinity and that **II** is recovered when treated with water. H_2O sorption measurements demonstrate that the water molecules can be desorbed *in vacuo* and confirm the number of water molecules determined from TG experiments and elemental analysis.

Because of the large potential of PONbs in various fields of possible applications, an efficient synthetic strategy with short reaction times and high yields is crucial to explore the potential of these new materials in a reasonable time scale. Because PONb based materials are often synthesized under hydrothermal conditions, systematic evaluations of the influence of a single reaction parameter onto product formation is necessary to understand the formation pathways. It is well documented that the products of hydrothermal syntheses are often inhomogeneous caused by concentration gradients in the reaction slurries. We demonstrated that phase pure products can be obtained stirring the reaction mixture which leads to a homogeneous distribution of the reactants in solution. Furthermore, a shortening of the reaction time is advantageous for screening of the parameter space, thus allowing fast optimization of reaction parameters. Currently, we are systematically exploring if this approach is suitable for the efficient synthesis of new PONbs exhibiting new structural features and chemical compositions.

■ ASSOCIATED CONTENT

Supporting Information

The Supporting Information is available free of charge on the ACS Publications website at DOI: 10.1021/acs.cgd.8b00548.

Additional tables with selected bond lengths and angles and bond valence sum analyses, images of the structures, powder patterns, DTA/TG curves of both compounds, DSC diagrams of compound **II**, IR spectra and assignments of the infrared absorption bands of both compounds, Kubelka−Munk plots (PDF)

Accession Codes

CCDC 1835027−1835028 contain the supplementary crystallographic data for this paper. These data can be obtained free of charge via www.ccdc.cam.ac.uk/data_request/cif, or by emailing data_request@ccdc.cam.ac.uk, or by contacting The Cambridge Crystallographic Data Centre, 12 Union Road, Cambridge CB2 1EZ, UK; fax: +44 1223 336033.

■ AUTHOR INFORMATION

Corresponding Author

*E-mail: wbensch@ac.uni-kiel.de.

ORCID

Christian Näther: 0000-0001-8741-6508

Wolfgang Bensch: 0000-0002-3111-580X

Author Contributions

The manuscript was written through contributions of all authors. All authors have given approval to the final version of the manuscript.

Notes

The authors declare no competing financial interest.

■ ACKNOWLEDGMENTS

The authors gratefully acknowledge financial support of the State Schleswig-Holstein and Lisa K. Mahnke for her help with the TOC graphic.

■ REFERENCES

(1) Ogata, A.; Yanagie, H.; Ishikawa, E.; Morishita, Y.; Mitsui, S.; Yamashita, A.; Hasumi, K.; Takamoto, S.; Yamase, T.; Eriguchi, M. Antitumour effect of polyoxomolybdates: Induction of apoptotic cell death and autophagy in in vitro and in vivo models. *Br. J. Cancer* **2008**, *98*, 399−409.

(2) Mitsui, S.; Ogata, A.; Yanagie, H.; Kasano, H.; Hisa, T.; Yamase, T.; Eriguchi, M. Antitumor activity of polyoxomolybdate, $[NH_3Pr^i]_6[Mo_7O_{24}]\cdot 3H_2O$, against, human gastric cancer model. *Biomed. Pharmacother.* **2006**, *60*, 353−358.

(3) Long, D.-L.; Tsunashima, R.; Cronin, L. Polyoxometalates: Building Blocks for Functional Nanoscale Systems. *Angew. Chem., Int. Ed.* **2010**, *49*, 1736−1758.

(4) Thompson, K. Coordination chemistry of vanadium in metallopharmaceutical candidate compounds. *Coord. Chem. Rev.* **2001**, *219*−*221*, 1033−1053.

(5) Streb, C. New trends in polyoxometalate photoredox chemistry: From photosensitisation to water oxidation catalysis. *Dalton Trans.* **2012**, *41*, 1651−1659.

(6) Rao, K. V.; Rao, P. S. N.; Nagaraju, P.; Prasad, P. S.; Lingaiah, N. Room temperature selective oxidation of toluene over vanadium substituted polyoxometalate catalysts. *J. Mol. Catal. A: Chem.* **2009**, *303*, 84−89.

(7) Hill, C. L. Progress and challenges in polyoxometalate-based catalysis and catalytic materials chemistry. *J. Mol. Catal. A: Chem.* **2007**, *262*, 2−6.

(8) Han, X.-B.; Zhang, Z.-M.; Zhang, T.; Li, Y.-G.; Lin, W.; You, W.; Su, Z.-M.; Wang, E.-B. Polyoxometalate-Based Cobalt-Phosphate Molecular Catalysts for Visible Light-Driven Water Oxidation. *J. Am. Chem. Soc.* **2014**, *136*, 5359−5366.

(9) Dianat, S.; Bordbar, A. K.; Tangestaninejad, S.; Yadollahi, B.; Zarkesh-Esfahani, S. H.; Habibi, P. ctDNA binding affinity and in vitro antitumor activity of three Keggin type polyoxotungestates. *J. Photochem. Photobiol., B* **2013**, *124*, 27−33.

DOI: 10.1021/acs.cgd.8b00548
Cryst. Growth Des. 2018, 18, 4130−4139

(10) Kozhevnikov, I. V. Catalysis by Heteropoly Acids and Multicomponent Polyoxometalates in Liquid-Phase Reactions. *Chem. Rev.* **1998**, *98*, 171−198.
(11) Katsoulis, D. E. A. Survey of Applications of Polyoxometalates. *Chem. Rev.* **1998**, *98*, 359−388.
(12) Ji, Y.; Huang, L.; Hu, J.; Streb, C.; Song, Y.-F. Polyoxometalate-functionalized nanocarbon materials for energy conversion, energy storage and sensor systems. *Energy Environ. Sci.* **2015**, *8*, 776−789.
(13) Yu, F.; Kong, X.-J.; Zheng, Y.-Y.; Ren, Y.-P.; Long, L.-S.; Huang, R.-B.; Zheng, L.-S. pH-dependent assembly of 0D to 3D Keggin-based coordination polymers: Structures and catalytic properties: Structures and catalytic properties. *Dalton Trans.* **2009**, 9503−9509.
(14) Yang, H.; Gao, S.; Lü, J.; Xu, B.; Lin, J.; Cao, R. pH-Dependent Syntheses and Crystal Structures of a Series of Organic-Inorganic Hybrids Constructed from Keggin or Wells-Dawson Polyoxometalates and Silver Coordination Compounds. *Inorg. Chem.* **2010**, *49*, 736−744.
(15) Sha, J.-Q.; Sun, J.-W.; Wang, C.; Li, G.-M.; Yan, P.-F.; Li, M.-T. Syntheses Study of Keggin POM Supporting MOFs System. *Cryst. Growth Des.* **2012**, *12*, 2242−2250.
(16) Li, S.; Zhang, L.; Chai, D.; Pang, H.; Ma, H. Self-assembly of polyoxometalate-based hybrid aggregates: From a monomer to dimers by changing the pH value of reaction systems. *New J. Chem.* **2017**, *41*, 10148−10154.
(17) Li, S.; Ma, H.; Pang, H.; Zhang, L. Assembly of Six Polyoxometalate-Based Hybrid Compounds from a Simple Supramolecule to a Complicated Pseudorotaxane Framework via Tuning the pH of the Reaction Systems. *Cryst. Growth Des.* **2014**, *14*, 4450−4460.
(18) Hu, Y.; An, H.; Liu, X.; Yin, J.; Wang, H.; Zhang, H.; Wang, L. pH-controlled assembly of hybrid architectures based on Anderson-type polyoxometalates and silver coordination units. *Dalton Trans.* **2014**, *43*, 2488−2498.
(19) Chi, Y.-N.; Cui, F.-Y.; Jia, A.-R.; Ma, X.-Y.; Hu, C.-W. pH-Dependent syntheses of copper−quinoxaline−polyoxotungstate hybrids: Variable role of Keggin-type polyanion in different pH conditions. *CrystEngComm* **2012**, *14*, 3183−3188.
(20) Li, F.; Xu, L. Coordination assemblies of polyoxomolybdate cluster framework: From labile building blocks to stable functional materials. *Dalton Trans.* **2011**, *40*, 4024−4034.
(21) Wu, H.-L.; Zhang, Z.-M.; Li, Y.-G.; Wang, X.-L.; Wang, E.-B. Recent progress in polyoxoniobates decorated and stabilized *via* transition metal cations or clusters. *CrystEngComm* **2015**, *17*, 6261−6268.
(22) Molina, P. I.; Sures, D. J.; Miró, P.; Zakharov, L. N.; Nyman, M. Bridging the opposite chemistries of tantalum and tungsten polyoxometalates. *Dalton Trans.* **2015**, *44*, 15813−15822.
(23) Wendt, M.; Näther, C.; Bensch, W. High Nuclearity Antimonato-Polyoxovanadate Cluster $\{V_{15}Sb_6O_{42}\}$ as a Synthon for the Solvothermal in situ Generation of α- and β-$\{V_{14}Sb_8O_{42}\}$ Isomers. *Chem. - Eur. J.* **2016**, *22*, 7747−7751.
(24) Nyman, M. Polyoxoniobate chemistry in the 21st century. *Dalton Trans.* **2011**, *40*, 8049−8058.
(25) Wendt, M.; Mahnke, L. K.; Heidenreich, N.; Bensch, W. Nucleation and Crystal Growth of a $\{V_{14}Sb_8O_{42}\}$ Cluster from a $\{V_{15}Sb_6O_{42}\}$ Polyoxovanadate: In Situ XRD Studies. *Eur. J. Inorg. Chem.* **2016**, *2016*, 5393−5398.
(26) Bontchev, R. P.; Nyman, M. Evolution of polyoxoniobate cluster anions. *Angew. Chem., Int. Ed.* **2006**, *45*, 6670−6672.
(27) Nyman, M.; Burns, P. C. A comprehensive comparison of transition-metal and actinyl polyoxometalates. *Chem. Soc. Rev.* **2012**, *41*, 7354−7367.
(28) Nyman, M.; Criscenti, L. J.; Bonhomme, F.; Rodriguez, M. A.; Cygan, R. T. Synthesis, structure, and molecular modeling of a titanoniobate isopolyanion. *J. Solid State Chem.* **2003**, *176*, 111−119.
(29) Ohlin, C. A.; Villa, E. M.; Casey, W. H. One-pot synthesis of the decaniobate salt $[N(CH_3)_4]_6[Nb_{10}O_{28}] \cdot 6H_2O$ from hydrous niobium oxide. *Inorg. Chim. Acta* **2009**, *362*, 1391−1392.
(30) Anderson, T. M.; Alam, T. M.; Rodriguez, M. A.; Bixler, J. N.; Xu, W.; Parise, J. B.; Nyman, M. Cupric Siliconiobate. Synthesis and Solid-State Studies of a Pseudosandwich-Type Heteropolyanion. *Inorg. Chem.* **2008**, *47*, 7834−7839.
(31) Nyman, M.; Bonhomme, F.; Alam, T. M.; Rodriguez, M. A.; Cherry, B. R.; Krumhansl, J. L.; Nenoff, T. M.; Sattler, A. M. A General Synthetic Procedure for Heteropolyniobates. *Science* **2002**, *297*, 996−998.
(32) Bonhomme, F.; Larentzos, J. P.; Alam, T. M.; Maginn, E. J.; Nyman, M. Synthesis, Structural Characterization, and Molecular Modeling of Dodecaniobate Keggin Chain Materials. *Inorg. Chem.* **2005**, *44*, 1774−1785.
(33) Nyman, M.; Bonhomme, F.; Alam, T. M.; Parise, J. B.; Vaughan, G. M. B $[SiNb_{12}O_{40}]^{16-}$ and $[GeNb_{12}O_{40}]^{16-}$: Highly Charged Keggin Ions with Sticky Surfaces. *Angew. Chem., Int. Ed.* **2004**, *43*, 2787−2792.
(34) Zhang, Z.; Lin, Q.; Kurunthu, D.; Wu, T.; Zuo, F.; Zheng, S.-T.; Bardeen, C. J.; Bu, X.; Feng, P. Synthesis and Photocatalytic Properties of a New Heteropolyoxoniobate compound: $K_{10}[Nb_2O_2(H_2O)_2][SiNb_{12}O_{40}] \cdot 12H_2O$. *J. Am. Chem. Soc.* **2011**, *133*, 6934−6937.
(35) Son, J.-H.; Ohlin, C. A.; Johnson, R. L.; Yu, P.; Casey, W. H. A Soluble Phosphorus-Centered Keggin Polyoxoniobate with Bicapping Vanadyl Groups. *Chem. - Eur. J.* **2013**, *19*, 5191−5197.
(36) Son, J.-H.; Ohlin, C. A.; Larson, E. C.; Yu, P.; Casey, W. H. Synthesis and Characterization of a Soluble Vanadium-Containing Keggin Polyoxoniobate by ESI-MS and ^{51}V NMR: $(TMA)_5[V_3Nb_{12}O_{42}] \cdot 18H_2O$. *Eur. J. Inorg. Chem.* **2013**, *2013*, 1748−1753.
(37) Son, J.-H.; Casey, W. H. Reversible capping/uncapping of phosphorous-centered Keggin-type polyoxoniobate clusters. *Chem. Commun.* **2015**, *51*, 1436−1438.
(38) Yuan, Y.; Li, F.; Fu, X.; Ma, P. Crystal Structure of a new 3D polyoxoniobate based on Lindqvist type polyoxoanion. *Huaxue Yanjiu* **2011**, 19−24.
(39) Fullmer, L. B.; Mansergh, R. H.; Zakharov, L. N.; Keszler, D. A.; Nyman, M. Nb_2O_5 and Ta_2O_5 Thin Films from Polyoxometalate Precursors: A Single Proton Makes a Difference. *Cryst. Growth Des.* **2015**, *15*, 3885−3892.
(40) Nyman, M.; Alam, T. M.; Bonhomme, F.; Rodriguez, M. A.; Frazer, C. S.; Welk, M. E. Solid-state Structures and Solution Behavior of Alkali Salts of the $[Nb_6O_{19}]^{8-}$ Lindqvist Ion. *J. Cluster Sci.* **2006**, *17*, 197−219.
(41) Alam, T. M.; Nyman, M.; Cherry, B. R.; Segall, J. M.; Lybarger, L. E. Multinuclear NMR Investigations of the Oxygen, Water, and Hydroxyl Environments in Sodium Hexaniobate. *J. Am. Chem. Soc.* **2004**, *126*, 5610−5620.
(42) Graeber, E. J.; Morosin, B. The Molecular Configuration of the Decaniobate Ion $(Nb_{10}O_{28}^{6-})$. *Acta Crystallogr., Sect. B: Struct. Crystallogr. Cryst. Chem.* **1977**, *33*, 2137−2143.
(43) Shen, L.; Li, C.-H.; Chi, Y.-N.; Hu, C.-W. Zn(2,2'-bipy)$_2$/Co(2,2'-bipy)$_2$ linked decaniobate $[Nb_{10}O_{28}]^{6-}$ clusters-zigzag neutral chains. *Inorg. Chem. Commun.* **2008**, *11*, 992−994.
(44) Niu, J.; Wang, G.; Zhao, J.; Sui, Y.; Ma, P.; Wang, J. Zero- or One-Dimensional Organic-Inorganic Hybrid Polyoxoniobates Constructed from Decaniobate Units and Transition-Metal Complexes. *Cryst. Growth Des.* **2011**, *11*, 1253−1261.
(45) Hou, Y.; Nyman, M.; Rodriguez, M. A. Soluble Heteropolyniobates from the Bottom of Group IA. *Angew. Chem.* **2011**, *123*, 12722−12725.
(46) Huang, P.; Qin, C.; Wang, X.-L.; Sun, C.-Y.; Xing, Y.; Wang, H.-N.; Shao, K.-Z.; Su, Z.-M. A new organic-inorganic hybrid based on the crescent-shaped polyoxoanion $[H_6SiNb_{18}O_{54}]^{8-}$ and copper-organic cations. *Dalton Trans.* **2012**, *41*, 6075−6077.
(47) Liu, B.-X.; Cai, Z.-W.; Yang, T.; Li, X.-X.; Yang, G.-Y.; Zheng, S.-T. A rare polyoxometalate based on mixed niobium-based polyoxoanions $[GeNb_{18}O_{54}]^{14-}$ and $[Nb_3W_3O_{19}]^{5-}$. *Inorg. Chem. Commun.* **2017**, *78*, 56−60.

DOI: 10.1021/acs.cgd.8b00548
Cryst. Growth Des. 2018, 18, 4130−4139

(48) Pienack, N.; Bensch, W. In-situ Monitoring of the Formation of Crystalline Solids. *Angew. Chem., Int. Ed.* **2011**, *50*, 2014−2034.
(49) Kortüm, G.; Braun, W.; Herzog, G. Prinzip und Meßmethodik der diffusen Reflexionsspektroskopie. *Angew. Chem.* **1963**, *75*, 653−661.
(50) Sheldrick, G.M.. *SHELXS-97: Program for the Solution of Crystal Structures*; University of Goettingen: Goettingen, 1997.
(51) Sheldrick, G.M.. *SHELXL-2014: Program for the Refinement of Crystal Structures*; University of Goettingen: Goettingen, 2014.
(52) Spek, A. L. PLATON SQUEEZE. A tool for the calculation of the disordered solvent contribution to the calculated structure factors. *Acta Crystallogr., Sect. C: Struct. Chem.* **2015**, *71*, 9−18.
(53) Filowitz, M.; Ho, R. K. C.; Klemperer, W. G.; Shum, W. Oxygen-17 nuclear magnetic resonance spectroscopy of polyoxometalates. 1. Sensitivity and resolution. *Inorg. Chem.* **1979**, *18*, 93−103.
(54) Tsunashima, R.; Long, D.-L.; Miras, H. N.; Gabb, D.; Pradeep, C. P.; Cronin, L. The Construction of High-Nuclearity Isopolyoxoniobates with Pentagonal Building Blocks: $[HNb_{27}O_{76}]^{16-}$ and $[H_{10}Nb_{31}O_{93}(CO_3)]^{23-}$. *Angew. Chem.* **2010**, *122*, 117−120.
(55) Hilbert, J.; Näther, C.; Bensch, W. Influence of the Synthesis Parameters onto Nucleation and Crystallization of Five New Tin-Sulfur Containing Compounds. *Inorg. Chem.* **2014**, *53*, 5619−5630.
(56) Fabbrizzi, L. A Lifetime Walk in the Realm of Cyclam. In *Macrocyclic and Supramolecular Chemistry*, 2016; pp 165−199. DOI:
(57) Villa, E. M.; Ohlin, C. A.; Balogh, E.; Anderson, T. M.; Nyman, M.; Casey, W. H. Reaction Dynamics of the Decaniobate Ion $[HxNb_{10}O_{28}]^{(6-x)-}$ in Water. *Angew. Chem.* **2008**, *120*, 4922−4924.
(58) Hou, Y.; Alam, T. M.; Rodriguez, M. A.; Nyman, M. Aqueous compatibility of group IIIA monomers and Nb-polyoxoanions. *Chem. Commun.* **2012**, *48*, 6004−6006.
(59) Liang, Z.; Zhang, D.; Wang, H.; Ma, P.; Yang, Z.; Niu, J.; Wang, J. The $\{Ni_{10}Nb_{32}\}$ aggregate: a perspective on isopolyniobates as ligands. *Dalton Trans.* **2016**, *45*, 16173−16176.
(60) Zhang, Y.; Shen, J.-Q.; Zheng, L.-H.; Zhang, Z.-M.; Li, Y.-X.; Wang, E.-B. Four Polyoxonibate-Based Inorganic−Organic Hybrids Assembly from Bicapped Heteropolyoxonibate with Effective Antitumor Activity. *Cryst. Growth Des.* **2014**, *14*, 110−116.
(61) Bondi, A. van der Waals Volumes and Radii. *J. Phys. Chem.* **1964**, *68*, 441−451.
(62) Pérez-Toro, I.; Domínguez-Martín, A.; Choquesillo-Lazarte, D.; Vílchez-Rodríguez, E.; González-Pérez, J. M.; Castiñeiras, A.; Niclós-Gutiérrez, J. Lights and shadows in the challenge of binding acyclovir, a synthetic purine-like nucleoside with antiviral activity, at an apical-distal coordination site in copper(II)-polyamine chelates. *J. Inorg. Biochem.* **2015**, *148*, 84−92.
(63) Tajidi, N. S. A.; Abdullah, N.; Arifin, Z. Diaqua-(1,4,8,11-tetraazacyclotetradecane-$\kappa^4N^1,N^4,N^8,N^{11}$)copper(II) didodeca-noate dihydrate. *Acta Crystallogr., Sect. E: Struct. Rep. Online* **2011**, *67*, m588−9.
(64) Tasker, P. A.; Sklar, L. Crystal and molecular structure of di(perchlorato)(1,4,8,11-tetraazacyclotetradecane)copper(II). Cu(cyclam)$(ClO_4)_2$. *J. Cryst. Mol. Struct.* **1975**, *5*, 329−344.
(65) Ahmad Tajidi, N. S.; Abdullah, N.; Arifin, Z.; Tan, K. W.; Ng, S. W. Diaqua-(1,4,8,11-tetraazacyclotetradecane-$\kappa^4N^1,N^4,N^8,N^{11}$)-copper(II) bis-(4-methyl-benzoate) monohydrate. *Acta Crystallogr., Sect. E: Struct. Rep. Online* **2010**, *66*, m890.
(66) Emsley, J.; et al. Hydrogen bonds between free fluoride ions and water molecules: two x-ray structures. *J. Mol. Struct.* **1990**, *220*, 1−12.
(67) Ahmad Tajidi, N. S.; Abdullah, N.; Arifin, Z.; Tan, K. W.; Ng, S. W. Diaqua-(1,4,8,11-tetraazacyclotetradecane-$\kappa^4N^1,N^4,N^8,N^{11}$)-copper(II)bis-(2,3,4,5,6-penta-fluoro-benzoate) dihydrate. *Acta Crystallogr., Sect. E: Struct. Rep. Online* **2010**, *66*, m889.
(68) Ahmad Tajidi, N. S.; Abdullah, N.; Arifin, Z.; Tan, K. W.; Ng, S. W. Diaqua-(1,4,8,11-tetraazacyclotetradecane-$\kappa^4N^1,N^4,N^8,N^{11}$)-copper(II) dihepta-noate dihydrate. *Acta Crystallogr., Sect. E: Struct. Rep. Online* **2010**, *66*, m887.
(69) Ahmad Tajidi, N. S.; Abdullah, N.; Arifin, Z.; Tan, K. W.; Ng, S. W. Diaqua-(1,4,8,11-tetraazacyclotetradecane-$\kappa^4N^1,N^4,N^8,N^{11}$)-copper(II) dideca-noate dihydrate. *Acta Crystallogr., Sect. E: Struct. Rep. Online* **2010**, *66*, m888.
(70) Martín-Caballero, J.; Wéry, A. S. J.; Artetxe, B.; Reinoso, S.; Felices, L. S.; Vilas, J. L.; Gutiérrez-Zorrilla, J. M. Sequential single-crystal-to-single-crystal transformations promoted by gradual thermal dehydration in a porous metavanadate hybrid. *CrystEngComm* **2015**, *17*, 8915−8925.
(71) Shannon, R. D. Revised Effective Ionic Radii and Systematic Studies of Interatomic Distances in Halides and Chalcogenides. *Acta Crystallogr., Sect. A: Cryst. Phys., Diffr., Theor. Gen. Crystallogr.* **1976**, *32*, 751−767.
(72) Rütter, H.; Mootz, D. Hydrate schwacher und starker Basen. V. Die Kristallstrukturen von KOH · $2H_2O$ (Substruktur) und KOH · $4H_2O$. *Z. Anorg. Allg. Chem.* **1991**, *601*, 73−82.
(73) Abramov, P. A.; Davletgildeeva, A. T.; Sokolov, M. N. Formation of Silicon-Containing Polyoxoniobates from Hexaniobate Under High Temperature Conditions. *J. Cluster Sci.* **2017**, *28*, 735−744.
(74) Infantes, L.; Chisholm, J.; Motherwell, S. Extended motifs from water and chemical functional groups in organic molecular crystals. *CrystEngComm* **2003**, *5*, 480−486.
(75) Infantes, L.; Motherwell, S. Water clusters in organic molecular crystals. *CrystEngComm* **2002**, *4*, 454−461.
(76) Bakaj, M.; Zimmer, M. Conformational analysis of copper(II) 1,4,8,11-tetraazacyclotetradecane macrocyclic systems. *J. Mol. Struct.* **1999**, *508*, 59−72.
(77) Kent Barefield, E. Coordination chemistry of N-tetraalkylated cyclam ligands—A status report. *Coord. Chem. Rev.* **2010**, *254*, 1607−1627.
(78) Matsumoto, M.; Ozawa, Y.; Yagasaki, A. Reversible dimerization of decaniobate. *Polyhedron* **2010**, *29*, 2196−2201.
(79) Boiocchi, M.; Broglia, A.; Fabbrizzi, L.; Fusco, N.; Mangano, C. Anion receptors containing coordinatively unsaturated metal ions: copper(II) complexes with cyclam derivatives. *Can. J. Chem.* **2014**, *92*, 794−802.
(80) Černák, J.; Kuchár, J.; Stolárová, M.; Kajňaková, M.; Vavra, M.; Potočňák, I.; Falvello, L. R.; Tomás, M. Preparation, spectroscopic and magnetic characterization of Cu(cyclam)$M(CN)_4$ complexes exhibiting one-dimensional crystal structures (cyclam = 1,4,8,11-tetraazacyclotetradecane, M = Ni, Pd, Pt). *Transition Met. Chem.* **2010**, *35*, 737−744.
(81) Prevedello, A.; Bazzan, I.; Dalle Carbonare, N.; Giuliani, A.; Bhardwaj, S.; Africh, C.; Cepek, C.; Argazzi, R.; Bonchio, M.; Caramori, S.; et al. Heterogeneous and Homogeneous Routes in Water Oxidation Catalysis Starting from Cu(II) Complexes with Tetraaza Macrocyclic Ligands. *Chem. - Asian J.* **2016**, *11*, 1281−1287.
(82) Stephan, H.; Geipel, G.; Appelhans, D.; Bernhard, G.; Tabuani, D.; Komber, H.; Voit, B. Pegylation of 1,4,8,11-tetraazacyclotetradecane (cyclam) and its Cu(II) complexation. *Tetrahedron Lett.* **2005**, *46*, 3209−3212.

DOI: 10.1021/acs.cgd.8b00548
Cryst. Growth Des. 2018, 18, 4130−4139

3.2 Der Einfluss der Titanquelle und der Temperatur auf die Bildung seltener Ti-PONbs mit Ni^{2+}-Kationen in unterschiedlichen Koordinationsumgebungen

Zusammenfassung der Publikation „On the influence of the titanium source on the composition and structure of novel titanoniobates“

In dieser Veröffentlichung werden die Ergebnisse der Synthese und der Einfluss von Titanquellen auf die Bildung neuer Titanoniobate vorgestellt. Unter hydrothermalen Bedingungen konnten mit *in-situ* generierten $[Ni(cyclam)]^{2+}$-Kationen, $[Nb_6O_{19}]^{8-}$-Anionen und $Ti(O^iPr)_4$ oder $K_2TiO(C_2O_4)\cdot 2H_2O$ fünf neue Titanoniobate mit zwei unterschiedlichen Ti-Substitutionsgraden und Ni^{2+}-Kationen in unterschiedlichen Koordinationsumgebungen hergestellt werden.

Mit $Ti(O^iPr)_4$ wurde $\{[Ni(cyclam)]_4[\mathbf{Ti_2Nb_8O_{28}}]\}n\cdot\sim 28nH_2O$ (**I**), ein Dititanoniobat, synthetisiert, in dessen Kristallstruktur jedes Anion über Ni-O-Bindungen von sechs $[Ni(cyclam)]^{2+}$-Kationen oktaedrischer Geometrie koordiniert ist. Zwei Ni^{2+}-Komplexe liegen in der *cis*-Konfiguration vor, was zu einer starken Verzerrung des cyclam-Moleküls führt. Die übrigen vier ÜM-Komplexe sind *trans*-konfiguriert. Wird $K_2TiO(C_2O_4)\cdot 2H_2O$ als Quelle eingesetzt, so werden vier Pseudo-Polymorphe $K[Ni(cyclam)]_3[\mathbf{TiNb_9O_{28}}]\cdot xH_2O$ (**II-IV**) (x = 10-18) erhalten, in deren Strukturen nur ein Nb^{5+}-Kation durch Ti^{4+} substituiert ist. In den Strukturen liegt Ni^{2+} quadratisch-planar koordiniert vor und sind isoliert zwischen den Anionen angeordnet. Besonders interessant ist, dass die Produktbildung bei den gewählten Reaktionsbedingungen selektiv ist, d.h. je nach verwendeter Titanquelle kristallisiert entweder **I** oder **II-IV**. Mit weiteren Experimenten konnte nachgewiesen werden, dass die Produktbildung von **II-IV** temperaturabhängig ist.

Zusätzlich konnte ausgeschlossen werden, dass die Bildung des Anions ausschließlich vom pH-Wert abhängig ist, denn bei entsprechenden Versuchen mit $K_2TiO(C_2O_4)\cdot 2H_2O$ wurden ebenfalls nur **II-IV** erhalten. Auch diese Verbindungen können z.T. reversibel Kristallwassermoleküle abgeben und aufnehmen.

Dalton Transactions

PAPER

View Article Online
View Journal | View Issue

Check for updates

Cite this: *Dalton Trans.*, 2018, **47**, 15103

On the influence of the titanium source on the composition and structure of novel titanoniobates†

Joanna Dopta, Sven Grzanna, Christian Näther and Wolfgang Bensch *

Received 10th July 2018,
Accepted 27th September 2018

DOI: 10.1039/c8dt02835d

rsc.li/dalton

Systematic variation of the titanium source and the reaction temperature applied during hydrothermal synthesis led to crystallization of four new titanoniobates: $\{[Ni(cyclam)]_4[Ti_2Nb_8O_{28}]\}_n \cdot \sim 28nH_2O$ (**I**), $K[Ni(cyclam)]_3[TiNb_9O_{28}] \cdot xH_2O$; x = 18 (**II**), x = 14 (**III**) and $x \sim 10$ (**IV**). These are the first titanoniobates with Ni^{2+}-centered amine complexes acting as counter cations and additionally, this is the first report of transition metal complexes expanded by monotitanoniobates. While **I** is obtained using $Ti(O^iPr)_4$, **II–IV** are formed using $K_2TiO(C_2O_4)\ 2H_2O$ as the educt. The presence of oxalate anions seems to influence the coordination environments of the Ni^{2+} cations that are octahedrally coordinated in **I**, and in a square-planar environment in **II–IV**. The titanium source also affects the degree of substitution of Nb^V by Ti^{IV}. Temperature-dependent syntheses demonstrate that the formation of **I** does not depend on the reaction temperature, while the formation of **II–IV** is clearly affected by this parameter. Regarding the arrangement of crystal water molecules, patterns of different dimensionalities ranging from 0D to 3D are formed which can be classified as water clusters. Each compound exhibits a pronounced plateau in the thermogravimetric curves after the removal of crystal H_2O molecules. Rehydration experiments after water removal proved that except for compound **III**, the re-integration of water was successful.

Introduction

Polyoxometalates (POMs) are anionic metal-oxo clusters that are formed by group V and VI transition metal cations. Due to their outstanding performance in *e.g.* catalysis, medicine and electrochemistry, the design of novel POMs is an important topic in current research.[1] Compared to polyoxovanadates, -molybdates and -tungstates, the chemistry of polyoxoniobates (PONbs) is less developed due to the synthetic limitations and chemical inertness of niobium oxo clusters.[2,3] Nevertheless, several novel cluster geometries were discovered in the past decade. In the field of hetero-PONbs, Si or Ge *e.g.* could be incorporated into Keggin anion containing compounds, *e.g.* in $Na_{16}[XNb_{12}O_{40}] \cdot 4H_2O$[4] (X = Si, Ge), or transition metal cations like Ni and V, *e.g.* in $K_{14}Na_6[H_4Ni_{10}(H_2O)_8Nb_{32}O_{102}] \cdot 73H_2O$[5] or $Na_{18}[Nb_{48}V_8(OH)_{30}O_{130}] \cdot 33H_2O$[6] and also lanthanide ions, *e.g.* in $(CN_3H_6)_7K_3H_{17}\{Eu_3(H_2O)_9Nb_{48}O_{138}(H_2O)_6\} \cdot 40H_2O$.[7]

The first examples of Ti^{IV} integration into the PONb structure were $A_{12}[Ti_2O_2][XNb_{12}O_{40}] \cdot nH_2O$ (A = Na, K; X = Si, Ge) featuring the Keggin-type $[XNb_{12}O_{40}]^{16-}$ anions, which are linked into chains *via* $[Ti_2O_2]^{4+}$ cations with Ti^{IV} in a strongly distorted octahedral environment.[8,9] These new compounds also represent the first PONb Keggin-type ions. In 2003, Nyman *et al.* described the synthesis of a dititanoniobate $[Ti_2Nb_8O_{28}]^{8-}$ anion containing compound for the first time.[10] A hydrothermal reaction of $Nb_2O_5 \cdot xH_2O$, $Ti(O^iPr)_4$, NaOH and $TMAOH \cdot 5H_2O$ yielded $Na_8[Ti_2Nb_8O_{28}] \cdot 34H_2O$. Its cluster anion exhibits the decaniobate $[Nb_{10}O_{28}]^{6-}$ geometry, where two interior Nb^V positions are substituted by Ti^{IV} ions. Molecular modeling of the possible isomers revealed that interior cluster positions are favored for substitution, suggesting that repulsion is minimized when the number of edges shared by TiO_6 octahedra is as large as possible. A few years later, the "missing link" between the $[Ti_2Nb_8O_{28}]^{8-}$ anion and $[Nb_{10}O_{28}]^{6-}$ – the monotitanoniobate anion – was reported.[11] The new compound $(TMA)_7[TiNb_9O_{28}] \cdot 22H_2O$ offered the opportunity for more systematic studies on the influence of substitution on the stability of the decametalate anions.

Integration of Ti into PONb cores may also lead to cluster geometries different from decametalates or Keggin geometry. Attempting to crystallize the monotitanoniobate salt, the $[Ti_{12}Nb_6O_{44}]^{10-}$ anion was discovered. This Lindqvist type

Institut für Anorganische Chemie, Christian-Albrechts-Universität zu Kiel, 24118 Kiel, Germany. E-mail: wbensch@ac.uni-kiel.de

†Electronic supplementary information (ESI) available: Crystal structure refinement results, geometric parameters, additional figures of the structures, XRD patterns, DTA-TG curves, and IR- and UV/Vis spectra. CCDC 1854782, 1854780 and 1854781. For ESI and crystallographic data in CIF or other electronic format see DOI: 10.1039/c8dt02835d

"superoctahedron" consists of edge sharing TiO_6 octahedra with NbO_5 units capping each face.[12] In the aspiring research on polyoxotantalates, upon Ti substitution the same cluster geometries are observed. Using a similar preparation procedure to Ti-PONbs, $[Ti_{12}Ta_6O_{44}]^{10-}$ and $[Ti_2Ta_8O_{28}]^{8-}$ anions were obtained.[13] The latter is stable in aqueous solution in contrast to the unsubstituted $[Ta_{10}O_{28}]^{6-}$ anion, which so far is accessible only in non-aqueous solutions[14] and, unlike in the PONb chemistry, could not even be detected with the aid of ESI-MS in titanometalate solutions.[13]

Until today, only a single report about a TM (TM = transition metal)-substituted titanoniobate is available, which was synthesized by reacting Cu^{2+} ions, ethylenediamine, titanium isopropoxide $Ti(O^iPr)_4$ and potassium hexaniobate $K_7HNb_6O_{19}{\cdot}13H_2O$ hydrothermally.[15] The compound $[Cu(en)_2][Cu(en)_2(H_2O)_2]_3[Ti_2Nb_8O_{28}]{\cdot}8H_2O$ (en = ethylenediamine) consists of isolated $[Ti_2Nb_8O_{28}]^{8-}$ clusters charge balanced by $[Cu(en)(H_2O)_2]^{2+}$ and $[Cu(en)_2]^{2+}$ molecules. This was a promising result, although the employment of other amine molecules or other TM cations did not lead to crystalline products under these reaction conditions.

Through the substitution of Nb^V ions for Ti^{IV}, the pH stability of decaniobate derivatives can be strongly affected, a phenomenon which was also observed for the titanotantalates.[13] As mentioned above, only the interior Nb^{5+} cations are substituted by Ti^{4+}. This results in the reduction of the formal charge on the μ_3-oxo sites, which are the key for the dissociation of $[Nb_{10}O_{28}]^{6-}$ to $[Nb_6O_{19}]^{8-}$ in basic media.[16,17] ^{17}O NMR experiments of aqueous solutions of dititanoniobate anions proved that the integration of Ti^{IV} leads to a stabilization of the molecule and inhibits the base-enhanced dissociation at higher pH values.[17] With the discovery of monotitanoniobate where only a single Nb^V is substituted,[11] a systematic study was possible and a similar effect was observed: the dissociation of the $[TiNb_9O_{28}]^{7-}$ anion takes place at pH $\geq$ 12,[18] while the $[Nb_{10}O_{28}]^{6-}$ anion starts to form $[Nb_6O_{19}]^{8-}$ already at pH $\geq$ 7.5.[19] For each ion, the pK_a values were determined, which increase with a higher substitution degree.[18] The experimentally determined pH-dependencies of oxygen exchange rates could be understood later by a theoretical approach.[20]

The chemical properties of PONbs may also be influenced *via* integration of TM complexes, but this approach still remains a challenge and as mentioned above, the examples are rare. Through their enhanced pH stability, titanoniobate clusters may be good candidates to introduce TM complexes into PONb clusters.

Herein, we present three new compounds composed of titanoniobate units, $\{[Ni(cyclam)]_4[Ti_2Nb_8O_{28}]\}_n{\cdot}{\sim}28nH_2O$ (**I**), $K[Ni(cyclam)]_3[TiNb_9O_{28}]{\cdot}18H_2O$ (**II**) and $K[Ni(cyclam)]_3[TiNb_9O_{28}]{\cdot}14H_2O$ (**III**) (cyclam = 1,4,8,11-tetraazacyclotetradecane). In addition to interesting structural features, *e.g.* arrangement of water molecules with different dimensionalities, these compounds and their syntheses possess several intriguing features:

(1) this is the first time that macrocyclic amine molecules and Ni^{2+} ions are incorporated into a titanoniobate network;

(2) compounds **II** and **III** are the first examples of inorganic–organic hybrids with $[TiNb_9O_{28}]^{7-}$ anions as central structural motifs;

(3) the choice of the titanium source influences

(a) the number of Ti^{4+} ions in the cluster;

(b) the geometry of the nickel complex present in the structure and the resulting color of the products; in compound **I**, *cis*- and *trans*-configured isomers coexist;

(4) the compounds are obtained within short reaction times and the reaction temperature influences the formation of compounds **II** and **III**.

Experimental section

Syntheses

All chemicals except $K_7HNb_6O_{19}{\cdot}13H_2O$ were purchased and used without further purification. (Nb_2O_5: abcr, 99.5% Nb; KOH: abcr, 85%; $Ni(NO_3)_2{\cdot}6H_2O$: Merck, >99%; 1,4,8,11-tetraazacyclotetradecane: Alfa Aesar, >98%; $Ti(O^iPr)_4$: Merck, 98%; $K_2TiO(C_2O_4){\cdot}2H_2O$: Sigma-Aldrich, 90%, $K_2C_2O_4{\cdot}H_2O$: Merck, 99%, $NaHCO_3$: Gruessing, 99%.) $K_7HNb_6O_{19}{\cdot}13H_2O$ was synthesized following a literature method.[21] Solid reactants were dispersed in 3 mL of distilled water. The pH value was adjusted with 1 M KOH. All reactions were carried out under hydrothermal conditions in DURAN® glass tubes with an inner volume of 11 mL.

Synthesis of $\{[Ni(cyclam)]_4[Ti_2Nb_8O_{28}]\}_n{\cdot}{\sim}28nH_2O$ (I)

0.2 mmol $K_7HNb_6O_{19}{\cdot}13H_2O$, 0.4 mmol $Ni(NO_3)_2{\cdot}6H_2O$ and 0.4 mmol 1,4,8,11-tetraazacyclotetradecane (cyclam) were dispersed in 3 mL H_2O. 0.034 mmol (0.1 mL) $Ti(O^iPr)_4$ was added and the slurry was thoroughly mixed. Afterwards, the pH was adjusted with 0.2 mL 1 M KOH to 12.2 (after reaction: ~10.7). The mixture was reacted at 130 °C for 24 h. Light violet crystals of **I** (Fig. S1a†) and colourless X-ray amorphous powder were obtained. Yield: ~40 mg (~83% based on Ti). $C_{40}H_{140}N_{16}Ni_4Nb_8Ti_2O_{50}$: calcd in %: C 17.00, H 5.42, N 7.93; found C 16.55, H 5.01, N 7.63. TG analysis gives a hint that approx. two water molecules may be emitted during sample preparation.

Synthesis of $K[Ni(cyclam)]_3[TiNb_9O_{28}]{\cdot}18H_2O$ (II)

The same method was applied as that for the synthesis of compound **I**, except that $Ti(O^iPr)_4$ was replaced by 0.034 mmol $K_2TiO(C_2O_4){\cdot}2H_2O$. After adding 0.2 mL 1 M KOH to the reaction mixture, the pH value was 11.3 (after reaction: ~9.5). The product crystallized as yellow block-like crystals (Fig. S1b†). Yield: 60 mg (71% based on Ti). $C_{30}H_{108}N_{16}Ni_3Nb_9TiO_{46}$: calcd in %: C 14.57, H 4.40, N 6.80; found C 14.67, H 4.40, N 6.87.

Synthesis of $K[Ni(cyclam)]_3[TiNb_9O_{28}]{\cdot}14H_2O$ (III)

A few single crystals of compound **III** were found in a batch of **II**. The product crystallized as yellow block-like crystals (Fig. S1c†). Yield: <1 mg (~1% based on Ti) under given reac-

tion conditions (see Results) $C_{30}H_{100}N_{16}Ni_3Nb_9TiO_{42}$: calcd in %: C 15.01, H 4.20, N 7.00; found C 15.10, H 4.30, N 7.17.

We note that all compounds are stable in air for several weeks.

Structure determination

Data collection was performed using a STOE Imaging Plate Diffraction System (IPDS-2) with MoKα (λ = 0.71073 Å) and for all compounds, a numerical absorption correction was performed. The structures were solved with the program SHELXS-97 [22] and refined was performed against F^2 using SHELXL-2014.[23] The details of data collection and of the structure refinements are summarized in Table S1.†

All non-hydrogen atoms were refined anisotropically. The C–H and N–H H atoms were positioned with idealized geometry and refined isotropically with $U_{iso}(H) = 1.2U_{eq}(C,N)$ using a riding model. The O–H H atoms were not located but considered in the calculation of the molecular formula and the molecular weight. In compound **I**, there is additional electron density indicating for disordered water molecules, for which no reasonable structure model was found. Therefore, the data were corrected for the disordered solvent using the Squeeze option in Platon.[24] During the SQUEEZE procedure, 140 electrons were collected. The accessible free space was calculated to be 360.5 Å^3 (7.6% of unit cell volume). One of the two cyclam ligands is disordered and was refined using a split model. In compound **II**, the Ti atom is located on the same position as Nb5 and both atoms were refined with an occupancy of 0.5. The position of the K^+ cation is only half occupied and the other half was assigned to disordered water. In this case the model agrees with elemental analysis and if the K^+ cation is refined with full occupancy much too large displacement parameters are obtained. The low reliability factors originate from a poor crystal quality and contributions of at least a second much smaller individual. This kind of twinning cannot be resolved. In compound **III**, Nb9/Ti9 and Nb10/Ti10 occupy the same crystallographic positions and were refined with occupancies of 0.75/0.25 as well as 0.25/0.75 using restraints (EXYZ and EADP). The K^+ cation is also disordered and was refined using a split model.

Several water O atoms were found in the structure of **III**; two positions are not fully occupied with s.o.f. = 0.4, two O atoms have an occupancy of 0.6 and two further O atoms 0.5. Ten positions of O atoms are fully occupied and one O atom (O47) is disordered with a ratio of 50 : 50, giving rise to about fourteen water molecules per formula unit.

CCDC 1854782 (**I**), CCDC 1854780 (**II**), and CCDC 1854781 (**III**) contain the supplementary crystallographic data for this paper.†

X-ray powder diffraction

Phase purity of the compounds was checked with X-ray powder diffraction patterns that were measured with Cu-Kα_1 radiation on a STOE Stadi-P diffractometer (Ge monochromator) with a Mythen 1 K detector (Fig. S2†).

Infrared spectroscopy

Infrared spectra were recorded on a Bruker Alpha-P IR spectrometer from 4000–400 cm^{-1} at room temperature.

Ultraviolet–visible spectroscopy

A UV/Vis two-channel spectrometer Cary 5 from Varian Techtron Pty was used to collect the UV/Vis reflection data using $BaSO_4$ as a white standard. The data were calculated with the Kubelka–Munk relation for diffuse reflectance data.[25]

Elemental analysis

Elemental analyses were performed on a EURO EA elemental analyzer (EURO VEKTOR).

Difference thermogravimetry (TG)

A Netzsch STA 409 CD was used to obtain the TG curves under N_2 flow with a heating rate of 4 K min^{-1}.

Results and discussion

Synthetic aspects

Recently, we used cyclam as a tetradentate ligand for the synthesis of TM-substituted PONbs, resulting in two novel compounds with $[Cu(cyclam)]^{2+}$ complexes as charge balancing agents.[26] Both compounds could be obtained in a short reaction time. Since the targeted integration of heteroatoms in the Cu^{2+}/cyclam/Nb^{5+} system was not yet successful, we replaced Cu^{2+} by Ni^{2+} ions as the TM source. Under similar reaction conditions to Cu–PONbs, we were able to prepare four novel titanoniobates $\{[Ni(cyclam)]_4[Ti_2Nb_8O_{28}]\}_n \cdot \sim 28nH_2O$ (**I**), $K[Ni(cyclam)]_3[TiNb_9O_{28}] \cdot xH_2O$ with x = 18 for **II**, x = 14 for **III** and $x \approx 10$ for **IV**. The first experiments were carried out with Ti(O^iPr)$_4$, which undergoes a hydrolysis in aqueous solution, forming ^{i}PrOH and titanium-oxo/hydroxo species.[27] On heating the reaction mixture solvothermally at 130 °C for 24 h, **I** was obtained from the orange-brown colored mother liquor as violet block shaped crystals (Fig. S1a†). Employing $K_2TiO(C_2O_4) \cdot 2H_2O$ and leaving all other reaction parameters constant, compound **II** was isolated as block-shaped yellow crystals (Scheme 1, Fig. S1b†).

When the red-violet colored mother liquor was evaporated, crystals of *cis*-$[Ni_2(cyclam)_2(ox)](NO_3)_2$ [28] were obtained. In a batch of **II**, a very small amount of **III** was found as yellow platelet-like crystals (Fig. S1c†). In order to improve the yield for further characterization, temperature dependent syntheses from 80 to 180 °C were performed, and fortunately, the yield of

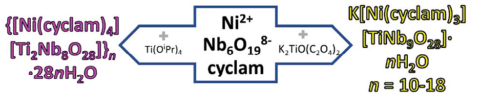

Scheme 1 Synthesis scheme for the preparation of the title compounds.

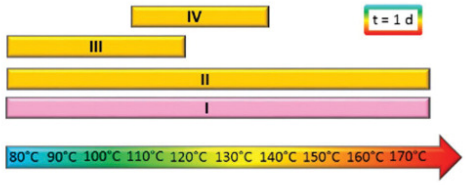

Scheme 2 Influence of the reaction temperature on the formation of compounds **II**–**IV**.

III could be increased to ~35 mg (~43%) at reaction temperatures of 110 °C and lower. During the temperature dependent investigations (Scheme 2), another type of yellow crystals (**IV**) was obtained as very thin yellow platelets (Fig. S1d†), which were not appropriate for single crystal structure analysis. All attempts to improve the crystal quality failed. The material was fully characterized and all analytical data indicate that **IV** is a pseudo-polymorph of the compounds **II** and **III** with the general formulae $K[Ni(cyclam)]_3[TiNb_9O_{28}]\cdot xH_2O$ with $x \approx 10$ for compound **IV**.‡

We want to note that compound **I** can also be isolated under stirring 'dynamic' conditions in comparable yields. Dynamic conditions also lead to formation of **II**, which crystallizes from the mother liquor, while **IV** can be recovered from the same reaction mixture directly by filtration. This demonstrates that dynamic conditions are beneficial not only for the efficient synthesis of iso- but also of heteropolyoxoniobates. Interestingly, the formation of **III** could not be observed on applying stirring conditions.

It is not yet clear why the formation of the dititanoniobate is favored when $Ti(O^iPr)_4$ is employed and the monotitanoniobate is dominating when $K_2TiO(C_2O_4)\cdot 2H_2O$ is applied. But it is not surprising that the formation depends on the change of a single reaction parameter, since in aqueous solutions of the $[TiNb_9O_{28}]^{7-}$ anion the $[Ti_2Nb_8O_{28}]^{8-}$ cluster is present as a byproduct.[11]

On reacting $Ti(O^iPr)_4$ and $K_2TiO(C_2O_4)\cdot 2H_2O$ simultaneously in equimolar proportion, solely the $[TiNb_9O_{28}]^{7-}$ containing compounds **II** and **IV** were obtained. The formation of the *cis*-$[Ni_2(cyclam)_2(ox)](NO_3)_2$ complex, which crystallizes as a by-product might influence different coordination environments of the Ni^{II} ion in compound **I** compared to compounds **II**–**IV**.

Carrying out the experiments using $Ti(O^iPr)_4$ as a source and $NaHCO_3$ as an additive (pH = 11.1), only compound **IV** crystallized.

To investigate whether the formation of the dititanoniobate (**I**) or the monotitanoniobate anions (**II**–**IV**) predominantly depend on the pH value, the syntheses were conducted at pH values ranging from 9 to 13. Applying $K_2TiO(C_2O_4)\cdot 2H_2O$ as the titanium source, only X-ray amorphous powders were obtained for pH = 12–13, while between 9 and 11 only the compounds with the monotitanoniobate anion are obtained. Using $Ti(O^iPr)_4$ as the reactant, at higher pH values the dititanoniobate compound **I** exclusively crystallized, whereas at lower pH values phase mixtures of the mono- and dititanoniobate compounds **I** and **II** are formed. From these results it is obvious that the formation of the mono- and dititanoniobate anions do not only depend on the actual pH value but also on the titanium source. Here we want to note that solvothermal reactions are complex and that changing one parameter inevitably leads to the alteration of all other parameters.

Since the presence of $C_2O_4^{2-}$ seems to influence the number of Ti^{4+} cations in the cluster, it is possible that these anions interact with niobate fragments. In the $[VNb_{12}O_{40}\{NbO(CO_3)\}_2]^{13-}$ and $[H_{10}Nb_{31}O_{93}(CO_3)]^{23-}$ anions, the carbonate ligands are coordinated to Nb^{5+} *via* two O^{2-} anions and the sevenfold coordination is completed by five O^{2-} anions of the PONb anion in the solid state.[29] Therefore, it is imaginable that such intermediates are present, leading to a preferred crystallization of one product with a distinct composition.

Further investigations on the influence of $C_2O_4^{2-}$ and other additives onto the formation of titanoniobates are underway.

Crystal structures

Crystal structure of $\{[Ni(cyclam)]_4[Ti_2Nb_8O_{28}]\}_n\cdot\sim 28nH_2O$ (I). The compound $\{[Ni(cyclam)]_4[Ti_2Nb_8O_{28}]\}_n\cdot 28nH_2O$ (**I**) crystallizes in the monoclinic space group *C*2/*m* with $Z = 2$. Ti1, O2, O8, Ni2, N11, N13, and four water O atoms lie on a crystallographic mirror plane. Two water O atoms (O7, O17) are located on the twofold rotational axis and the second crystallographically independent Ni^{2+} (Ni2) ion on a center of inversion. The main structural motif consists of a titanoniobate cluster anion, which is decorated by Ni^{2+} centered complexes (Fig. 1).

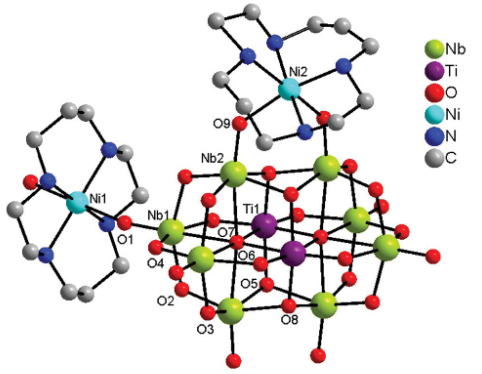

Fig. 1 Representation of the main structural motif in the structure of **I**. Only selected atoms are labeled. H atoms are omitted for clarity. Only one orientation of the disordered cyclam ligand is shown.

‡Analytical data; optical micrographs (Fig. S1†), XRD patterns (Fig. S2†), IR (Fig. S17†), UV/Vis (Fig. S21†) spectra and DTA-TG curves (Fig. S25†) can be found in the ESI.†

The anionic unit displays the Nyman-type cluster geometry $[Ti_2Nb_8O_{28}]^{8-}$ with Nb^{5+} and Ti^{4+} cations octahedrally coordinated by oxygen.[10] In analogy to the known decaniobate geometry,[30–33] three octahedra are connected *via* edge-sharing and these are attached to another trimer by sharing the edges, forming a 2 × 3 rectangle. The rectangle is capped by two edge-sharing octahedra at the top and the bottom, respectively. The results of bond valence sum (BVS) analysis are in line with oxidation states +5 for Nb, +4 for Ti, and +2 for Ni (Table S2†). The Nb=O_t (t = terminal), Nb-μ_2-O, Nb-μ_3-O and Nb-μ_6-O bonds (Table S3†) are in the range of 1.752(2)–1.768(2) Å, 1.924(2)–2.0213(19) Å, 2.0787(17)–2.0852(17) Å and 2.3829(3)–2.4305(19) Å, respectively, a bond length distribution that is known for other decaniobate compounds.[30–33] As expected, the TiO_6 octahedron has no terminal Ti=O bonds. Like in Ti-PONbs, Ti-POWs and Ti-POMos, terminal Ti=O bonds were not observed, and Ti^{4+} always prefers bonds to bridging O^{2-} anions, favouring positions with lower distortion.[10] This is in agreement with the structures of layered Ti^{IV}/Nb^{V} perovskite materials where Ti^{4+} octahedra are located in the interior slab sites.[34–37] The Ti-μ_2-O, Ti-μ_3-O and Ti-μ_6-O bond lengths are 1.812(2), 1.962(3)–1.983(3) and 2.1889(17) Å, respectively and show the general trend of increasing bond lengths with an increasing number of bridging oxygen atoms.[10] The O–Ti–O angles (Table S4†) demonstrate a severe deviation from ideal geometry (O–Ti–O: 80.93–167.86°). Compared to the two literature known $[Ti_2Nb_8O_{28}]^{8-}$ containing compounds $(Na_8[Ti_2Nb_8O_{28}]\cdot 34H_2O$[10] and $[Cu(en)_2][Cu(en)_2(H_2O)_2]_3[Ti_2Nb_8O_{28}]\cdot 8H_2O$[15]) there are some slight differences in certain bond lengths as displayed in Fig. S3† and summarized in Table S5.† These differences are most probably caused by the multiple coordinations of the $[Ni(cyclam)]^{2+}$ units. The M-μ_3-O (M = Ti/Nb) and the Nb-μ_6-O bond lengths are slightly shorter and the Ti-μ_6-O distances are longer than reported for the two other compounds.

The O–Nb–O angles are 75.75–178.15° for Nb1 and 74.87–171.08° for Nb2 (Table S4†), demonstrating a stronger distortion of the NbO_6 octahedra which share more edges with neighboring units. Charge compensation in compound **I** is achieved through four Ni^{2+} centered amine complexes per formula unit. The octahedral coordination sphere of the two unique Ni^{2+} ions is formed by the four N atoms of one cyclam molecule and two terminal O^{2-} anions of the $[Ti_2Nb_8O_{28}]^{8-}$ cluster.

Each $[Ti_2Nb_8O_{28}]^{8-}$ unit is decorated by two $[Ni(cyclam)]^{2+}$ molecules *via* two terminal cluster O atoms in the *cis*-position. The cyclam molecule is disordered over two positions in ratio 50 : 50 (Fig. 2a). The Ni–N and the Ni–O bond lengths are 2.058(7)–2.138(6) Å and 2.111(2) Å, respectively (Table S6†). The corresponding values for equatorial N–Ni–N/O angles are 83.7(2)–99.3(2)° and for the *trans* N–Ni–N/O angles are 168.8(2)–174.8(2)°, reflecting a significant distortion of the octahedral geometry. Besides the Ni(2)–N(12/13) bond lengths which are shorter (2.058(7)–2.080(5) Å) than most of the reported values but not unprecedented in complexes,[28,38–41] all geometrical parameters are in good agreement with those in similar complexes with *cis*-configured cyclam molecules, *e.g.* $[Ni_2(C_2O_4)(cyclam)_2](ClO_4)_2$.[39] The anionic cluster is further expanded by four *trans*-$[Ni(cyclam)]^{2+}$ cations, where the O atoms of two neighboring clusters occupy the vertices of Ni^{2+} centered octahedra with cyclam N-donors in axial positions (Fig. 2b). The Ni–N and the Ni–O distances (Table 1) match well with the literature data.[42–44] The equatorial N–Ni–N/O angles scatter between 85.81(12)–94.19(12)° and the *trans* N–Ni–N/O angles are 180.00°, being closer to ideal octahedral geometry compared to the complex discussed above.

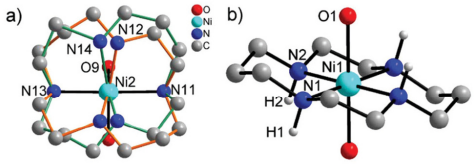

Fig. 2 Coordination spheres around the two crystallographically independent Ni^{2+} ions in the structure of **I**. The disorder of the cyclam ligand coordinated to Ni2 is indicated by orange and green lines (left).

Table 1 Comparison of the geometrical parameters of the two crystallographically independent $[Ni(cyclam)]^{2+}$ complexes in the structure of **I**

Type of bond /angle	*trans*-$[Ni(cyclam)]^{2+}$	*cis*-$[Ni(cyclam)]^{2+}$
Ni–N/Å	2.062(3)–2.073(3)	2.058(7)–2.138(6)
Ni–O/Å	2.087(2) Å	2.111(2)
eq. N–Ni–N/O/°	85.81(12)–94.19(12)°	83.7(2)–99.3(2)°
trans N–Ni–N/O/°	180.00°	168.8(2)–174.8(2)°

It is unusual that the disordered cyclam molecule coordinated to Ni2 adopts *cis*-configuration, while the cyclam molecule surrounding Ni1 exhibits a *trans*-configuration, which is the most common configuration for metal cation centered cyclam complexes.[45] The coexistence of *cis*- and *trans*-isomers in the solid state is rare and was reported only for $[Ni_2(cyclam)_2(\mu_3\text{-}C_2O_4)]\cdot(ClO_4)_2\cdot H_2O$.[40]

Overall, each $[Ti_2Nb_8O_{28}]^{8-}$ unit is connected to four *trans*-$[Ni(cyclam)]^{2+}$ and two *cis*-$[Ni(cyclam)]^{2+}$ cations and may be viewed as a hexadentate ligand for the complexes. The *trans*-$[Ni(cyclam)]^{2+}$ moieties connect the anionic clusters in the *ab* plane into layers (Fig. S4†). The layers are separated by the *cis*-$[Ni(cyclam)]^{2+}$ complexes, which are arranged in a wave-like manner (Fig. 3).

H-bonding interactions are observed, which may explain some structural peculiarities (Table S7†). The Nb(2)–O(9)–Ni(2) angle is 134.04(12)° and significantly differs from the ideal value of 180°. This can be explained with the presence of H-bonds between the N–H and C–H atoms of the cyclam molecule and Nb-μ_2-O bridging atoms (N–H···O = 2.953(5) Å; < (NHO) = 146.3°; C–H···O = 3.391(17) Å; <(CHO) = 163.8°) which lead to a tilting of the *cis*-$[Ni(cyclam)]^{2+}$ complex relative to the anion (Fig. S5a†). Furthermore, a crystal H_2O molecule located near the amine molecule is also involved in H-bonding with

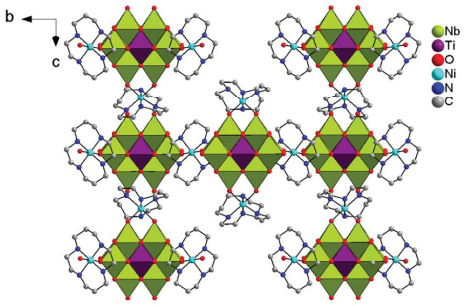

Fig. 3 View of the layers in the structure of **I** along [100]. H and water O atoms are omitted for clarity. Only one orientation of the disordered cyclam ligand is shown. Green polyhedra: NbO_6, violet polyhedra: TiO_6.

the N–H H atoms, additionally stabilizing the folded geometry of the cyclam ligand (Fig. S5b†), (N–H···O = 3.114(7)–3.122(7) Å; <(NHO) = 161.3–167.3°). The tilting in the second unique *trans*-$[Ni(cyclam)]^{2+}$ cation is less pronounced (Nb(1)–O(1)–Ni (1): 166.26(13)°) and only C–H groups are involved in H-bonding (Fig. S5c†), (C–H···O = 3.160(4) Å–3.553(4) Å; <(CHO) = 112.5–169.0°). One N–H H atom of the *trans*-configured cyclam molecule interacts with a crystal water molecule (N–H···O = 3.147(4) Å; <(NHO) = 155.6°).

Single crystal structure analysis revealed that there are 22 water molecules per formula unit in the structure of **I**. The water H atoms could not be located, but the water O atoms (O···O-distances up to the sum of the van der Waals radii: 3.05 Å, Table S8†) show an unusual arrangement. Following the notation of Infantes *et al.*,[46,47] the H_2O molecules form a L4(2)4(4)28(14) wallpaper-like layer-type water cluster, *i.e.* there are four-membered rings which share water molecules with two adjacent rings, a second type of four-membered ring surrounded by four other rings and 28-membered rings enclosed with 14 rings (Fig. 4). Bucket-like 4-membered fragments decorate the 4(4) rings (Fig. S6†). In the 28-membered rings, the $[Ti_2Nb_8O_{28}]^{8-}$ anions are located, whereas the *cis*-$[Ni(cyclam)]^{2+}$ molecules are located in the plane formed by the rings (Fig. S7a†), and the *trans*-$[Ni(cyclam)]^{2+}$ molecules are found below and above these planes (Fig. S7b†).

Crystal structures of $K[Ni(cyclam)]_3[TiNb_9O_{28}]\cdot 18H_2O$ (II) and $K[Ni(cyclam)]_3[TiNb_9O_{28}]\cdot 14H_2O$ (III). $K[Ni(cyclam)]_3[TiNb_9O_{28}]\cdot 18H_2O$ (**II**) crystallizes in the monoclinic space group *C*2/*c* with four formula units in the unit cell. All atoms except the central Ti/Nb cations, the K^+ cation and a H_2O molecule are located at general positions. In the decaniobate cluster one Nb^{5+} cation is replaced by a Ti^{4+} ion (Fig. 5).

Similar to compound **I** and other titanoniobates, the Ti^{4+} cation is located on an interior position of the anion, and in **II** these positions are occupied with 50% Ti and 50% Nb. For Nb and Ni, BVS provides oxidation states of +5 and +2, respectively. To calculate the BVS for Ti and Nb on the sites with mixed occupancy, the R_0 values were weighted according to the

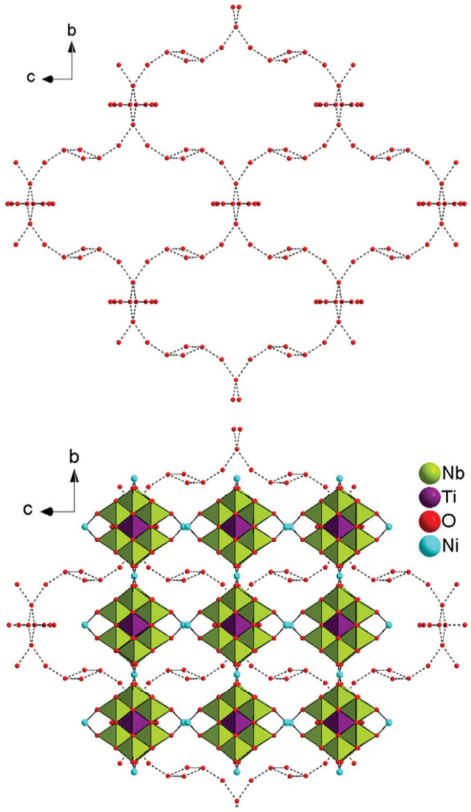

Fig. 4 Arrangement of the crystal water molecules building a L4(2)4(4)28(14) type cluster in the structure of **I** (top, H-bonds dashed lines), and location of the anions (bottom). C, N and H atoms are not displayed for clarity. Green: NbO_6, violet: TiO_6.

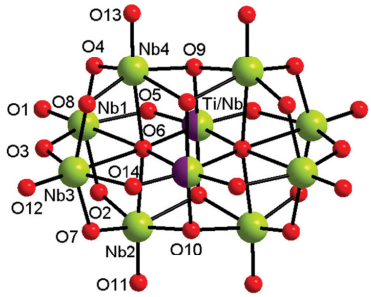

Fig. 5 View of the anionic cluster in the structure of compound **II**.

occupation factor leading to 4.52 (Table S2†), in accordance with the average oxidation state for Ti^{IV} and Nb^{V} on the interior position. The Nb–O bond lengths in the $[TiNb_9O_{28}]^{7-}$ anion are 1.741(6)–1.763(4) Å for Nb=O_t, 1.905(4)–2.068(4) Å for Nb-μ_2-O, 2.098(4)–2.116(4) Å for Nb-μ_3-O and 2.390(4)–2.496(4) Å for Nb-μ_6-O (Table S9†) and agree with the data for decaniobates.[31] The Ti–/Nb–O bonds with values of 1.815(4)–1.827(4) Å for μ_2- and 1.992(4)–1.999(4) Å for μ_3-O atoms differ only slightly from other $[TiNb_9O_{28}]^{7-}$ cluster containing compounds (Table S10†)[11] with Ti/Nb-μ_6-O bonds with 2.191(4)–2.208(4) Å matching the reported data. The O–Nb–O angles are comparable to that observed for **I**. The negative charge of $[TiNb_9O_{28}]^{7-}$ is compensated through three $[Ni(cyclam)]^{2+}$ complexes and a K^+ cation. In contrast to compound **I**, the two crystallographically independent Ni^{2+} ions are in a square-planar coordination of four N atoms of the cyclam molecule (Fig. S8†). The nearest possible axial ligands are cluster O^{2-} anions at 3.534(4) and 3.669(4) Å, which are too far away for bonding interactions. The Ni–N bonds (1.923(6)–1.941(6) Å) are significantly shorter than those in **I**, but are in agreement with the data reported for low-spin Ni^{II} amine complexes.[38,41,48–51] The angles around Ni^{2+} (Table S11†) are typical of square-planar $[Ni(cyclam)]^{2+}$ moieties.[38,41,48,50–52]

Each $[TiNb_9O_{28}]^{7-}$ anion is surrounded by six $[Ni(cyclam)]^{2+}$ molecules (Fig. S9†), yielding a layer-like arrangement (Fig. 6).

The K^+ cation is surrounded by five H_2O molecules and two terminal O atoms of the anion, leading to the coordination number (CN) 7 (Fig. S10a†). The K–O distances scatter from 2.734(12) to 3.054(8) Å (Table S12,† average: 2.874 Å), and are partially longer than expected (2.81–2.84 Å,[53] depending on CN) but they are not unusual.[54] The KO_7 polyhedra share no atoms with each other and are arranged in a wave-like fashion along [010] (Fig. 7, Fig. S11†).

The C–H and N–H H atoms of the cyclam ligands are involved in intermolecular H bonding interactions with cluster O atoms (Table S13, Fig. S12†). (N–H···O = 2.828(7) Å–3.238(8) Å; C–H···O − 3.194(9)–3.574(9) Å; <(NHO) − 143.1–170.4°; <(CHO) = 131.2–165.0°). Furthermore, H_2O also exhibits hydrogen bonding interactions with ligand C–H H atoms (C–H···O = 3.23(1) Å–3.595(9) Å; <(CHO) = 122.7–163.1°).

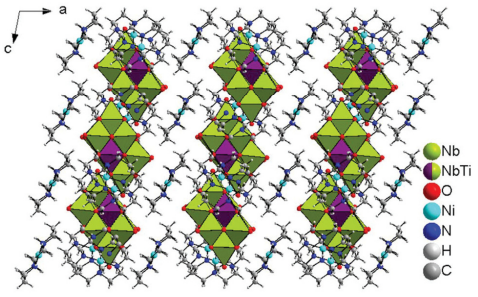

Fig. 6 Arrangement of the $[TiNb_9O_{28}]^{7-}$ anions and $[Ni(cyclam)]^{2+}$ cations in the structure of compound **II**. Green polyhedra: NbO_6, violet polyhedra: TiO_6.

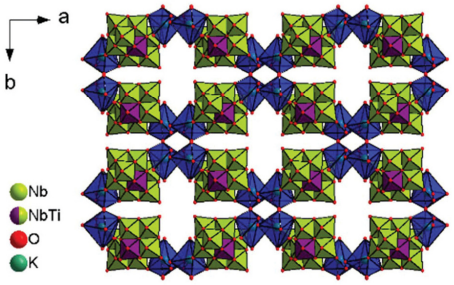

Fig. 7 Arrangement of the KO_7 polyhedra (blue) and $[TiNb_9O_{28}]^{7-}$ anions in the structure of **II**. The $[Ni(cyclam)]^{2+}$ cations and water O atoms which are not involved in K–O interactions are omitted. Green: NbO_6, violet: Ti/NbO_6, blue: KO_7 polyhedra.

The water O atoms in the structure of **II** form a layered cluster and considering only fully occupied water O atom positions, a L5(4)L30(18) type cluster along [010] can be identified (Fig. S13a†). Eight fragments consisting of two O atoms decorate each 30-membered ring. The layers are connected along the *b* axis *via* two H_2O molecules (Fig. 13b†), forming a 3-dimensional network (Fig. S14†).

Because **II** and **III** are pseudopolymorphs, mainly the structural differences of $K[Ni(cyclam)]_3[TiNb_9O_{28}]\cdot 18H_2O$ (**III**) compared to **II** are discussed. Compound **III** crystallizes in the triclinic space group $P\bar{1}$ with two formula units in the unit cell. All atoms except Ni3 and Ni4 are located at general positions. In analogy to **II**, the Ti^{4+} and Nb^{5+} ions in the interior position of the $[TiNb_9O_{28}]^{7-}$ anion are disordered over the same crystallographic position, but with a different site occupancy of 25% (Ti9/Nb10)/75%(Nb9/Ti10). The K^+ cation is disordered over two positions with a 60 : 40 occupancy. Each of the K^+ cations is in a different coordination environment of H_2O and cluster-μ_2-O atoms. Using a cut-off at 3.2 Å for K–O interactions, K^+ (60% occupancy) is surrounded by six H_2O molecules and two O^{2-} anions and two symmetry related face-sharing KO_8 polyhedra are linked with two $[TiNb_9O_{28}]^{7-}$ anions (Fig. 8, top). The second K^+ cation (s.o.f. = 0.4) is coordinated by six H_2O molecules, building distorted edge-sharing octahedra (Fig. 8, bottom). Geometric parameters for the KO_x (x = 8, 6), for the $[Ni(cyclam)]^{2+}$ cations and the hydrogen bonding interactions are listed in Tables S12 and S14.†

Considering only fully occupied water O atoms (O–O distances: 2.698–3.038 Å (Table S8,† average: 2.791 Å), hexameric isolated R6 water clusters are found. Taking into account cluster O atoms being involved in H bonds, an extended water motif is formed (Fig. 9). Two adjacent cluster anions are linked *via* two water molecules along the *c* axis, which interact with terminal cluster O atoms building a four-membered ring. A second arrangement of H_2O molecules and cluster O atoms connect the anions along the *a* axis, which may be denoted as

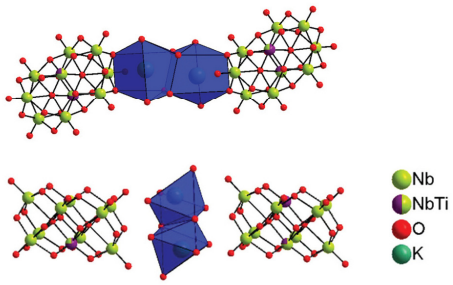

Fig. 8 Different coordination environments of the disordered K^+ cation in the structure of III; s.o.f = 0.6 (top), 0.4 (bottom) and the arrangement of the resulting K–O polyhedra (blue).

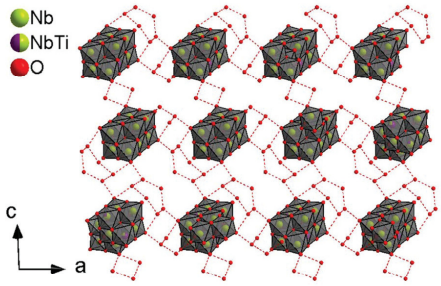

Fig. 9 View on the extended water motif along [010] in the structure of III. O–O distances below the sum of the van der Waals radii shown in dashed lines. For clarity, the $[Ni(cyclam)]^{2+}$ and K^+ cations are not shown. Grey polyhedra: Ti/NbO_6.

R6(2), *i.e.* there are five hexameric rings which share two O atoms with adjacent rings (Fig. S15†) and are attached to the clusters *via* a H_2O molecule.

Spectroscopic investigations

In the IR spectrum of each compound (Fig. S16–19†), characteristic absorptions of the organic ligands are observed between 3250 and 1000 cm^{-1} (Table S15†). The O–H stretching vibrations of the crystal water molecules appear as very broad bands in the characteristic region at 3600–3300 cm^{-1}.[55] Below 1000 cm^{-1}, a definite assignment of the signals is difficult because the N–H and macrocyclic deformation vibrations occur in the same region as that of the Nb–O vibrations. The $Nb–O_t$ absorptions are found at 965, 885 and 857 cm^{-1} for **I**, 880 and 864 cm^{-1} for **II** and 876 and 857 cm^{-1} for **III**. The bands below 800 cm^{-1} are most probably caused by bridging $M–O_b–M$ (M = Ti, Nb) vibrations.

In the UV/Vis spectrum of compound **I**, the characteristic transitions of high-spin octahedral Ni^{2+} complexes are observed (Fig. S20†). The bands at 354, 554 and 889 nm can be assigned to the $^3A_{2g} \rightarrow {}^3T_{1g}(^3P)$, $^3A_{2g} \rightarrow {}^3T_{1g}(^3F)$ and $^3A_{2g} \rightarrow {}^3T_{2g}$ d–d transitions, respectively.[28,56,57] The signal at 308 nm is most probably the O → Nb CT transition, which is typically observed between 200 and 300 nm.[7,58–61] But this band is missing in the absorption spectra of compounds **II** and **III** and in the UV/Vis spectrum of the copper ethylenediamine salt of the $[Ti_2Nb_8O_{28}]^{8-}$ anion.[15] Therefore, we assume that the band arises from splitting of the $^3A_{2g} \rightarrow {}^3T_{1g}(^3P)$ d–d transition due to the different coordination geometries of the $[Ni(cyclam)]^{2+}$ complexes.

In the UV/Vis spectra of **II–IV**, a single broad band around 455 nm is observed (Fig. S21–23†), which is in accordance with the yellow color of the compounds. This band is most probably caused by the d–d transition in the low-spin square-planar $[Ni(cyclam)]^{2+}$ complex.[48]

Thermoanalytical investigations and dehydration experiments

Compound **I** decomposes in at least two steps (Fig. S24†). The first mass loss of ~17% is accompanied by an endothermic signal at a peak temperature (T_p) of 76 °C and can be assigned to the emission of crystal water molecules (calcd 17.8%). A plateau is observed ranging from ~110 to 180 °C, followed by successive decomposition steps. From ~200 to 630 °C, the mass loss of ~30% may be explained by the emission of the cyclam molecules (calcd 28.4%). In the DTA curve, two exothermic signals are observed at T_p ~ 250 °C and ~460 °C (Fig. S24a†). Beyond 650 °C, no significant mass loss occurs and the yellow residue recovered after heating the sample to 1000 °C was identified as a mixture of $NiTiNb_2O_8$ and $Ni_{0.5}Ti_{0.5}NbO_4$. The occurrence of exothermic signals during the decomposition of the sample under an inert atmosphere was unexpected. For TG measurements, the sample chamber is flushed with dry N_2. To avoid the desorption of crystal H_2O molecules, the chamber was not evacuated prior to the measurement. The residual moisture or air impurities may lead to chemical reactions when decomposing sensitive samples. We repeated the experiment thoroughly evacuating the chamber and in the resulting DTA curve, only a single endothermic event at T_p = 381 °C is present (Fig. S24b†). The decomposition steps are not well resolved. The first mass loss until 200 °C of ~6.2% may be assigned to the residual crystal H_2O molecules. The following steps from 200 to 900 °C are accompanied by a mass loss of ~33%, but the decomposition is not finished at 1000 °C. In the XRDP (X-ray diffraction pattern) of the black powder that was recovered after heating of **I** to 1000 °C, most reflections are assignable to Ni and $Ni_{0.5}Ti_{0.5}NbO_4$.

In the DTA-TG curves of **II** the first thermal event is finished at about 200 °C (Fig. S25†) and the mass loss of 13.1% is in excellent agreement with the removal of crystal water molecules (calcd 13.1%). The DTG and DTA (two endothermic events, T_p = 89, 126 °C) curves show that the dehydration process occurs in two not well resolved steps. A distinct plateau is observed after the removal of the H_2O molecules followed by the next thermal reaction starting at about 270 °C which is accompanied by an endothermic signal in the DTA

curve at T_p = 393 °C. Upon further heating, the compound decomposes in at least two steps and the thermal reaction is not finished at 1000 °C. From 270 to 900 °C the mass loss of 24.0% may be explained by the emission of the cyclam molecules (calcd 24.3%), and the dark-green residue contains $NiTiNb_2O_8$, $(NiNb_2O_6)_{0.6667}$ and NiO but we note that not all reflections could be assigned.

The TG curve of **III** is similar to that of **II** (Fig. S26†) with two not well resolved thermal events between 50 °C and ~200 °C, where the mass loss of 10.5% is most likely caused by removal of the crystal H_2O molecules (calcd for $14H_2O$ = 10.5%). The mass loss is accompanied by a peak at T_p = 96 °C and a second signal with low intensity at T_p = 134 °C. The following endothermic decomposition step (T_p = 400 °C) starts at ~300 °C and ends at ~550 °C (Δm = −10.5%). A further mass decrease is observed between 600 and 900 °C (16.3%), but the thermal decomposition is not finished at the highest temperature of 1000 °C. The overall mass loss of 26.8% between 300 and 900 °C is in good agreement with the removal of the cyclam molecules (calcd 25.0%). In the XRDP of the dark green residue obtained after heating to 1000 °C, most reflections could be assigned to $NiTiNb_2O_8$, $Ni_{0.5}Ti_{0.5}NbO_4$ and Nb_2O_5.

The TG curve of compound **IV** exhibits a mass loss of 8.2% caused by the removal of about $11H_2O$ molecules (calcd 8.4%) (Fig. S27†). The thermal reaction is accompanied by an endothermal signal at T_p = 138 °C. The second endothermic event (T_p = 394 °C) and the third decomposition step from 600 °C to ~900 °C lead to an overall mass loss of 27.5%, indicating the removal of the cyclam molecules (calcd 25.6%). In analogy to **II** and **III**, the decomposition is not finished at 1000 °C. The XRDP of the residue contains reflections of $Ti_{0.67}Nb_{1.33}O_4$, TiO_2 and NiO.

In the TG curves of the title compounds, distinct plateaus occur after dehydration. This encouraged us to stop the decomposition after water removal and investigate whether the crystal structure is affected and if rehydration recovers the starting material.

For **I** the decomposition was stopped at 160 °C and the color turned from violet to brownish. The XRDP of the dehydrated material differs significantly from that of the as-synthesized samples and demonstrates that the water free compound exhibits a reasonable good crystallinity after H_2O removal (Fig. S28†). Immersing the sample in H_2O leads to a brownish material exhibiting a similar powder pattern to **I** before dehydration, but with broader and low intensity reflections typical of a reduced crystallinity.

In the XRDP of the dark yellow colored material obtained after heating compound **II** to 250 °C, only three very broad reflections are observed (Fig. S29†). After stirring the sample in H_2O, the XRDP matches well with that of the as-synthesized material demonstrating the reversibility of the water removal. Compound **III** was heated to 250 °C that led to partial decomposition of the sample, which is indicated by XRDP measurements, that shows only two not well resolved broad reflections between 6 and 8° 2θ, respectively, as well as two reflections of weaker intensity at ~10° 2θ (Fig. S30†). In the XRDP of the recovered material after H_2O treatment, a few reflections of low intensity are present between 6 and 10° 2θ, which do not match with reflections of the starting material, *i.e.* the dehydration seems to be not reversible. The XRDP of dehydrated compound **IV** is dominated by three broad and intense reflections. Interestingly, the XRD pattern of a dehydrated sample of compound **IV** shows some similarity to that of compound **II** (Fig. S31†). After recovering the sample treated in water, the XRDP shows a good crystallinity, but the reflections can be clearly assigned to compound **II**.

On storing the samples at room-temperature, no removal of water could be observed, which might be explained by the pronounced hydrogen bonding network between the crystal H_2O molecules forming water clusters, several H-bonding interactions between cyclam molecules and water or cluster O^{2-} anions and close $K–O_{cluster}$ distances.

pH value stability investigations

To estimate the pH stabilities of the compounds, samples of **I** and **II** were immersed for 24 h in an aqueous solution of HCl or KOH at defined pH values. The powder XRD patterns of the samples (Fig. S32 and S33†) indicate that compound **I** is stable between pH 2 and 13. At pH = 14, the compound starts to decompose, clearly visible by the appearance of additional reflections. For compound **II**, a pH stability window from 2 to 13 was determined, while at pH = 14 the reflections start to diminish indicating decomposition. For pH < 2 both compounds decompose to form X-ray amorphous materials. Summarizing, the compounds exhibit good pH stability from pH = 2 to pH = 13.

Conclusion

Employing $[Ni(cyclam)]^{2+}$ cations for charge compensation, we synthesized four novel titanoniobates with Ni^{II} in two different spin states and different degrees of substitution of Nb^{V} for Ti^{IV}. These are the first titanoniobates with Ni^{2+}-centered amine complexes and the first transition metal expanded monotitanoniobates. The anions are derivatives of the $[Nb_{10}O_{28}]^{6-}$ decaniobate anion, where one or both interior Nb^{V} positions are substituted with Ti^{IV}, yielding the dititanoniobate $[Ti_2Nb_8O_{28}]^{8-}$ or monotitanoniobate $[TiNb_9O_{28}]^{7-}$ anion. In compound **I**, the Ni^{2+} cation of the $[Ni(cyclam)O_2]^{2-}$ complex is in a high-spin state. The O^{2-} anions occupy both the *trans*- and the *cis*-positions in the two crystallographically independent complexes, which is very rare. In compounds **II–IV**, a low-spin square-planar coordinated $[Ni(cyclam)]^{2+}$ cation is present. The different spin states of the Ni^{2+} centers lead to different electronic transitions in the UV/Vis spectra and result in the different colors of the compounds. In the structure of the title compounds the crystal water molecules are joined by H-bonds yielding patterns of different dimensionalities.

Beyond the interesting structural characteristics, the product formation can be controlled to a certain extent.

Employing $Ti(O^iPr)_4$ as a titanium source, $\{[Ni(cyclam)]_4[Ti_2Nb_8O_{28}]\}_n \cdot \sim 28nH_2O$ (**I**) with octahedrally coordinated Ni^{2+} and a disubstituted anion is obtained, while the usage of $K_2TiO(C_2O_4)\cdot 2H_2O$ leads to $K[Ni(cyclam)]_3[TiNb_9O_{28}]\cdot xH_2O$ (**II–IV**) with a square planar environment around Ni^{2+} and the monosubstituted anion. Further experiments demonstrated that the oxalate anion plays a crucial role in the preferential crystallization of one distinct compound.

The substitution of Nb^V for Ti^{IV} leads to an enhanced stability of the PONb anions in a wider range of the pH scale, extending the working pH range for future applications. The good pH stability of the compounds presented here was demonstrated with XRD experiments.

Therefore, the study presented here contributes to the systematic evaluation of the parameters that influence the formation of such compounds, which is the key for the efficient design of novel multifunctional materials.

Conflicts of interest

There are no conflicts to declare.

Acknowledgements

This work was supported by the State of Schleswig-Holstein. The authors thank Lisa K. Mahnke for her kind support with the TOC graphic.

References

1 (*a*) K. Thompson, *Coord. Chem. Rev.*, 2001, **219–221**, 1033–1053; (*b*) C. Streb, *Dalton Trans.*, 2012, **41**, 1651–1659; (*c*) K. V. Rao, P. S. N. Rao, P. Nagaraju, P. S. Prasad and N. Lingaiah, *J. Mol. Catal. A: Chem.*, 2009, **303**, 84–89; (*d*) A. Ogata, H. Yanagie, E. Ishikawa, Y. Morishita, S. Mitsui, A. Yamashita, K. Hasumi, S. Takamoto, T. Yamase and M. Eriguchi, *Br. J. Cancer*, 2008, **98**, 399–409; (*e*) D.-L. Long, R. Tsunashima and L. Cronin, *Angew. Chem., Int. Ed.*, 2010, **49**, 1736–1758; (*f*) D. E. Katsoulis, *Chem. Rev.*, 1998, **98**, 359–388; (*g*) C. L. Hill, *J. Mol. Catal. A: Chem.*, 2007, **262**, 2–6; (*h*) A. Bijelic, M. Aureliano and A. Rompel, *Chem. Commun.*, 2018, **54**, 1153–1169; (*i*) S. Herrmann, C. Ritchie and C. Streb, *Dalton Trans.*, 2015, **44**, 7092–7104.

2 (*a*) M. Nyman, *Dalton Trans.*, 2011, **40**, 8049–8058; (*b*) M. Nyman and P. C. Burns, *Chem. Soc. Rev.*, 2012, **41**, 7354–7367; (*c*) B. W. Dale, J. M. Buckley and M. T. Pope, *J. Chem. Soc. A*, 1969, 301–304.

3 M. Nyman, J. P. Larentzos, E. J. Maginn, M. E. Welk, D. Ingersoll, H. Park, J. B. Parise, I. Bull and F. Bonhomme, *Inorg. Chem.*, 2007, **46**, 2067–2079.

4 M. Nyman, F. Bonhomme, T. M. Alam, J. B. Parise and G. M. B. Vaughan, *Angew. Chem., Int. Ed.*, 2004, **43**, 2787–2792.

5 Z. Liang, D. Zhang, H. Wang, P. Ma, Z. Yang, J. Niu and J. Wang, *Dalton Trans.*, 2016, **45**, 16173–16176.

6 Y.-T. Zhang, C. Qin, X.-L. Wang, P. Huang, B.-Q. Song, K.-Z. Shao and Z.-M. Su, *Inorg. Chem.*, 2015, **54**, 11083–11087.

7 S. Chen, P. Ma, H. Luo, Y. Wang, J. Niu and J. Wang, *Chem. Commun.*, 2017, **53**, 3709–3712.

8 M. Nyman, F. Bonhomme, T. M. Alam, M. A. Rodriguez, B. R. Cherry, J. L. Krumhansl, T. M. Nenoff and A. M. Sattler, *Science*, 2002, **297**, 996–998.

9 F. Bonhomme, J. P. Larentzos, T. M. Alam, E. J. Maginn and M. Nyman, *Inorg. Chem.*, 2005, **44**, 1774–1785.

10 M. Nyman, L. J. Criscenti, F. Bonhomme, M. A. Rodriguez and R. T. Cygan, *J. Solid State Chem.*, 2003, **176**, 111–119.

11 C. A. Ohlin, E. M. Villa, J. C. Fettinger and W. H. Casey, *Dalton Trans.*, 2009, 2677–2678.

12 C. A. Ohlin, E. M. Villa, J. C. Fettinger and W. H. Casey, *Angew. Chem., Int. Ed.*, 2008, **120**, 5716–5718.

13 J.-H. Son and W. H. Casey, *Chem. – Eur. J.*, 2016, **22**, 14155–14157.

14 M. Matsumoto, Y. Ozawa, A. Yagasaki and Y. Zhe, *Inorg. Chem.*, 2013, **52**, 7825–7827.

15 Y.-T. Zhang, P. Huang, C. Qin, L.-K. Yan, B.-Q. Song, Z.-X. Yang, K.-Z. Shao and Z.-M. Su, *Dalton Trans.*, 2014, **43**, 9847–9850.

16 E. M. Villa, C. A. Ohlin, E. Balogh, T. M. Anderson, M. D. Nyman and W. H. Casey, *Angew. Chem., Int. Ed.*, 2008, **120**, 4922–4924.

17 E. M. Villa, C. A. Ohlin, J. R. Rustad and W. H. Casey, *J. Am. Chem. Soc.*, 2009, **131**, 16488–16492.

18 E. M. Villa, C. A. Ohlin and W. H. Casey, *J. Am. Chem. Soc.*, 2010, **132**, 5264–5272.

19 E. M. Villa, C. A. Ohlin, E. Balogh, T. M. Anderson, M. Nyman and W. H. Casey, *Angew. Chem., Int. Ed.*, 2008, **120**, 4922–4924.

20 J. R. Rustad and W. H. Casey, *Nat. Mater.*, 2012, **11**, 223–226.

21 M. Filowitz, R. K. C. Ho, W. G. Klemperer and W. Shum, *Inorg. Chem.*, 1979, **18**, 93–103.

22 G. M. Sheldrick, *SHELXS-97: Program for the Solution of Crystal Structures*, University of Goettingen, Goettingen, 1997.

23 G. M. Sheldrick, *SHELXL-2014: Program for the Refinement of Crystal Structures*, University of Goettingen, Goettingen, 2014.

24 A. L. Spek, *Acta Crystallogr., Sect. C: Struct. Chem.*, 2015, **71**, 9–18.

25 G. Kortüm, W. Braun and G. Herzog, *Angew. Chem., Int. Ed.*, 1963, **75**, 653–661.

26 J. Dopta, D.-C. Krause, C. Näther and W. Bensch, *Cryst. Growth Des.*, 2018, 4130–4139.

27 U. Schubert, *J. Mater. Chem.*, 2005, **15**, 3701–3715.

28 L. P. Battaglia, A. Bianchi, A. B. Corradi, E. Garcia-España, M. Micheloni and M. Julve, *Inorg. Chem.*, 1988, 4174–4179.

29 (*a*) P. A. Abramov, A. T. Davletgildeeva, N. K. Moroz, N. B. Kompankov, B. Santiago-Schübel and M. N. Sokolov, *Inorg. Chem.*, 2016, **55**, 12807–12814; (*b*) R. Tsunashima, D.-L. Long, H. N. Miras, D. Gabb, C. P. Pradeep and L. Cronin, *Angew. Chem., Int. Ed.*, 2010, **122**, 117–120.
30 L. Shen, C.-H. Li, Y.-N. Chi and C.-W. Hu, *Inorg. Chem. Commun.*, 2008, **11**, 992–994.
31 J. Niu, G. Wang, J. Zhao, Y. Sui, P. Ma and J. Wang, *Cryst. Growth Des.*, 2011, **11**, 1253–1261.
32 E. J. Graeber and B. Morosin, *Acta Crystallogr., Sect. B: Struct. Crystallogr. Cryst. Chem.*, 1977, 2137–2143.
33 M. Matsumoto, Y. Ozawa and A. Yagasaki, *Polyhedron*, 2010, 2196–2201.
34 A. R. Drews, W. Wong-Ng, T. A. Vanderah and R. S. Roth, *J. Alloys Compd.*, 1997, 243–247.
35 A. R. Drews, W. Wong-Ng, R. S. Roth and T. A. Vanderah, *Mater. Res. Bull.*, 1996, **31**, 153–162.
36 J. Gopalakrishnan, S. Uma and V. Bhat, *Chem. Mater.*, 1993, 132–136.
37 Y.-S. Hong, S.-J. Kim, S.-J. Kim and J.-H. Choy, *J. Mater. Chem.*, 2000, **10**, 1209–1214.
38 E. K. Barefield, A. Bianchi, E. J. Billo, P. J. Connolly, P. Paoletti, J. S. Summers and D. G. van Derveer, *Inorg. Chem.*, 1986, 4197–4202.
39 H. Liu, W. Gu, X.-L. Tong, Y.-Y. Kou and S.-P. Yan, *Acta Crystallogr., Sect. E: Struct. Rep. Online*, 2006, **62**, m2704–m2705.
40 H. Liu, W. Gu, G. Xu, Y. Feng, Y. Kou, L. Feng, S. Yan, D. Liao and P. Cheng, *Inorg. Chem. Commun.*, 2007, **10**, 1099–1101.
41 E. Pardo, R. Ruiz-García, F. Lloret, M. Julve, J. Cano, J. Pasán, C. Ruiz-Pérez, Y. Filali, L.-M. Chamoreau and Y. Journaux, *Inorg. Chem.*, 2007, **46**, 4504–4514.
42 C. Glidewell, G. Ferguson, R. M. Gregson and A. J. Lough, *Acta Crystallogr., Sect. C: Cryst. Struct. Commun.*, 2000, 174–176.
43 C. M. Zakaria, G. Ferguson, A. J. Lough and C. Glidewell, *Acta Crystallogr., Sect. B: Struct. Sci.*, 2002, 78–93.
44 Y. D. Lampeka, L. V. Tsymbal, A. V. Barna, Y. L. Shuĺga, S. Shova and V. B. Arion, *Dalton Trans.*, 2012, **41**, 4118–4125.
45 *Macrocyclic and Supramolecular Chemistry. A lifetime walk in the Realm of Cyclam*, ed. J. Wiley, John Wiley@Sons LTD, Chichester, 2016.
46 L. Infantes, J. Chisholm and S. Motherwell, *CrystEngComm*, 2003, **5**, 480–486.
47 L. Infantes and S. Motherwell, *CrystEngComm*, 2002, **4**, 454–461.
48 M. Boiocchi, L. Fabbrizzi, F. Foti and M. Vazquez, *Dalton Trans.*, 2004, 2616–2620.
49 A.-L. Cheng, N. Liu, J.-Y. Zhang and E.-Q. Gao, *Inorg. Chem.*, 2007, **46**, 1034–1035.
50 A. C. Cerdeira, D. Belo, S. Rabaça, L. C. J. Pereira, J. T. Coutinho, D. Simão, R. T. Henriques, O. Jeannin, M. Fourmigué and M. Almeida, *Eur. J. Inorg. Chem.*, 2013, 4612–4618.
51 L. Prasad, S. C. Nyburg and A. McAuley, *Acta Crystallogr., Sect. C: Cryst. Struct. Commun.*, 1987, **43**, 1038–1042.
52 M. P. Suh, J. W. Jeon, H. R. Moon, K. S. Min and H. J. Choi, *C. R. Chim.*, 2005, **8**, 1543–1551.
53 R. D. Shannon, *Acta Crystallogr., Sect. A: Cryst. Phys., Diffr., Theor. Gen. Crystallogr.*, 1976, **32**, 751–767.
54 (*a*) H. Rütter and D. Mootz, *Z. Anorg. Allg. Chem.*, 1991, 73–82; (*b*) P. A. Abramov, A. T. Davletgildeeva and M. N. Sokolov, *J. Cluster Sci.*, 2017, **28**, 735–744.
55 G. Socrates, *Infrared and Raman Characteristic Group Frequencies*, John Wiley@Sons LTD, Manchester, New York, Weinheim, Toronto, Brisbane, Singapore, 2001.
56 S. P. Roe, J. O. Hill and R. J. Magee, *Monatsh. Chem.*, 1991, **122**, 467–478.
57 M. P. Suh, K. S. Min, J. W. Ko and H. J. Choi, *Eur. J. Inorg. Chem.*, 2003, 1373–1379.
58 L. Li, Y. Niu, K. Dong, P. Ma, C. Zhang, J. Niu and J. Wang, *RSC Adv.*, 2017, **7**, 28696–28701.
59 Z. Liang, J. Sun, D. Zhang, P. Ma, C. Zhang, J. Niu and J. Wang, *Inorg. Chem.*, 2017, **56**, 10119–10122.
60 J.-H. Son, C. A. Ohlin, E. C. Larson, P. Yu and W. H. Casey, *Eur. J. Inorg. Chem.*, 2013, 1748–1753.
61 J.-H. Son, C. A. Ohlin and W. H. Casey, *Dalton Trans.*, 2012, **41**, 12674–12677.

4. Unveröffentlichte Ergebnisse

4.1 Untersuchungen zur Kristallwasserabgabe eines wasserreichen Polyoxoniobates

Zusammenfassung des Manuskripts „ Unveiling the Structural Changes Induced by Water Removal from a Water-rich Polyoxoniobate Using in-situ X-ray Powder Diffraction and Pair Distribution Function Analysis“

Mit den Edukten Cu^{2+}/cyclam/$[Nb_6O_{19}]^{8-}$ wurden bereits viel versprechende Ergebnisse erhalten, so dass überprüft werden sollte, ob sich gezielt Heteroatome in PONbs einbringen lassen. Um dies zu erreichen wurde $Ti(O^iPr)_4$ als Quelle eingesetzt und die molaren Verhältnisse von Ti:Nb variiert. Die Integration war auch bei großem Ti^{4+}-Überschuss nicht erfolgreich. Stattdessen konnte das neue wasserreiche Polyoxoniobat $[Cu(cyclam)(H_2O)_2]\{[Cu(cyclam)]_2[Nb_{10}O_{28}]\}\cdot 27\ H_2O$ isoliert werden, welches sowohl unter statischen Bedingungen als auch dynamisch hergestellt werden konnte. XRD-Untersuchungen haben ergeben, dass die Hälfte der Kristallwassermoleküle bereits an Luft bei Raumtemperatur abgegeben werden, die wasserreiche Verbindung allerdings durch Suspendieren in H_2O wieder erhalten werden kann. Die Kristallwasserabgabe wurde mit Synchrotron-XRD-Messungen untersucht. Die Ergebnisse belegen, dass die Wasserabgabe und die damit einhergehende Strukturumwandlung beim Heizen spontan verlaufen. Allerdings konnte mit den Beugungsdaten der wasserarmen Form keine Strukturlösung erfolgen. Mit der Analyse der Totalstreudaten (Pair Distribution Function, PDF) konnte ein detailliertes Histogramm der Bindungslängen sowohl der wasserreichen als auch der wasserarmen Form berechnet und miteinander verglichen werden, so dass deutliche Unterschiede in der Anordnung der Konstituenten in den Strukturen nachgewiesen werden konnten.

4.1.2 Manuskript: Unveiling the Structural Changes Induced by Water Removal from a Water-rich Polyoxoniobate Using in-situ X-ray Powder Diffraction and Pair Distribution Function Analysis

Unveiling the Structural Changes Induced by Water Removal from a Water-rich Polyoxoniobate Using in-situ X-ray Powder Diffraction and Pair Distribution Function Analysis

Joanna Dopta[1], Anna-Lena Hansen[1], Nicole Pienack[1], Lisa K. Mahnke[1], Helge Reinsch[1], Martin Etter[2], Christian Näther[1], Wolfgang Bensch[1]*

[1]Institut für Anorganische Chemie, Christian-Albrechts-Universität Kiel, Max-Eyth-Straße 2, D-24118 Kiel, Germany; wbensch@ac.uni-kiel.de

[2]Deutsches Elektronen-Synchrotron (DESY), Notkestr. 85, D-22607 Hamburg, Germany

Abstract

The new polyoxoniobate $[Cu(cyclam)(H_2O)_2]\{[Cu(cyclam)]_2[Nb_{10}O_{28}]\} \cdot 27\ H_2O$ (cyclam = 1,4,8,11-tetraazacyclotetradecane) was obtained under solvothermal conditions as violet crystals. Removing the crystals from the mother liquor and storing at room temperature under ambient conditions leads to emission of half of the lattice water molecules within a short time period. The loss of crystal water molecules is accompanied by a change of the crystal structure while crystallinity of the samples remains intact. The emission of H_2O was investigated by in-situ synchrotron XRPD (X-ray powder diffraction). The resulting partially dehydrated material is microcrystalline in nature and was characterized by PDF (pair distribution function) to investigate the structural differences between the water-rich and water-poor phase.

Introduction

The chemistry of polyoxometalates (POMs) with M = V, Mo and W was well developed during the past decades[1] while for Nb progress was only made during the last few years. For the synthesis of polyoxomolybdates (POMo) and polyoxotungstates (POW) a variety of starting materials are at hand consisting of high-nuclearity clusters, and the preparation of new compounds is mainly done under mild conditions. In contrast, the number of starting compounds for the synthesis of polyoxoniobates (PONbs) is limited and the preparation mainly requires high pH values and solvothermal conditions.[2] Because PONb based materials exhibit promising properties like e.g. photocatalytic H_2 evolution[3], nerve agent degradation[4] or photoluminescence [5],[6], progress has been made in the last years in terms of novel, medium to high (>20 Nb centers) nuclearity clusters and extended networks [7][8] or the investigation of polyoxoniobate (and -tantalate) solutions.[9]] Recently, the largest PONb anion $[Nb_{288}O_{768}(OH)_{48}(CO_3)_{12}]^{180-}$ was reported, which is the second highest nuclearity POM ever since the commonly known $\{Mo_{368}\}$ cluster. [4][10].

Many POM compounds are characterized by an appreciable large number of co-crystallized crystal water molecules which could be often removed under mild conditions or even they are emitted in ambient atmosphere. Water loss can be accompanied by decomposition and degradation of crystallinity as reported for the two compounds $[N(CH_3)_4]_4[Na_2Nb_{10}O_{28}]\cdot 8H_2O\cdot ½CH_3OH$ and $[N(CH_3)_4]_6[Nb_{10}O_{28}]\cdot 6H_2O$ [11], or for $Na_8[Nb_8Ti_2O_{28}]\cdot 34H_2O$. [12] When exposed to air, the crystals showed cracks and lost their transparency. In the latter case measured and calculated XRD patterns showed differences which were assigned to the loss of the crystal water molecules; and redissolution and recrystallization of the compound proved that the $[Nb_8Ti_2O_{28}]^{8-}$ anion stays intact after dehydration/hydration.

2

For $\{[M(2,2'\text{-bipy})_2]_3[Nb_{10}O_{28}]\cdot xH_2O\}_n$ (M = Ni, Co; x = 1.5-3) thermogravimetric investigations demonstrated that the release of water molecules starts as low as around 55 °C[13]. In contrast $[M(phen)_3]\{[M(phen)_2]_2[Nb_{10}O_{28}]\}\cdot 8H_2O$ (M = Ni, Zn, Co), $[Ni(2,2'\text{-bipy})_3]\{[Ni(2,2'\text{-bipy})_2]_2[Nb_{10}O_{28}]\cdot 8.5H_2O$ and $[Ni(2,2'\text{-bipy})_2]_3[Nb_{10}O_{28}]\cdot 2H_2O$[13] did not show loss of crystal water molecules which was explained a more stable structural network. For $[Cu(cyclam)]\{[Cu(cyclam)]_2[V_{10}O_{28}]\}\cdot 10\ H_2O$ removal of crystal water molecules did not significantly affected crystallinity. The removal of H_2O at 130 °C occurred with a single-crystal-to-single-crystal (SCSC) transformation[14]. Recently, we reported reversible dehydration and rehydration of $\{[Cu(cyclam)(H_2O)]_2[Cu(cyclam)]_2[Nb_{10}O_{28}]\}n \cdot 9n\ H_2O$ being accompanied by changing significantly the crystal structure. Until now, not much efforts were undertaken to fully characterize the processes and structural changes occurring during water removal/water uptake by POM compounds. In addition, to the best of our knowledge, it was not systematically investigated whether water-rich POMs can used as starting materials for the preparation of water-poor new products.

Here, we present results of investigations of water loss by means of temperature dependent *in situ* synchrotron X-ray diffraction (XRD) and total scattering experiments to calculate the corresponding pair distribution function (PDF) of the novel polyoxoniobate $[Cu(cyclam)(H_2O)_2]\{[Cu(cyclam)]_2[Nb_{10}O_{28}]\}\cdot 27\ H_2O$ (cyclam = 1,4,8,11-tetraazacyclotetradecane). Ex-situ experiments demonstrated that removal of crystals from mother liquor leads to loss of crystal H_2O molecules to form a crystalline compound with an altered crystal structure. The H_2O molecules can be reintegrated by treating the sample with H_2O.

Experimental Section

3

General. All chemicals except of $K_7HNb_6O_{19}\cdot 13H_2O$ were purchased and used without further purification: 1,4,8,11-tetraazacyclotetradecane (98+%, Alfa Aesar), $Cu(NO_3)_2\cdot 3H_2O$ (>99%, Merck), $Ti(O^iPr)_4$ (>98%, Merck). $K_7HNb_6O_{19}\cdot 13H_2O$ was synthesized by a known literature method[15]. After dispersing the solid reactants in 3 mL of distilled water, $Ti(O^iPr)_4$ was added and subsequently, pH was adjusted with 1 M aq. KOH. All reactions were carried out under hydrothermal conditions in DURAN® glass tubes with an inner volume of 11 mL. After cooling, the reaction mixtures were filtered and the mother liquors were transferred into straight glass tubes and solvent was left to evaporate at room temperature. The resulting products were washed with dest. H_2O and dried on air.

Synthesis. 0.2 mmol $K_7HNb_6O_{19}\cdot 13H_2O$, 0.4 mmol $Cu(NO_3)_2\cdot 3H_2O$ and 0.4 mmol 1,4,8,11-tetraazacyclotetradecane (cyclam) were placed in a DURAN® glass tube (V=11 mL) and after 3 mL H_2O and 0.034 mmol $Ti(O^iPr)_4$ was added, the pH was adjusted with 0.2 mL 1 M KOH to ~11. After reacting the mixture hydrothermally at 130 °C for 3 h under stirring, the mixture was cooled down in an ice bath and filtered. After slow evaporation of the solvent, violet block shaped crystals were obtained and washed with minute amounts of distilled water. Yield: 137.0 mg (46 % based on Nb). Note that stirring is not necessary to obtain the compound.

X-Ray powder diffraction

Laboratory powder patterns were recorded with Cu $K_{\alpha 1}$ radiation (λ=1.5406 Å) on a STOE Stadi-P powder diffractometer with a Ge monochromator and a Mythen detector.

Synchrotron X-Ray Diffraction and PDF analyses

Synchrotron X-ray powder diffraction (XRPD) and X-ray total scattering data at higher *Q* range for the calculation of the corresponding pair distribution function (PDF) were collected at the PETRA III P02.1 beamline (DESY, Hamburg) at temperatures

between RT and 65 °C using a Nitrogen Gas Blower @60 keV, λ = 0.20717 Å. To determine the detector characteristics, the sample-to-detector distance (SDD) and to account for the instrumental contribution to the PDF (Q_{damp}), LaB_6 was used as calibration standard. For XRPD, the SDD was 1012.18 mm and for PDF it was set to 363.5 mm. The samples were measured in Kapton capillaries. To obtain the water-rich compound, the solid sample of the water poor material was suspended in water and the suspension was transferred via syringe into the capillaries. The scattering data were corrected by subtracting the contribution of the empty capillaries, which were measured under identical conditions.

The integration of the data was performed using Fit2D[16]. Desy data helper und Multi power x-ray diffraction data tool for data integration and plotting was used[17]. The mathematical transformations, background subtractions and PDF calculation of various structural models were done with xPDFsuite[18].

Spectroscopic investigations

A Bruker Alpha-P ATR IR spectrometer was used to record MIR spectra in a range of 400 – 4000 cm^{-1}. UV-Vis diffuse reflectance spectra were collected on an UV/Vis-NIR two-channel spectrometer Cary 5 from Carian Techtron Pty using $BaSO_4$ as reference. The IR spectrum (Fig. S8) and the band assignment (Tab. S7) as well as the UV-Vis spectra (Fig. S9+S10) and their interpretation are displayed in the Supporting Information.

Elemental analysis

CHN analyses were done with an EURO EA elemental analyzer (EURO VEKTOR).

Single crystal structure analysis

Single crystal X-ray intensity data were collected with a STOE Imaging Plate Diffraction System (IPDS-1) with Mo-K_α radiation (λ = 0.71073 Å) at 170 K. A numerical absorption correction was performed ($T_{min/max}$: 0.5656/0.7633).The crystal

5

structure was solved with the SHELXS-97[19] and refined against F^2 using SHELXL-2014[20]. All non H atoms except some of the disordered water O atoms of lower occupancy were refined anisotropic. The C-H and N-H H atoms were positioned with idealized geometry and refined isotropic with $U_{iso}(H) = 1.2\ U_{eq}(C)$ using a riding model. The O-H H atoms were not located but considered in the calculation of the molecular formula. One cyclam ligand is disordered in two orientations and was refined with restraints using a split model. The water O atoms are also disordered and were refined using a split model. Eight are fully occupied (O22-O25, O29-O32), seven half occupied (O26-28, O37-O40), two oxygen atoms possess an occupancy of 80% (O33, O34) and two are 20 % occupied (O35, O36), resulting in 13.5 water molecules in the asymmetric unit or 27 crystal water molecules per formula unit.

Synthetic aspects, Dehydration and Crystal Structure

Since alkaline pH values are required for the synthesis of PONbs, one strategy to obtain new compounds with TMs is to prevent the formation of hydroxides by complexing with amine molecules[21]. $[Co(en)]^{2+}$ and $[Cr(en)]^{2+}$ cations were the first complexes which were integrated in polyoxoniobates[22]. Meanwhile, Cu^{2+}-cetered seem most appropriate because most TM containing PONbs were reported with Cu^2. This may be due to the high stability constants of copper amine complexes and the strong Jahn-Teller-distortions of Cu^{II}, which result in flexible coordination geometries[23].

The title compound is obtained at 130°C after a reaction time of 3h. Stirring the slurry the product crystallizes as a violet crystalline powder and can be obtained by filtration immediately after solvothermal treatment. Single crystals are obtained either by leaving the filtrate at room temperature, allowing the solvent to slowly evaporate, or by heating the mixture of starting materials hydrothermally without stirring.

6

We note that titanium is not integrated into the structure, but crucial for the formation of the title compound, indicating that the presence of titanium species is important for product formation. The sensitivity of polyoxoniobate formation towards the reaction conditions is a known phenomenon and several examples of additives, which are essential for the formation without being integrated in PONb structure were reported[24]]. We tried to force the integration of Ti by applying an excess of titanium isopropoxide, but no titanoniobate could be obtained. This just led to high amounts of titanium dioxide as byproduct and lowered the yield of the title compound.

In order to proof phase purity, an XRDP pattern was recorded. Comparison with the pattern calculated from single crystal data revealed a mismatch of both patterns, which may explained by the fact that single crystal data were collected at 170 K while the powder pattern was measured at RT. In addition, crystal water may be lost handling the sample in laboratory conditions. Storing the samples in a humid atmosphere did not alter the XRD pattern and two different strategies were tested to prove whether the material absorb additional water: i) submersing the sample in a water-filled glass tube overnight and ii) suspending the compound in a small amount of water and transferring it into Kapton capillaries. The amount of water was chosen to be sparse, because the compound is soluble in water to a minor extent.

$[Cu(cyclam)(H_2O)_2]\{[Cu(cyclam)]_2[Nb_{10}O_{28}]\} \cdot 27\ H_2O$ crystallizes in the monoclinic space group $P2_1/c$ with two formula units per unit cell. The details of structure determination and refinement are listed in Tab. S1. The structure consists of the literature-known $[Nb_{10}O_{28}]^{8-}$ anion and two crystallographically independent $[Cu(cyclam)(H_2O)x]^{2+}$ cations (x=0,2, Fig. 1). One of the cyclam ligands is disordered. Besides the crystal H_2O molecules coordinated to Cu^{2+}, 27 further water oxygen atoms are located in the asymmetric unit. All atoms, except Cu2, are

crystallographically independent atoms located on general positions. A more detailed description of the structure is available in the Supporting Information.

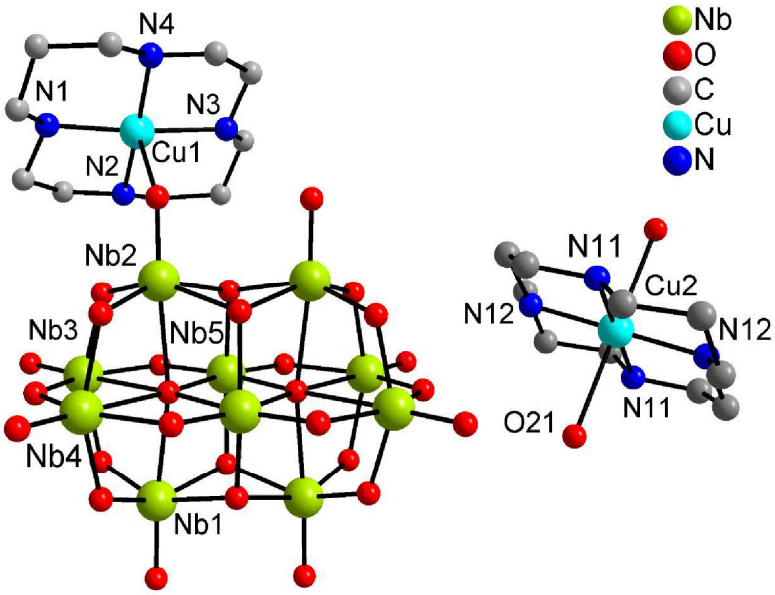

Figure 1. Structural unit of $[Cu(cyclam)(H_2O)_2]\{[Cu(cyclam)]_2[Nb_{10}O_{28}]\} \cdot 27\ H_2O$. The cyclam ligand with lower occupancy (0.45) is not displayed.

Characterization

In house XRPD

Both strategies explained in the experimental section to rehydrate the sample yielded powder patterns agreeing well with a pattern calculated from single crystal data for the water-rich compound, *i.e.* the integration is reversible (Fig. 2).

8

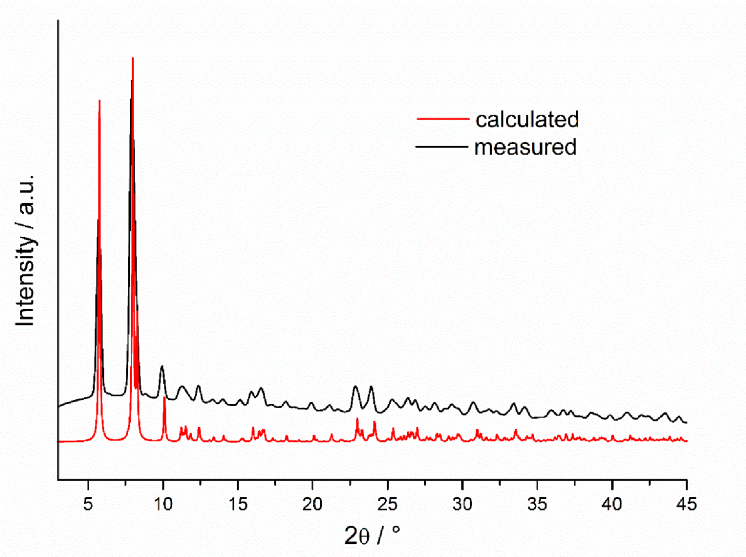

Figure 2. Comparison of XRDP of the moistened sample with data simulated from single crystal structure analysis. The data were calculated using CuK*α* radiation wavelength (1.5406 Å).

The PXRD pattern of the partially dehydrated sample could be successfully indexed using a monoclinic unit cell with extinction conditions suitable for the space group $P2_1/c$ using TOPAS Academics.[25] These indexed parameters were refined by structure-less Pawley refinement (Fig. 3), converging to sufficient figures of merit (R_{WP} = 3.3%, GoF = 1.1; a = 14.621(1) Å, b = 17.794(2) Å, c = 15.179(1) Å, β = 108.109(7) °).

9

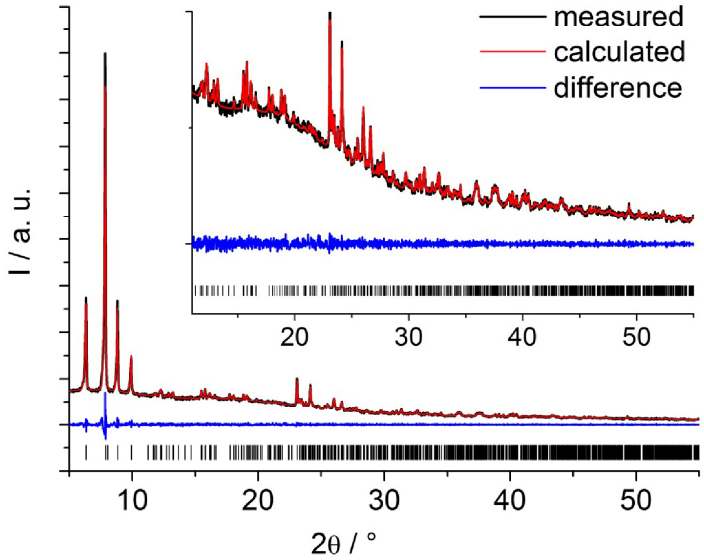

Figure 3. Plot of the structure-less Pawley refinement of the partially dehydrated compound for the determination of the unit cell parameters.

The cell dimensions and symmetry pointed at a direct structural relationship between the hydrated and the dehydrated compound. Hence, the crystal structure of the hydrated material was used as starting point for further modelling. The water molecules were removed from the structure and the indexed cell parameters were superimposed using the molecular modelling software Materials Studio.[26] The thus obtained model was further optimized by force-field calculations using the universal force-field as implemented in the Forcite routine in Materials Studio.[27] An attempted Rietveld refinement of this model was unsuccessful, most likely due to the complexity of the structure (56 non-hydrogen atoms of which 55 reside on general positions). Nevertheless, the theoretical pattern is in good agreement with the experimental data (Fig. 4). The intensity deviations could for example be due to textural effect or the partial re-adsorption of moisture from air.

10

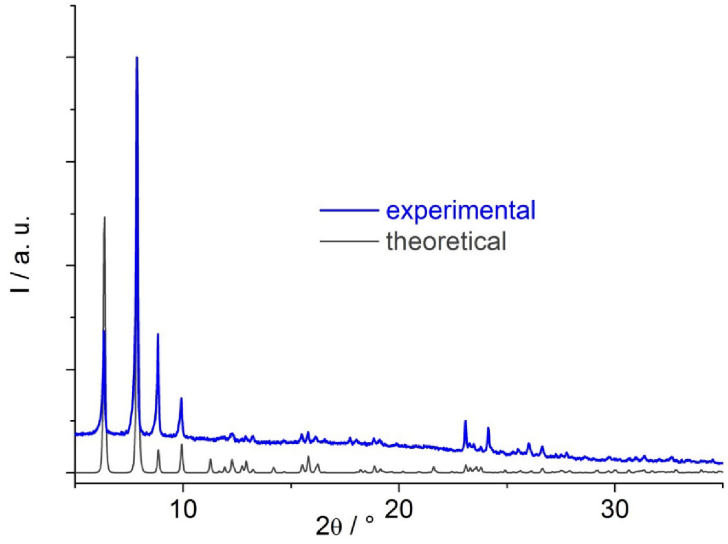

Figure 4. Comparison of the theoretical pattern for the model obtained by force-field calculations (grey) and the experimental data (blue).

Table 1. Comparison of the cell parameters.

	Nb_{10} · 29 H_2O	**Nb_{10} · ~14H_2O**
Spgr	*P*2$_1$/c	*P*2$_1$/*c*
a / Å	16.7620(4)	14.621(1)
b / Å	17.4987(5)	17.794(2)
c / Å	15.5807(4)	15.179(1)
α / °	90	90
β / °	113.719(2)	108.109(7)
γ / °	90	90
V / Å^3	4184.0	3753.5
l / Å	7.67	6.95

Comparing the cell parameters of the two phases (Table 1) reveals a shrinkage of the cell volume of about ~ 10 %, whereby the major deviation takes place in the crystallographic *a* direction. This becomes reasonable, having a look at the crystal structure along this direction (Fig. 5). The structure can be approximately described

11

as a layered structure with H_2O molecules distributed between alternating layers of decaniobate anions and $[Cu(cyclam)]^{2+}$ cations. The "interlayer" distance l was calculated to imply changes of the monoclinic angle β and the cell parameter a by $l = \frac{1}{2} a \sin \beta$. A reduction of the interlayer distance of ~ 9.4 % was observed.

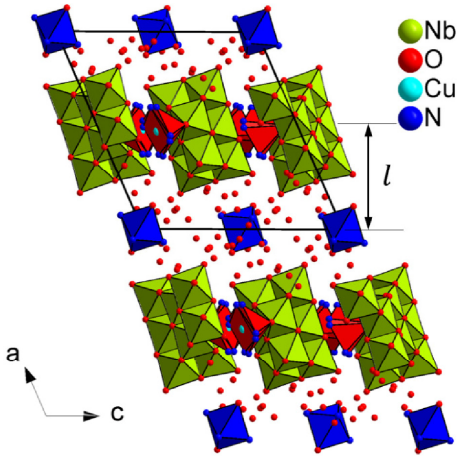

Figure 5. Representation of the crystal structure ||*a*; Green: NbO_6 octahedra; red: CuN_4O square pyramid; blue: CuN_4O_2 octahedra; red: oxygen atoms.

Elemental analysis and thermogravimetric measurements

To estimate the number of water molecules in the water poor phase, elemental analysis and thermogravimetric (TG) measurements were carried out. According to TG, the first mass loss takes place from RT to ~150 °C, where the crystal H_2O molecules are most probably emitted. This mass loss of 10.2 % would correspond to the emission of 13 - 14 H_2O molecules (calcd. 9.8% [13 H_2O] -10.4 % [14H_2O]) which is in very good agreement to the elemental analyses, calculated for 13 [14] H_2O in %: C 15.0 [14.9], H 4.1 [4.2], N 7.0 [6.9] found: C 15.0, H 4.0, N 7.0). On the base of these results, we assume that the water poor form contains ~14 H_2O. Consecutively, we use $Nb_{10}{\cdot}14H_2O$ for the water-poor and $Nb_{10}{\cdot}29H_2O$ for the water-rich material.

12

The spectroscopic investigations are displayed in detail in the Supporting Informations (Fig. S8: IR; Fig. S9: UV-Vis).

Synchrotron XRD investigations

As stated above, preliminary experiments revealed that the material emits ~ 13 crystal H_2O molecules when removed from mother liquor, passing a structural change clearly distinguishable in the XRDP. *In house* XRD measurements revealed that the water loss can be traced via XRD at room temperature, a slow process enduring several hours. However, water emission can be induced by heating the sample at moderate temperatures (< 65 °C). To trace the phase transition, the sample was heated to 40 °C and subsequently the temperature was increased in 2 °C steps (Fig. 6). The results of the corresponding Pawley refinements are shown in Figure 7. The cell parameters stay almost constant up to 52 °C, and the unit cell volume decreases by only 2.2 % between 46 °C and 52 °C, suggesting a minor emission of water molecules. Between 52 °C and 54 °C the structure changes abruptly, indicated by the disappearance of reflections associated with the water-rich form. An additional shrinkage of the unit cell volume could be observed, which amounts to -8.5 %. Again the main structural changes occur along the crystallographic *a* axis and for the monoclinic angle *β*, resulting in an interlayer distance being ~ 7 % smaller than before.

13

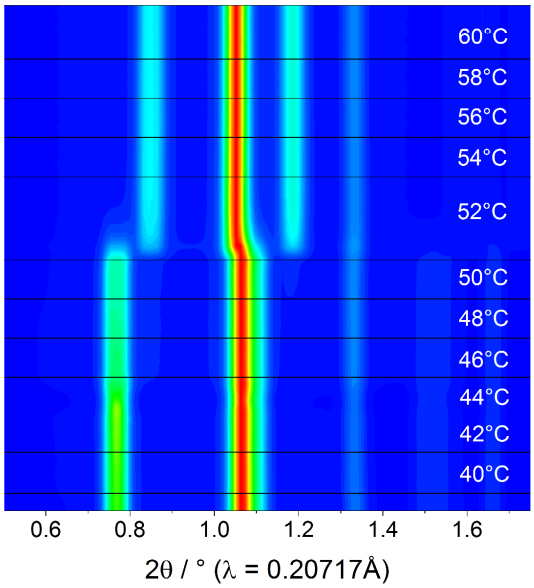

Figure 6. Temperature dependent plot of the evolution of the reflection intensities recorded on a sample suspended in water upon heating from 25°C – 60 °C.

14

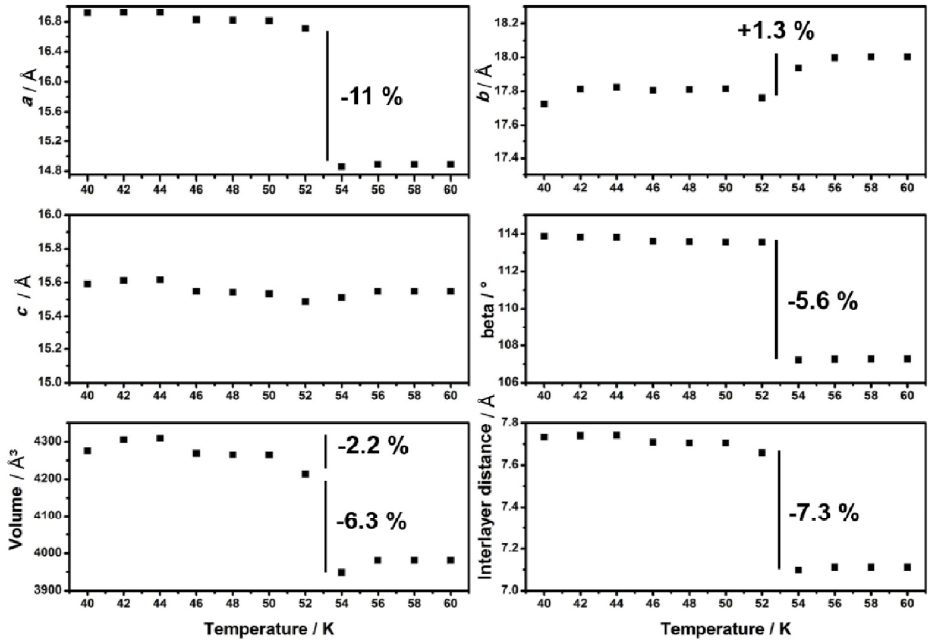

Figure 7. Results of Pawley Refinements. Estimated standard deviations are smaller than markers.

After the phase transition neither prolonged heating nor rising the temperature to 65 °C lead to any further changes in the XRPD. (Fig. S12). The powder pattern recorded at 60 °C corresponds to the partially dehydrated material. After heating, the sample was cooled to RT to check for structural changes caused by uptake of moisture, but no such effect was observed (Fig. S12).

Pair distribution function analyses

The pair distribution function is a powerful approach to gain structural information on the short and intermediate range order of a material. It is experimentally accessible from measured diffraction data, since Fourier transformation of the total scattering

15

structure function S(Q) corrected for experimental effects yields directly the probability to find a neighboring atom at a certain distance r (Eq.1).

$$G(r) = \frac{2}{\pi} \int_0^\infty Q\,[S(Q) - 1] \sin(Qr)\, dQ \qquad \text{Eq(1)}$$

Consequently, the PDF yields a histogram of distances between atoms in a material.[28][29][30]

As mentioned above structural model could be extracted from powder XRD data, but a Rietveld refinement was prevented by the large number of parameters. Hence, PDF analysis was performed to gain insight into the structural changes occurring during water removal. From the PDFs of both phases, the water-poor crystals of $Nb_{10}{\cdot}14H_2O$ obtained after removing from mother liquor and the water-rich crystals of $Nb_{10}{\cdot}29H_2O$ formed when suspending $Nb_{10}{\cdot}14H_2O$ in water, several intense signals attributable to five different Nb-Nb intramolecular distances in the $[Nb_{10}O_{28}]^{6-}$ anion are distinguishable at ~3.4, 4.8, 5.7, 6.5 and 7.4 Å (Figures 8 and 9).

16

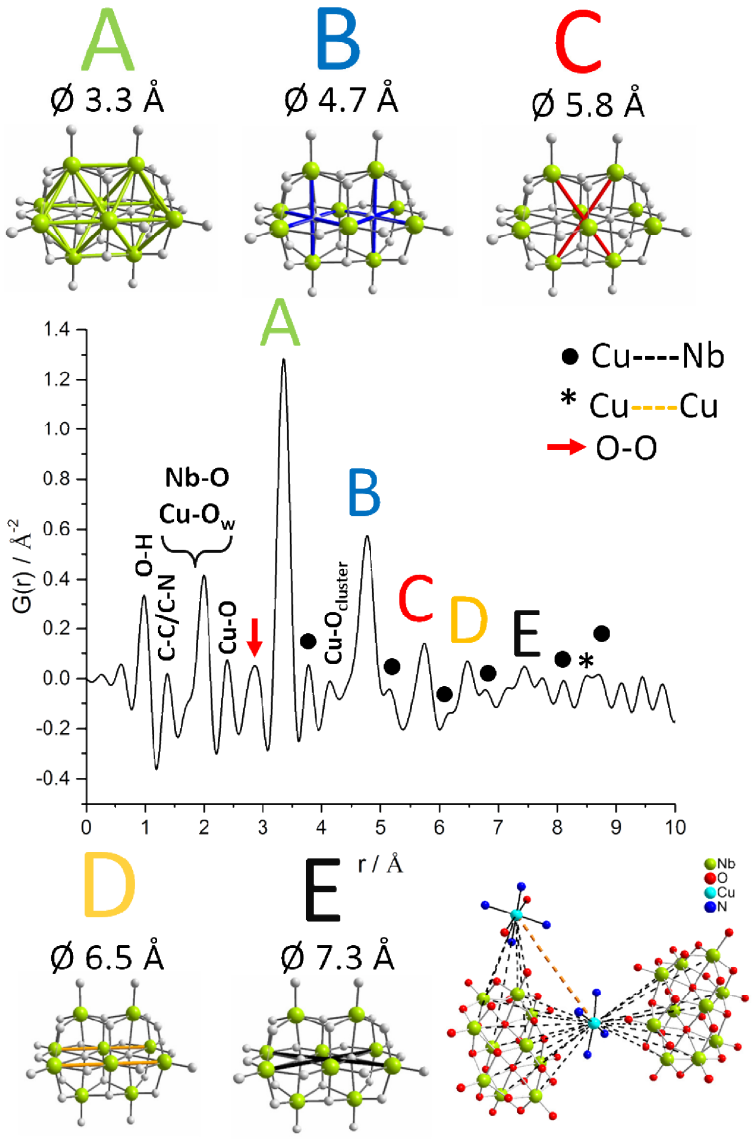

Figure 8. Representation of the distances estimated from PDF exemplified by $Nb_{10}{\cdot}29H_2O$.

At low r-values, the C-C and C-H bonds in the cyclam molecule at ~1.4 Å (1.37(3)-1.57(4) Å) are visible. The Cu-N at ~2.0 Å as well as the Cu-$O_{cluster}$ and Cu-O_{H2O} bonds at ~2.4 and ~2.5 Å are superimposed by the signals for Nb-O bridging and

17

terminal bonds at 1.7-2.5 Å. At 2.9 Å, the O_{H2O}-O_{H2O} distances are observed, which are 2.8 Å for the average O-O distances in the water cluster in $Nb_{10}{\cdot}29H_2O$ as well as in liquid water (Fig. S13). At 3.8 and 5.2 Å, the Cu-Nb distances are located, originating from the Cu^{2+} in the $[Cu(cyclam)]^{2+}$ molecule attached to the cluster (Cu1-Nb1: 3.7 Å; Cu1-Nb1/3: 5.1 Å). At higher r-values, the Cu-Cu and Cu-Nb pair distances appear. Some of the distances are slightly longer than estimated from single crystal structure analysis (e.g exp. 6.1 / 7.1 Å compared to calc. 5.9 / 6.9 Å), but note that the single crystal data was collected at lower temperatures. Compared to $Nb_{10}{\cdot}29H_2O$, the intensity of the signals in the PDF of $Nb_{10}{\cdot}14H_2O$ are more intense and beyond the range of 6 Å, a strong broadening of the peaks occurs, indicating that the constituents in $Nb_{10}{\cdot}29H_2O$ are more rigid or "fixed" than in $Nb_{10}{\cdot}14H_2O$. Additionally, some of the peaks attributable to Cu-Nb distances are missing, indicating that they might have moved or twisted relative to the cluster. Another hint for the displacement of the $[Cu(cyclam)]^{2+}$ cations is the diminished intensity of the Cu-Cu distance at ~8.5 Å in the water-poor phase relative to the Cu/Nb-Nb distances.

18

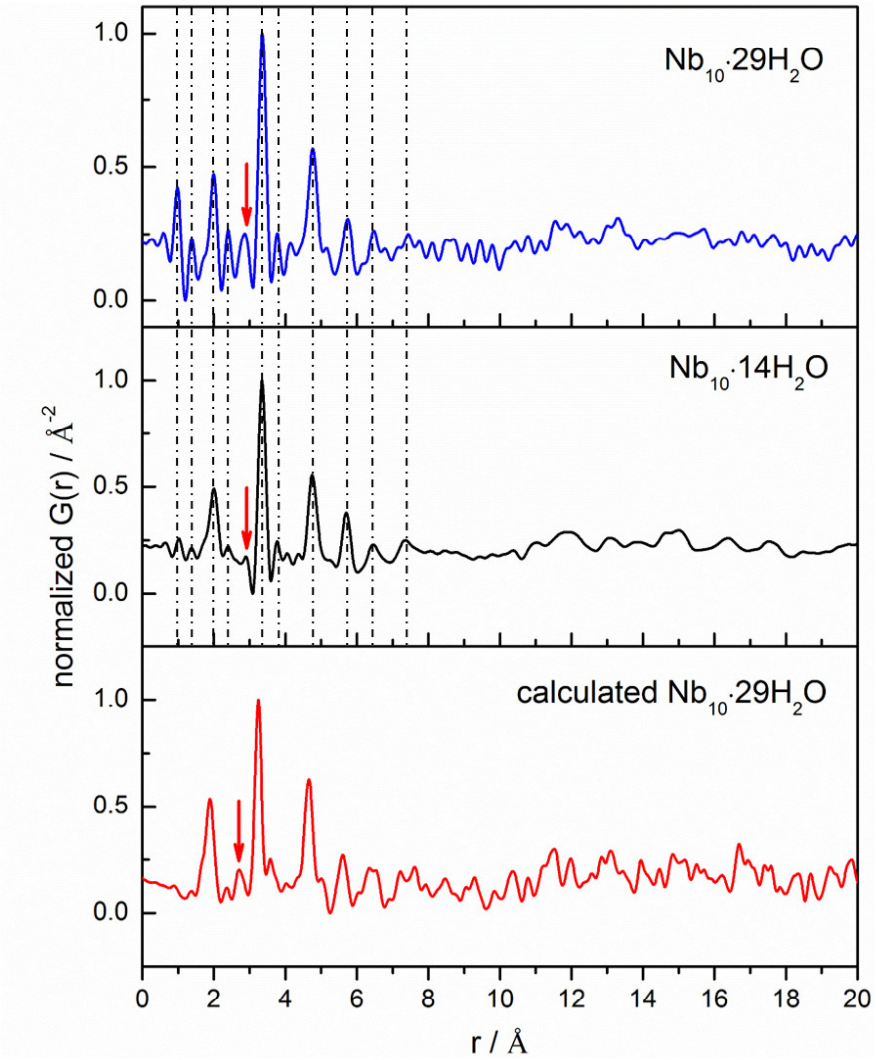

Figure 9. PDFs of the $Nb_{10}{\cdot}29H_2O$ (top) and $Nb_{10}{\cdot}14H_2O$ (middle) compared to the calculated (bottom) pair distances marked with red arrows. Note that calculated PDF is based on low T single crystal (170 K) data. Dotted lines are a guide to the eye to emphazise the structural integrity of the main features diplayed in Figure 8.

19

Table 2. Assignment of the bond lengths observed in the PDFs of $Nb_{10}{\cdot}14H_2O$ and $Nb_{10}{\cdot}29H_2O$

Assignment	$Nb_{10}{\cdot}14H_2O$	$Nb_{10}{\cdot}29H_2O$[theo]
C-C, C-N	1.4	1.4
Nb-O	1.7	1.7
Nb-O, Cu-N	2.0	2.0
Nb-O, Cu-O	2.4	2.4
O-O	2.9	2.9
A Nb-Nb	3.4	3.4
Cu-Nb	3.8	3.8
$Cu\text{-}O_{cluster}$	4.1	4.2
$Cu\text{-}Nb/O_w\text{-}O_w$	4.4	
B Nb-Nb	4.7	4.8
Cu-Nb	5.2	5.2
C Nb-Nb	5.7	5.7
Cu-Nb		6.1[5.9]
D Nb-Nb	6.5	6.5
Cu-Nb		6.8
Cu-Nb		7.1[6.9]
E Nb-Nb/Cu-Nb	7.3	7.4
Cu-Nb		7.8
Cu-Nb	8.0	8.1
Cu-Cu /Nb-Nb	8.4	8.5
Cu-Nb	8.7	8.7

Indicated by the PDF in the long-range order of both phases, the distances between adjacent anions are apparently not altered significantly, being approx. 10 Å (Fig. 10). This is highly interesting because one would expect that the removal of ~13 crystal H_2O molecules, which is accompanied by a decrease of the unit cell volume, would bring the constituents closer together. But the electrostatic repulsion between the highly charged $[Nb_{10}O_{28}]^{6-}$ anions seems to hinder closer contacts resulting in displacement of the other components in the structure to prevent voids.

20

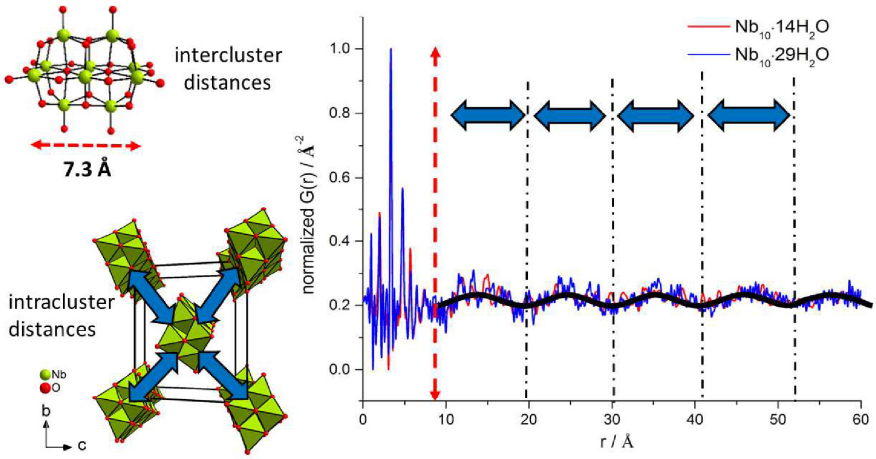

Figure 10. Comparison of the intracluster distances in the PDFs of $Nb_{10}{\cdot}29H_2O$ (top) and $Nb_{10}{\cdot}14H_2O$ (bottom). The dotted lines are a guide for the eyes.

Conclusion

The new polyoxoniobate $[Cu(cyclam)(H_2O)_2]\{[Cu(cyclam)]_2[Nb_{10}O_{28}]\} \cdot 27\ H_2O$ ($Nb_{10}{\cdot}29H_2O$) was prepared *via* solvothermal synthesis within 3h applying static or dynamic conditions. Synchrotron and in house XRPD measurements revealed that the water rich crystals emit approximately half of the lattice water molecules after removing from mother liquor, yielding a water-poor phase ($Nb_{10}{\cdot}14H_2O$) with a different crystal structure. The emission is reversible and the water molecules can be reintegrated by suspending the sample in a small amount of water. The water loss results in a shrinkage of the unit cell mainly in the *a* direction, which can be understood by analyzing the distribution of the lattice water molecules in $Nb_{10}{\cdot}\ 29H_2O$. The water poor phase $Nb_{10}{\cdot}14H_2O$ is a microcrystalline powder, but a Rietveld refinement was unsuccessful due to the complexity of the structure. Applying PDF, we were able to gain insights into the structural changes. First, the evaluation of the PDF for $Nb_{10}{\cdot}29H_2O$ is in excellent agreement with the data obtained from single crystal structure

21

analysis, supporting the results of the XRD measurements which proved the reversibility of the water loss. Investigating the short range order in the PDF of $Nb_{10}{\cdot}14H_2O$, we found that the Cu-Nb pair distances are strongly broadened, giving a hint for a higher flexibility of this building units in contrast to the corresponding sharp signals for Cu-Nb in the PDF of $Nb_{10}{\cdot}\ 29H_2O$. The evaluation in the long range order revealed, that in both phases the distances between the anions remain unchanged, indicating that the electrostatic repulsion between the highly charged $\{Nb_{10}\}$ clusters hinders a closer contact. Therefore, the other constituents need to be reorganized to prevent voids, like evidenced from the pair distances in the short range order.

Acknowledgements

Financial support by the State of Schleswig-Holstein is gratefully acknowledged.

22

References

[1] D.-L. Long, R. Tsunashima, L. Cronin, *Angew. Chem. Int. Ed.* **2010**, *49*, 1736.

[2] M. Nyman, *Dalton Trans.* **2011**, *40*, 8049.

[3] J.-H. Son, J. Wang, F. E. Osterloh, P. Yu, W. H. Casey, *Chem. Commun.* **2014**, *50*, 836.

[4] Y.-L. Wu, X.-X. Li, Y.-J. Qi, H. Yu, L. Jin, S.-T. Zheng, *Angew. Chem., Int. Ed.* **2018**, *57*, 8572.

[5] J.-Y. Niu, G. Chen, J.-W. Zhao, P.-T. Ma, S.-Z. Li, J.-P. Wang, M.-X. Li, Y. Bai, B.-S. Ji, *Chem. Eur. J.* **2010**, *16*, 7082.

[6] S. Chen, P. Ma, H. Luo, Y. Wang, J. Niu, J. Wang, *Chem. Commun.* **2017**, *53*, 3709.

[7] R. P. Bontchev, M. Nyman, *Angew. Chem., Int. Ed.* **2006**, *45*, 6670.

[8] L. Jin, Z.-K. Zhu, Y.-L. Wu, Y.-J. Qi, X.-X. Li, S.-T. Zheng, *Angew. Chem., Int. Ed.* **2017**, *56*, 16288.

[9] M. R. Antonio, M. Nyman, T. M. Anderson, *Angew. Chem.* **2009**, *121*, 6252.

[10] A. Müller, E. Beckmann, H. Bögge, M. Schmidtmann, A. Dress, *Angew. Chem. Int. Ed.* **2002**, *41*, 1162.

[11] E. J. Graeber, B. Morosin, *Acta Crystallogr. B.* **1977**, 2137.

[12] M. Nyman, L. J. Criscenti, F. Bonhomme, M. A. Rodriguez, R. T. Cygan, *J. Solid State Chem.* **2003**, *176*, 111.

[13] L. Shen, C.-H. Li, Y.-N. Chi, C.-W. Hu, *Inorg. Chem. Commun.* **2008**, *11*, 992.

[14] J. Martín-Caballero, A. San José Wéry, S. Reinoso, B. Artetxe, L. San Felices, B. El Bakkali, G. Trautwein, J. Alcañiz-Monge, J. L. Vilas, J. M. Gutiérrez-Zorrilla, *Inorg. Chem.* **2016**, *55*, 4970.

[15] M. Filowitz, Ho, R. K. C., W. G. Klemperer, W. Shum, *Inorg. Chem.* **1979**, *18*, 93.

[16] A. P. Hammersley, *FIT2D: An Introduction and Overview*, ESRF97HA02T, **1997**.

[17] a) M. Köppen, *Desy data helper for FIT2D*, **2015**; b) M. Köppen, *Multi purpose powder x-ray diffraction data tool*, **2015**.

[18] P. Juhas, T. Davis, C. L. Farrow, S. J. L. Billinge, *J. Appl. Cryst.* **2013**, *46*, 560.

[19] G.M. Sheldrick, *SHELXS-97: Program for the Solution of Crystal Structures*, University of Goettingen, Goettingen, **1997**.

[20] G.M. Sheldrick, *SHELXL-2014: Program for the Refinement of Crystal Structures*, University of Goettingen, Goettingen, **2014**.

[21] H.-L. Wu, Z.-M. Zhang, Y.-G. Li, X.-L. Wang, E.-B. Wang, *CrystEngComm* **2015**, *17*, 6261.

[22] C. M. Flynn, G. D. Stucky, *Inorg. Chem.* **1969**, 178.

[23] G. A. Carlson, J. P. McReynolds, F. H. Verhoek, *J. Am. Chem. Soc.* **1945**, 1334.

[24] R. Tsunashima, D.-L. Long, H. N. Miras, D. Gabb, C. P. Pradeep, L. Cronin, *Angew. Chem.* **2010**, *122*, 117.

[25] Coelho Software, *Topas Academics*, Brisbane, **2007**.

[26] Accelrys Inc., *Materials Studio Version 5.0*, San Diego, **2009**.

[27] C. J. Casewit, K. S. Colwell, A. K. Rappe, *J. Am. Chem. Soc.* **1992**, *114*, 10046.

[28] T. Egami, S. J.L. Billinge, *Underneath the Bragg peaks. Structural analysis of complex materials*, Pergamon, Amsterdam, **2012**.

[29] S. J. L. Billinge, M. G. Kanatzidis, *Chem. Commun.* **2004**, 749.

[30] S. J.L. Billinge, *J. Solid State Chem.* **2008**, *181*, 1695.

24

5. Zusammenfassung und Ausblick

Im Rahmen der Doktorarbeit konnten insgesamt sieben neue Polyoxoniobate synthetisiert und umfassend charakterisiert werden.

In Gegenwart von $[Cu(cyclam)]^{2+}$ Komplexen und dem $[Nb_6O_{19}]^{8-}$ -Anion konnte die neue Verbindung $K_5[Cu(H_2O)_2(cyclam)]_{1.5}\{[Cu(cyclam)][Cu(H_2O)(cyclam)]_2\mathbf{HSiNb_{18}O_{54}}\}\cdot 30H_2O$ hydrothermal hergestellt werden, in deren Struktur das seltene Anion $[SiNb_{18}O_{54}]^{18-}$ vorhanden ist. Die Erniedrigung des pH-Wertes auf <10.3 führte zur Kristallisation der Verbindung $\{[Cu(cyclam)(H_2O)]_2[Cu(cyclam)][\mathbf{Nb_{10}O_{28}}]\}_n\cdot 9nH_2O$ mit zwei unterschiedlich koordinierten Cu^{2+}-Kationen. In den Strukturen der beiden Verbindungen sind die $[Cu(cyclam)]^{2+}$-Komplexe über Cu-O-Bindungen an den anionischen Cluster kovalent gebunden. Die Ausbeute und die Reaktionszeit beider Verbindungen konnte durch Rühren des Gemisches (dynamische Bedingungen) dahingehend optimiert werden, dass beide Substanzen bereits nach 30 min Reaktionszeit in guten Ausbeuten isoliert werden konnten. Durch kombinierte thermoanalytische und Röntgenbeugungsuntersuchungen konnte nachgewiesen werden, dass die dekaniobathaltige Verbindung dehydratisiert und rehydratisiert werden kann. Bei der Dehydratisierung wird eine Phasenumwandlung unter Erhaltung der Kristallinität beobachtet. Bei der thermischen Zersetzung an Luft wird ein neues nanokristallines Material gebildet, dessen Struktur bisher nicht aufgeklärt werden konnte.

Bei der Verwendung von $Ti(O^iPr)_4$ als Heteroatomquelle kristallisiert das wasserreiche Dekaniobat $[Cu(cyclam)(H_2O)_2]\{[Cu(cyclam)]_2[\mathbf{Nb_{10}O_{28}}]\}\cdot 27\ H_2O$. Bei Lagerung an Luft wird innerhalb kurzer Zeit die Hälfte der Kristallwassermoleküle abgegeben, wobei die gute Kristallinität erhalten bleibt. Dieser Wasserverlust kann durch Dispergieren in Wasser wieder rückgängig gemacht werden. Die Struktur der wasserarmen Form konnte aus Röntgenpulverdaten nicht gelöst werden. Die während der Wasserabgabe beobachtete Phasenumwandlung wurde mit Röntgenbeugung am DESY untersucht und die Paarverteilungsfunktion (PDF) sowohl für die wasserarme als auch für die wasserreiche Form ermittelt. Die aus der PDF extrahierten interatomaren Abstände der wasserreichen Verbindung stimmen sehr gut mit den Daten der Einkristallstrukturanalyse überein. Aus der PDF der wasserarmen Form kann geschlossen werden, dass sich der Abstand zwischen den Anionen nicht signifikant verändert und dass die $[Cu(cyclam)]^{2+}$-Moleküle ihre Position in der Struktur verändert haben müssen.

Durch die Verwendung von $Ti(O^iPr)_4$ oder $K_2TiO(C_2O_4)_2$ als Heteroatomquellen konnten mit Ni^{2+} und cyclam als Ligand vier weitere Verbindungen hergestellt werden:

{[Ni(cyclam)]$_4$[**Ti$_2$Nb$_8$O$_{28}$**]}n~28nH$_2$O und drei pseudo-polymorphe Verbindungen K[Ni(cyclam)]$_3$[**TiNb$_9$O$_{28}$**]·xH$_2$O (x = 10-18), in denen entweder Mono- oder Dititanoniobatanionen vorliegen. In der ersten Verbindung sind die [Ni(cyclam)]$^{2+}$-Komplexe oktaedrisch koordiniert, wobei neben den 4 N-Atomen des cyclam-Liganden zwei Cluster-Sauerstoffanionen die Koordinationssphäre vervollständigen. Diese O^{2-}-Ionen befinden sich in den zwei kristallographisch unabhängigen Komplexen entweder *trans* zueinander und verknüpfen die Clusteranionen zu einer Schichtstruktur, oder die O^{2-}-Ionen sind in *cis*-Stellung, was zu einer starken Verzerrung des Liganden führt. Die Clusteranionen in den drei pseudo-polymorphen Verbindungen liegen isoliert vor und sind von quadratisch-planar koordinierten Ni^{2+}-Kationen umgeben. Ein ausgeprägtes Wasserstoffbrückenbindungsnetzwerk stabilisiert die strukturelle Anordnung der Anionen und Kationen. Unter den gewählten Reaktionsbedingungen bilden sich Mono- und Dititanoniobat selektiv und phasenrein in Abhängigkeit von der eingesetzten Titanquelle. Das Monotitanoniobat kristallisiert, wenn $K_2TiO(C_2O_4)_2$ eingesetzt wird, während Dititanoniobatcluster bei der Verwendung von Ti(O^{i}Pr)$_4$ gebildet werden. Die Ergebnisse von Synthesen mit unterschiedlichen pH-Werten belegen, dass dieser Parameter nicht allein die Geometrie des Cluster bestimmt, Untersuchungen zur Stabilität der Verbindungen bei verschiedenen pH-Werten ergaben, diese zwischen pH = 2 und pH = 13 stabil sind. Mit Thermogravimetrie und Röntgenbeugungsuntersuchungen konnte nachgewiesen werden, dass das Kristallwasser der Verbindungen {[Ni(cyclam)]$_4$[**Ti$_2$Nb$_8$O$_{28}$**]}n~28nH$_2$O und K[Ni(cyclam)]$_3$[**TiNb$_9$O$_{28}$**]·18H$_2$O unter Erhalt der Kristallinität entfernt werden kann und nach Behandlung mit Wasser die Ausgangsverbindungen gebildet werden.

Wie im Rahmen der Arbeit gezeigt werden konnte, ist die Hydrothermalsynthese besonders gut geeignet, neue PONbs zu synthetisieren. Welche Rolle das Alkalimetallkation im Ausgangsmaterial $K_7HNb_6O_{19}·13H_2O$ auf die Produktbildung ausübt, würde bisher nicht systematisch untersucht. Daher lohnt es sich in Zukunft sowohl leichter (Rb, Cs) als auch schwerer lösliche (Li, Na) Salze des Hexaniobats einzusetzen, insbesondere da vor kurzer Zeit von *Nyman et al.* gezeigt werden konnte, dass die Größe und Konzentration des Alkalimetallions die Größe des Polyoxoniobatclusters stark beeinflusst.[40] Zusätzlich stellen (Aza-)Kronenether hervorragende makrozyklische Liganden für Alkalimetallionen dar[128], und die Verwendung dieser Liganden könnte zu völlig neuen Strukturen führen.

Herausfordernd ist die Synthese von Polyoxoniobaten mit integrierten Seltenerdionen, da bei basischen Bedingungen Lanthanoidionen als Hydroxide ausfallen. Aber lanthanoidhaltige

PONbs wären interessant für Lumineszenzanwendungen, da die Lumineszenz der Seltenerdionen stark von der Koordinationsumgebung abhängt. Zusätzlich könnte die Dotierung von PONbs mit Seltenerdionen die Möglichkeit eröffnen, mit der ILACS-Methode (*In-situ* luminescence analysis of coordination sensors) an der Kieler *in-situ*-Kristallisationszelle das Ionen-Assoziationsverhalten sowie die Bildung kristalliner Produkte zu untersuchen.[129][130][131]

Synthesen von PONbs in ionischen Flüssigkeiten sind attraktive Alternativen zu den bisher fast ausschließlich in wässrigen Lösungen durchgeführten Synthesen. Viel versprechend kann auch die Integration von PONb in MOFs sein, so dass Verbindungen erhalten werden, welche die Eigenschaften der beiden Stoffklassen synergetisch vereinigen. Die thermische Stabilität und elektrische Leitfähigkeit von POMs in MOFs kann dann durch ionische Flüssigkeiten verbessert werden.[132][133]

Wie am Beispiel von {[Cu(cyclam)(H_2O)]$_2$[Cu(cyclam)][**$Nb_{10}O_{28}$**]}$_n$·9$n$$H_2O$ gezeigt, können PONbs als Ausgangsmaterial für neue (nanostrukturierte) Materialien verwendet werden, welche sonst nur schwer zugänglich sind.

6. Anhang

6.1 Hintergrundinformationen zu den Publikationen

6.1.1 Zusatzinformation zur Publikation „Controlling Nucleation and Crystallization of Two New Polyoxoniobates

Controlling Fast Nucleation and Crystallization of Two New Polyoxoniobates

*Joanna Dopta, Dana-Céline Krause, Christian Näther, Wolfgang Bensch**

Institute of Inorganic Chemistry, Christian-Albrechts-University of Kiel, Max-Eyth-Str. 2, 24118 Kiel, Germany

* Corresponding Author,

Email: wbensch@ac.uni-kiel.de

Phone: +49 431 880 2419

Fax: +49 431 880 1520

1

Table of contents

2

Table S1. Selected crystal data for both compounds and details of the structure refinement.

	Compound I	Compound II
Sum formula	$C_{90}H_{216}N_{38}K_{10}Cu_9Si_2Nb_{36}O_{184}$	$C_{30}H_{84}N_{12}Cu_3Nb_{10}O_{34}$
Crystal system	triclinic	monoclinic
Space group	*P*-1	*C*2/c
a / Å	13.3241(3)	26.9392(5)
b / Å	19.7074(5)	11.4146(2)
c / Å	25.7409(5)	22.5881(5)
α / °	92.185(2)	90
β / °	100.535(2)	100.196(2)
γ / °	92.564(2)	90
V / Å^3	6631.2(3)	6836.2(2)
Z	1	4
Formula weight / g · mol-1	9138.80	2276.81
ρcalc. / g · cm^{-3}	2.288	2.212
λ / Å	0.71073	0.71073
Scan mode	Omega scan	Omega scan
2θ range / °	1.342 ≤ θ ≤ 26.755	1.942 ≤ θ ≤ 27.005
Crystal dimensions / mm	0.06 x 0.15 x 0.21	0.09 x 0.14 x 0.19
Crystal colour	purple	purple
Temperature / K	170	170
Index range	-16 ≤ h ≤ 19 -19 ≤ k ≤ 24 -32 ≤ l ≤ 31	-32 ≤ h ≤ 34 -14 ≤ k ≤ 14 -28 ≤ l ≤ 28
Reflections collected	64749	47935
Independent reflections	27878	7467
Reflections with $F_0>4\sigma(F_0)$	22634	6761
R_{int}	0.0351	0.0396
μ / mm-1	2.472	2.608
Number of parameters	1661	404
Transm min/max	0.6356/0.7561	0.5409/0.7507
R_1 $F_0>4\sigma(F_0)$	0.0537	0.0396
R_1 (all data)	0.0684	0.0440
wR_2 (all data)	0.1495	0.1090
ΔF /e ·Å^{-3}	1.415/ -0.998	0.699 / -0.740
GOF	1.035	1.077

3

Table S2. Nb-O bond lengths / Å in the siliconiobate anion of **I** sorted by type; O_t: terminal O atoms; Si/Nb-μ_n-O: bridging O atoms.

Nb-O_t		Nb(18)-O(50)	1.753(5)	Nb(13)-O(28)	2.121(4)	Si(1)-O(34)	1.637(5)
Nb(1)-O(29)	1.745(5)	**Si/Nb-μ_3-O**		Nb(16)-O(17)	2.068(5)	**Nb-μ_6-O**	
Nb(2)-O(23)	1.739(5)	Nb(1)-O(22)	2.099(4)	Nb(16)-O(5)	2.134(4)	Nb(3)-O(8)	2.232(4)
Nb(4)-O(47)	1.770(5)	Nb(3)-O(5)	2.107(4)	Nb(18)-O(5)	2.018(4)	Nb(4)-O(8)	2.515(4)
Nb(7)-O(43)	1.763(5)	Nb(3)-O(24)	2.193(4)	Si(1)-O(24)	1.650(4)	Nb(5)-O(26)	2.230(4)
Nb(8)-O(53)	1.760(5)	Nb(5)-O(22)	2.077(4)	Si(1)-O(27)	1.639(4)	Nb(6)-O(26)	2.209(4)
Nb(9)-O(54)	1.749(5)	Nb(5)-O(27)	2.235(4)	**Si/Nb-μ_4-O**		Nb(8)-O(26)	2.530(4)
Nb(10)-O(51)	1.756(5)	Nb(6)-O(28)	2.111(4)	Nb(1)-O(21)	2.374(4)	Nb(9)-O(8)	2.542(4)
Nb(11)-O(18)	1.758(5)	Nb(6)-O(27)	2.198(4)	Nb(2)-O(21)	2.491(4)	Nb(11)-O(8)	2.444(4)
Nb(13)-O(39)	1.745(5)	Nb(7)-O(28)	2.021(4)	Nb(7)-O(34)	2.332(4)	Nb(12)-O(8)	2.231(4)
Nb(14)-O(49)	1.745(5)	Nb(10)-O(17)	2.126(4)	Nb(10)-O(17)	2.371(4)	Nb(13)-O(26)	2.356(4)
Nb(15)-O(45)	1.750(5)	Nb(12)-O(17)	2.070(4)	Nb(17)-O(34)	2.491(4)	Nb(14)-O(26)	2.467(4)
Nb(16)-O(52)	1.743(5)	Nb(12)-O(24)	2.207(4)	Nb(18)-O(34)	2.358(4)	Nb(15)-O(26)	2.546(4)
Nb(17)-O(48)	1.764(5)	Nb(13)-O(22)	2.106(4)	Si(1)-O(21)	1.626(4)	Nb(16)-O(8)	2.338(4)
Nb-μ_2-O							
Nb(1)-O(1)	1.965(5)	Nb(5)-O(10)	1.846(5)	Nb(9)-O(16)	2.024(5)	Nb(14)-O(11)	2.027(4)
Nb(1)-O(30)	1.984(5)	Nb(5)-O(11)	1.908(4)	Nb(10)-O(36)	1.952(5)	Nb(14)-O(32)	2.046(5)
Nb(1)-O(20)	2.001(4)	Nb(6)-O(12)	1.821(5)	Nb(10)-O(20)	1.977(5)	Nb(15)-O(41)	1.962(5)
Nb(2)-O(3)	1.917(5)	Nb(6)-O(13)	1.881(5)	Nb(10)-O(3)	1.989(5)	Nb(15)-O(19)	1.976(5)
Nb(2)-O(30)	1.920(5)	Nb(6)-O(32)	1.885(4)	Nb(11)-O(35)	1.951(5)	Nb(15)-O(40)	1.996(4)
Nb(2)-O(4)	2.055(4)	Nb(7)-O(1)	1.916(4)	Nb(11)-O(9)	1.967(5)	Nb(15)-O(13)	2.047(5)
Nb(2)-O(2)	2.073(4)	Nb(7)-O(44)	2.017(4)	Nb(11)-O(38)	2.026(4)	Nb(16)-O(37)	1.933(5)
Nb(3)-O(6)	1.811(5)	Nb(7)-O(14)	2.076(5)	Nb(11)-O(7)	2.043(4)	Nb(16)-O(25)	1.951(5)
Nb(3)-O(7)	1.868(4)	Nb(8)-O(41)	1.945(5)	Nb(12)-O(2)	1.834(5)	Nb(17)-O(44)	1.916(5)
Nb(3)-O(46)	1.888(5)	Nb(8)-O(33)	1.961(4)	Nb(12)-O(16)	1.863(5)	Nb(17)-O(42)	1.947(4)
Nb(4)-O(31)	1.949(5)	Nb(8)-O(15)	1.985(5)	Nb(12)-O(38)	1.895(4)	Nb(17)-O(12)	2.046(5)
Nb(4)-O(25)	1.960(5)	Nb(8)-O(10)	2.058(5)	Nb(13)-O(15)	1.915(5)	Nb(17)-O(6)	2.055(5)
Nb(4)-O(9)	1.986(5)	Nb(9)-O(31)	1.960(5)	Nb(13)-O(40)	1.970(5)	Nb(18)-O(36)	1.921(5)
Nb(4)-O(46)	2.047(5)	Nb(9)-O(35)	1.971(4)	Nb(14)-O(33)	1.960(5)	Nb(18)-O(42)	2.026(4)
Nb(5)-O(4)	1.822(5)	Nb(9)-O(37)	2.012(4)	Nb(14)-O(19)	1.996(5)	Nb(18)-O(14)	2.064(5)

4

Table S3. Results of bond valence analysis for **I** and **II**.

$K_5[Cu(H_2O)_2(cyclam)]_{1.5}\{[Cu(cyclam)][Cu(H_2O)(cyclam)]_2HSiNb_{18}O_{54}\}(NO_3)\cdot 30H_2O$ (I)					
Nb1	5.11	Nb7	5.12	Nb13	5.05
Nb2	5.27	Nb8	5.15	Nb14	5.07
Nb3	5.16	Nb9	5.14	Nb15	5.11
Nb4	5.13	Nb10	5.09	Nb16	5.11
Nb5	5.13	Nb11	5.12	Nb17	5.15
Nb6	5.11	Nb12	5.12	Nb18	5.13
Average: 5.13					
Si1	4.73				
Terminal O atoms					
O29	1.72	O54	1.61	O45	1.60
O23	1.65	O51	1.58	O52	1.63
O47	1.52	O18	1.57	O48	1.54
O43	1.55	O39	1.62		
O53	1.56	O49	1.62		
Average: 1.60					
μ_2-bridging O atoms					
O1	1.92	O25	1.84	O33	1.81
O30	1.86	O9	1.74	O15	1.88
O3	1.86	O10	1.93	O35	1.81
O4	2.02	O11	1.80	O37	1.77
O2	1.95	O12	2.04	O16	1.95
O20	1.68	O13	1.84	O36	1.94
O6	2.16	O32	1.83	O38	1.84
O7	1.89	O44	1.80	O40	1.71
O46	1.82	O14	1.35	O19	1.69
O31	1.84	O41	1.85	O42	1.70
Average: 1.88					
μ_3-bridging O atoms					
O22	1.90				
O5	1.96				
O24	2.09				
O27	2.09				
O28	1.96				
O17	1.93				
Average: 1.99					
μ_4-bridging O atoms					
O21	2.03				
O34	2.04				
μ_6-bridging O atoms					
O26	1.82				
O34	1.84				
$\{[Cu(cyclam)(H_2O)]_2[Cu(cyclam)][Nb_{10}O_{28}]\}_n\cdot 9nH_2O$ (II)					
Nb1	5.05				
Nb2	5.07				
Nb3	5.05				
Nb4	5.09				
Nb5	4.96				
Average: 5.05					

5

Table S4. Selected bond lengths / Å and angles / ° for the five unique $[Cu(cyclam)]^{2+}$ complexes in **I**.

Cu(1)-N(1)	2.033(7)	N(4)-Cu(1)-N(2)	179.1(3)	N(3)-Cu(1)-O(77)	90.3(2)
Cu(1)-N(2)	2.003(7)	N(4)-Cu(1)-N(1)	93.5(3)	N(4)-Cu(1)-O(77)	96.6 (2)
Cu(1)-N(3)	2.034(6)	N(2)-Cu(1)-N(1)	85.7(3)	N(1)-Cu(1)-O(29)	96.9(2)
Cu(1)-N(4)	2.000(7)	N(4)-Cu(1)-N(3)	86.0(2)	N(2)-Cu(1)-O(29)	86.9(2)
Cu(1)-O(77)	2.529(7)	N(2)-Cu(1)-N(3)	94.7(3)	N(3)-Cu(1)-O(29)	83.4(2)
Cu(1)-O(29)	2.698(4)	N(1)-Cu(1)-N(3)	179.5(3)	N(4)-Cu(1)-O(29)	93.5(2)
		N(1)-Cu(1)-O(77)	89.5(2)	O(77)-Cu(1)-O(29)	167.6(2)
		N(2)-Cu(1)-O(77)	83.0(3)		
Cu(2)-N(11)	2.028(6)	N(13)-Cu(2)-N(12)	94.4(2)	N(13)-Cu(2)-O(69)	89.0(2)
Cu(2)-N(12)	2.014(6)	N(13)-Cu(2)-N(11)	179.3(2)	N(14)-Cu(2)-O(69)	92.1(2)
Cu(2)-N(13)	2.011(6)	N(12)-Cu(2)-N(11)	86.3(3)	N(11)-Cu(2)-O(65)	89.7(2)
Cu(2)-N(14)	2.034(6)	N(13)-Cu(2)-N(14)	85.6(2)	N(12)-Cu(2)-O(65)	86.8(2)
Cu(2)-O(65)	2.541(5)	N(12)-Cu(2)-N(14)	179.4(3)	N(13)-Cu(2)-O(65)	90.2(2)
Cu(2)-O(69)	2.647(6)	N(11)-Cu(2)-N(14)	93.7(3)	N(14)-Cu(2)-O(65)	93.8(2)
		N(11)-Cu(2)-O(69)	91.1(2)	O(69)-Cu(2)-O(65)	174.0(2)
		N(12)-Cu(2)-O(69)	87.3(2)		
Cu(3)-N(21)	1.995(6)	N(21)-Cu(3)-N(24)	93.8(3)	N(23)-Cu(3)-O(70)	86.2(2)
Cu(3)-N(22)	2.027(6)	N(21)-Cu(3)-N(23)	178.2(3)	N(24)-Cu(3)-O(70)	88.2(3)
Cu(3)-N(23)	2.026(7)	N(24)-Cu(3)-N(23)	85.4(3)	N(21)-Cu(3)-O(51)	88.0(2)
Cu(3)-N(24)	2.024(7)	N(21)-Cu(3)-N(22)	86.0(3)	N(22)-Cu(3)-O(51)	86.4(2)
Cu(3)-O(70)	2.648(6)	N(24)-Cu(3)-N(22)	178.7(3)	N(23)-Cu(3)-O(51)	93.7(2)
Cu(3)-O(58)	2.558(5)	N(23)-Cu(3)-N(22)	94.8(3)	N(24)-Cu(3)-O(51)	94.9(2)
		N(21)-Cu(3)-O(70)	93.1(2)	O(70)-Cu(3)-O(51)	176.8(2)
		N(22)-Cu(3)-O(70)	90.4(2)		
Cu(4)-N(31)	2.024(6)	N(34)-Cu(4)-N(32)	177.2(3)	N(33)-Cu(4)-O(54)	90.2(2)
Cu(4)-N(32)	2.018(6)	N(34)-Cu(4)-N(33)	86.4(3)	N(31)-Cu(4)-O(54)	95.9(2)
Cu(4)-N(33)	2.020(7)	N(32)-Cu(4)-N(33)	94.9(3)	N(34)-Cu(4)-O(45)	91.6 (2)
Cu(4)-N(34)	2.016(6)	N(34)-Cu(4)-N(31)	92.6(3)	N(32)-Cu(4)-O(45)	87.6(2)
Cu(4)-O(54)	2.401(6)	N(32)-Cu(4)-N(31)	85.9(3)	N(33)-Cu(4)-O(45)	82.2 (2)
Cu(4)-O(45)	3.031(6)	N(33)-Cu(4)-N(31)	173.8(3)	N(31)-Cu(4)-O(45)	90.5(2)
		N(34)-Cu(4)-O(54)	89.6(2)	O(45)-Cu(4)-O(54)	172.4(2)
		N(32)-Cu(4)-O(54)	92.5(2)		
Cu(5)-N(41)	1.996(8)	N(42)-Cu(5)-N(42)	180.0	N(42)-Cu(5)-N(42)	180.00
Cu(5)-N(42)	2.014(7)	N(41)-Cu(5)-N(42)	94.9(3)	N(41)-Cu(5)-O(78)	90.5(3)
Cu(5)-O(78)	2.451(8)	N(41)-Cu(5)-N(42)	85.1(3)	N(42)-Cu(5)-O(78)	96.4(3)
		N(41)- Cu(5)- N(42)	85.1(3)	O(78)-Cu(5)-O(78)	180.00
		N(41)- Cu(5)-N(42)	94.9(3)		

6

Table S5. K-O distances in **I** / Å. Distances longer than the sum of ionic radii are marked in grey.

K(1)-O(1)	2.729(5)	K(4)-O(7)	2.913(5)	K(3)-O(48)	2.729(5)
K(1)-O(29)	2.958(5)	K(4)-O(11)	3.102(5)	K(3)-O(48)#1	2.839(5)
K(1)-O(39)	2.842(5)	K(4)-O(24)	2.882(4)	O(48)-K(3)#1	2.839(5)
K(1)-O(43)	2.840(5)	K(4)-O(27)	2.904(4)	K(3)-O(72)	2.801(6)
K(1)-O(50)	2.675(5)	K(4)-O(32)	2.905(5)	O(72)-K(3)#2	2.801(6)
O(50)-K(1)#2	2.675(5)	K(4)-O(38)	3.079(5)	K(3)-O(81)	2.806(6)
K(1)-O(85)	2.858(6)	K(4)-O(66)	2.653(5)	K(3)-O(85)	2.841(6)
K(1)-O(80)	2.912(8)	K(4)-O(65)	2.866(5)	K(3)-O(85)#4	2.841(6)
K(1)-O(64)	3.097(6)	K(5)-O(96)	2.60(3)	O(85)-K(3)#2	2.841(6)
K(2)-O(36)	2.701(5)	K(5)-O(96´)	2.92(3)	K(3)-O(68)#1	3.061(7)
K(2)-O(43)	2.680(5)	K(5)-O(97)	2.85(4)	O(68)-K(3)#1	3.061(7)
O(43)-K(2)#2	2.680(5)	K(5)-O(80)#2	2.896(7)		
K(2)-O(50)	2.882(5)	O(80)-K(5)#2	2.896(7)		
K(2)-O(51)	2.962(5)	K(5)-O(68)	2.965(7)		
K(2)-O(52)	2.940(5)	K(5)-O(25)	2.740(5)		
K(2)-O(94)	2.760(1)	K(5)-O(50)	2.792(6)		
K(2)-O(72)	2.892(6)	K(5)-O(52)	2.995(6)		
K(2)-O(64)	3.086(6)	K(5)-O(98)	3.12(3)		

Table S6. O···O distances in the layered water cluster in **I**.

Atom 1	Atom 2	Distance / Å	Atom 1	Atom 2	Distance / Å
O92	O89	2.616	O93	O79	2.778
O88	O78	2.619	O95	O79	2.785
O93	O94	2.643	O87	O68	2.792
O92	O82	2.655	O81	O87	2.797
O92	O90	2.697	O73	O66	2.820
O88	O83	2.705	O67	O85	2.821
O90	O73	2.707	O83	O70	2.830
O89	O77	2.721	O67	O72	2.833
O91	O83	2.723	O91	O75	2.840
O71	O81	2.725	O86	O70	2.856
O84	O73	2.729	O84	O74	2.889
O90	O88	2.751	O89	O84	2.903
O84	O74	2.755	O93	O79	2.908
O77	O75	2.762	O64	O67	2.984
O94	O80	2.777	O95	O86	2.987
Average: 2.779					

7

Table S7. Nb-O bond lengths / Å in the decaniobate anion of **II** sorted by type.

O_t: terminal O atoms; Nb-μ_n-O: bridging O atoms.

Nb-Ot		Nb-μ2-O		Nb-μ3-O		Nb-μ6-O	
Nb(1)-O(3)	1.744(3)	Nb(1)-O(4)	1.923(3)	Nb(1)-O(1)	2.138(3)	Nb(1)-O(2) #1	2.414(2)
Nb(2)-O(8)	1.744(3)	Nb(1)-O(6)	1.932(3)	O(1)-Nb(1)#1	2.138(3)	O(2)-Nb(1)#1	2.414(2)
Nb(3)-O(12)	1.753(3)	Nb(2)-O(7)	1.951(3)	Nb(1)-O(5)	2.100(3)	Nb(2)-O(2) #1	2.536(2)
Nb(4)-O(11)	1.738(3)	Nb(2)-O(9) #1	2.097(3)	Nb(3)-O(1) #1	2.118(2)	O(2)-Nb(2)#1	2.536(2)
		O(9)-Nb(2)#1	2.097(3)	O(1)-Nb(3)#1	2.118(2)	Nb(3)-O(2)	2.405(2)
		Nb(2)-O(10) #1	1.990(3)	Nb(3)-O(5)	2.129(3)	Nb(4)-O(2)	2.545(2)
		O(10)-Nb(2)#1	1.990(3)	Nb(5)-O(1)	2.009(3)	Nb(4)-O(2)#1	2.545(2)
		Nb(2)-O(4)	1.978(3)	Nb(5)-O(5)	2.020(3)	O(2)-Nb(4)#1	2.545(2)
		Nb(3)-O(10)	1.916(3)			Nb(5)-O(2)	2.218(2)
		Nb(3)-O(13)	1.918(3)			Nb(5)-O(2)#1	2.218(2)
		Nb(4)-O(6)	1.995(2)			O(2)-Nb(5)#1	2.218(2)
		Nb(4)-O(7)	1.953(3)			Nb(5)-O(2)	2.225(2)
		Nb(4)-O(14)	2.076(3)				
		Nb(4)-O(13)	1.990(3)				
		Nb(4)-O(13)#1	1.990(3)				
		O(13)-Nb(4)#1	1.990(3)				
		Nb(5)-O(9)	1.830(3)				
		Nb(5)-O(14)	1.833(3)				

Symmetry transformations used to generate equivalent atoms: #1 -x+3/2,-y+1/2,-z+1.

Table S8. Selected bond angles / ° in the decaniobate anion of **II**.

O(3)-Nb(1)-O(6)	107.03(13)	O(1)#1-Nb(3)-O(5)	73.48(10)
O(4)-Nb(1)-O(6)	94.69(12)	O(12)-Nb(3)-O(2)	173.85(12)
O(3)-Nb(1)-O(5)	103.62(12)	O(10)-Nb(3)-O(2)	79.49(10)
O(4)-Nb(1)-O(5)	149.94(10)	O(13)-Nb(3)-O(2)	79.99(10
O(6)-Nb(1)-O(5)	91.40(11)	O(1)#1-Nb(3)-O(2)	73.47(9)
O(3)-Nb(1)-O(1)#1	99.13(12)	O(5)-Nb(3)-O(2)	73.37(9)
O(4)-Nb(1)-O(1)#1	87.99(11)	O(11)-Nb(4)-O(7)	103.17(14)
O(6)-Nb(1)-O(1)#1	152.38(11)	O(11)-Nb(4)-O(13)#1	103.06(15)
O(5)-Nb(1)-O(1)#1	73.65(10)	O(7)-Nb(4)-O(13)#1	88.47(11)
O(3)-Nb(1)-O(2)#1	172.25(12)	O(11)-Nb(4)-O(6)	105.60(15)
O(4)-Nb(1)-O(2)#1	78.53(10)	O(7)-Nb(4)-O(6)	88.74(11)
O(6)-Nb(1)-O(2)#1	80.40(10)	O(13)#1-Nb(4)-O(6)	151.08(11)
O(5)-Nb(1)-O(2)#1	73.52(9)	O(11)-Nb(4)-O(14)	106.42(14)
O(1)#1-Nb(1)-O(2)#1	73.19(9)	O(7)-Nb(4)-O(14)	150.41(11)
O(3)-Nb(1)-O(4)	102.65(13)	O(13)#1-Nb(4)-O(14)	84.32(11)
O(8)-Nb(2)-O(7)	103.18(13)	O(6)-Nb(4)-O(14)	84.03(11)
O(8)-Nb(2)-O(4)	104.57(12)	O(11)-Nb(4)-O(2)#1	178.30(14)
O(7)-Nb(2)-O(4)	89.66(11)	O(7)-Nb(4)-O(2)#1	77.22(10)
O(8)-Nb(2)-O(10)#1	105.76(12)	O(13)#1-Nb(4)-O(2)#1	75.27(9)
O(7)-Nb(2)-O(10)#1	89.42(11)	O(6)-Nb(4)-O(2)#1	76.04(9)
O(4)-Nb(2)-O(10)#1	149.03(11)	O(14)-Nb(4)-O(2)#1	73.19(9)
O(8)-Nb(2)-O(9)#1	105.53(12)	O(9)-Nb(5)-O(14)	109.55(12)

8

O(7)-Nb(2)-O(9)#1	151.29(11)	O(9)-Nb(5)-O(1)	97.86(11)
O(4)-Nb(2)-O(9)#1	83.22(11)	O(14)-Nb(5)-O(1)	98.15(11)
O(10)#1-Nb(2)-O(9)#1	82.87(11)	O(9)-Nb(5)-O(5)	97.62(11)
O(8)-Nb(2)-O(2)#1	178.98(11)	O(14)-Nb(5)-O(5)	96.88(12)
O(7)-Nb(2)-O(2)#1	77.49(10)	O(1)-Nb(5)-O(5)	153.39(10)
O(4)-Nb(2)-O(2)#1	74.62(9)	O(9)-Nb(5)-O(2)#1	164.31(11)
O(10)#1-Nb(2)-O(2)#1	74.98(9)	O(14)-Nb(5)-O(2)#1	86.13(11)
O(9)#1-Nb(2)-O(2)#1	73.81(9)	O(1)-Nb(5)-O(2)#1	79.77(9)
O(12)-Nb(3)-O(10)	104.30(12)	O(5)-Nb(5)-O(2)#1	79.48(9)
O(12)-Nb(3)-O(13)	104.19(14)	O(9)-Nb(5)-O(2)	86.92(10)
O(10)-Nb(3)-O(13)	96.06(12)	O(14)-Nb(5)-O(2)	163.51(11)
O(12)-Nb(3)-O(1)#1	101.81(12)	O(1)-Nb(5)-O(2)	79.89(9)
O(10)-Nb(3)-O(1)#1	150.78(10)	O(5)-Nb(5)-O(2) 7	79.47(9)
O(13)-Nb(3)-O(1)#1 9	90.03(11)	O(2)#1-Nb(5)-O(2)	77.39(10)
O(12)-Nb(3)-O(5)	101.68(13)	Nb(3)-O(13)-Nb(4)#1	118.43(13)
O(10)-Nb(3)-O(5)	88.50(11)	Nb(5)-O(14)-Nb(4) 1	113.92(13)
O(13)-Nb(3)-O(5)	151.68(10)		

Symmetry transformations used to generate equivalent atoms: #1 -x+3/2,-y+1/2,-z+1.

Table S9. Selected bond lengths/ Å and angles/ ° for the two unique $[Cu(cyclam)]^{2+}$ molecules in **II**.

Cu(1)-N(1)	2.030(4)	N(3)-Cu(1)-N(2)	94.6(2)	N(2)-Cu(1)-N(1)	86.6(2)
Cu(1)-N(2)	2.019(4	N(3)-Cu(1)-N(4)	85.6(2)	N(4)-Cu(1)-N(1)	93.2(2)
Cu(1)-N(3)	2.013(4)	N(2)-Cu(1)-N(4)	179.5(2)	N(1)-Cu(1)-O(3)	90.9(1)
Cu(1)-N(4)	2.027(3)	N(1)-Cu(1)-O(21)	81.2(2)	N(2)-Cu(1)-O(3)	91.4(1)
Cu(1)-O(3)	2.469(3)	N(2)-Cu(1)-O(21)	87.7(1)	N(3)-Cu(1)-O(3)	91.2(1)
Cu(1)-O(21)	2.594(5)	N(3)-Cu(1)-O(21)	96.8(2)	N(4)-Cu(1)-O(3)	89.1(1)
		N(4)-Cu(1)-O(21)	91.8(1)	O(3)-Cu(1)-O(21)	172.1(1)
		N(3)-Cu(1)-N(1)	177.6(2)		
Cu(2)-N(11)	2.005(3)	N(11)-Cu(2)-N(11)#2	180.0(4)	N(11)-Cu(2)-N(12)#2	94.2(2)
Cu(2)-N(11)#2	2.005(3)	N(11)-Cu(2)-N(12)	85.9(2)	N(11)#2-Cu(2)-N(12)#2	85.9(2)
Cu(2)-N(12)	2.027(4)	N(11)#2-Cu(2)-N(12)	94.1(2)	N(12)-Cu(2)-N(12)#2	180.0
Cu(2)-N(12)#2	2.027(4)	N(11)-Cu(2)-O(11)	94.5(1)	O(11)-Cu(2)-O(11)	180.0
Cu(2)-O(11)	2.721(4)	N(11) #2-Cu(2)-O(11)	85.5(1)		
		N(12)-Cu(2)-O(11)	89.4(1)		
		N(12) #2-Cu(2)-O(11)	90.6(1)		

Symmetry transformations used to generate equivalent atoms: #2 -x+1,-y+1,-z.

9

Table S10. Geometrical parameters of hydrogen bonds in **II** / Å and / °.

D-H...A	d(D-H)	d(H...A)	d(D...A)	<(DHA)
N-H···O bonding interactions between cyclam molecules and cluster O atoms				
N(2)-H(2)...O(4)	1.00	2.13	3.018(5)	146.5
N(3)-H(3)...O(12)	1.00	2.03	2.968(5)	156.1
N(4)-H(4)...O(10)#3	1.00	2.17	3.049(4)	145.9
N(11)-H(11)...O(7)#4	1.00	2.01	2.988(4)	166.0
N(12)-H(12)...O(13)#7	0.99	1.96	2.949(4)	168.4
N-H···O bonding interactions between cyclam molecules and water O atoms				
N(1)-H(1)...O(21)	1.00	2.52	3.038(6)	111.6
C-H···O bonding interactions between cyclam molecules and cluster O atoms				
C(1)-H(1A)...O(4)	0.99	2.47	3.241(6)	134.6
C(4)-H(4A)...O(1)#1	0.99	2.55	3.480(6)	156.4
C(7)-H(7A)...O(5)#3	0.99	2.65	3.365(5)	128.8
C(8)-H(8A)...O(3)	0.99	2.55	3.210(5)	123.6
C(11)-H(11B)...O(8)#5	1.00	2.53	3.472(6	158.3
C(14)-H(14A)...O(10)#7	1.00	2.50	3.429(6)	156.1
C(15)-H(15A)...O(11)#4	0.99	2.56	3.248(6)	126.4
C-H···O bonding interactions between cyclam molecules and water O atoms				
C(9)-H(9B)...O(23)	0.99	2.58	3.258(6)	125.8
C(12)-H(12A)...O(22)#6	0.99	2.62	3.579(7)	163.6
C(15)-H(15B)...O(23)#8	0.99	2.54	3.515(7)	169.9
O-H···O bonding interactions between water molecules and water O atoms				
O(22)-H(4O)...O(23)#10	0.84	1.92	2.755(6)	175.4
O-H···O bonding interactions between water molecules and cluster O atoms				
O(21)-H(2O)...O(12)#3	0.99	1.92	2.746(5)	167.7
O(22)-H(3O)...O(6)#9	0.84	2.31	2.992(5)	139.1
O(22)-H(3O)...O(7)#9	0.84	2.53	3.217(5)	139.1
O(23)-H(5O)...O(8)#11	0.84	2.06	2.876(5)	164.7
O(23)-H(6O)...O(8)#9	0.84	1.96	2.798(4)	171.3

Symmetry transformations used to generate equivalent atoms: #1 -x+3/2,-y+1/2,-z+1; #2 -x+1,-y+1,-z; #3 -x+3/2,y+1/2,-z+3/2; #4 x-1/2,-y+1/2,z-1/2; #5 -x+3/2,y-1/2,-z+1/2; #6 x-1/2,y-1/2,z-1; #7 x,-y+1,z-1/2; #8 -x+3/2,-y+3/2,-z+1; #9 x,-y+1,z+1/2; #10 -x+2,-y+1,-z+2 #11 -x+2,y,-z+3/2.#

10

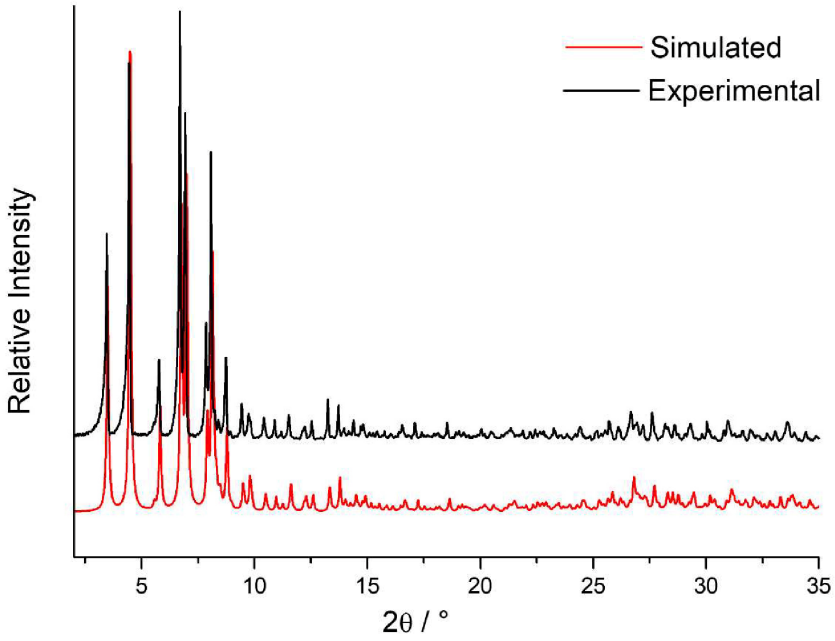

Figure S1. Comparison of simulated (red) and experimental (black) powder patterns for **I**.

11

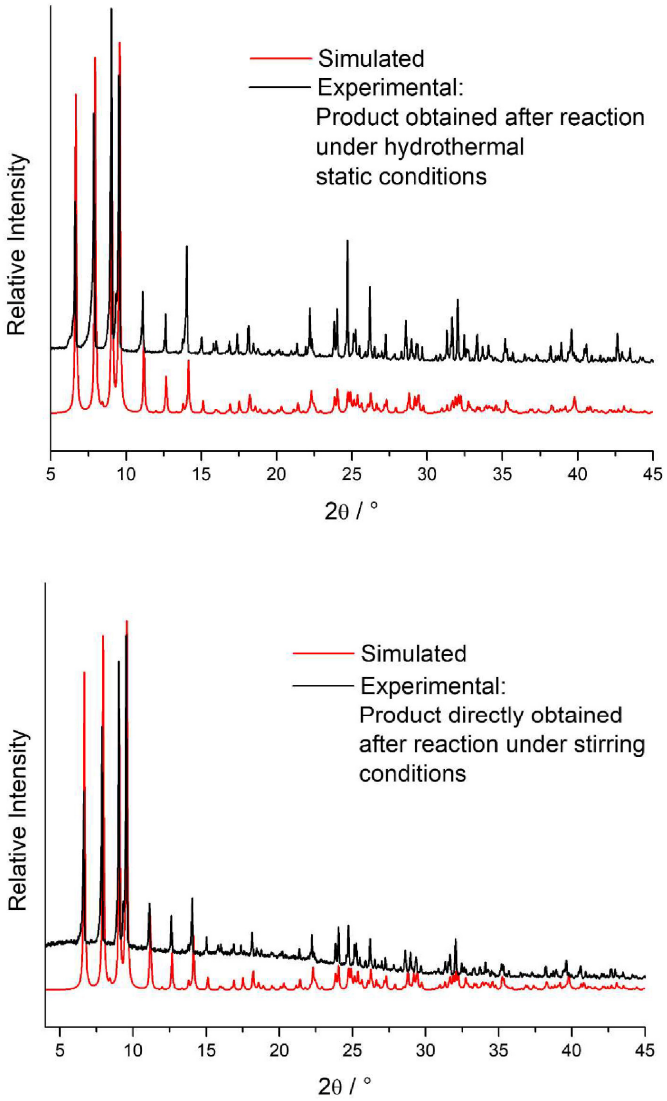

Figure S2. Comparison of simulated (red) and experimental (black) powder patterns of **II** obtained after dynamic (top) and static (bottom) reaction conditions.

12

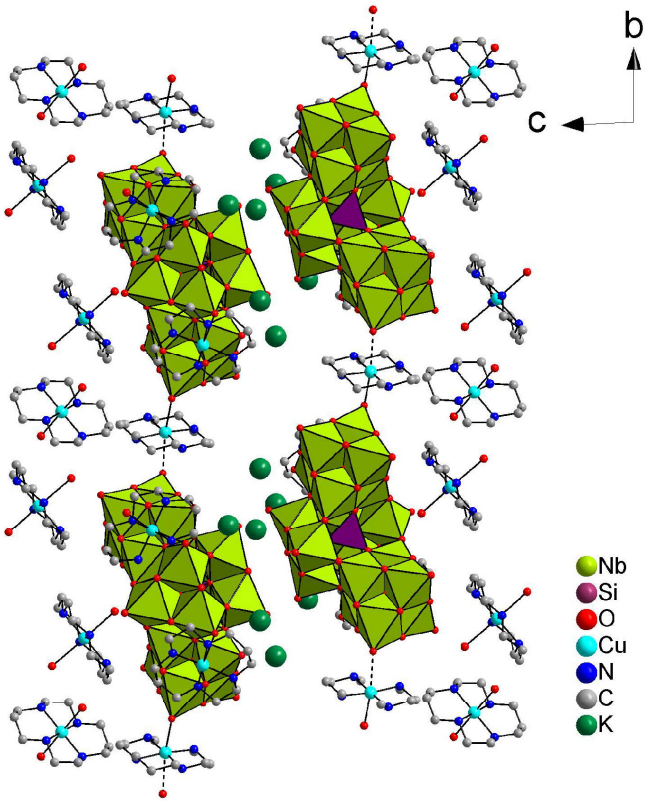

Figure S3. View on the bc plane in the structure of **I**. $\{HSiNb_{18}O_{54}\}$ clusters and $[Cu(cyclam)]^{2+}$ cations build a 1D pseudo-chain. The longest Cu-O distances are shown in dashed lines. Green polyhedra: NbO_6 units; purple polyhedra: SiO_4 units. Crystal water O atoms and H atoms are omitted.

13

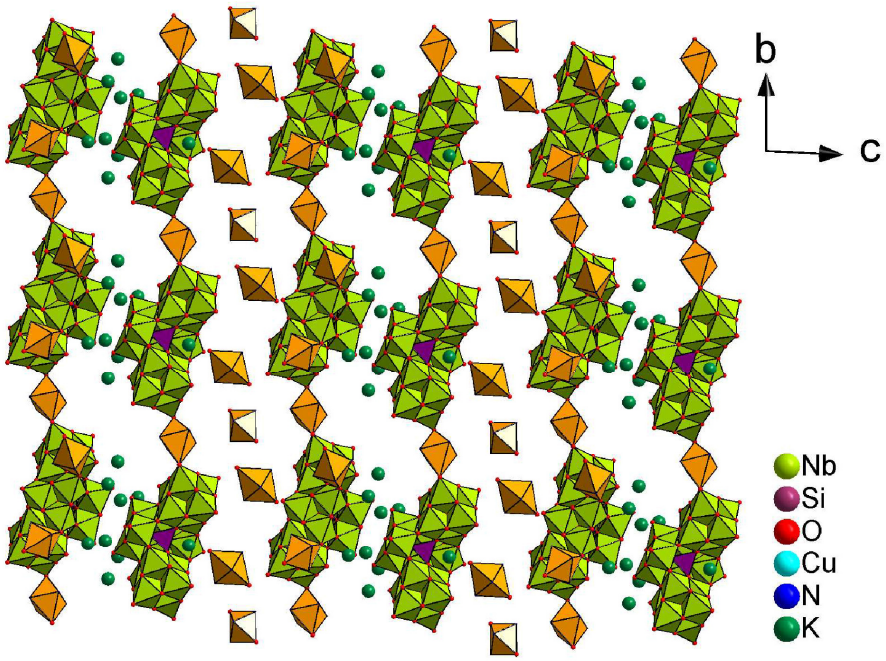

Figure S4. View along a axis on the arrangement of anionic and cationic units in **I**. Green polyhedra: NbO_6; purple polyhedra: SiO_4; orange polyhedra: CuO_2N_4. C, H and water O atoms are not displayed.

14

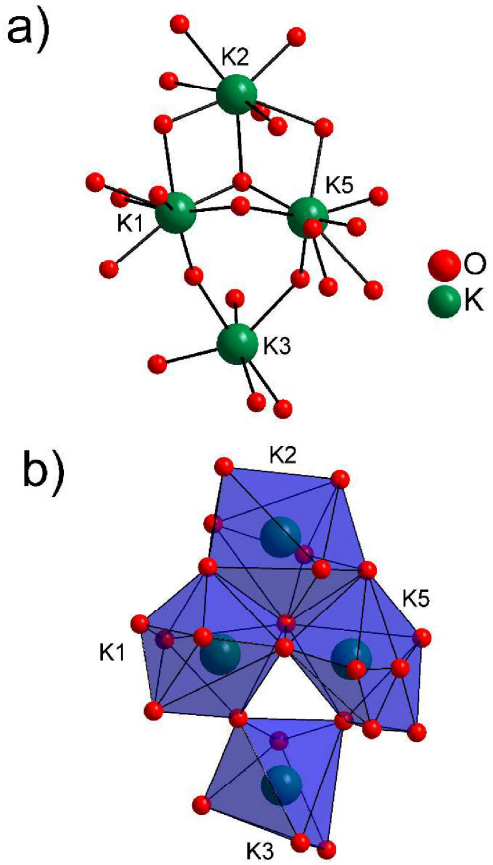

Figure S5a-b. Coordination environments around the K^+ ions in **I**. Blue polyhedra: KO_x (X=.6-9).The K^+ ion in the pocket of the cluster (K4) is not displayed.

15

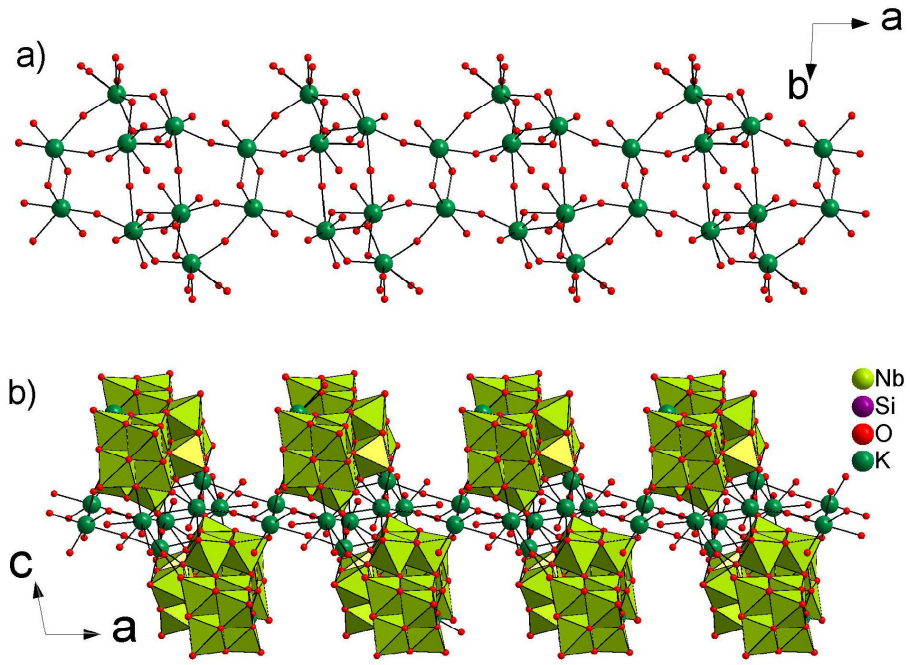

Figure S6a-b. a) Channel-like arrangement of the potassium ions surrounded by water molecules in **I** along [001]. b) View along b axis on the K-O_{water} channels between the $[HSiNb_{18}O_{54}]^{13-}$ anions. Green polyhedra: NbO_6 octahedra. Please note that some atoms are omitted for clarity.

16

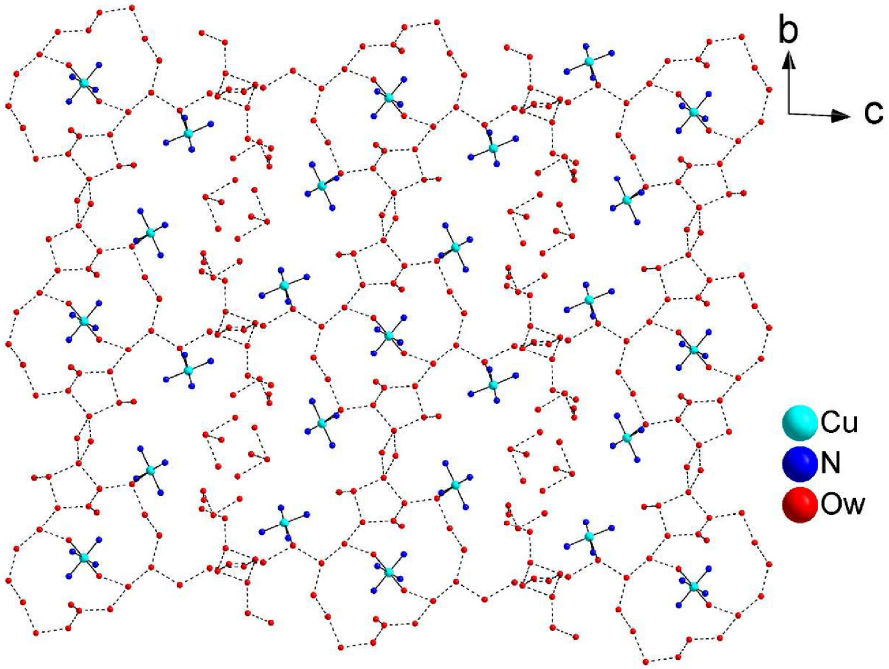

Figure S7. View on the bc plane: Arrangement of water oxygen atoms (O_w) in compound **I**, building a layered L4(2)4(4)5(4)10(4)16(6)42(14) motif. For clarity, the majority of atoms are omitted.

17

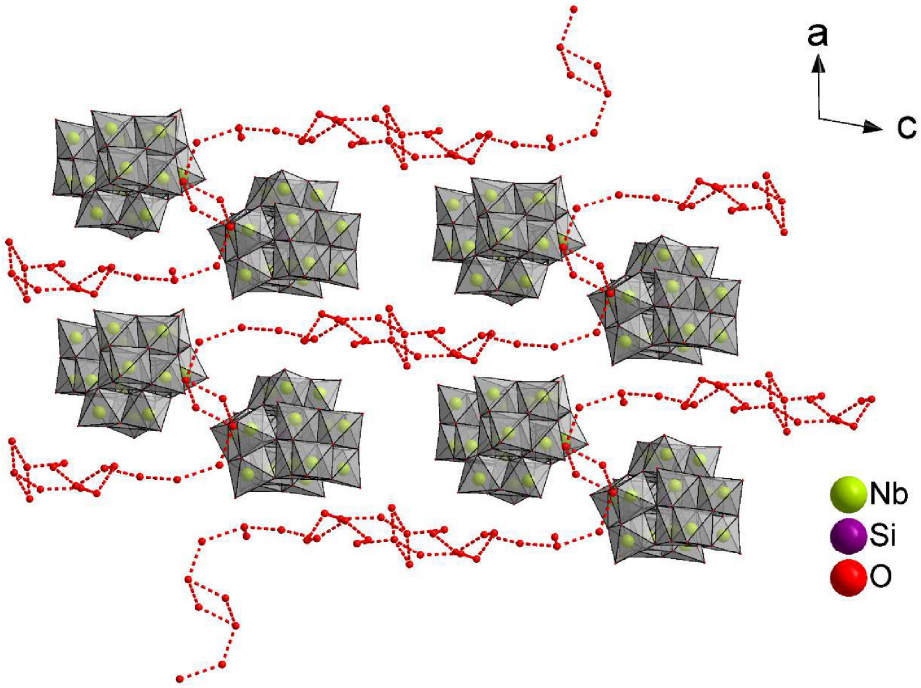

Figure S8. View on the arrangement of the water cluster in **I** along [010]. Grey polyhedra: NbO_6 units; For sake of clarity, most of the atoms are omitted.

18

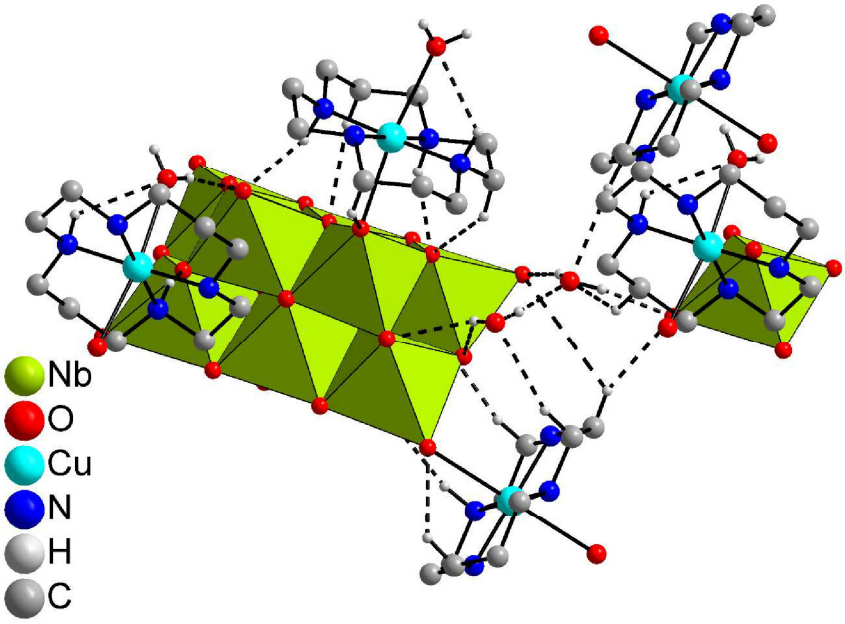

Figure S9. View on the hydrogen bonding in **II**. Green polyhedra: NbO_6 units; all hydrogen atoms (except water H atoms) which are not involved in hydrogen bonding are not displayed.

19

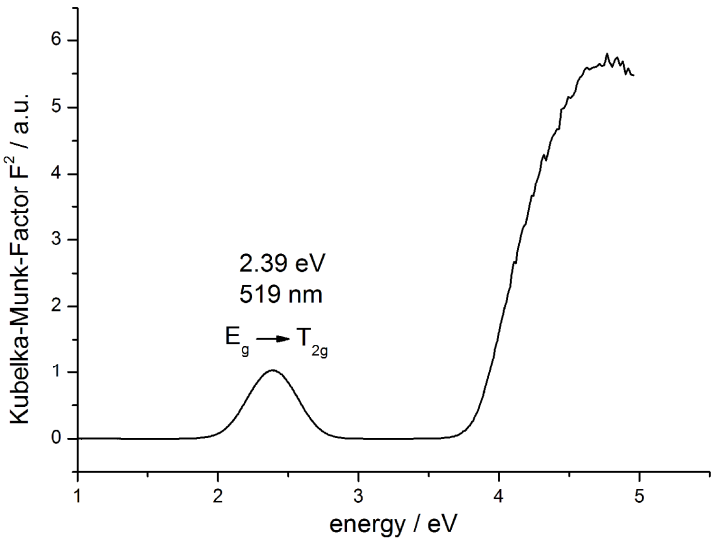

Figure S10. Kubelka Munk Factor F^2 plotted against energy for

$K_5[Cu(H_2O)_2(cyclam)]_{1.5}\{[Cu(cyclam)][Cu(H_2O)(cyclam)]_2HSiNb_{18}O_{54}\}(NO_3)\cdot 30H_2O$ (**I**).

20

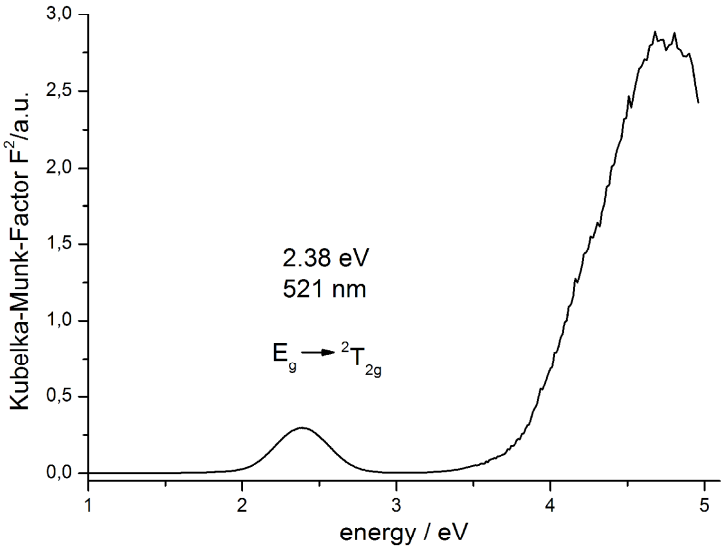

Figure S11. Kubelka Munk Factor F^2 plotted against energy for $\{[Cu(cyclam)(H_2O)]_2[Cu(cyclam)][Nb_{10}O_{28}]\}_n \cdot 9nH_2O$ (**II**).

21

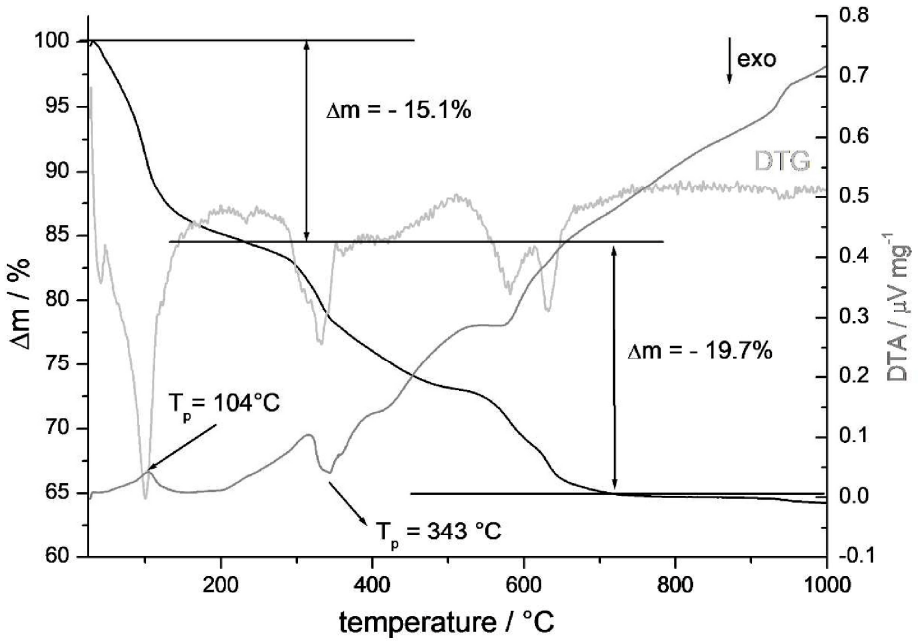

Figure S12. DTA, TG and DTG curves of compound **I** (air atmosphere).

22

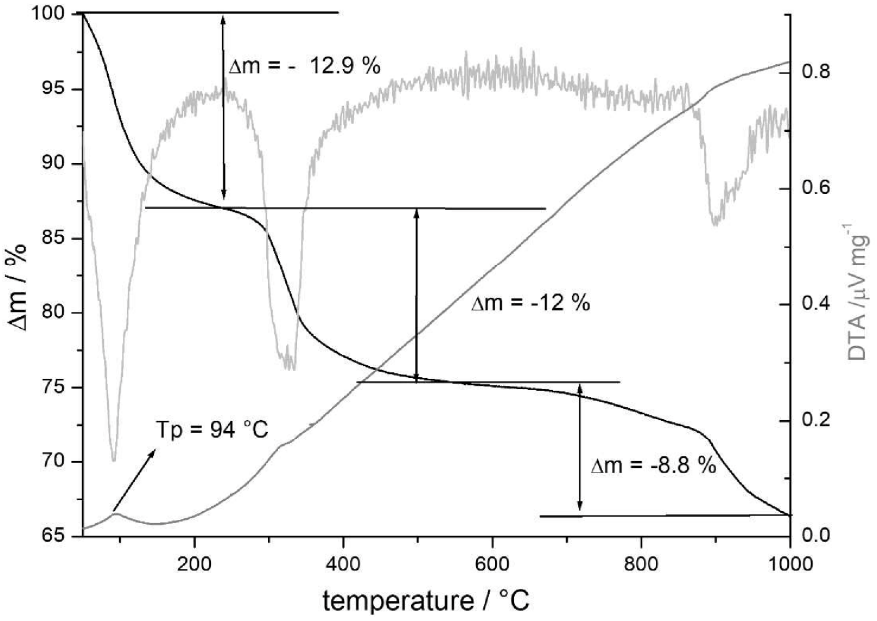

Figure S13. DTA, TG and DTG curves of compound **I** (N_2 atmosphere).

23

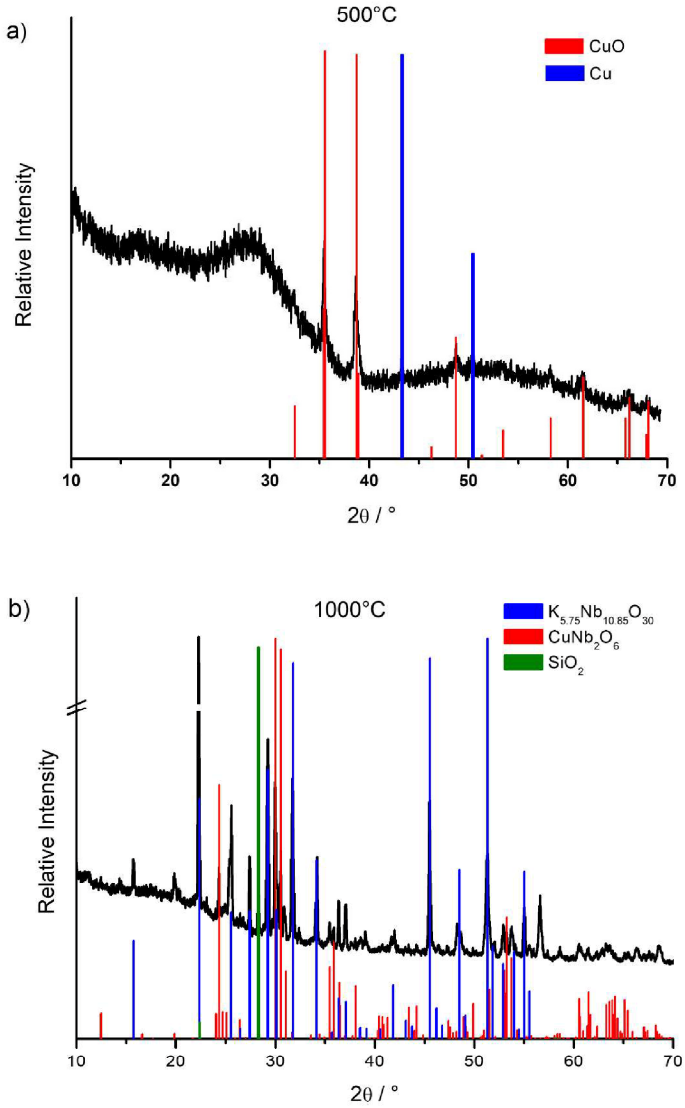

Figure S14a-b. XRD patterns of compound **I** decomposed in air atmosphere at 500 °C (top) and 1000 °C (bottom) together with the assignment of the reflections to known compounds.

24

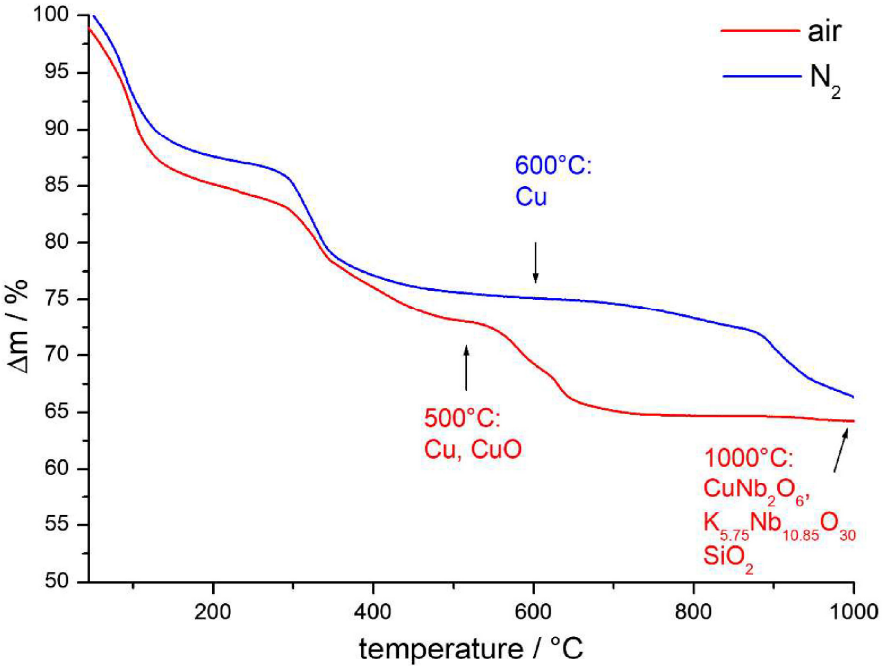

Figure S15. TG curves and decomposition products of compound **I** measured in N_2 atmosphere (blue) and air atmosphere (red).

25

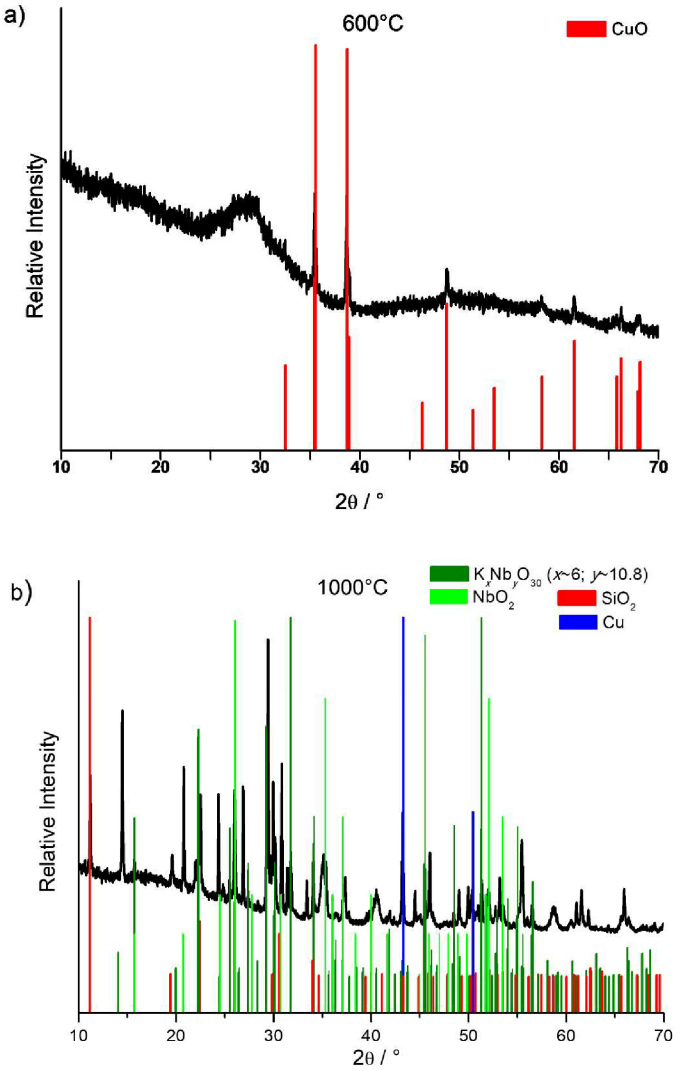

Figure S16a-b. XRD patterns of compound **I** decomposed in N_2 atmosphere at 600 °C (top) and 1000 °C (bottom) together with the assignment of the reflections to known compounds.

26

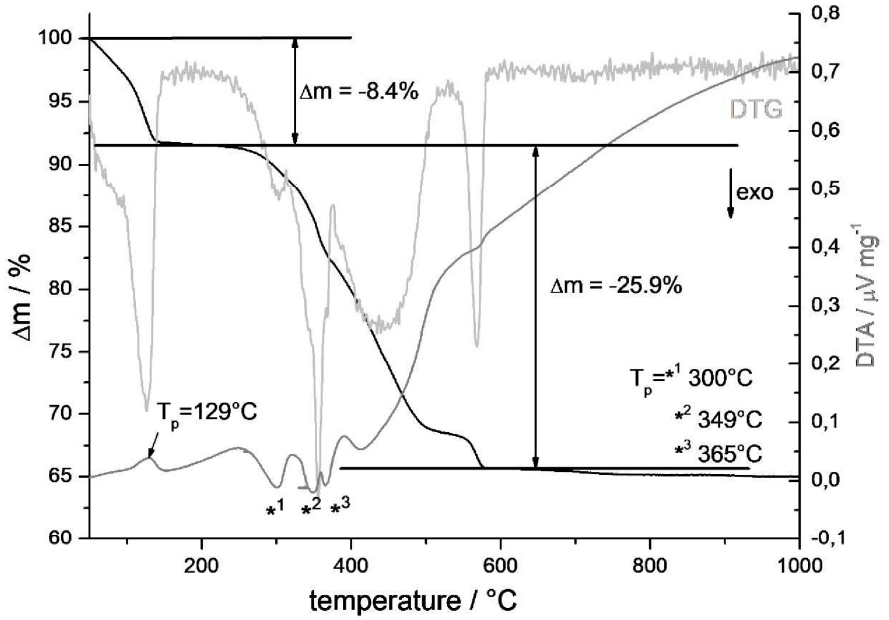

Figure S17. DTA, TG and DTG curves of compound **II** (air atmosphere).

27

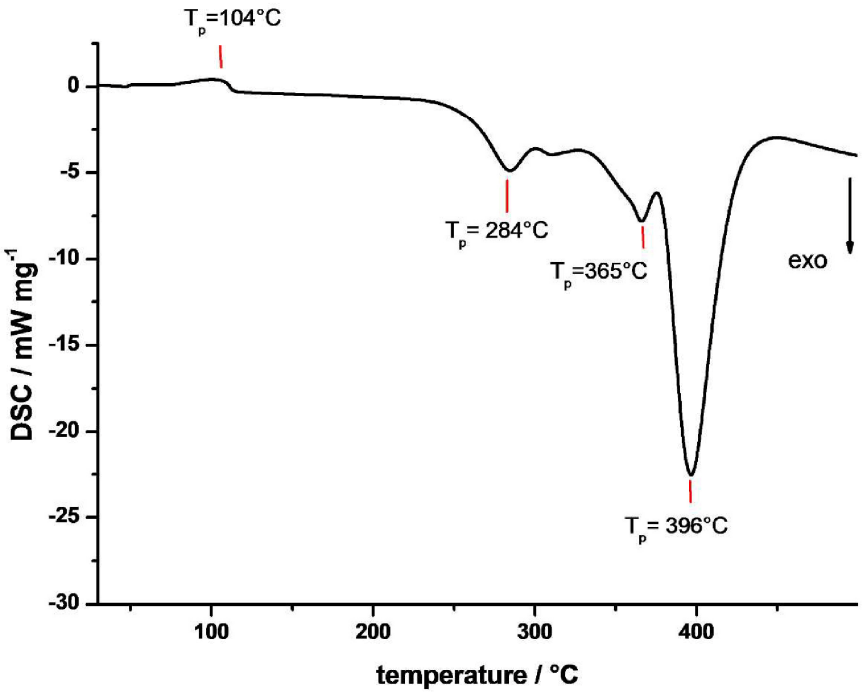

Figure S18. DSC curve of compound **II** measured in air atmosphere.

28

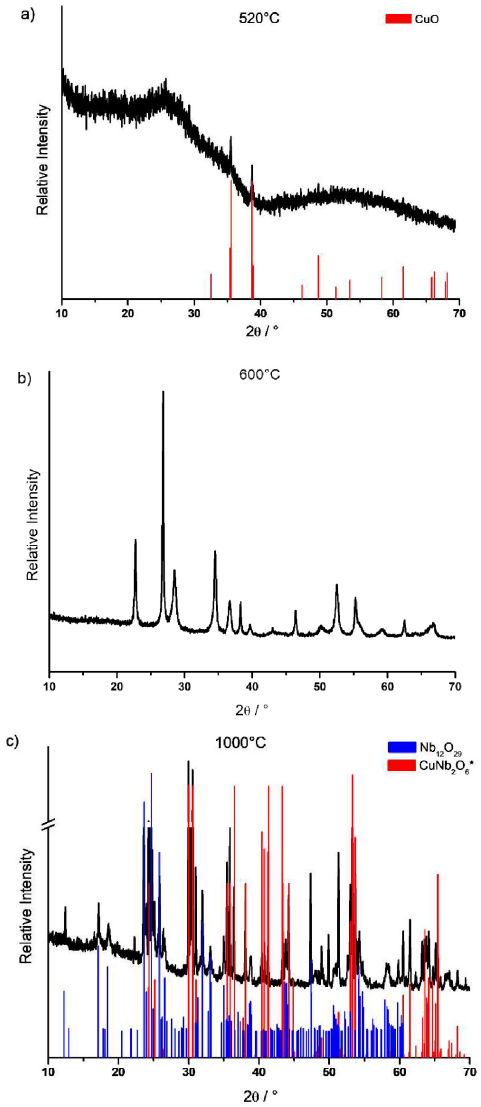

Figure S19. XRD patterns of compound **II** decomposed in air atmosphere at 520°C (top), 600°C (mid) and 1000°C (bottom) together with the assignment of the reflections to CuO, $CuNb_2O_6$ or $Nb_{12}O_{28}$. * Please note that two modifications of $CuNb_2O_6$ are observed.

29

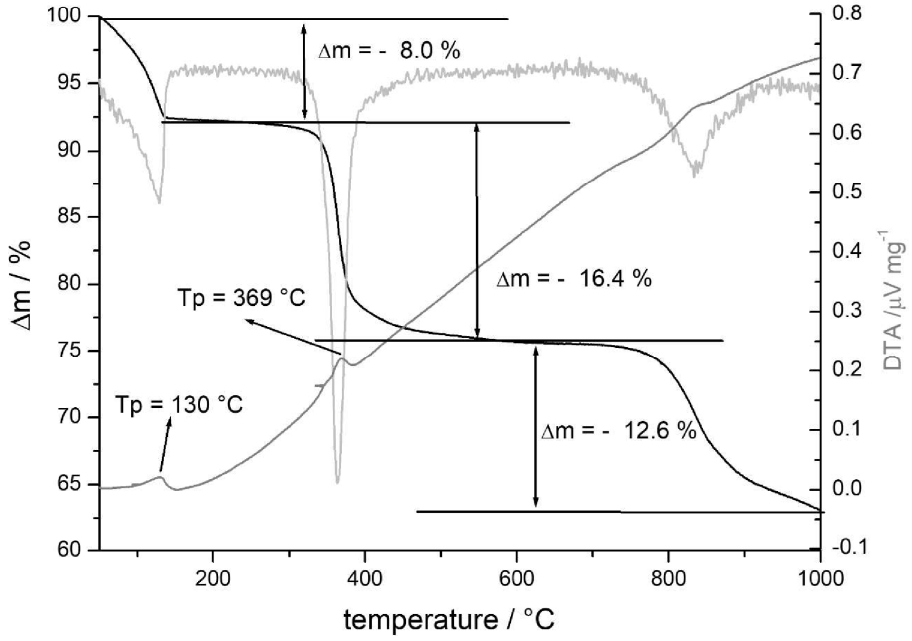

Figure S20. DTA, TG and DTG curves of compound **II** (N_2 atmosphere).

30

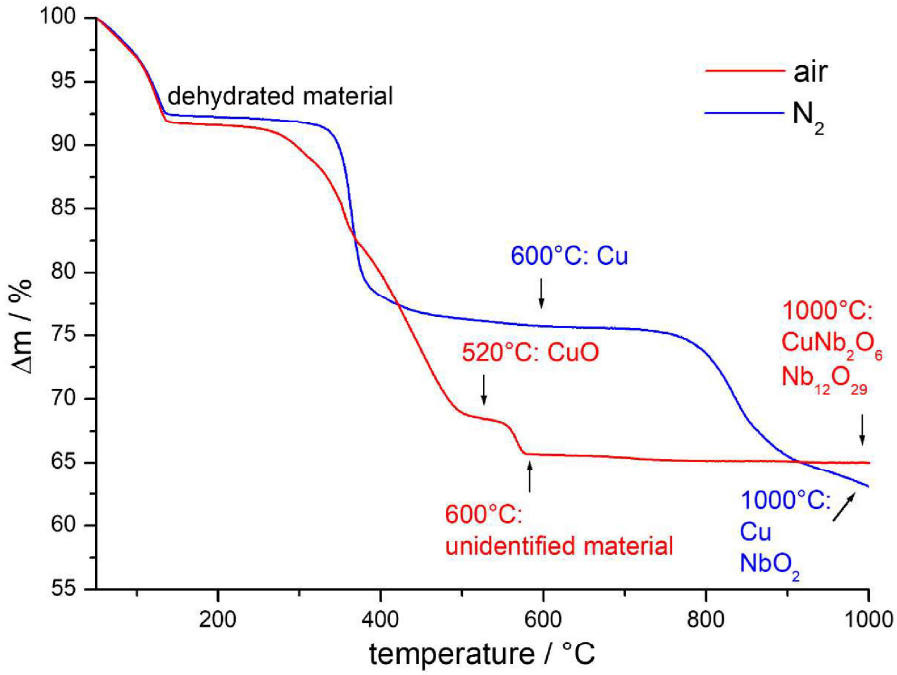

Figure S21. TG curves and decomposition products of compound **II** measured in N_2 atmosphere (blue) and air atmosphere (red).

31

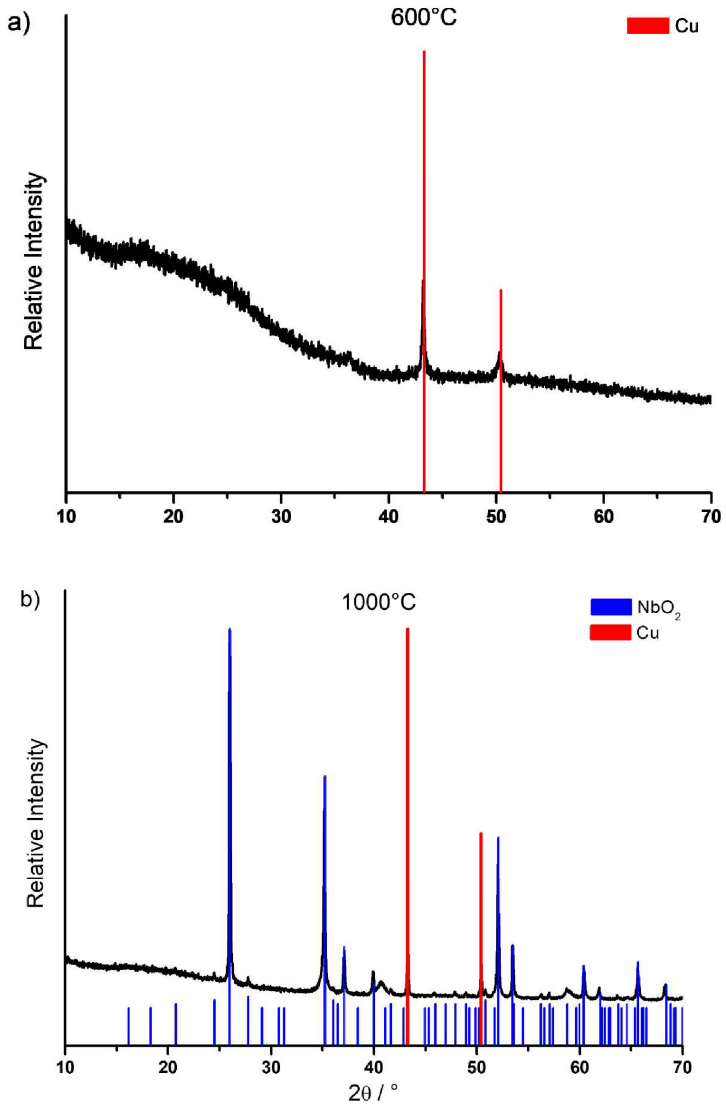

Figure S22a-b. XRD patterns of compound **II** decomposed in N_2 atmosphere at 600 °C (top) and 1000 °C (bottom) together with assignment of the reflections to Cu and NbO_2.

32

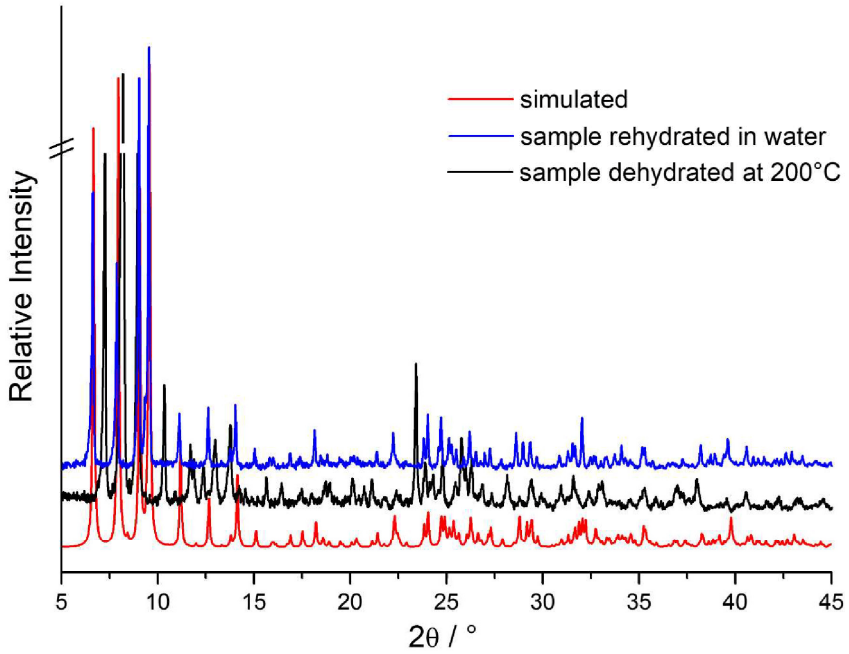

Figure S23. Powder patterns of compound **II** dehydrated at 200 °C (black), compound **II** rehydrated (blue) compared to simulated powder pattern (red).

33

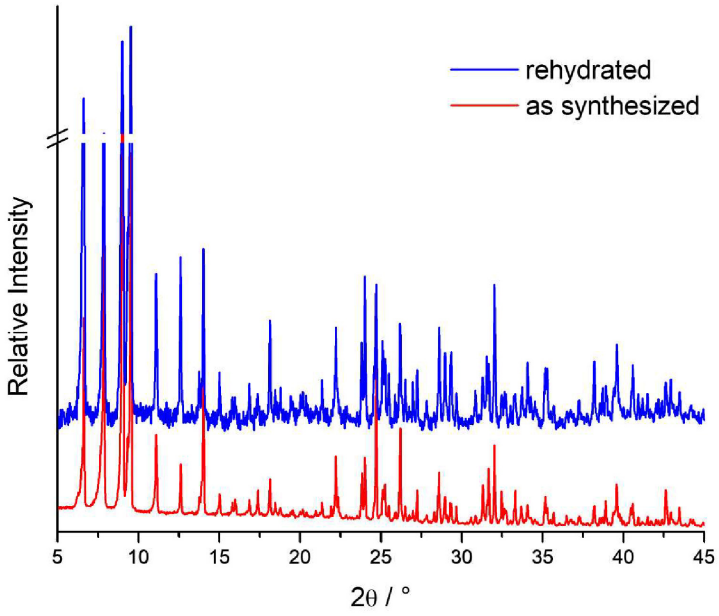

Figure S24. Powder patterns of compound **II** as synthesized (red) compared to the powder pattern of the rehydrated material (blue).

34

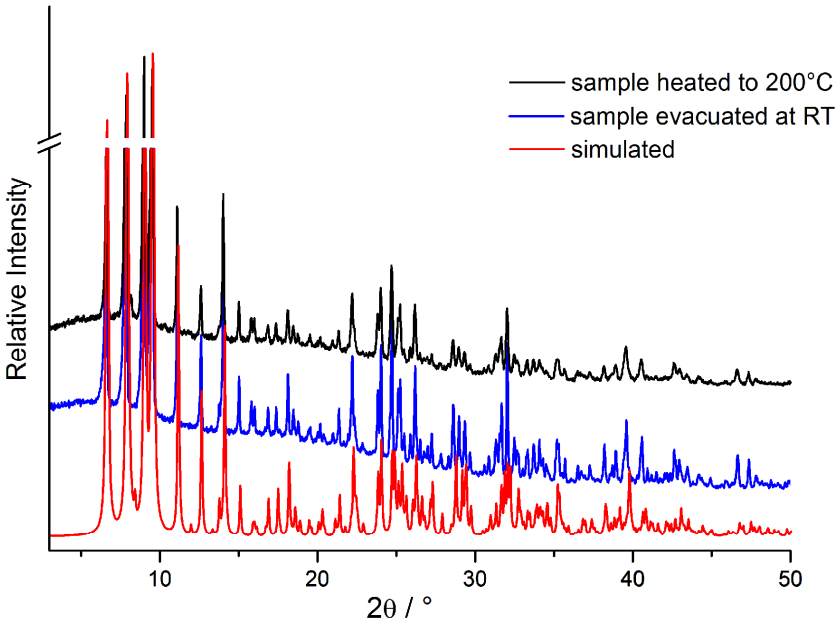

Figure S25. Powder patterns of compound **II** after sorption measurements: sample heated to 200 °C (black) and after evacuation at room temperature (blue) compared to simulated powder pattern (red).

35

Infrared spectroscopy

In the infrared (IR) spectra (Fig. S10+11) of both compounds, O-H absorptions of the crystal water molecules are observed at ~ 3340 cm^{-1} and ~1650–1600 cm^{-1} (Tab. S11)[1]. The typical absorptions of the amine molecules are located between ~3200–1030 cm^{-1} [2]. In the fingerprint region, an unambiguous assignment of the bands is difficult due to the overlap of Nb-O-Nb and Nb-O_t absorptions with those of the $[Cu(cyclam)]^{2+}$ complexes. Compared to the literature-known $[Cu(en)_2]_3\{[Cu(en)_2][H_6SiNb_{18}O_{54}]\}\cdot 22H_2O$[3], three additional bands (828, 767, 549 cm^{-1}) are observed in the IR spectrum of **I**. The band at 828 cm^{-1} may be assigned to the nitrate ion; the two remaining additional bands are weak and could be explained by the multiple attachment of copper amine complexes to the PONb anion[4,5].

In the fingerprint region in the IR spectra of **II**, some bands are missing compared to $\{[TM(2,2'\text{-bipy})]_3[Nb_{10}O_{28}]\cdot xH_2O\}_n$ (TM = Ni^{2+}, Co^{2+}; x = 1.5, 3, Tab. S11)[6]. Those are most probably covered by intense broad bands at ~890 and ~726 cm^{-1}.

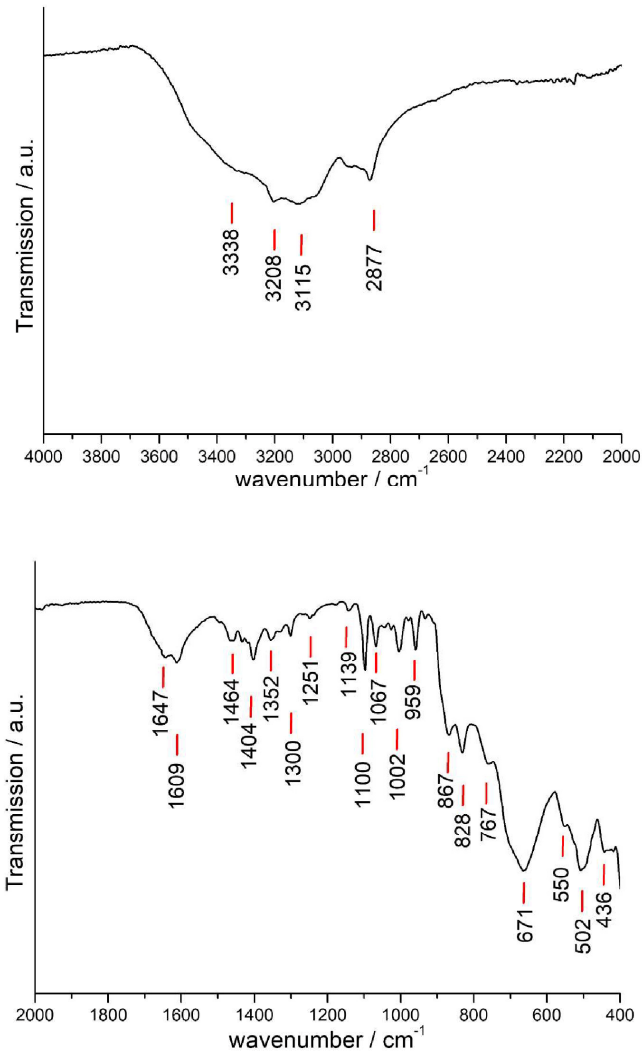

Figure S26. IR spectrum of $K_5[Cu(H_2O)_2(cyclam)]_{1.5}\{[Cu(cyclam)][Cu(H_2O)(cyclam)]_2HSiNb_{18}O_{54}\}(NO_3)\cdot 30H_2O$ (**I**).

37

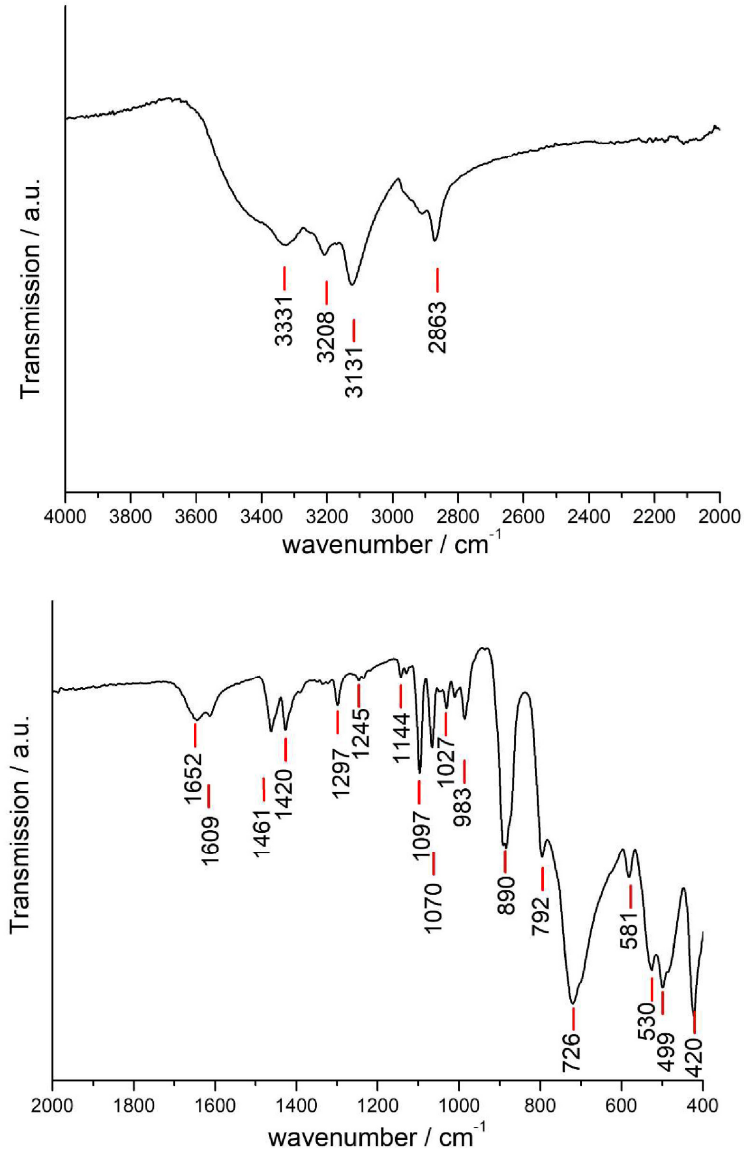

Figure S27. IR spectrum of $\{[Cu(cyclam)(H_2O)]_2[Cu(cyclam)][Nb_{10}O_{28}]\}_n \cdot 9nH_2O$ (**II**).

38

Table. S11. Assignment of the IR absorptions[1-3, 6-8].

Compound I	assignment	$\{SiNb_{18}O_{54}\}^{3}$	Compd.II powder	Compd.II crystals	assignment	$\{Nb_{10}O_{28}\}^{6}$
3338	O-H stretch		3331	3341	O-H stretch	
3208	N-H stretch		3208	3210	N-H stretch	
3115	N-H stretch		3131	3129	N-H stretch	
2877	C-H stretch		2863	2871	C-H stretch	
1647	H-O-H def.		1652	1644	H-O-H def.	
1609	H-O-H def.		1609	1614	H-O-H def.	
1464	C-H def		1461	1469	C-H def	
1404	C-N stretch C-C stretch		1420	1426	C-N stretch C-Cstretch	
1300	C-N stretch C-C stretch		1297	1300	C-N stretch C-C stretch	
1251	C-N stretch C-C stretch		1245	1248	C-N stretch C-C stretch	
1139	C-N stretch C-C stretch		1144	1144	C-N stretch C-C stretch	
1100	C-N stretch C-C stretch Nb-Ot	1105	1097	1100	C-N stretch C-C stretch	
1067	C-N stretch C-C stretch Nb-Ot	1047	1070	1065	C-N stretch C-C stretch	
1002	N-H def.		1027	1027	N-H def.	
958	Nb-Ot/ N-H def.	961	983	991	Nb-Ot	1018
867	Nb-Ot	866	890	887	Nb-Ot/ C-H def.	886, 859
828	Nb-Ot/NO3					
			792	792	Nb-O-Nb	778, 765
767	Nb-O-Nb		726	721	Nb-O-Nb	746, 734
641	Nb-O-Nb	673	581	582	Nb-O-Nb	
549	Nb-O-Nb		530	530	Nb-O-Nb	534
502	Nb-O-Nb	508	499	497	Nb-O-Nb	507
436	Nb-O-Nb/ Stretch Cu-N Def. Cu-N		420	420	Nb-O-Nb/ Cu-N stretch Cu-N def.	434 416

39

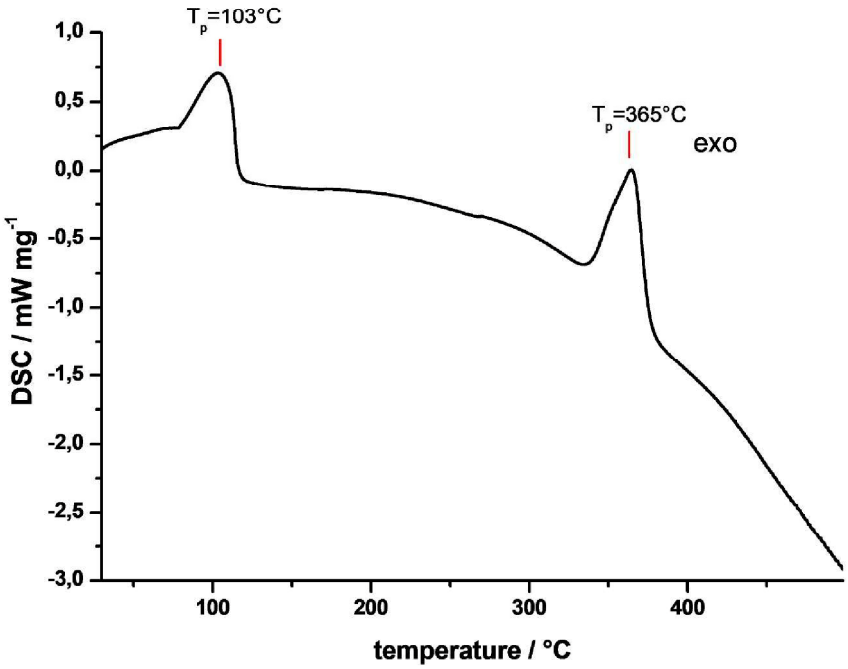

Figure S28. DSC curve of compound **II** measured in N_2 atmosphere.

40

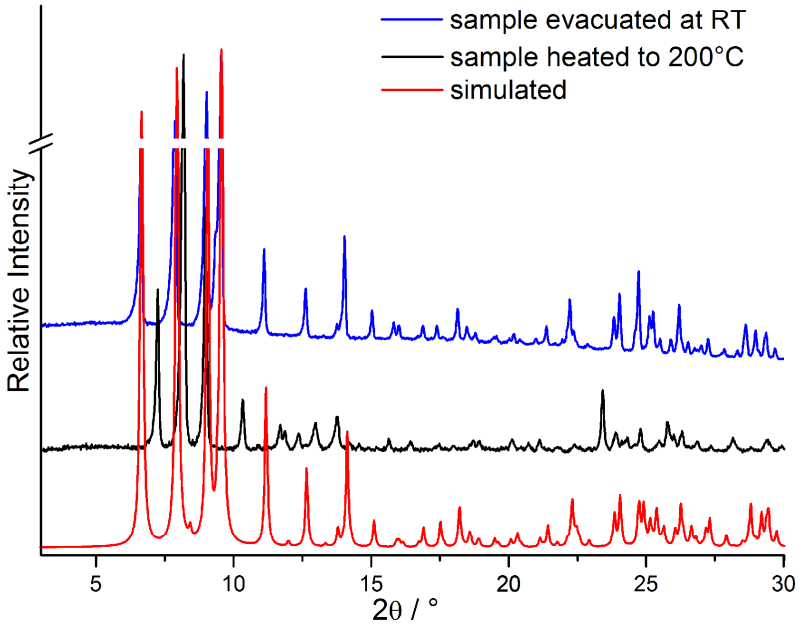

Figure S29. Powder patterns of compound **II**: sample heated to 200 °C (black) and after evacuation at room temperature (blue) compared to simulated powder pattern (red).

41

References

(1) Socrates, G. *Infrared and Raman Characteristic Group Frequencies*; John Wiley@Sons LTD: Manchester, New York, Weinheim, Toronto, Brisbane, Singapore, 2001.

(2) Diaz F., G.; Clavijo C., R.E.; Campos-Vallette, M. M.; Saavedra S, M.; Diez, S.; Muñoz, R. Specular reflectance infrared spectra of the macrocycles cyclam and cyclamdione and their Cu(II) complexes deposited onto a smooth copper surface. *Vib. Spectrosc.* **1997**, *15*, 201–209.

(3) Huang, P.; Qin, C.; Wang, X.-L.; Sun, C.-Y.; Xing, Y.; Wang, H.-N.; Shao, K.-Z.; Su, Z.-M. A new organic-inorganic hybrid based on the crescent-shaped polyoxoanion $[H_6SiNb_{18}O_{54}]^{8-}$ and copper-organic cations. *Dalton Trans.* **2012**, *41*, 6075–6077.

(4) Wang, J.-P.; Niu, H.-Y.; Niu, J.-Y. A novel Lindqvist type polyoxoniobate coordinated to four copper complex moieties: $\{Nb_6O_{19}[Cu(2,2'\text{-bipy})]_2[Cu(2,2'\text{-bipy})_2]_2\} \cdot 19H_2O$. *Inorg. Chem. Commun.* **2008**, *11*, 63–65.

(5) Tan, H.; Chen, W.; Liu, D.; Li, Y.; Wang, E. A new polyoxoniobate with $Nb^{IV}O_8$ center and Cu_{24} core. *Inorg. Chem. Commun.* **2010**, *13*, 1354–1356.

(6) Shen, L.; Li, C.-H.; Chi, Y.-N.; Hu, C.-W. $Zn(2,2'\text{-bipy})_2$/$Co(2,2'\text{-bipy})_2$ linked decaniobate $[Nb_{10}O_{28}]^{6-}$ clusters-zigzag neutral chains. *Inorg. Chem. Commun.* **2008**, *11*, 992–994.

(7) Son, J.-H.; Ohlin, C. A.; Casey, W. H. A new class of soluble and stable transition-metal-substituted polyoxoniobate: $[Cr_2(OH)_4Nb_{10}O_{30}]^{8-}$. *Dalton Trans.* **2012**, *41*, 12674–12677.

(8) Niu, J.; Wang, G.; Zhao, J.; Sui, Y.; Ma, P.; Wang, J. Zero- or One-Dimensional Organic-Inorganic Hybrid Polyoxoniobates Constructed from Decaniobate Units and Transition-Metal Complexes. *Cryst. Growth Des.* **2011**, *11*, 1253–1261.

6.1.2 Zusatzinformation zur Publikation „On the influence of the titanium sources on the composition and structure of novel titanoniobates"

Supporting Information

"On the influence of the titanium source on the composition and structure of novel titanoniobates "

*Joanna Dopta, Sven Grzanna, Christian Näther, Wolfgang Bensch**

Institute of Inorganic Chemistry, Christian-Albrechts-University of Kiel, 24118 Kiel, Germany

* Corresponding Author: Wolfgang Bensch, E-mail: wbensch@ac.uni-kiel.de, Fax: +49 431 880 1520, Tel: +49 880 2091

Content

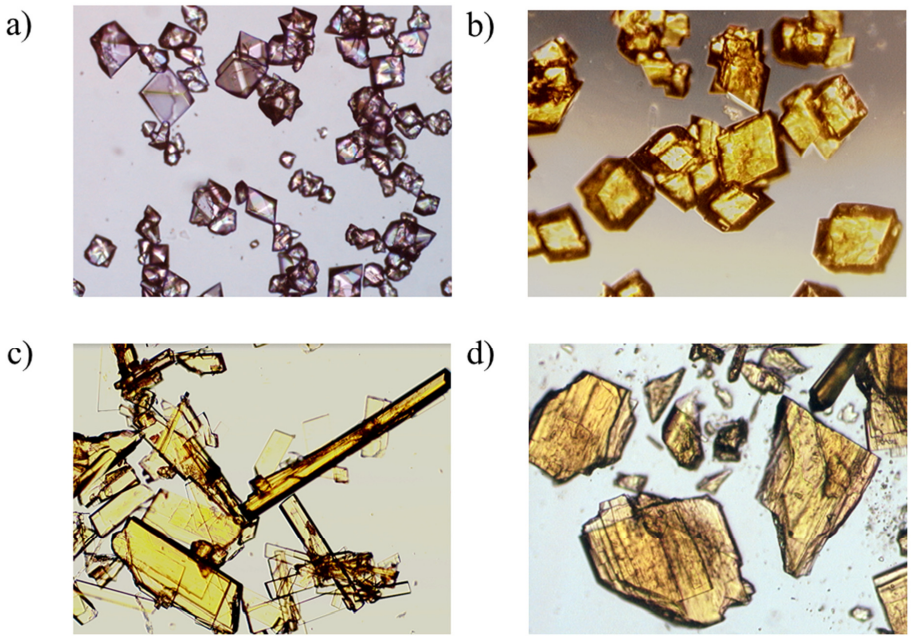

Figure S1a-d: Optical micrographs of the crystals of $\{[Ni(cyclam)]_4[Ti_2Nb_8O_{28}]\}_n \cdot 22nH_2O$ (a), $K[Ni(cyclam)]_3[TiNb_9O_{28}] \cdot 18H_2O$ (b), $K[Ni(cyclam)]_3[TiNb_9O_{28}] \cdot 14H_2O$ (c) and $K[Ni(cyclam)]_3[TiNb_9O_{28}] \cdot \sim 10H_2O$ (d)

3

Table S1: Selected crystal data for all compounds and details of the structure refinement.

	Compound **I**	Compound **II**	Compound **III**
Sum formula	$C_{40}H_{140}N_{16}Ni_4Nb_8Ti_2O_{50}$	$C_{30}H_{108}KN_{12}Nb_9Ni_3O_{46}Ti$	$C_{30}H_{100}KN_{12}Nb_9Ni_3O_{42}Ti$
Crystal system	monoclinic	monoclinic	triclinic
Space group	*C*2/m	*C*2/c	*P*-1
a / Å	18.8775(6)	25.3130(6)	11.6781(5)
b / Å	21.9384(5)	19.1246(5)	13.7488(8)
c / Å	14.6624(4)	15.9741(4)	22.6762(13)
α / °	90	90	103.762(4)
β / °	128.456(2)	100.847(2)	90.404(4)
γ / °	90	90	98.135(4)
V / Å^3	4755.1(2)	7594.9(3)	3497.6(3)
Z	2	4	2
Formula weight / g · mol^{-1}	2719.59	2472.44	2400.53
$\rho_{calc.}$ / g · cm^{-3}	1.899	2.197	2.279
λ / Å	0.71073	0.71073	0.71073
Scan mode	Omega scan	Omega scan	Omega scan
2θ range / °	1.661 ≤ θ ≤ 27.005	1.343 ≤ θ ≤ 27.005	1.542 ≤ θ ≤ 27.005
Crystal dimensions / mm	0.06 x 0.11 x 0.16	0.07 x 0.09 x 0.12	0.06 x 0.09 x 0.12
Crystal colour	pale purple	yellow	yellow
Temperature / K	170(2)	170(2)	170(2)
Index range	-24 ≤ h ≤ 24	-29 ≤ h ≤ 32	-14 ≤ h ≤ 14
	-28 ≤ k ≤ 28	-24 ≤ k ≤ 24	-17 ≤ k ≤ 17
	-17 ≤ l ≤ 18	-20 ≤ l ≤ 20	-28 ≤ l ≤ 28
Reflections collected	34711	30337	40100
Independent reflections	5340	8279	15247
R_{int}	4859	0.0449	0.0684
Reflections with $F_0>4\sigma(F_0)$)	0.0433	7724	10775
μ / mm^{-1}	1.948	2.337	2.470
Number of parameters	349	475	932
Transm min/max	0.5950/0.8078	0.6517/0.7340	0.6356/0.7561
*R*1 ($F_0>4\sigma(F_0)$)	0.0299	0.0522	0.0573
*R*1 (all data)	0.0348	0.0604	0.0864
*wR*2 (all data)	0.863	0.1415	0.1548
ΔF /e ·Å^{-3}	0.611/-0.813	0.834/-1.119	0.920/-1.266
GOF	1.057	1.184	1.021

4

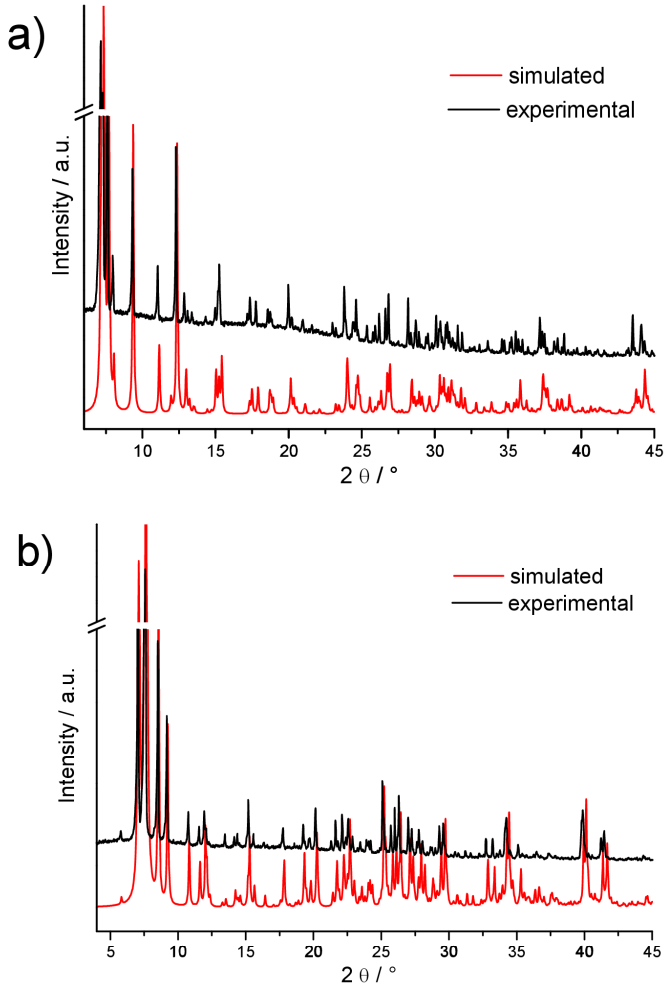
a)
simulated
experimental
Intensity / a.u.
10
15
20
25
30
35
40
45
2 θ / °
b)
simulated
experimental
Intensity / a.u.
5
10
15
20
25
30
35
40
45
2 θ / °

5

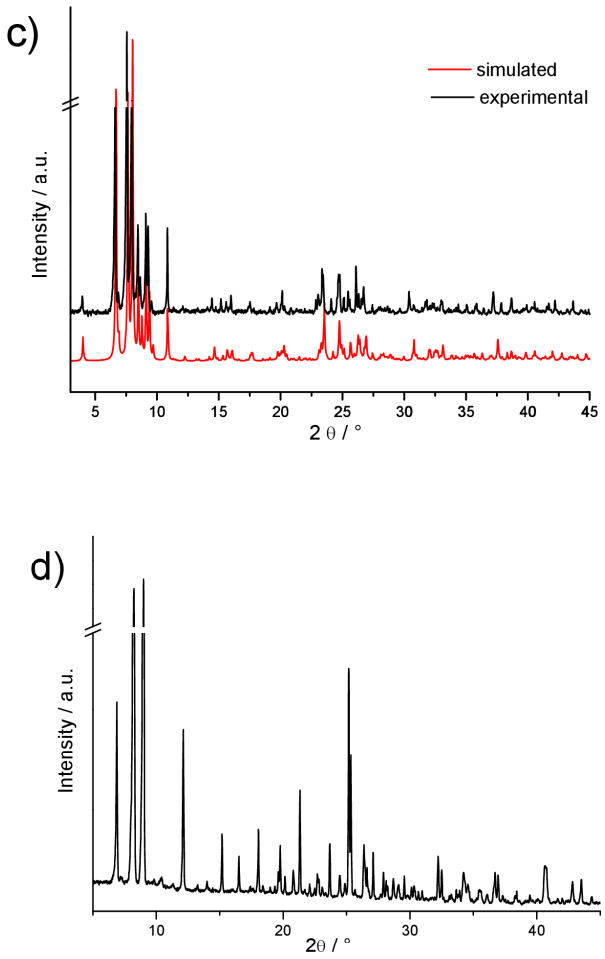

Figures S2a-d. Experimental (black) and simulated X-ray powder patterns (red) of compounds **I-III** (a-c) and experimental XRDP of **IV** (d).

6

Table S2. Results of bond valence sum analysis. In the sites of mixed occupancy (Ti(9)/Nb(9) and Ti(10)/Nb(10)), the atom with a site occupancy of 75% is highlighted in bold.

BVS for **I**					
Nb(1)	5.09	Ti(1)	4.04	Ni(1)	2.25
Nb(2)	5.12			Ni(2)	2.21
BVS for **II**					
Nb(1)	5.15	Ti(1)/Nb(5)	4.52	Ni(1)	2.41
Nb(2)	5.13			Ni(2)	2.41
Nb(3)	5.12				
Nb(4)	5.07				
BVS for **III**					
Nb(1)	5.09	Ti(9)/**Nb(9)**	4.79	Ni(1)	2.42
Nb(2)	5.11	**Ti(10)**/Nb(10)	4.27	Ni(2)	2.38
Nb(3)	5.12			Ni(3)	2.37
Nb(4)	5.11			Ni(4)	2.36
Nb(5)	5.12				
Nb(6)	5.13				
Nb(7)	5.07				
Nb(8)	5.07				

Table S3. Nb-O bond lengths in the titanoniobate unit in **I** sorted by type of bridging mode.

Bond type	Atoms	Bond length /Å	Bond type	Atoms	Bond length /Å
Nb=O_t	Nb(1)-O(1)	1.752(2)		Nb(2)-O(8)#2	2.0852(17)
	Nb(2)-O(9)	1.768(2)	Nb-μ_6-O	Nb(1)-O(7)#2	2.4305(19)
Nb-μ_2-O	Nb(1)-O(4)	1.9888(14)		Nb(2)-O(7)#2	2.3829(3)
	Nb(1)-O(2)	1.995(2)		O(7)-Nb(2)#2	2.3829(3)
	Nb(1)-O(3)#1	2.005(2)		O(7)-Nb(2)#3	2.3829(3)
	Nb(1)-O(6)	2.0213(19)		O(7)-Nb(1)#2	2.4305(18)
	Nb(2)-O(3)	1.924(2)		O(7)-Nb(1)#3	2.4305(18)
	Nb(2)-O(2)	1.927(2)	Ti-μ_2-O	Ti(1)-O(6)#3	1.8124(19)
	O(3)-Nb(1)#1	2.005(2)		Ti(1)-O(6)	1.812(2)
	O(4)-Nb(1)#1	1.9888(14)	Ti-μ_3-O	Ti(1)-O(8)	1.962(3)
Nb-μ_3-O	O(8)-Nb(2)#2	2.0850(17)		Ti(1)-O(5)	1.983(3)
	O(8)-Nb(2)#1	2.0850(17)	Ti-μ_6-O	Ti(1)-O(7)	2.1889(17)
	O(5)-Nb(2)#3	2.0787(17)		Ti(1)-O(7)#2	2.1889(17)
	Nb(2)-O(5)	2.0787(17)		O(7)-Ti(1)#2	2.1889(17)

Symmetry transformations used to generate equivalent atoms: #1 -x+1,y,-z+2 #2 -x+1,-y+1,-z+2 #3 x,-y+1,z.

7

Table S4. Bond angles / ° in the titanoniobate unit in **I**.

O(1)-Nb(1)-O(4)	104.52(10)	O(2)-Nb(2)-O(8)#2	153.39(10)
O(1)-Nb(1)-O(2)	103.59(9)	O(5)-Nb(2)-O(8)#2	74.86(9)
O(4)-Nb(1)-O(2)	87.26(6)	O(9)-Nb(2)-O(7)#2	171.10(9)
O(1)-Nb(1)-O(3)#1	101.91(9)	O(3)-Nb(2)-O(7)#2	79.71(7)
O(4)-Nb(1)-O(3)#1	88.51(6)	O(2)-Nb(2)-O(7)#2	79.84(7)
O(2)-Nb(1)-O(3)#1	154.40(8)	O(5)-Nb(2)-O(7)#2	74.53(9)
O(1)-Nb(1)-O(6)	102.69(9)	O(8)#2-Nb(2)-O(7)#2	74.74(9)
O(4)-Nb(1)-O(6)	152.78(9)	O(6)#3-Ti(1)-O(6)	105.62(13)
O(2)-Nb(1)-O(6)	86.35(8)	O(6)#3-Ti(1)-O(8)	97.99(8)
O(3)#1-Nb(1)-O(6)	85.95(8)	O(6)-Ti(1)-O(8)	97.99(8)
O(1)-Nb(1)-O(7)#2	178.15(8)	O(6)#3-Ti(1)-O(5)	95.80(8)
O(4)-Nb(1)-O(7)#2	77.03(8)	O(6)-Ti(1)-O(5)	95.80(8)
O(2)-Nb(1)-O(7)#2	77.41(6)	O(8)-Ti(1)-O(5)	157.08(12)
O(3)#1-Nb(1)-O(7)#2	77.04(6)	O(6)#3-Ti(1)-O(7)	86.38(8)
O(6)-Nb(1)-O(7)#2	75.76(7)	O(6)-Ti(1)-O(7)	167.87(8)
O(9)-Nb(2)-O(3)	107.30(10)	O(8)-Ti(1)-O(7)	81.76(6)
O(9)-Nb(2)-O(2)	104.69(9)	O(5)-Ti(1)-O(7)	80.93(6)
O(3)-Nb(2)-O(2)	94.01(9)	O(6)#3-Ti(1)-O(7)#2	167.86(9)
O(9)-Nb(2)-O(5)	97.54(10)	O(6)-Ti(1)-O(7)#2	86.39(8)
O(3)-Nb(2)-O(5)	152.43(10)	O(8)-Ti(1)-O(7)#2	81.76(6)
O(2)-Nb(2)-O(5)	90.99(8)	O(5)-Ti(1)-O(7)#2	80.93(6)
O(9)-Nb(2)-O(8)#2	99.51(10)	O(7)-Ti(1)-O(7)# 2	81.56(10)
O(3)-Nb(2)-O(8)#2	89.15(8)	O(6)#3-Ti(1)-O(6)	105.62(13)

Symmetry transformations used to generate equivalent atoms: #1 -x+1,y,-z+2; #2 -x+1,-y+1,-z+2; #3 x,-y+1,z

8

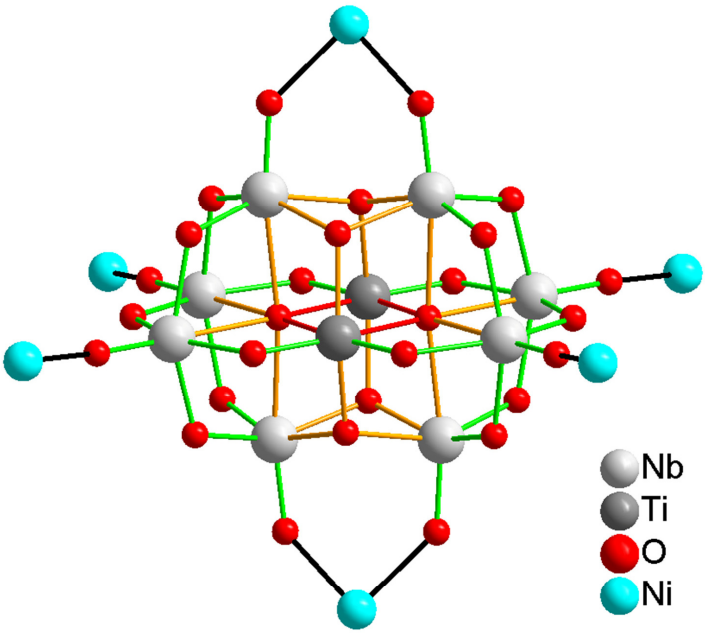

Figure S3. View on the anionic cluster in compound **I**. The bond lengths were compared to known $[Ti_2Nb_8O_{28}]^{8-}$ containing compounds[1][2] and colored as follows: green: good agreement; red: longer bonds; light orange: shorter bonds than reported in literature.

Table. S5. M-O bond lengths (M=Ti/Nb) / Å in title compound sorted by number of bridging atoms and comparison to the bond lengths in the two known dititanioniobates[1][2]. Color code: green: good agreement; red: longer bonds; light orange: shorter bonds than literature-known compounds.

	$[Ni(cyclam)]_4$ $[Ti_2Nb_8O_{28}]\cdot 22H_2O$	$[Cu(en)_2(H_2O)_2]_3$ $[Cu(en)_2][Ti_2Nb_8O_{28}]\cdot 8H_2O$	$Na_8[Ti_2Nb_8O_{28}]\cdot 34H_2O$
Nb=O_t	**1.752(2)-1.768(2)**	1.750(4)-1.764(4)	1.759(2)-1.765(2)
Nb-μ_2-O	**1.924(2)-2.0213(19)**	1.919(4)-2.026(4)	1.921(2)-2.032(2)
Nb-μ_3-O	**2.0787(17)-2.0850(17**	2.091(4)-2.098(4)	2.099(2)-2.104(2)
Nb-μ_6-O	**2.3829(3)-2.4305(18)**	2.415(4)-2.501(4)	2.409(2)-2.481(2)
Ti-μ_2-O	**1.812(2)**	1.811(4)-1.833(4)	1.817(2)-1.824(2)
Ti-μ_3-O	**1.963(3)-1.983(3)**	1.990(4)-2.011(4)	1.999(2)-2.001(2)
Ti-μ_6-O	**2.1889(17)**	2.134(4)-2.153(4)	2.150(2)-2.167(2)

9

Table S6. Bond lengths / Å and angles / ° for the coordination environment around Ni^{2+} in **I**.

Ni(1)-N(1)	2.062(3)	Ni(2)-N(12)	2.058(7)
Ni(1)-N(1)#4	2.062(3)	Ni(2)-N(13)	2.080(5)
Ni(1)-N(2)	2.073(3)	Ni(2)-N(11)	2.105(5)
Ni(1)-N(2)#4	2.073(3)	Ni(2)-O(9)#3	2.111(2)
Ni(1)-O(1)#4	2.087(2)	Ni(2)-N(14)	2.138(6)
N(1)-Ni(1)-N(1)#4	180.0	N(12)-Ni(2)-N(13)	93.9(4)
N(1)-Ni(1)-N(2)	85.81(12)	N(12)-Ni(2)-N(11)	83.7(3)
N(1)#4-Ni(1)-N(2)	94.19(12)	N(13)-Ni(2)-N(11)	174.8(2)
N(1)-Ni(1)-N(2)#4	94.19(12)	N(12)-Ni(2)-O(9)	87.2(2)
N(1)#4-Ni(1)-N(2)#4	85.81(12)	N(13)-Ni(2)-O(9)	88.0(3)
N(2)-Ni(1)-N(2)#4	180.00(11)	N(11)-Ni(2)-O(9)	96.4(2)
N(1)-Ni(1)-O(1)	89.82(10)	N(12)-Ni(2)-O(9)#3	168.8(2)
N(1)#4-Ni(1)-O(1)	90.18(10)	N(13)-Ni(2)-O(9)#3	95.0(3)
N(2)-Ni(1)-O(1)	91.27(9)	N(11)-Ni(2)-O(9)#3	87.9(2)
N(2)#4-Ni(1)-O(1)	88.73(9)	O(9)-Ni(2)-O(9)#3	86.37(12)
N(1)-Ni(1)-O(1)#4	90.18(10)	N(12)-Ni(2)-N(14)	99.3(2)
N(1)#4-Ni(1)-O(1)#4	89.83(10)	N(13)-Ni(2)-N(14)	83.9(4)
N(2)-Ni(1)-O(1)#4	88.73(9)	N(11)-Ni(2)-N(14)	92.0(3)
N(2)#4-Ni(1)-O(1)#4	91.27(9)	O(9)-Ni(2)-N(14)	169.9(2)
O(1)-Ni(1)-O(1)#4	180.0	O(9)#3-Ni(2)-N(14)	88.32(19)

Symmetry transformations used to generate equivalent atoms: #1 -x+1,y,-z+2; #2 -x+1,-y+1,-z+2; #3 x,-y+1,z ; #4 -x+1/2,-y+1/2,-z+2.

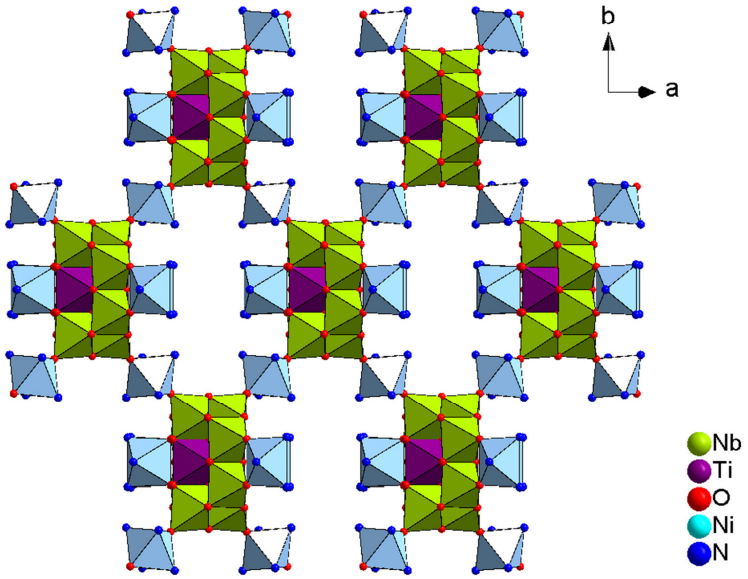

10

Figure S4. View on the layered structure of $[Ni(cyclam)_4][Ti_2Nb_8O_{28}] \cdot 22H_2O$ (**I**) along [001]; green polyhedra: NbO_6; violet polyhedra: TiO_6; blue polyhedra: NiN_4O_2.

Table S7. Geometrical parameters of hydrogen bonds in **I**.

D-H···A	d(D-H)	d(H···A)	d(D···A)	>(DHA)
N-H…O bonding interactions between cyclam molecules and water or cluster O atoms				
N(2)-H(2)...O(13)#5	1.00	2.21	3.147(4)	155.6
N(11)-H(11)...O(5)	1.00	2.07	2.953(5)	146.3
N(12)-H(12)...O(16)	1.00	2.16	3.114(7)	167.3
N(14)-H(14)...O(16)	1.00	2.16	3.122(7)	161.3
C-H…O bonding interactions between cyclam molecules and cluster O atoms				
C(2)-H(2B)...O(6)	0.99	2.58	3.553(4)	169.0
C(5)-H(5B)...O(1)	0.99	2.65	3.160(4)	112.5
C(13)-H13(B)…O(9)	0.99	2.58	3.093(7)	112.3
C(20)-H(20A)...O(2)#3	0.96	2.43	3.391(7)	163.8

Symmetry transformations used to generate equivalent atoms: #1 -x+1,y,-z+2 #2 -x+1,-y+1,-z+2 #3 x,-y+1,z #4 -x+1/2,-y+1/2,-z+2 #5 x-1/2,-y+1/2,z

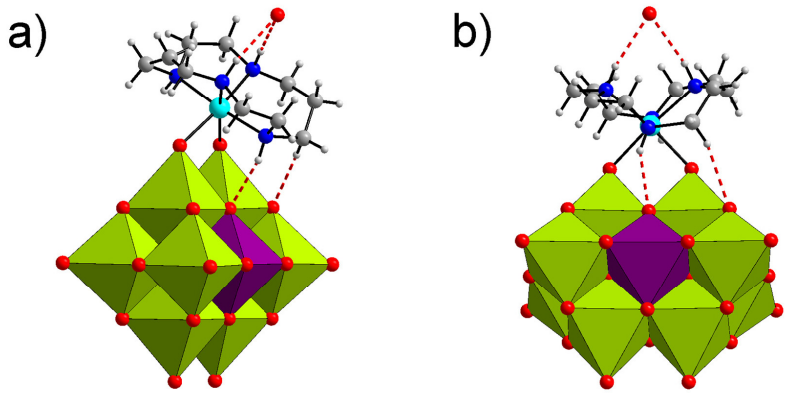

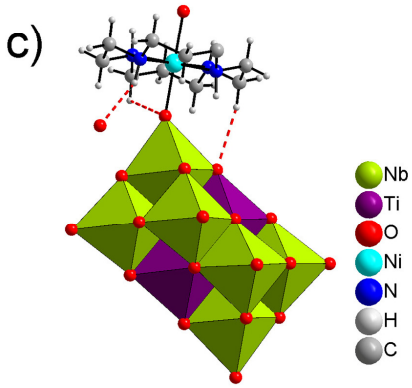

Figure S5a-c. Representation on the H-bonding interactions (dashed lines) in compound **I** involving the *cis*- and the *trans*-[Ni(cyclam)]$^{2+}$ (bottom) molecules in **I**. Only one orientation of the disordered ligand is shown. Green polyhedra: NbO_6, violet polyhedra: TiO_6.

12

Table S8. O – O distances in water clusters for compounds **I-III**.

atom 1	atom 2	distance / Å
compound I		
O(15)	O(16)	2.778
O(12)	O(13)	2.802
O(14)	O(18)	2.828
O(17)	O(14)	2.840
O(11)	O(12)	2.856
O(12)	O(17)	2.875
O(11)	O(12)	2.894
O(14)	O(16)	2.904
Average: 2.847		
compound II		
O(24)	O(29)	2.730
O(24)	O(30)	2.736
O(23)	O(26)	2.738
O(25)	O(26)	2.753
O(22)	O(25)	2.770
O(21)	O(24)	2.778
O(28)	O(28)	2.787
O(21)	O(25)	2.822
O(22)	O(24)	2.824
O(22)	O(28)	2.837
O(27)	O(27)	2.859
O(24)	O(30)	2.873
O(23)	O(27)	2.873
O(22)	O(23)	2.891
O(23)	O(23)	2.910
Average: 2.812		
compound II		
O(36)	O(42)	2.698
O(42)	O(35)	2.725
O(7)	O(41)	2.725
O(38)	O(6)	2.732
O(43)	O(44)	2.751
O(35)	O(3)	2.765
O(36)	O(40)	2.769
O(37)	O(4)	2.769
O(40)	O(43)	2.790
O(41)	O(39)	2.802
O(8)	O(43)	2.806
O(39)	O(3)	2.811
O(8)	O(40)	2.840
O(41)	O(38)	2.847
O(42)	O(41)	2.871
O(37)	O(32)	2.948
Average: 2.791		

13

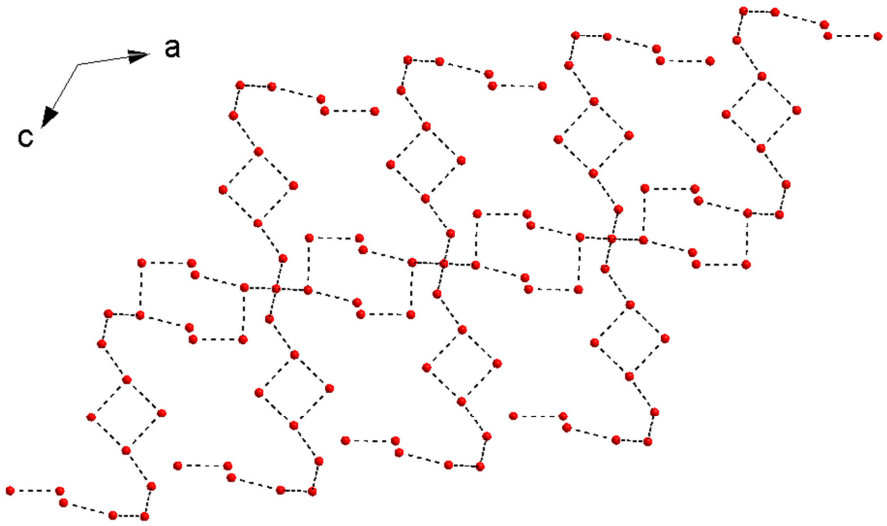

Figure S6. View on the arrangement of water O atoms in the water cluster in **I** along b axis. O – O distances up to 3.04 Å shown in dashed lines.

14

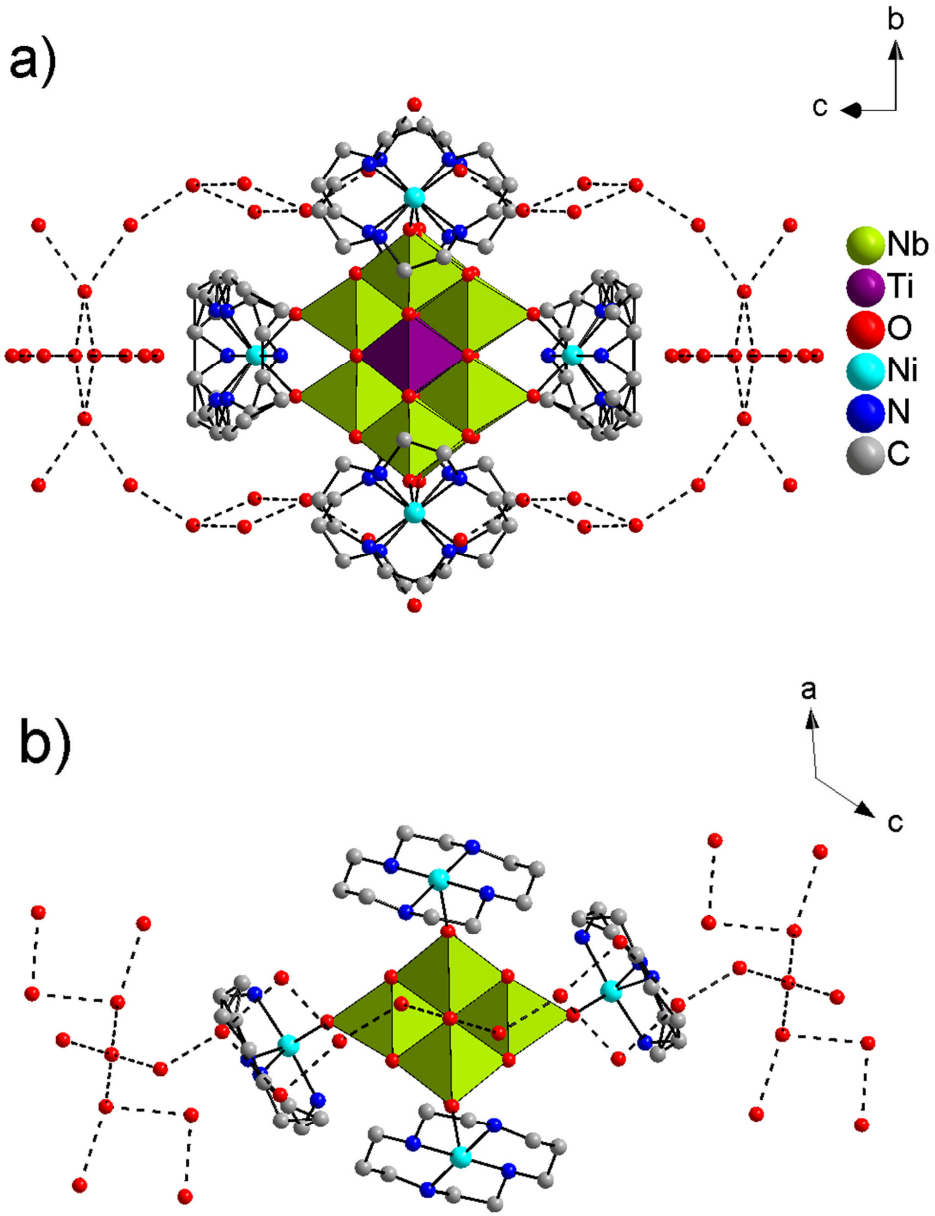

Figure S7a-b. Arrangement of the differently coordinated $[Ni(cyclam)]^{2+}$ molecules in **I** with respect to the water cluster. O – O distances up to 3.04 Å shown in dashed lines. Green polyhedra: NbO_6, violet polyhedra: TiO_6. H atoms omitted for clarity.

15

Table S9. Nb-O bond lengths / Å in the titanoniobate unit in **II** sorted by type of bridging mode.

Bond type	Atoms	Bond length /Å	Bond type	Atoms	Bond length /Å
Nb=O_t	Nb(1)-O(1)	1.741(6)		Nb(4)-O(10) #1	2.106(4)
	Nb(2)-O(11)	1.756(4)		O(9)-Nb(2)#1	2.102(4)
	Nb(3)-O(12)	1.743(5)		O(10)-Nb(4)#1	2.106(4)
	Nb(4)-O(13)	1.763(4)	Nb-μ_6-O	Nb(1)-O(6) #1	2.486(4)
Nb-μ_2-O	Nb(1)-O(2)	1.995(4)		Nb(2)-O(6)#1	2.390(4)
	Nb(1)-O(3)	1.953(4)		Nb(3)-O(6)#1	2.496(4)
	Nb(1)-O(5)	2.065(4)		O(6)-Nb(4)#1	2.399(4)
	Nb(1)-O(4)	1.982(4)		O(6)-Nb(2)#1	2.390(4)
	Nb(2)-O(2)	1.923(4)		O(6)-Nb(1)#1	2.486(4)
	Nb(2)-O(7)	1.905(4)		O(6)-Nb(3)#1	2.493(4)
	Nb(3)-O(3)	1.944(4)		Nb(3)-O(6)#1	2.493(4)
	Nb(3)-O(7)	1.985(4)		Nb(4)-O(6)#1	2.399(4)
	Nb(3)-O(8)	2.012(4)	Ti/Nb-μ_2-O	Ti(1)/Nb(5)-(O14)	1.815(4)
	Nb(3)-O(14)#1	2.068(4)		Ti(1)/Nb(5)-(O5)	1.827(4)
	Nb(4)-O(4)	1.913(4)	Ti/Nb -μ_3-O	Ti(1)/Nb(5)-(O9)	1.999(4)
	Nb(4)-O(8)	1.933(4)		Ti(1)/Nb(5)-(O10)	1.992(4)
	O(14)-Nb(3)#1	2.068(4)	Nb/Ti-μ_6-O	Ti(1)/Nb(5)-(O6)	2.191(4)
Nb-μ_3-O	Nb(2)-O(9)#1	2.102(4)		O(6)- Ti(1)/Nb(5)#1	2.208(4)
	Nb(2)-O(10)	2.116(4)		Ti(1)/Nb(5)-O(6)#1	2.208(4)
	Nb(4)-O(9)	2.098(4)			

Symmetry transformations used to generate equivalent atoms: #1 -x+3/2,-y+3/2,-z+1; #2 -x+2,y,-z+3/2.

Table S10. Comparison of the bond lengths / Å in the anionic units of compounds **II** and **III** with those reported for $(TMA)_7[TiNb_9O_{28}]\cdot 22H_2O$[3].

Bond type	Compound **II**	Compound **III**	$TiNb_9$[3]
Nb=O_t	1.741(6)- 1.763(4)	1.737(5)- 1.768(5)	1.746(4)-1.770(4)
Nb-μ_2-O	1.905(4)- 2.068(4)	1.907(5)- 2.098(5)	1.900(4)-2.078(4)
Nb-μ_3-O	2.098(4)- 2.116(4)	2.074(5)- 2.119(4)	2.086(4)-2.127(4)
Nb-μ_6-O	2.390(4)- 2.496(4)	2.394(4)- 2.520(4)	2.398(4)-2.512(4)
Ti/Nb-μ_2-O	1.815(4)- 1.827(4)	1.808(5)- 1.826(5)	1.809(4)-1.815(4)
Ti/Nb-μ_3-O	1.992(4)- 1.999(4)	1.994(4)- 2.023(4)	2.001(4)-2.028(4)
Ti/Nb-μ_6-O	2.191(4)- 2.208(4)	2.182(5)- 2.228(5)	2.183(4)-2.222(4)

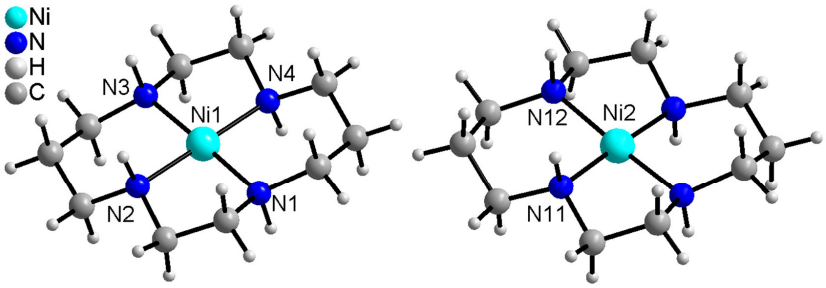

Figure S8. Coordination environment of the $[Ni(cyclam)]^{2+}$ cations in the structure of **II**.

Table S11. Ni-N bond lengths / Å and N-Ni-N bond angles / ° for the $[Ni(cyclam)]^{2+}$ cations in compound **II**.

Ni(1)-N(1)	1.923(6)	Ni(2)-N(11)	1.923(6)
Ni(1)-N(2)	1.941(6)	Ni(2)-N(11)#2	1.923(6)
Ni(1)-N(3)	1.933(6)	Ni(2)-N(12)#2	1.938(5)
Ni(1)-N(4)	1.926(6)	Ni(2)-N(12)	1.938(5)
N(1)-Ni(1)-N(4)	94.1(3)	N(11)#2-Ni(2)-N(11)	86.2(3)
N(1)-Ni(1)-N(3)	178.4(2)	N(11)#2-Ni(2)-N(12)#2	93.5(2)
N(1)-Ni(1)-N(2)	86.0(3)	N(11)-Ni(2)-N(12)#2	176.1(2)
N(4)-Ni(1)-N(2)	179.7(2)	N(11)#2-Ni(2)-N(12)	176.1(2)
N(4)-Ni(1)-N(3)	86.8(3)	N(11)-Ni(2)-N(12)	93.5(2)
N(3)-Ni(1)-N(2)	93.2(3)	N(12)#2-Ni(2)-N(12)	87.1(3)

Symmetry transformations used to generate equivalent atoms: #1 -x+3/2,-y+3/2,-z+1 #2 -x+2,y,-z+3/2.

17

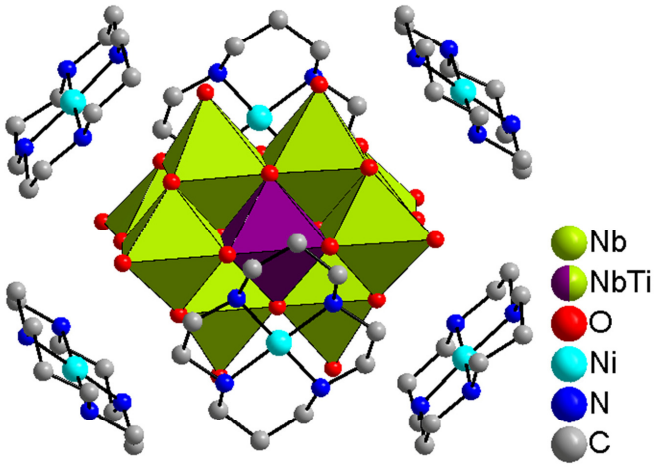

Figure S9. The $[TiNb_9O_{28}]^{7-}$ anion in the structure of **II** surrounded by six $[Ni(cyclam)]^{2+}$ cations. H and K atoms are not displayed. Green polyhedra: NbO_6, violet polyhedra: TiO_6.

18

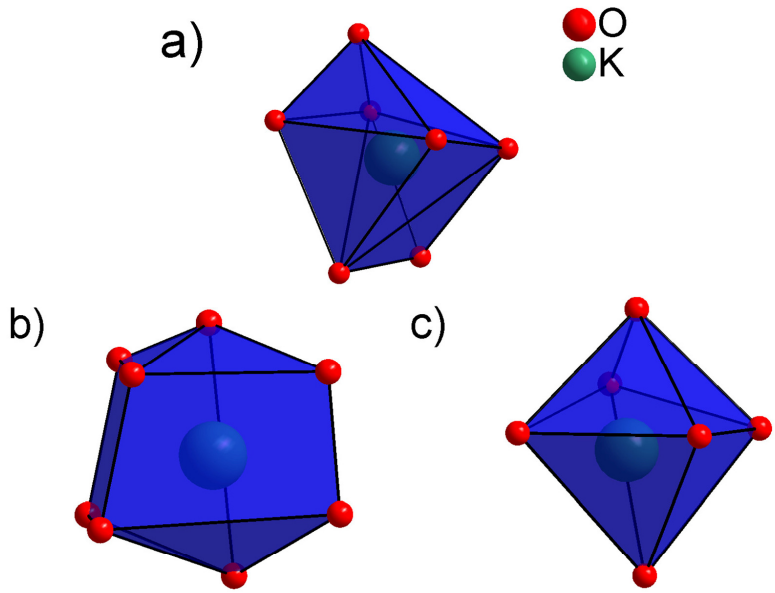

Figure S10a-c. Coordination environment of K^+ cations in the structure of **II** (a) and **III** (b-c) surrounded by water molecules and cluster O atoms.

Table S12. K-O bond lengths / Å in the structure of compounds **II** and **III**.

Compound **II**		Compound **III**			
atoms	distance / Å	atoms	distance / Å	atoms	distance / Å
K(1)-O(11)	2.841(6)	K(1)-O(13)	3.035(6)	K´(1)- O(33)	2.952(16)
K(1)#1-O(13)	2.874(6)	K(1)-O(15)	3.079(6)	K´(1)- O(33)	2.691(16)
K(1)-O(13)#1	2.874(6	K(1)-O(31)	2.697(12)	K´(1)- O(34)	2.831(13)
K(1)-O(24)	2.806(7)	K(1)-O(31)	3.133(13)	K´(1)- O(37)	2.601(7)
K(1)-O(25)	2.796(7)	K(1)-O(32)	3.060(14)	K´(1)- O(39)	3.057(8)
K(1)-O(26)	3.016(9)	K(1)-O(32)	3.104(15)	K´(1)- O(46)	2.815(13)
K(1)-O(29)	3.054(8)	K(1)-O(39)	2.774(8)		
K(1)-O(30)	2.734(12)	K(1)-O(46)	3.052(12)		
Average: 2.874		**Average:** 2.920			

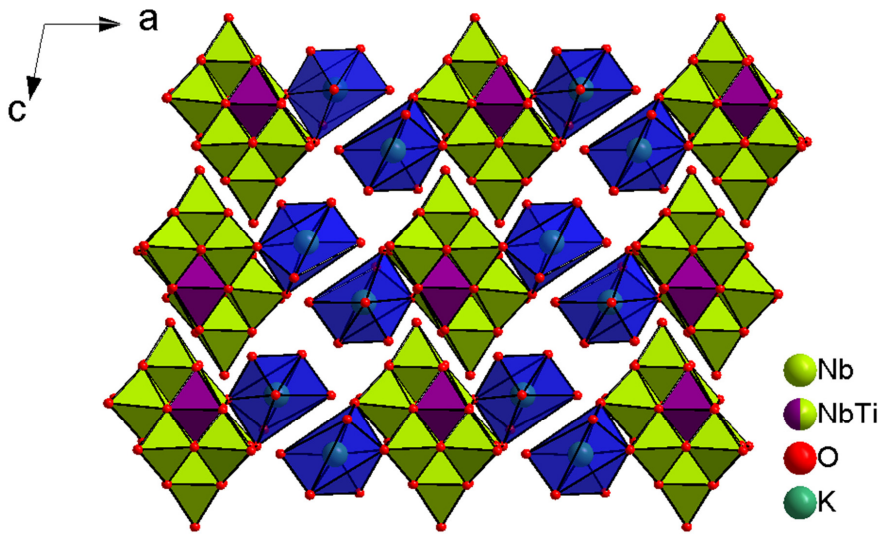

Figure S11. Arrangement of the KO_7 polyhedra and $[TiNb_9O_{28}]^{7-}$ anions in the structure of **II** along [010]. The $[Ni(cyclam)]^{2+}$ cations and water O atoms which are not involved in K-O interactions are omitted. Green: NbO_6, violet: Ti/NbO_6, blue: KO_7 polyhedra.

20

Table S13. Geometrical parameters of hydrogen bonds in **II**.

D-H...A	d(D-H)	d(H...A)	d(D...A)	<(DHA)
N-H…O bonding interactions between cyclam molecules and cluster O atoms				
N(1)-H(1)...O(14)	1.00	2.01	2.937(7)	152.9
N(2)-H(2)...O(1)#3	1.00	2.37	3.238(8)	145.1
N(2)-H(2)...O(2)#3	1.00	2.47	3.302(7)	139.9
N(3)-H(3)...O(2)#3	1.00	2.61	3.395(7)	135.9
N(3)-H(3)...O(11)#3	1.00	2.17	3.031(7)	143.1
N(4)-H(4)...O(5)	1.00	1.85	2.837(7)	169.4
N(11)-H(11)...O(13)	1.00	1.84	2.828(7)	170.4
N(12)-H(12)...O(8)	1.00	2.03	2.996(7)	160.6
C-H…O bonding interactions between cyclam molecules and cluster O atoms				
C(1)-H(1B)...O(3)#3	0.99	2.53	3.446(9)	153.5
C(2)-H(2A)...O(12)#1	0.99	2.63	3.454(9)	140.5
C(3)-H(3A)...O(7)#1	0.99	2.65	3.574(9)	156.3
C(6)-H(6A)...O(4)	0.99	2.41	3.373(9)	165.0
C(7)-H(7A)...O(11)#3	0.99	2.45	3.194(9)	131.2
C(8)-H(8B)...O(7)#3	0.99	2.58	3.493(9)	152.9
C(10)-H(10A)...O(12)#3	0.99	2.59	3.507(9)	153.5
C(12)-H(12B)...O(4)#2	0.99	2.62	3.514(8)	150.1
C(14)-H(14A)...O(1)#2	0.99	2.64	3.540(9)	150.5
C(15)-H(15A)...O(3)#2	0.99	2.47	3.421(8)	161.2
C-H…O bonding interactions between cyclam molecules and water O atoms				
C(4)-H(4A)...O(25)#3	0.99	2.59	3.517(11)	155.3
C(5)-H(5B)...O(30)#3	0.99	2.48	3.434(15)	163.1
C(9)-H(9B)...O(23)	0.99	2.64	3.558(10)	153.7
C(11)-H(11A)...O(30)#4	0.99	2.58	3.229(14)	122.7
C(13)-H(13B)...O(22)#5	0.99	2.64	3.595(9)	162.3

Symmetry transformations used to generate equivalent atoms:#1 -x+3/2,-y+3/2,-z+1; #2 -x+2,y,-z+3/2; #3 -x+3/2,y-1/2,-z+3/2; #4 x+1/2,y-1/2,z; #5 x+1/2,-y+3/2,z-1/2.

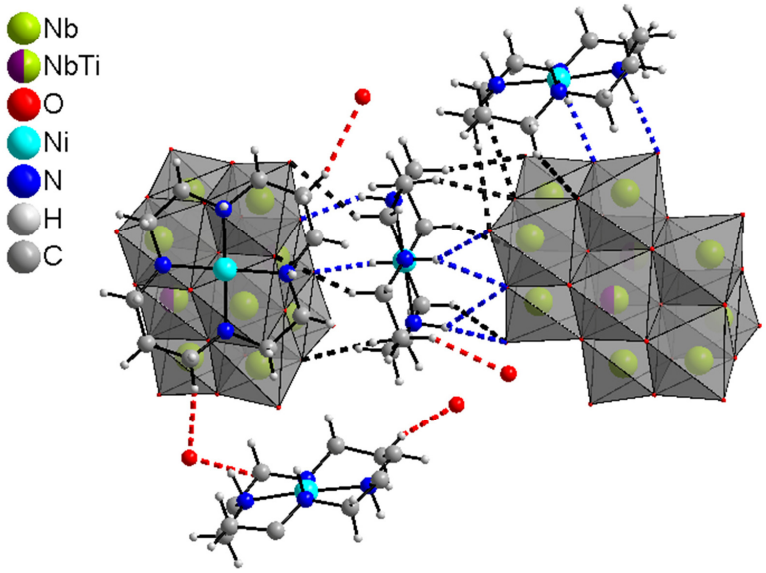

Figure S12. H bonding interactions in the structure of compound **II** shown in dashed lines. Color code: N-H···O(cluster): blue, C-H···O(cluster): black, C-H···O(water): red. Grey polyhedra: Ti/NbO_6 units.

22

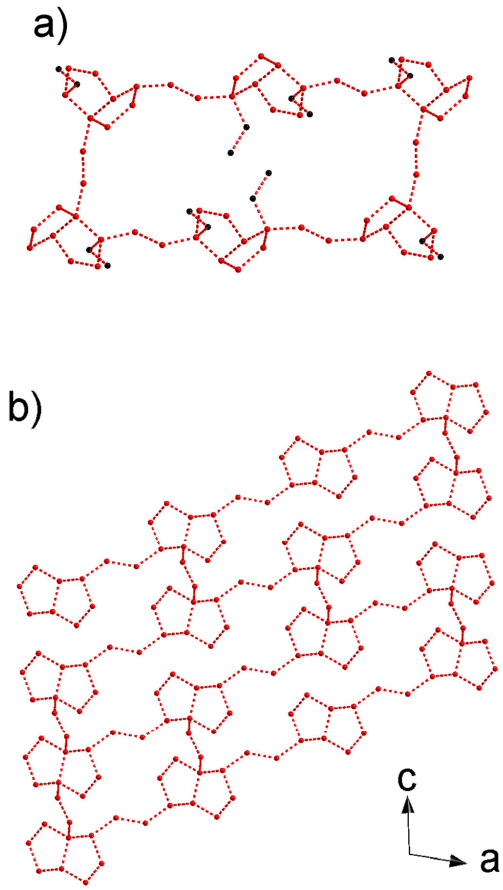

Figure S13a-b. View on the arrangement of water O atoms in **II**. O-O distances below the sum of the van der Waals radii in dashed lines. a) View on the L5(4)30(18) building unit. The isolated fragments consisting of two water molecules (O24,O29) attached to the water cluster are displayed in black and omitted in b) View on the L5(4)30(18) type water cluster along [010].

23

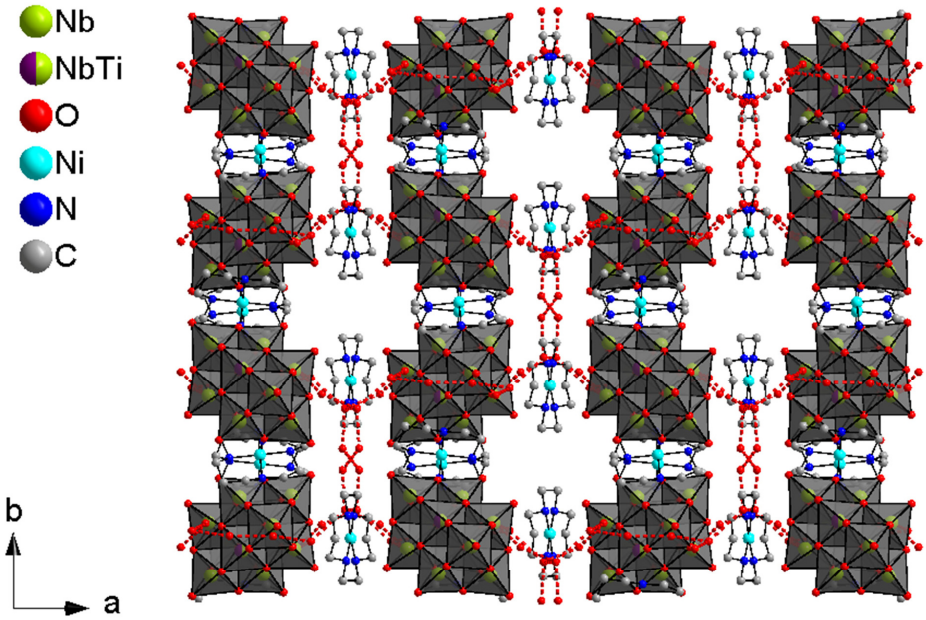

Figure S14. The L5(4)L30(18) water cluster in the structure of **II** (grey polyhedra: Ti/NbO_6), which are connected via two water O atoms along b axis. The water O atoms that do not expand the network (O24+O29), K and H atoms omitted.

Table S14. Comparison of selected bond lengths and angles in compound **II** and **III**.

	$Nb=O_t$ bond lengths / Å	$Nb-\mu_2$-O bond lengths / Å	$Nb-\mu_3$-O bond lengths / Å
II	1.741(6) – 1.763(4)	1.905(4) – 2.068(4)	2.098(4) – 2.116(4)
III	1.737(5) – 1.768(5)	1.907(5) – 2.098(5)	2.074(5) – 2.119(4)
	$Nb-\mu_6$-O bond lengths / Å	$Ti/Nb-\mu_2$-O bond lengths / Å	$Ti/Nb-\mu_3$-O bond lengths / Å
II	2.390(4) -2.496(4)	1.815(4) – 1.827(4)	1.992(4) - 1.999(4)
III	2.394(4) – 2.520(4)	1.808(5) – 1.826(5)	1.994(4) – 2.023(4)
	$Ti/Nb-\mu_6$-O bond lengths / Å	Nb-O-Nb angles / °	Ni-N bond lengths /Å
II	2.191(4) - 2.208(4)	73.6(1) – 178.2(2)	1.923(6) – 1.941(6)
III	2.182(5) – 2.228(5)	73.45(17) – 177.9(2)	1.919(6) – 1.941(6)
	Ti/Nb-O-Ti/Nb angles / °	Ni-N *cis*-angles / °	Ni-N *trans*-angles / °
II	79.37(15) – 166.30(16)	86.0(3) – 93.5(2)	176.1(2) – 179.7(2)
III	80.03(17) – 166.5(2)	86.5(3) – 93.4(3)	177.2(2) – 180.0
	$N-H\cdots O_{cluster}$ / Å	$C-H\cdots O_{cluster}$ / Å	$C-H\cdots O_{water}$ / Å
II	2.828(7) – 3.238(8)	3.194(9) – 3.574(9)	3.23(1) – 3.595(9)
III	2.830(8) – 3.465(7)	3.130(10) – 3.523(11)	3.191(14) – 3.522(10)
	< (NHO) / °	< ($CHO_{cluster}$) / °	< (CHO_{water}) / °
II	143.1 – 170.4	131.2 – 165.0	122.7 – 163.1
III	138.6 – 171.6	137.0 – 178.3	137.0 – 178.3

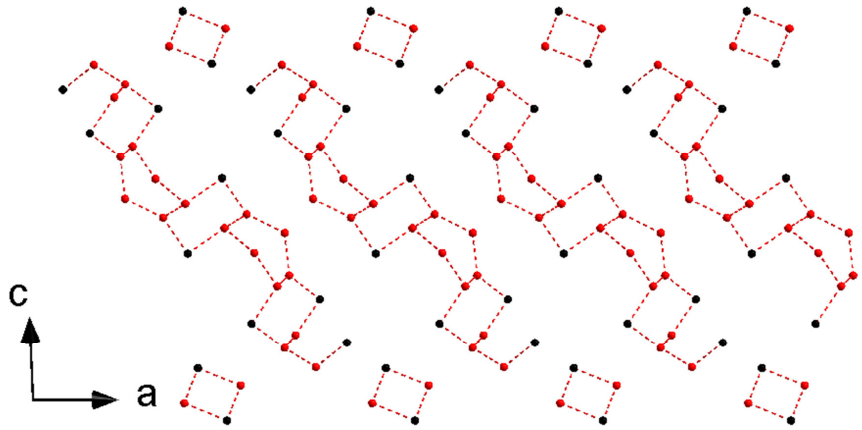

Figure S15. The extended water motif involving water (red) and cluster (black) O atoms in the structure of compound **III.**

25

Infrared spectroscopy

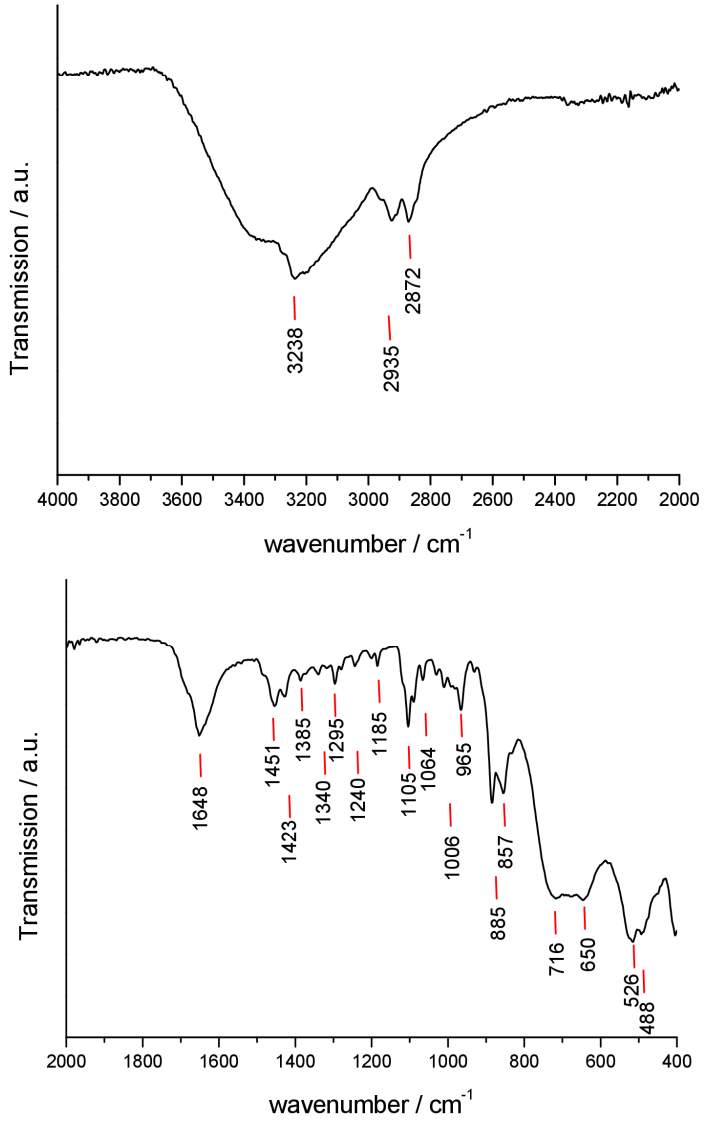

Figure S16. Infrared spectrum of compound **I**.

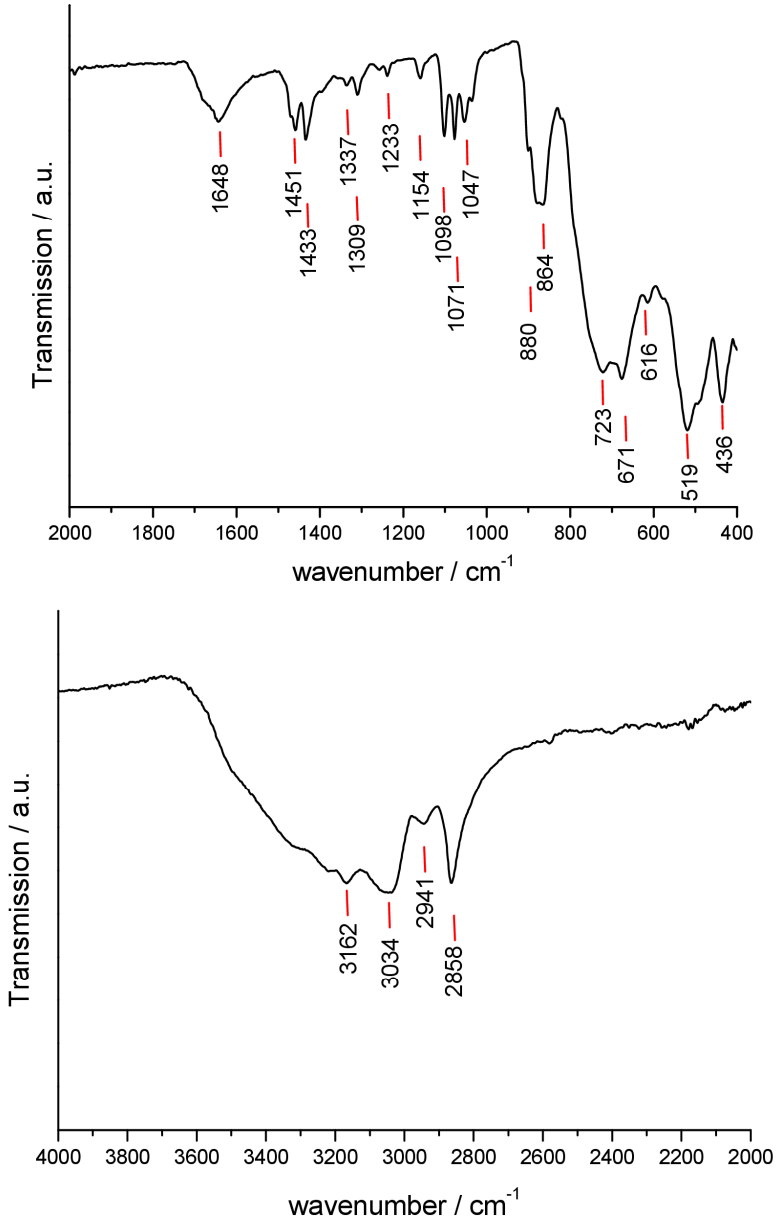

Figure S17. Infrared spectrum of compound **II**.

27

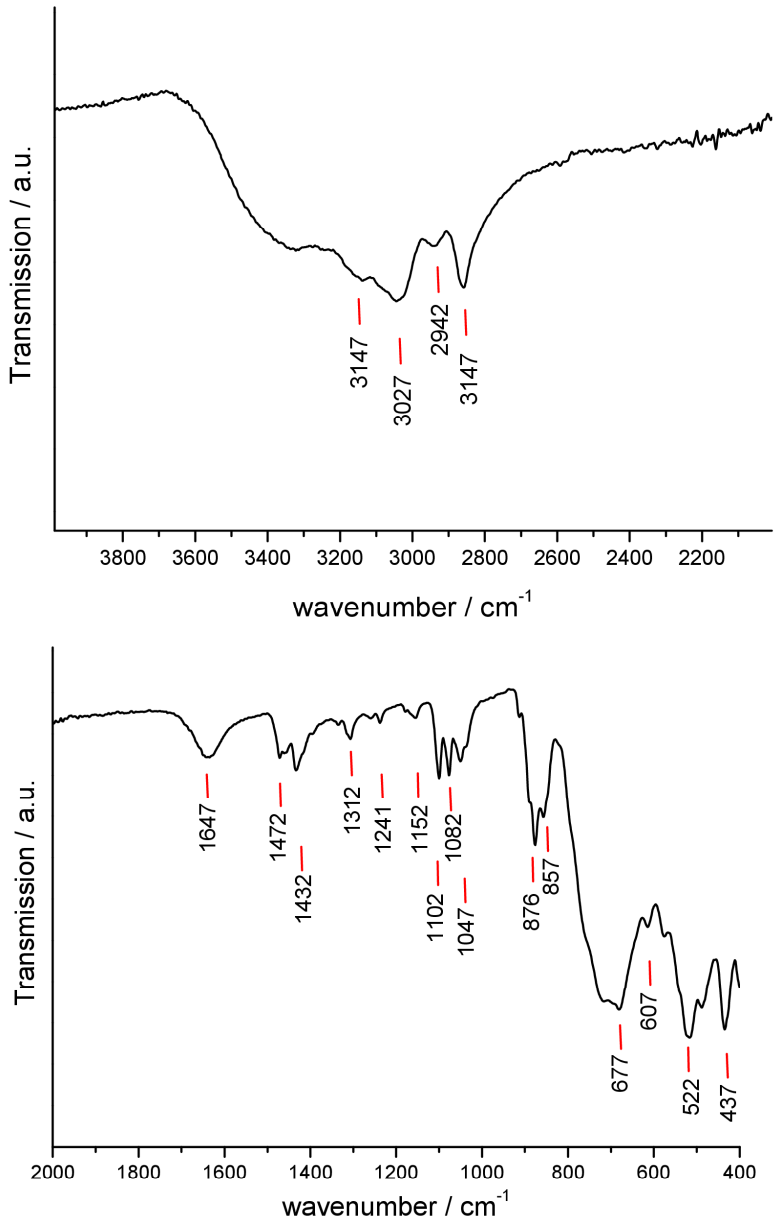

Figure S18. Infrared spectrum of compound **III**.

28

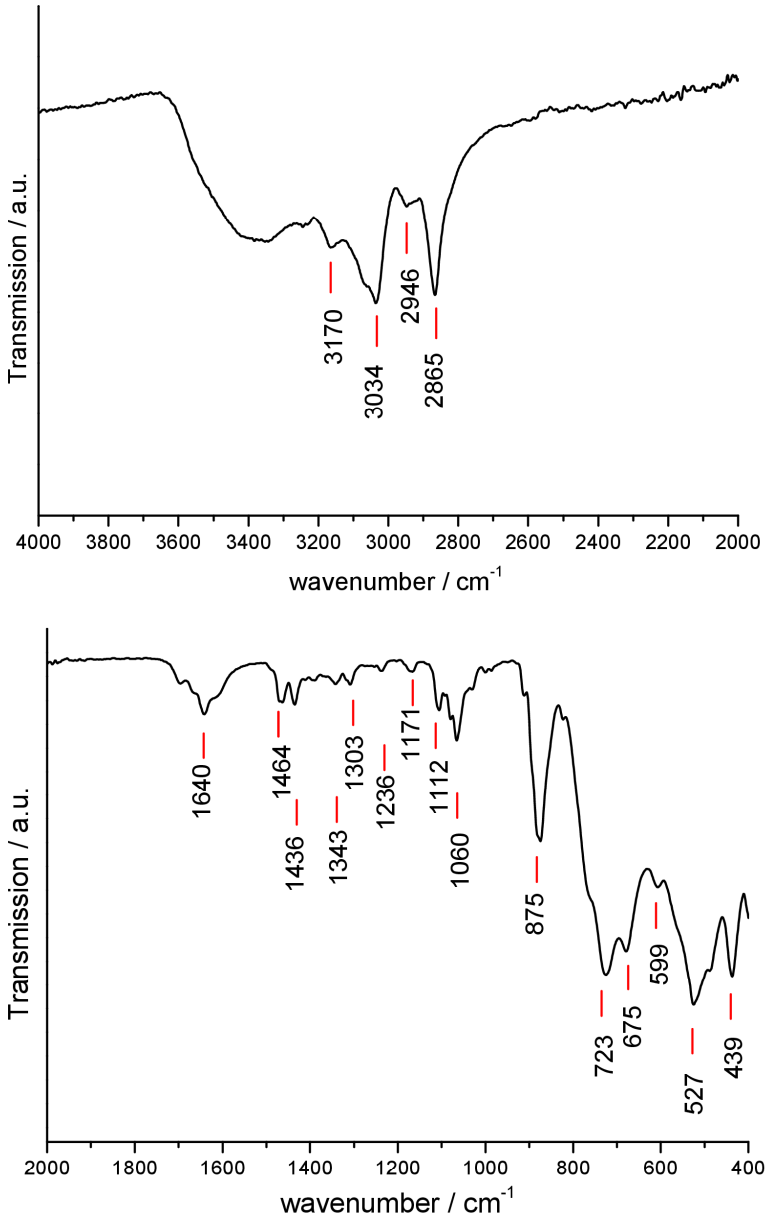

Figure S19. Infrared spectrum of compound **IV**.

29

Table S15. Assignment of the IR absorptions compared to literature-known compounds[4].

I	II	III	IV	assignment	$[Nb_{10}O_{28}]^{6-}$ [5]	$[Ti_2Nb_8O_{28}]^{8-}$ [2]
3238	3162	3147	3170	ν (N-H)		
	3034	3027	3034	ν (N-H)		
2935	2941	2942	2946	ν (C-H)		
2872	2858	2847	2865	ν (C-H)		
1648	1647	1647	1640	δ (O-H)		
1451	1458	1472	1464	ν (C-C) + ν (C-N)		
1423	1433	1432	1436	ν (C-C) + ν (C-N)		
1385				ν (C-C) + ν (C-N)		
1340	1337		1343	ν (C-C) + ν (C-N)		
1295	1309	1312	1303	ν (C-C) + ν (C-N)		
1240	1233	1241	1236	ν (C-N) + δ (C-H)		
1185	1154	1152	1171	ν (C-N) + δ (C-H)		
1105	1098	1102	1112	ν (C-C) + δ (C-N)		
1064	1071	1082	1060	ν (C-C) + δ (C-N)		
	1047	1047		ν (C-C) + δ (C-N)		
1006				ν (C-C) + δ (C-N)		
965				δ (N-H)/Nb-O_t		975
885	880	876	875	δ (N-H)/ Nb-O_t	886	
857	864	857		Nb-O_t	859	800
716	723		723	Ti/Nb-O-Ti/Nb	746,765	752
650	671	677	675	Ti/Nb-O-Ti/Nb	649	
	616	607	599	Ti/Nb-O-Ti/Nb		
526	519	522	527	macrocycl. def./ Nb-O-Nb	507, 534	524
488				Ti/Nb-O-Ti/Nb		
	436	437	439	Ti/Nb-O-Ti/Nb	434	

30

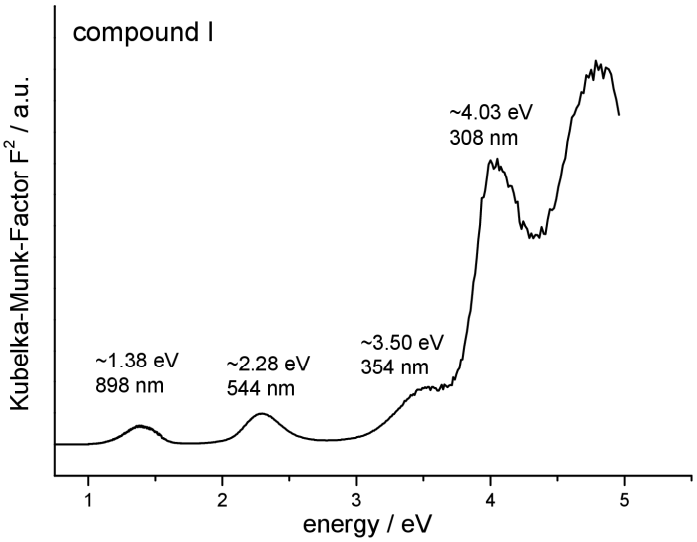

Figure S20. UV/Vis diffuse reflectance spectrum of compound **I**.

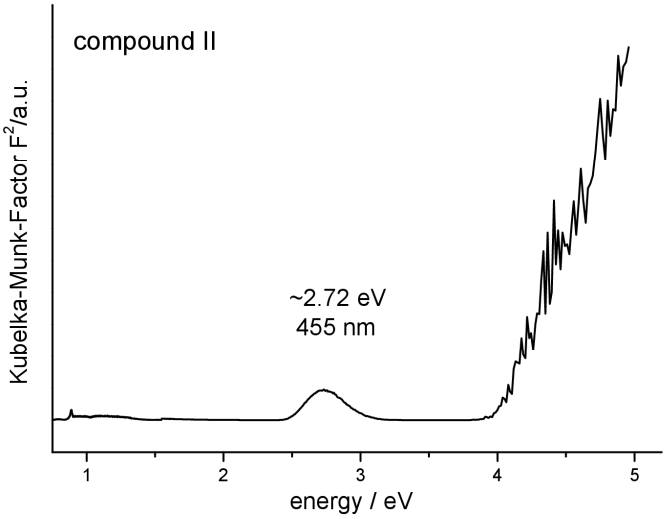

Figure S21. UV/Vis diffuse reflectance spectrum of compound**II**.

31

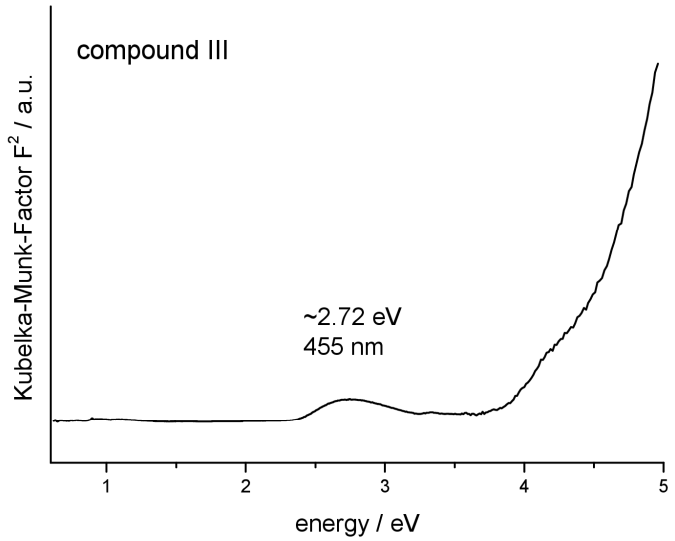

Figure S22. UV/Vis diffuse reflectance spectrum of compound **III**.

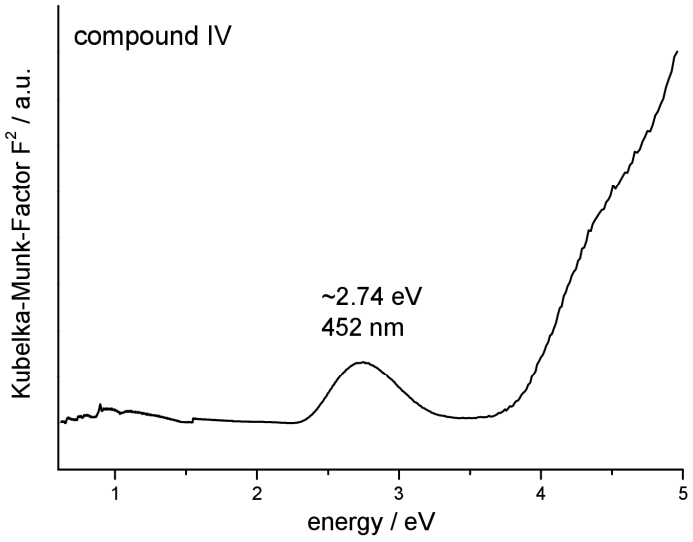

Figure S23. UV/Vis diffuse reflectance spectrum of compound **IV**.

32

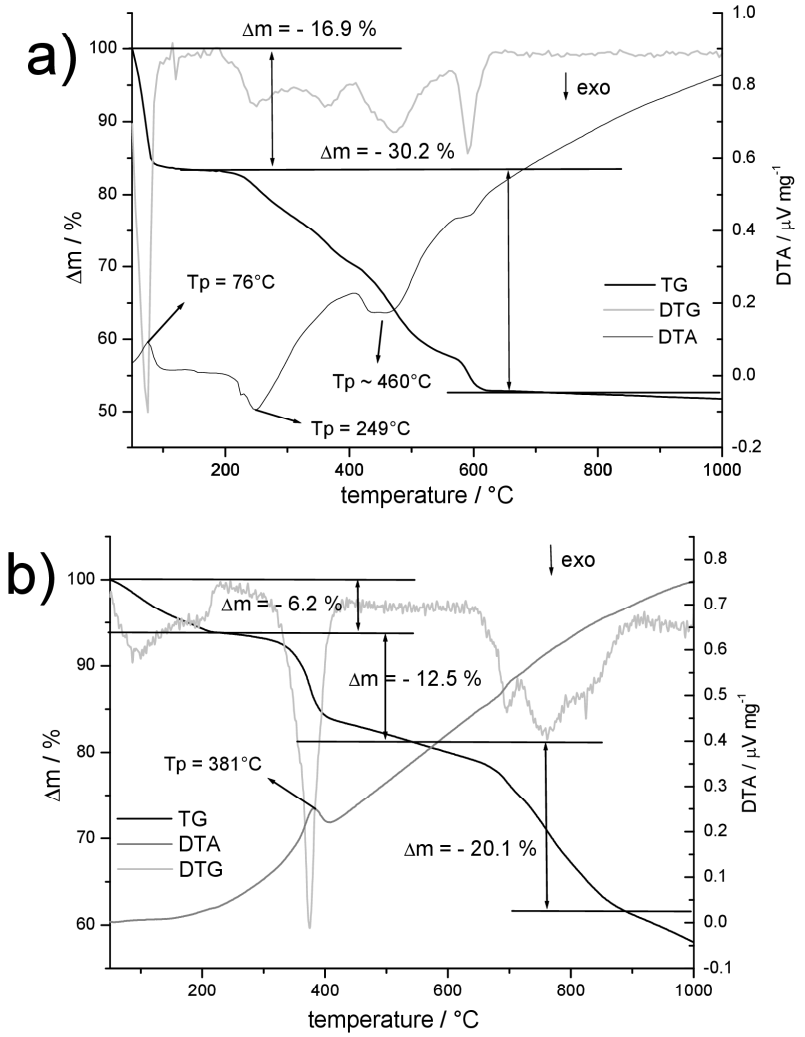

Figure S24a-b. DTA-TG curves of compound **I** without (a) and with (b) evacuating the sample chamber.

33

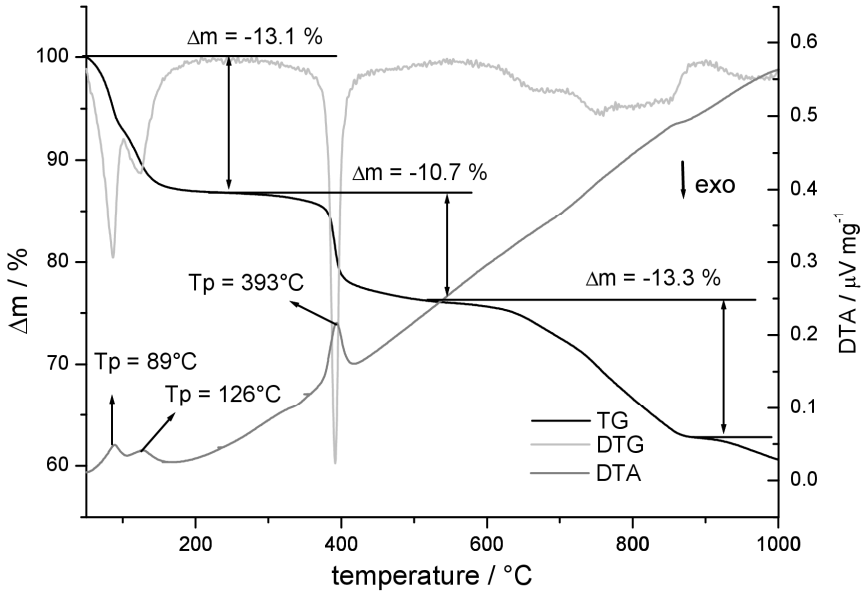

Figure S25. DTA-TG curves of compound **II**.

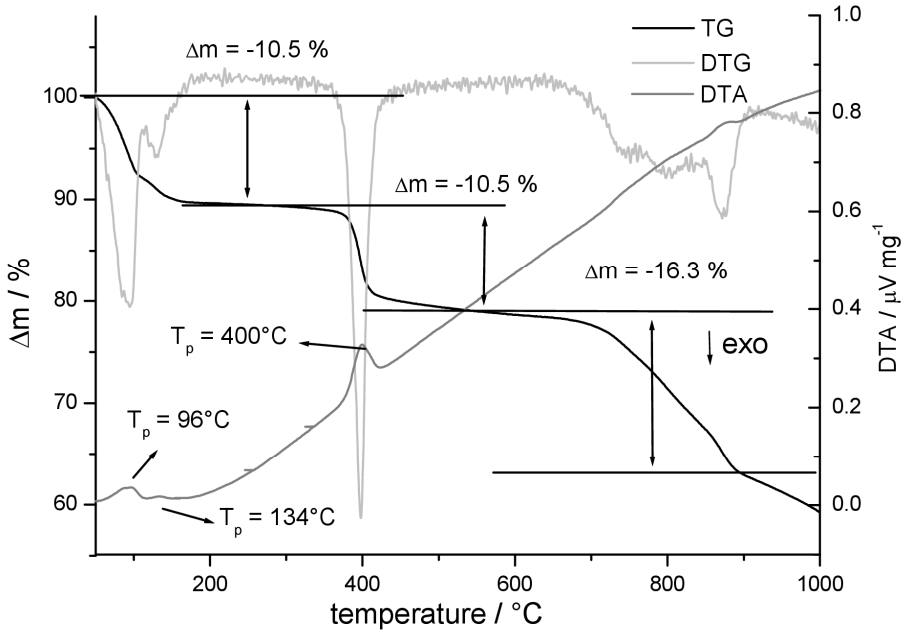

Figure S26. DTA-TG curves of compound **III**.

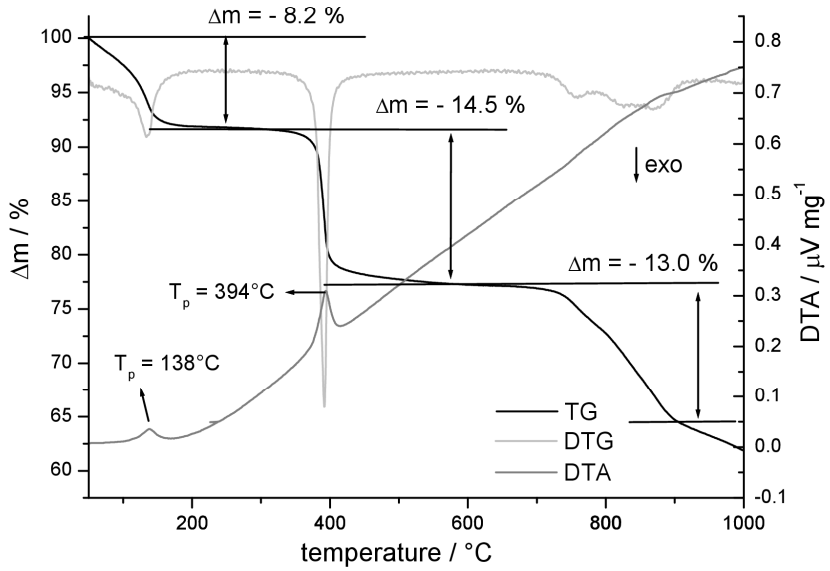

Figure S27. DTA-TG curves of compound **IV**.

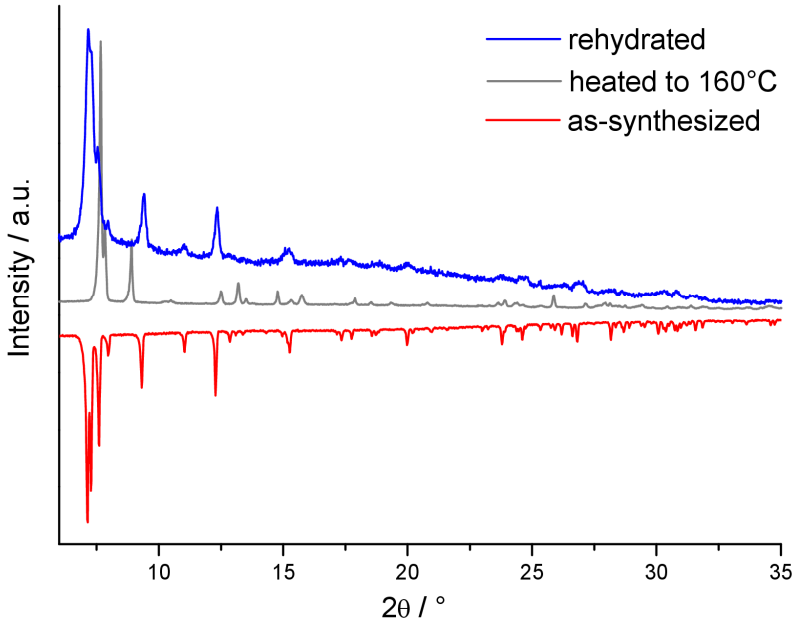

Figure S28. Comparison of XRDP of compound **I** as–synthesized (red), after heating to 160 °C (grey) and after rehydration experiment (blue).

35

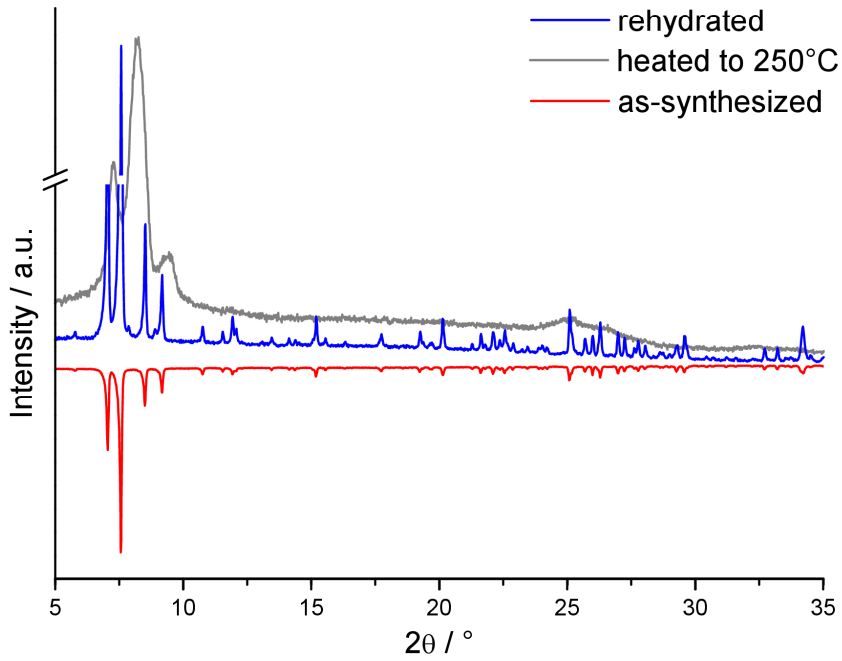

Figure S29. Comparison of XRDP of compound **II** as–synthesized (red), after heating to 250 °C (grey) and after rehydration experiment (blue).

36

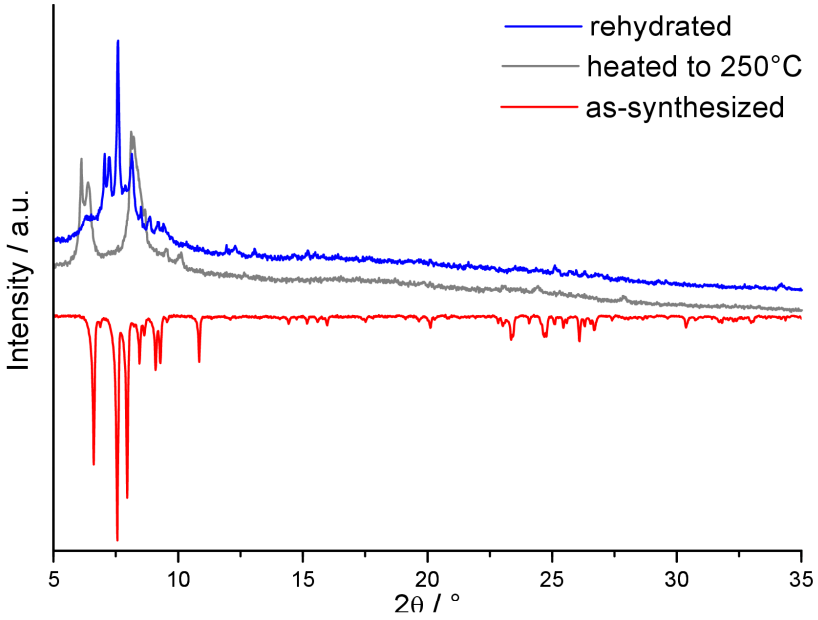

Figure S30. Comparison of XRDP of compound **III** as–synthesized (red), after heating to 250 °C (grey) and after rehydration experiment (blue).

37

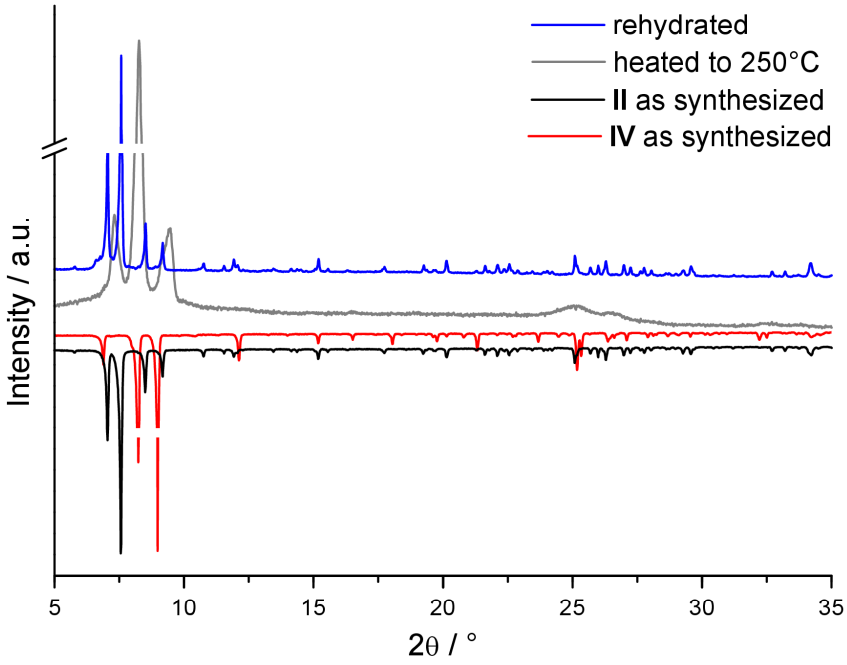

Figure S31. Comparison of XRDP of compound **II** (black) and **IV** (red) as–synthesized with the XRPD of **IV** after heating to 250 °C (grey) and after rehydration experiment (blue).

38

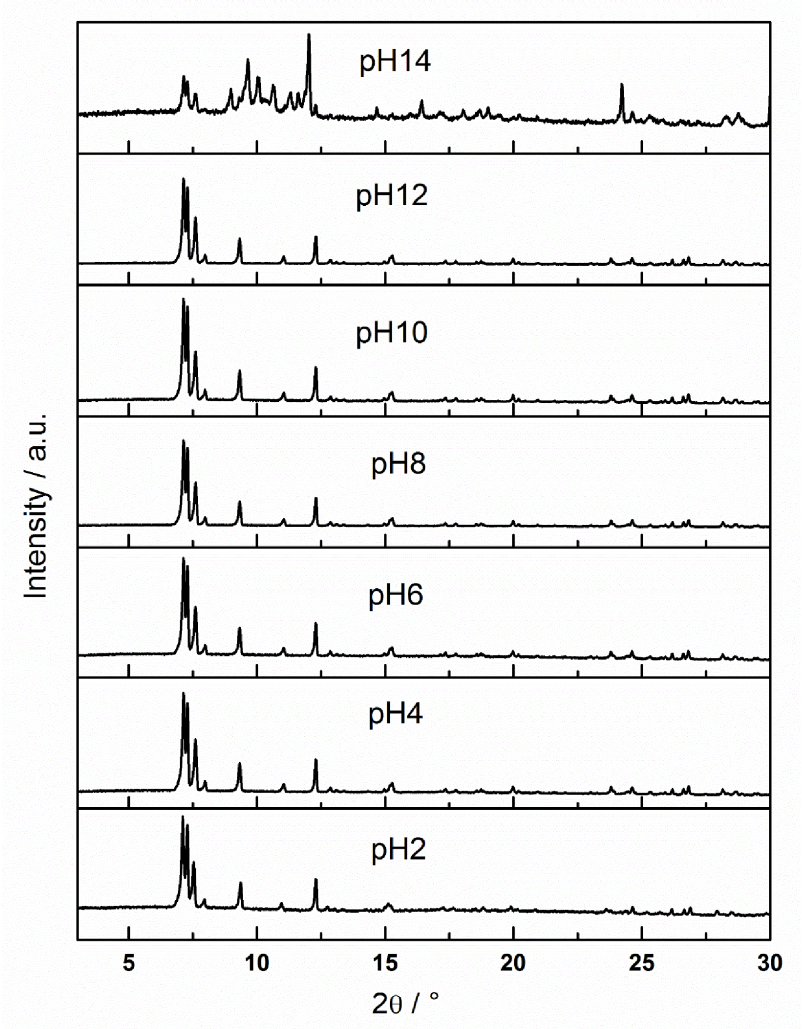

Figure S32. XRDP of compound **I** after immersing the samples in aqueous solutions of different pH values.

39

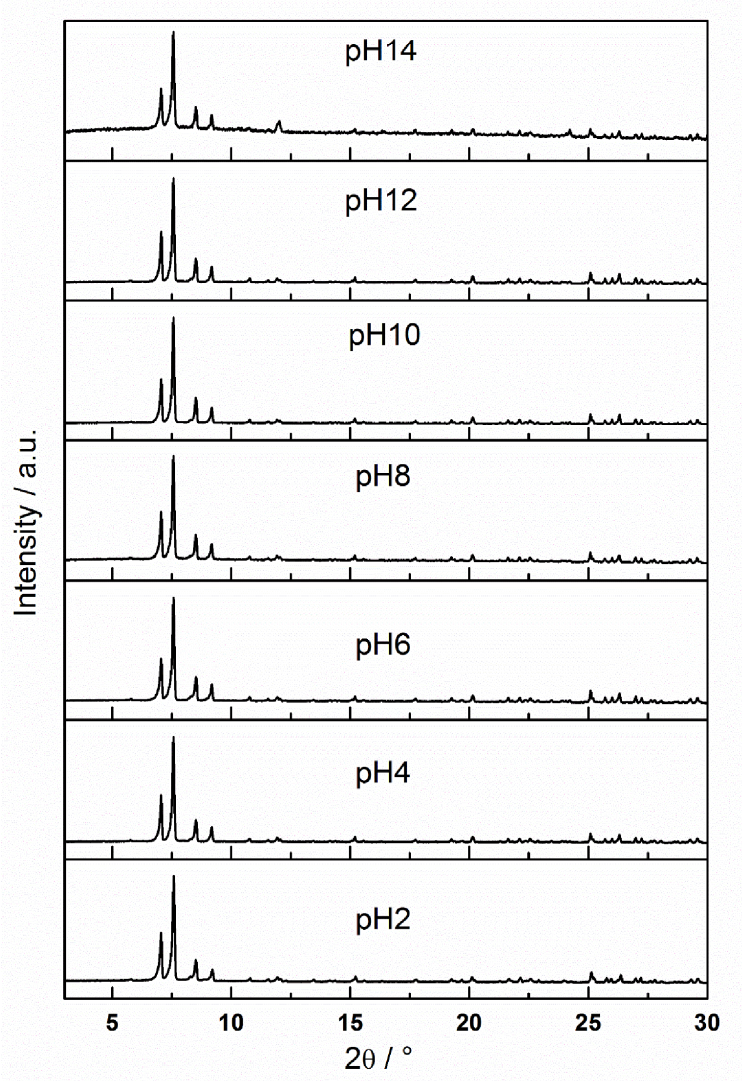

Figure S33. XRDP of compound **II** after immersing the samples in aqueous solutions of different pH values.

40

6.1.3 Zusatzinformation zum Manuskript „ Unveiling the Structural Changes Induced by Water Removal from a Water-rich Polyoxoniobate Using *in-situ* X-Ray Powder Diffraction and Pair Distribution Function Analysis"

Supporting Information

Unveiling the Structural Changes Induced by Water Removal from a Water-rich Polyoxoniobate Using in-situ X-ray Powder Diffraction and Pair Distribution Function Analysis

Joanna Dopta[1], Anna-Lena Hansen[1], Nicole Pienack[1], Lisa K. Mahnke[1], Helge Reinsch[1], Martin Etter[2], Christian Näther[1], Wolfgang Bensch[1]*

[1]Institut für Anorganische Chemie, Christian-Albrechts-Universität Kiel, Max-Eyth-Straße 2, D-24118 Kiel, Germany; wbensch@ac.uni-kiel.de

[2]Deutsches Elektronen-Synchrotron (DESY), Notkestr. 85, D-22607 Hamburg, Germany

Description of the crystal structure

The details of structure determination and refinement are listed in Tab. S1.

As mentioned in the main text, a decaniobate anion and $[Cu(cyclam)(H_2O)x]^{2+}$ cations (x=0,2) coexist in the structure of the title compound. In the anionic cluster, all ten Nb^{5+} cations are coordinated by six oxygen atoms, forming distorted NbO_6 octahedra, whereby the BVS confirms the oxidation state of +5 (Tab. S2) These are connected via edge-sharing mode, forming the decaniobate anion $[Nb_{10}O_{28}]^{6-}$ (Fig.1).

The Nb-O_t (t = terminal) bond lengths are in the range of 1.745(6)-1.752(6) Å, the Nb-μ_2-O- and the Nb-μ_3-O bonds are in the range of 1.819(6)-2.061(6) Å and 2.011(5)-2.106(6) Å, respectively; the Nb-μ_6-O distances represent the longest bonds (2.183(5)-2.504(5) Å, Tab. S3). All values are in good agreement with those reported in literature.[1] [2] [3]

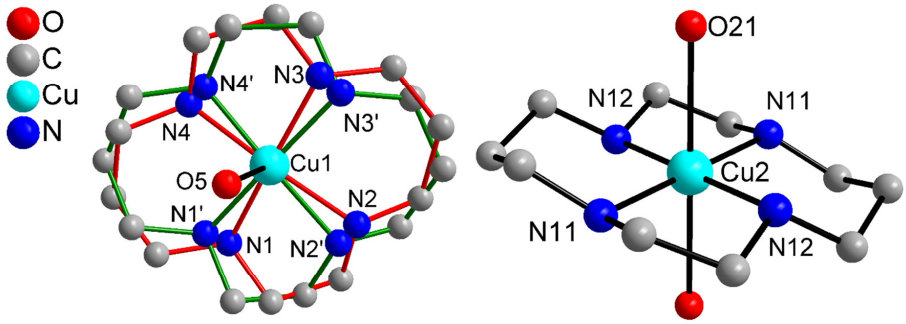

Figure S1. Coordination environments of the two crystallographically independent Cu^{2+} cations. Only selected atoms are labelled. The disorder of the cyclam molecule coordinating Cu1 is displayed using red and green bonds, respectively.

Charge compensation is achieved by three Cu^{2+} cations surrounded by four N atoms of the cyclam ligand in the basal plane and a terminal cluster O atom (Cu1) or two crystal H_2O molecules (Cu2, Fig. S1) at the apices. Two of them interact with the decaniobate cluster *via* terminal O atoms (Cu1), respectively. The corresponding cyclam ligand is disordered. The $\{[Cu(cyclam)]_2[Nb_{10}O_{28}]\}$ units are arranged along [010] axis with (Fig. S2) isolated $[Cu(cyclam)(H_2O)_2]^{2+}$ cations located between the

decaniobate units. The Cu-N-distances are in the range of 1.98(2) Å-2.015(19) Å (Tab. S4) and fit well those reported in literature. [4] [5] [6] [7] [8]

For the octahedrally coordinated $[Cu(cyclam)(H_2O)_2]^{2+}$ (Cu2), the *cis*-N-Cu-N angles are 85.3(3)- 94.7(3) ° and the *trans*-N-Cu-N angles are 180.0 °, also matching literature data. In contrast, the corresponding values for the square-pyramidal complex are 83.6(10)-95.3(11) ° for *cis*- and 169(14)-176.5(11) ° for *trans*-N-Cu-N angles and are slightly lower than literature data. Between this $[Cu(cyclam)]^{2+}$ molecule and the cluster anion, N-H and C-H H bonding interactions exist (N-H…O: 2.87(2)-3.13(3) Å, <(NHO): 3.20(3)-3.45(2) Å; <(NHO): 129.8-154.0 °, (Fig. S3, Tab. S5)) which may lead to a slight distortion of the molecule, being also reflected in the Nb-O-Cu angle with 126.0(3) °.

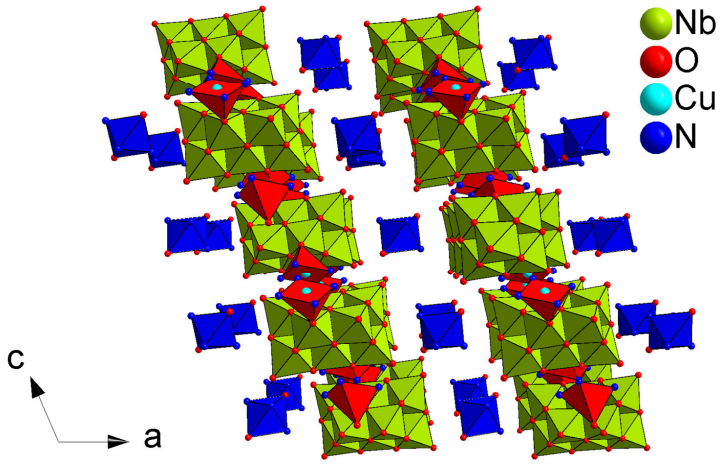

Figure S2. Representation of the arrangement of $[Nb_{10}O_{28}]^{6-}$ anions and $[Cu(cyclam)]^{2+}$ cations (*x*=1,2) along [110]; Green: NbO_6 octahedra; red: CuN_4O square pyramid; blue: CuN_4O_2 octahedra.

The two copper cations which interact with the terminal oxygen ions of the decaniobate unit are in a square pyramidal environment with a Cu(1)-O(5) distance of 2.358(6) Å and the nearest possible ligand beyond the range suitable for bonding interactions (Cu1-O4: 3.64 Å).

3

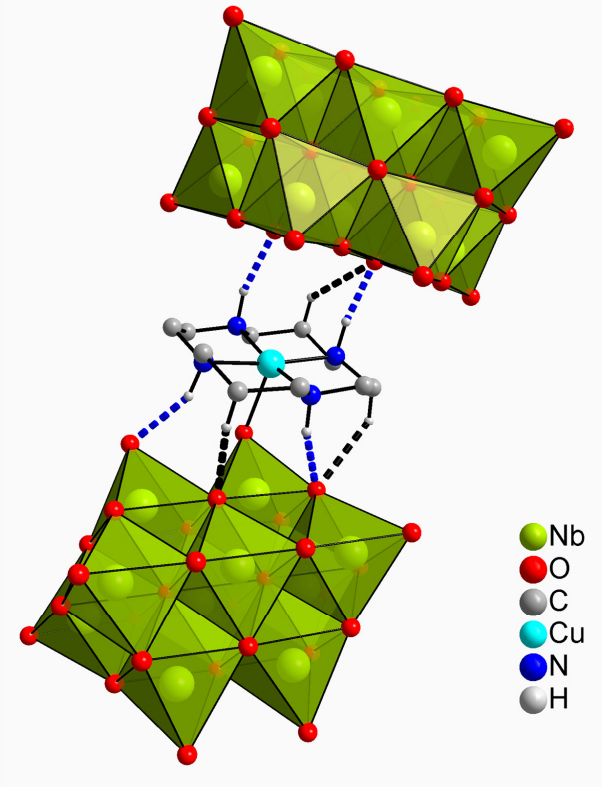

Figure S3. H bonding interactions between $[Cu(cyclam)]^{2+}$ cations and $[Nb_{10}O_{28}]^{6-}$ anions (dotted lines; blue: N-H H; black: C-H H bonding interactions.

The length of Cu-O distances to H_2O molecules in the octahedrally coordinated $[Cu(cyclam)(H_2O)_2]^{2+}$ complex (Cu(2)-O(21): 2.5242(9) Å) are also significantly longer than the sum of the ionic radii (2.01 Å[9]). The tetragonal elongation as an effect of Jahn-Teller distortion is often observed both in isolated copper cyclam complexes with apical oxygen-containing ligands[5] [10] as well as in copper-amine decorated polyoxoniobates.[11] [12] [13] [14] [15] [16]

Compared to the similar decavanadate compound $[Cu(cyclam)]\{[Cu(cyclam)]_2[V_{10}O_{28}]\} \cdot 10\ H_2O$, where $[Cu(cyclam)]^{2+}$ cations bridge the anionic clusters via terminal O atoms (Cu-O: 2.525(3)-2.604(3) Å), the Cu-O distances are shorter.[17]

The N atoms in both complexes are located in the basal plane, while the O atoms occupy the apices. This corresponds to a *trans* configuration of the cyclam molecules,

which is the commonest configuration in octahedral and square-planar copper macrocycle complexes.[18] Each $[Nb_{10}O_{28}]^{6-}$ anion is surrounded by six $[Cu(cyclam)]^{2+}$ cations in total (Fig. S4).

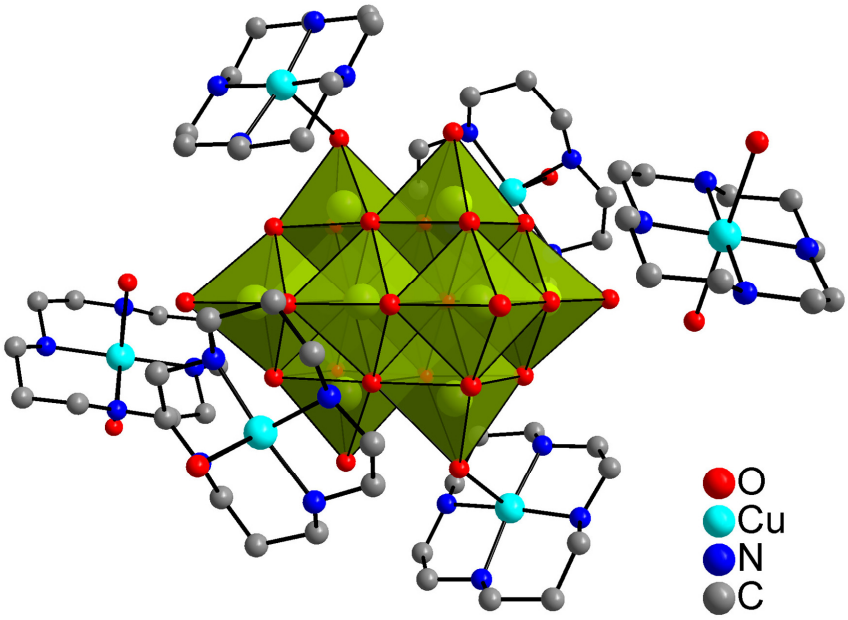

Figure S4. The decaniobate anion in the structure of the title compound surrounded by six $[Cu(cyclam)(H_2O)x]^{2+}$ molecules (x=0,2).

Besides the water molecules which complete the coordination sphere in the $[Cu(cyclam)(H_2O)_2]^{2+}$ cations, 27 further water oxygen atoms are located in the asymmetric unit. The arrangement of fully occupied water O atoms under consideration of the sum of the van der Waals radii (3.04 Å[9]) leads to an interesting pattern that can be classified using the notation of Infantes *et al.* for water clusters.[19] [20]

A layered network of alternating rings of two different sizes can be denoted as L16(4)20(8), i.e. the 16-membered rings share water O atoms with four other rings and the 20-membered ring are surrounded by eight adjacent rings (Fig. S5). The O-O distances scatter between 2.687 and 2.867 Å (Tab. S7, average: 2.797). In the 20-membered rings, the $[Cu(cyclam)(H_2O)_2]^{2+}$ cations and eight not fully occupied water

O atoms are located (O26,O28,O37,O40, s.o.f = 0.5), while the 16-membered rings surround the remaining water O atoms with lower occupancy (Fig. S6).

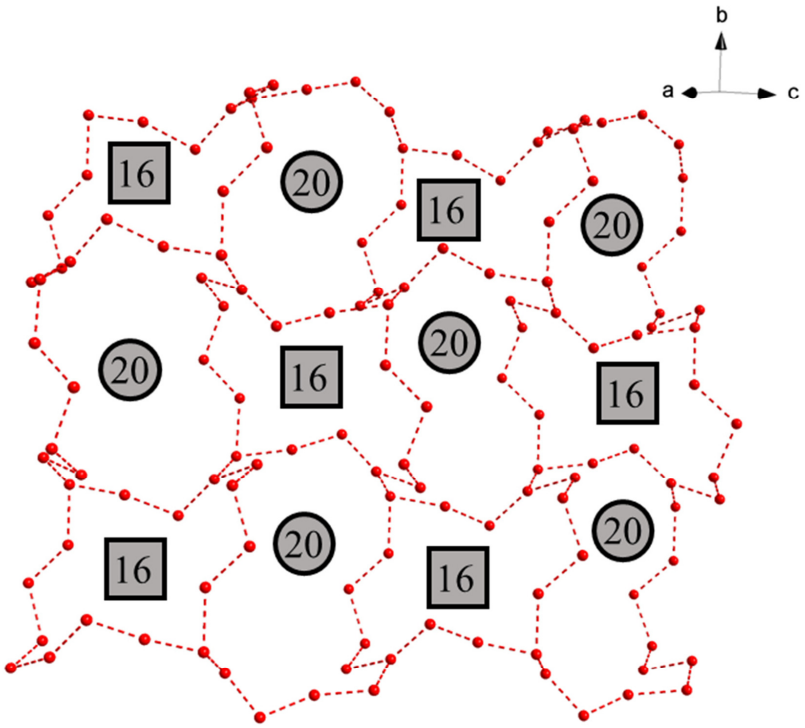

Figure S5. The arrangement of the fully occupied water O atoms into a L16(4)20(8) water cluster in the structure of $[Cu(cyclam)(H_2O)_2]\{[Cu(cyclam)]_2[Nb_{10}O_{28}]\} \cdot 27\ H_2O$; 16-and 20-membered rings alternate and are surrounded by four and eight adjacent rings, respectively.

6

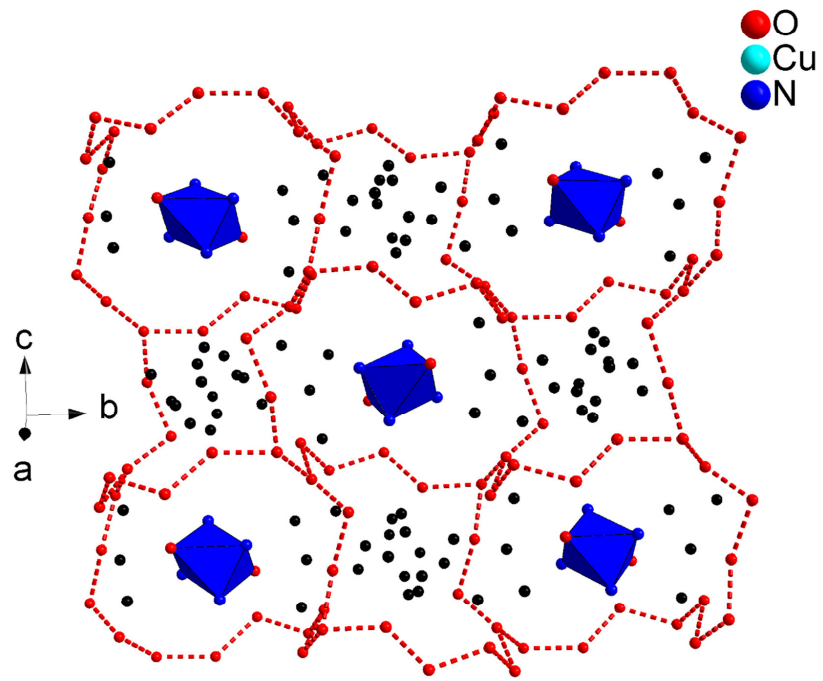

Figure S6. Arrangement of the two different types of rings in the layered L16(4)20(8) water cluster in the title compound. The 20-membered rings enclose the $[Cu(cyclam)(H_2O)_2]^{2+}$ cations and 8 H_2O molecules, while the 16-membered rings contain the residual H_2O molecules.

7

Table S1. Selected single crystal structure data and details of structure refinement.

[Cu(cyclam)(H$_2$O)$_2$]{[Cu(cyclam)]$_2$[Nb$_{10}$O$_{28}$]} · 27 H$_2$O	
Sum formula	$C_{30}H_{130}N_{12}Cu_3Nb_{10}O_{57}$
Crystal system	monoclinic
Space group	*P*2/c
a / Å	16.7620(4)
b / Å	17.4987(5)
c / Å	15.5807(4)
α / °	90
β / °	113.719(2)
γ / °	90
V / Å^3	4184.0(2)
Z	2
Formula weight / g · mol^{-1}	2691.17
$\rho_{calc.}$ / g · cm^{-3}	2.168
λ / Å	0.71073
Scan mode	Omega scan
2θ range / °	1.765 ≤ θ ≤ 25.004
Crystal dimensions / mm	0.09 x 0.15 x 0.20
Crystal colour	purple
Temperature / K	170
Index range	-16 ≤ h ≤ 19
	-20 ≤ k ≤ 20
	-20 ≤ l ≤ 18
Reflections collected	36212
Independent reflections	7352
R_{int}	0.0425
μ / mm^{-1}	2.168
Number of parameters	653
Transm min/max	0.5409/0.7507
R1 F_0>4σ(F_0))	0.0671
R1 (all data)	0.0721
wR2 (all data)	0.2016
∆F /e ·Å^{-3}	0.5656/0.7633
GOF	1.076

Table S2. Results of the bond valence sum calculations for Nb^{5+} cations.

Nb1	5.09
Nb2	5.21
Nb3	5.22
Nb4	5.10
Nb5	5.18
average	**5.16**

8

Table S3. Selected bond lengths / Å in the decaniobate unit sorted by type.

Bond type	Atoms	Bond length / Å	Bond type	Atoms	Bond length / Å
Nb=O_t	Nb(1)-O(3)	1.745(6)	Nb-μ_3-O	Nb(1)-O(10)	2.104(6)
	Nb(2)-O(5)	1.752(6)		Nb(1)-O(13)#1	2.116(6)
	Nb(3)-O(1)	1.745(6)		O(13)-Nb(1)#1	2.116(6)
	Nb(4)-O(2)	1.748(6)		O(10)-Nb(2)#1	2.082(6)
Nb-μ_2-O	Nb(1)-O(8)	1.920(6)		Nb(2)-O(10)#1	2.082(6)
	Nb(1)-O(11)	1.931(6)		Nb(2)-O(13)	2.106(6)
	Nb(2)-O(4)	1.915(6)		Nb(5)-O(13)	2.001(5)
	Nb(3)-O(8)	1.963(6)		Nb(5)-O(10)	2.031(5)
	Nb(3)-O(7)	1.966(6)	Nb-μ_6-O	Nb(1)-O(14)#1	2.420(5)
	Nb(3)-O(4)	1.967(6)		O(14)-Nb(1)#1	2.420(5)
	Nb(3)-O(9)	2.061(6)		Nb(2)-O(14)#1	2.407(5)
	Nb(4)-O(7)	1.957(6)		O(14)-Nb(2)#1	2.407(5)
	Nb(4)-O(11)	1.976(6)		Nb(3)-O(14)#1	2.492(5)
	Nb(4)-O(12)	2.004(6)		O(14)-Nb(3)#1	2.492(5)
	Nb(2)-O(12)	1.907(6)		Nb(4)-O(14)#1	2.504(5)
	Nb(4)-O(6)#1	2.061(6)		O(14)-Nb(4)#1	2.504(5)
	O(6)-Nb(4)#1	2.061(6)		Nb(5)-O(14)#1	2.183(5)
	Nb(5)-O(9)	1.819(6)		O(14)-Nb(5)#1	2.183(5)
	Nb(5)-O(6)	1.828(6)		Nb(5)-O(14)	2.189(5)

Symmetry transformations used to generate equivalent atoms: #1 -x+1,-y+1,-z+1

Table S4. Bond lengths / Å and angles / ° of the $[Cu(cyclam)]^{2+}$ cations.

Cu(1)-N(1)	1.98(2)	Cu(1)-N(2)	2.036(16)
Cu(1)-N(3')	2.00(2)	Cu(2)-N(12)	2.008(8)
Cu(1)-N(4')	2.00(2)	Cu(2)-N(12)#2	2.008(8)
Cu(1)-N(4)	2.002(19)	Cu(2)-N(11)#2	2.013(9)
Cu(1)-N(1')	2.015(19)	Cu(2)-N(11)	2.013(9)
Cu(1)-N(3)	2.02(2)	O(5)-Cu(1)	2.358(6)
Cu(1)-N(2')	2.03(2)		
N(3')-Cu(1)-N(4')	86.0(10)	N(3)-Cu(1)-O(5)	87.8(8)
N(1)-Cu(1)-N(4)	94.8(9)	N(2')-Cu(1)-O(5)	100.4(10)
N(3')-Cu(1)-N(1')	176.5(11)	N(2)-Cu(1)-O(5)	100.3(8)
N(4')-Cu(1)-N(1')	94.5(9)	N(3)-Cu(1)-N(2)	94.6(10)
N(1)-Cu(1)-N(3)	171.6(10)	N(4)-Cu(1)-N(2)	171.6(12)
N(4)-Cu(1)-N(3)	85.0(9)	N(1)-Cu(1)-O(5)	100.6(6)
N(3')-Cu(1)-N(2')	95.3(11)	N(3')-Cu(1)-O(5)	90.9(9)
N(4')-Cu(1)-N(2')	169.7(14)	N(4')-Cu(1)-O(5)	89.7(9)
N(1')-Cu(1)-N(2')	83.6(10)	N(4)-Cu(1)-O(5)	88.0(8)
N(1)-Cu(1)-N(2)	84.4(10)	N(1')-Cu(1)-O(5)	92.6(6)
Nb(2)-O(5)-Cu(1)	126.0(3)	N(3)-Cu(1)-O(5)	87.8(8)
N(4)-Cu(1)-N(2)	171.6(12)	N(12)-Cu(2)-N(12)#2	180.0
N(1)-Cu(1)-O(5)	100.6(6)	N(12)-Cu(2)-N(11)#2	94.7(3)
N(3')-Cu(1)-O(5)	90.9(9)	N(12)#2-Cu(2)-N(11)#2	85.3(3)
N(4')-Cu(1)-O(5)	89.7(9)	N(12)-Cu(2)-N(11)	85.4(3)
N(4)-Cu(1)-O(5)	88.0(8)	N(12)#2-Cu(2)-N(11)	94.7(3)
N(1')-Cu(1)-O(5)	92.6(6)	N(11)#2-Cu(2)-N(11)	180.0

Symmetry transformations used to generate equivalent atoms: #1 -x+1,-y+1,-z+1 #2 -x+2,-y+1,-z+1.

9

Table S5. Geometrical parameters of hydrogen bonds in title compound.

D-H...A	d(D-H)	d(H...A)	d(D...A)	<(DHA)
N-H…O bonding interactions between cyclam molecules and cluster O atoms				
N(1)-H(1N)...O(6)#3	1.00	1.94	2.88(2)	154.9
N(2)-H(2N)...O(4)	1.00	1.97	2.87(3)	149.2
N(3)-H(3N)...O(3)#1	1.00	2.21	3.13(3)	152.3
N(4)-H(4N)...O(9)#3	1.00	1.96	2.93(3)	162.5
N(1')-H(5N)...O(6)#3	1.00	1.98	2.96(2)	167.0
N(3')-H(7N)...O(3)#1	1.00	2.51	3.32(3)	137.9
N(3')-H(7N)...O(13)	1.00	2.53	3.42(3)	147.8
N(2')-H(6N)...O(4)	1.00	1.85	2.79(4)	154.3
N(4')-H(8N)...O(9)#3	1.00	2.06	2.98(3)	152.0
N(12)-H(10N)...O(7)	1.00	2.07	3.020(10)	158.7
N-H…O bonding interactions between cyclam molecules and water O atoms				
N(11)-H(9N)...O(26)	1.00	2.18	3.112(17)	155.4
C-H…O bonding interactions between cyclam molecules and cluster O atoms				
C(1)-H(1A)...O(4)	0.99	2.48	3.20(3)	129.8
C(4)-H(4B)...O(13)	0.99	2.54	3.45(2)	154.0
C(9)-H(9A)...O(6)#3	0.99	2.58	3.34(3)	132.7
C(6')-H(6D)...O(8)#3	0.99	2.61	3.54(4)	155.9
C(7')-H(7'2)...O(3)#1	0.99	2.51	3.27(3)	133.8
C(11)-H(11B)...O(1)	0.99	2.57	3.521(12)	161.3
C(11)-H(11B)...O(8)	0.99	2.59	3.261(12)	124.9
C-H…O bonding interactions between cyclam molecules and water O atoms				
C(4)-H(4A)...O(38)#4	0.99	2.57	3.15(4)	117.9
C(7)-H(7A)...O(24)#3	0.99	2.58	3.56(3)	168.1
C(9)-H(9B)...O(25)#5	0.99	2.50	3.48(2)	171.5
C(10)-H(10B)...O(36)#5	0.99	1.91	2.72(6)	137.1
C(1')-H(1C)...O(37)#2	0.99	2.56	3.36(4)	137.9
C(10')-H(10D)...O(36)#5	0.99	1.90	2.89(6)	178.4
C(10')-H(10D)...O(38)#7	0.99	2.62	3.37(5)	132.7
C(13)-H(13A)...O(34)#2	0.99	3.31	3.68(2)	104.0
C(15)-H(15A)...O(30)#2	0.99	2.64	3.430(18)	136.6

Symmetry transformations used to generate equivalent atoms: #1 -x+1,-y+1,-z+1 #2 -x+2,-y+1,-z+1 #3 -x+1,y+1/2,-z+1/2 #4 x-1,y,z #5 x,-y+3/2,z+1/2 #6 x,-y+3/2,z-1/2 #7 -x+2,y+1/2,-z+1/2

10

Table S6. O-O distances in the water cluster in $[Cu(cyclam)(H_2O)_2]\{[Cu(cyclam)]_2[Nb_{10}O_{28}]\} \cdot 27\ H_2O$.

Atom 1	Atom 2	Distance / Å
O(22)	O(32)	2.687
O(29)	O(30)	2.709
O(24)	O(25)	2.772
O(23)	O(31)	2.807
O(22)	O(24)	2.815
O(23)	O(25)	2.822
O(23)	O(30)	2.835
O(30)	O(32)	2.857
O(29)	O(31)	2.867
		Average: 2.797

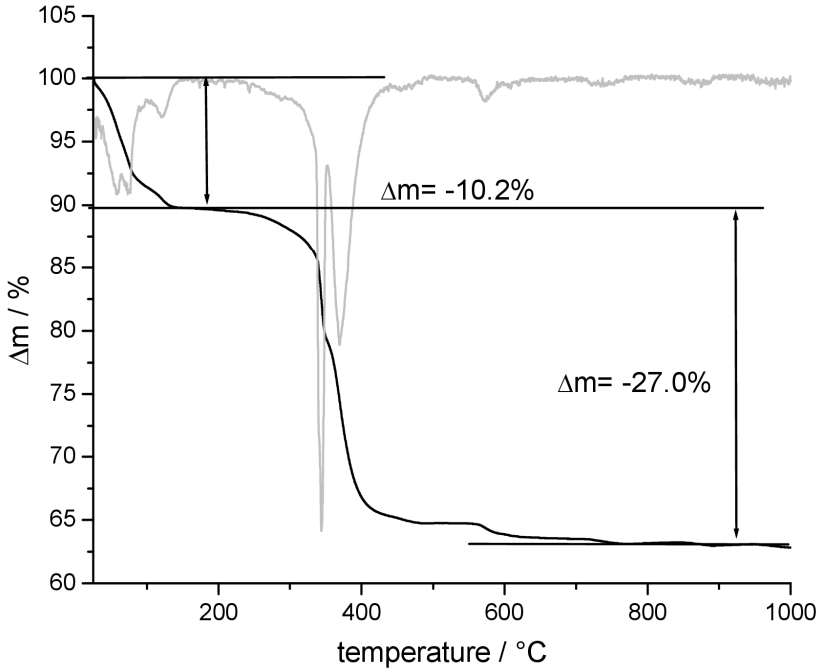

Figure S7. TG and DTG curves to estimate the water content in title compound.

Spectroscopic investigations

Infrared spectroscopy

In the IR spectrum of the title compound, the bands between 3377 cm^{-1} and 987 cm^{-1} are assigned to crystal water and cyclam molecules (Fig. S8). In the range between 892 cm^{-1} and 500 cm^{-1}, the peaks correspond to terminal Nb=O_t (892 cm^{-1}) and bridging Nb-O-Nb (721, 583 and 521 cm^{-1}) vibrations. The intense band at 424 cm^{-1} most likely represents the Cu-N stretching vibration of the $[Cu(cyclam)]^{2+}$ molecules. A more detailed assignment is presented in Tab. S7.

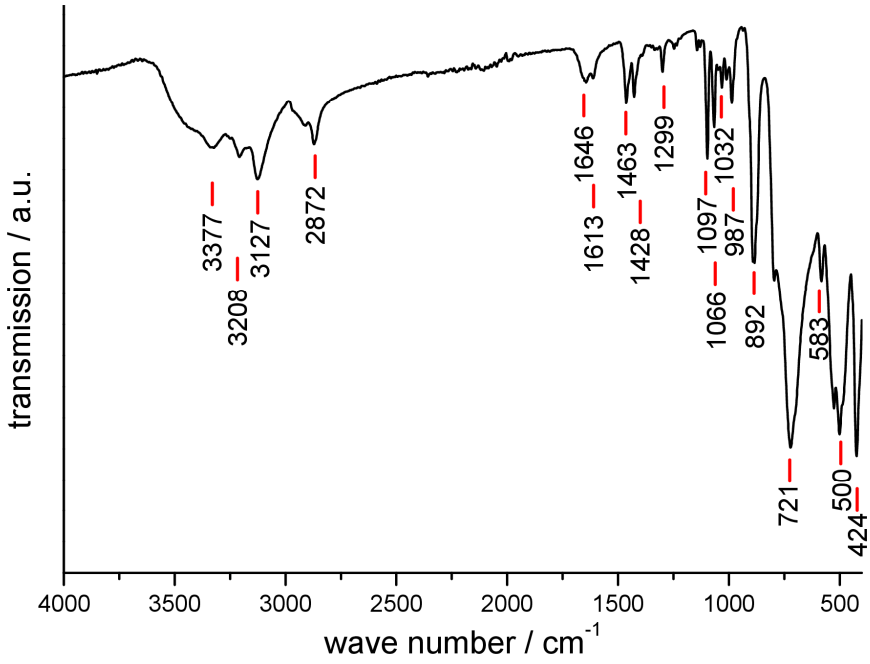

Figure S8. IR spectrum of the title compound.

12

Table S7. Assignment of the IR bands of the title compound compared to $[Cu(cyclam)]^{2+}$.

$[Cu(cyclam)]^{2+}$	Title compound	assignment [21],[22],[1],[23],[24]
3450	3377	O-H stretching
3230	3208	N-H stretching
3167	3127	N-H stretching
2903	2872	C-H stretching
-	1646	H-O-H def.
-	1613	H-O-H def.
1474	1463	C-H def.
1434	1428	C-H def.
1294	1299	C-N stretching C-C stretching
1110	1097	C-N stretching C-C stretching
1063	1066	C-N stretching C-C stretching
1015	1032	C-N stretching C-C stretching
963	987	N-H def.
-	892	Nb-Ot
-	721	Nb-O-Nb
-	583	Nb-O-Nb
-	500	Nb-O-Nb
427	424	Cu-N stretching

13

UV-Vis Spectroscopy

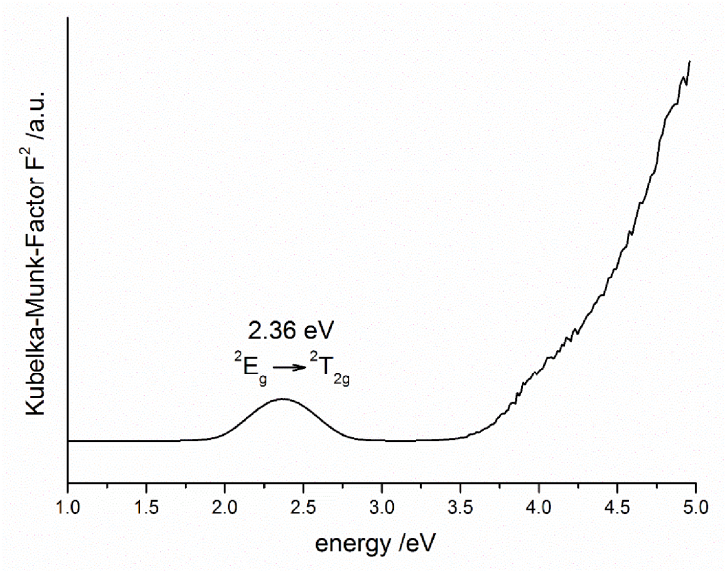

Figure S9. Kubelka-Munk-Factor plotted against energy.

The solid-state diffuse reflectance data were calculated with the Kubelka-Munk equation.[25] A broad absorption is found at 2.36 eV (525 nm/green, (Fig. S10), which corresponds to the $^2E_g \rightarrow {}^2T_{2g}$ d-d transition of Cu(II)[26][27][28][29] and agrees well with the violet color of the crystals. Compared to the $[Cu(cyclam)]^{2+}$ complex, where Cu^{II} is in an octahedral environment, this band is slightly red-shifted (Fig. S11). This can be explained by the formation of the square pyramidal complex, in which the copper ion is coordinated by four N ligands and one terminal O atom of the decaniobate unit, which leads to an energy decrease.[26]

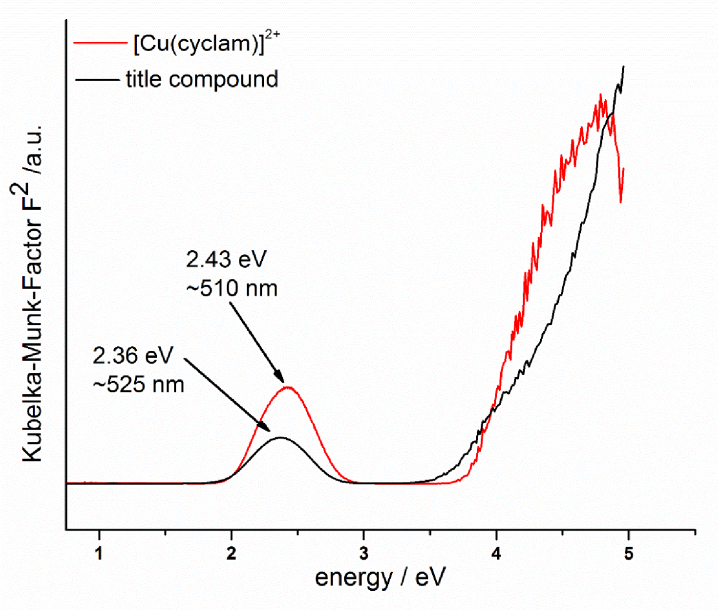

Figure S11. Kubelka-Munk-Factor plotted against energy for the title compound (red) and the $[Cu(cyclam)]^{2+}$ complex (black).

15

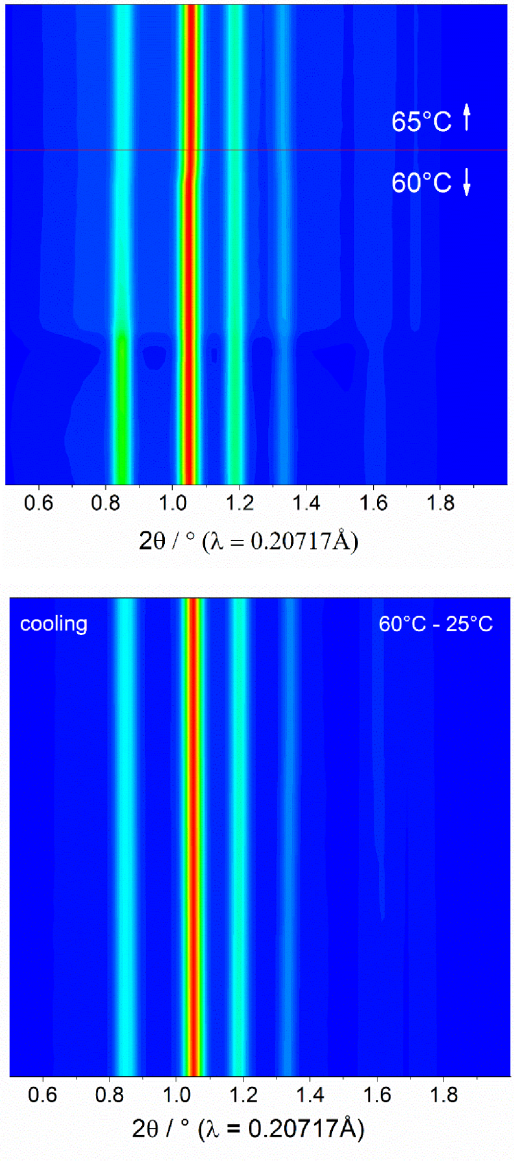

Figure S12. Contour plot of XRD patterns of sample upon heating to 65 °C (top) and cooling (bottom).

16

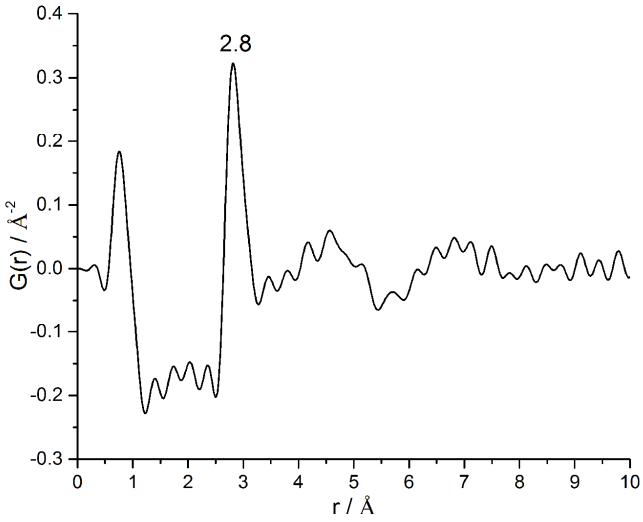

Figure S13. PDF of H_2O; the contribution of the Capton capillary was subtracted.

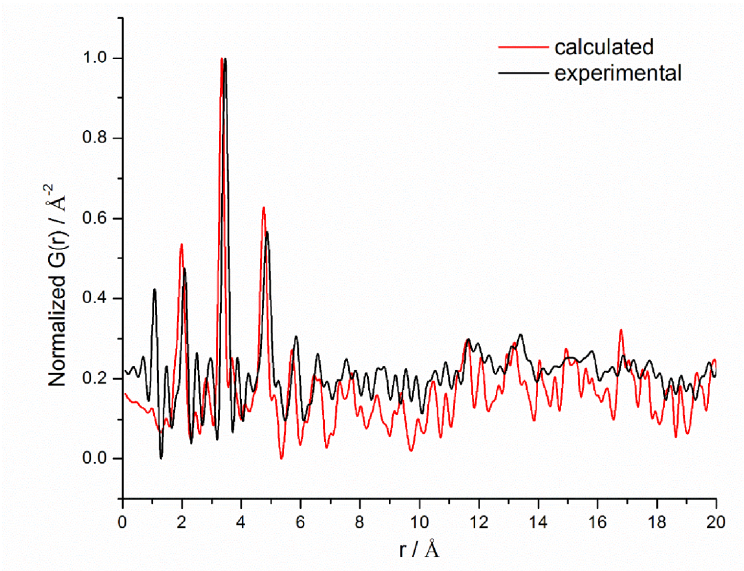

Figure S14. Comparison of the experimental PDF curve for $Nb_{10}{\cdot}29H_2O$ (black) with the curve calculated from single crystal structure data (red).

17

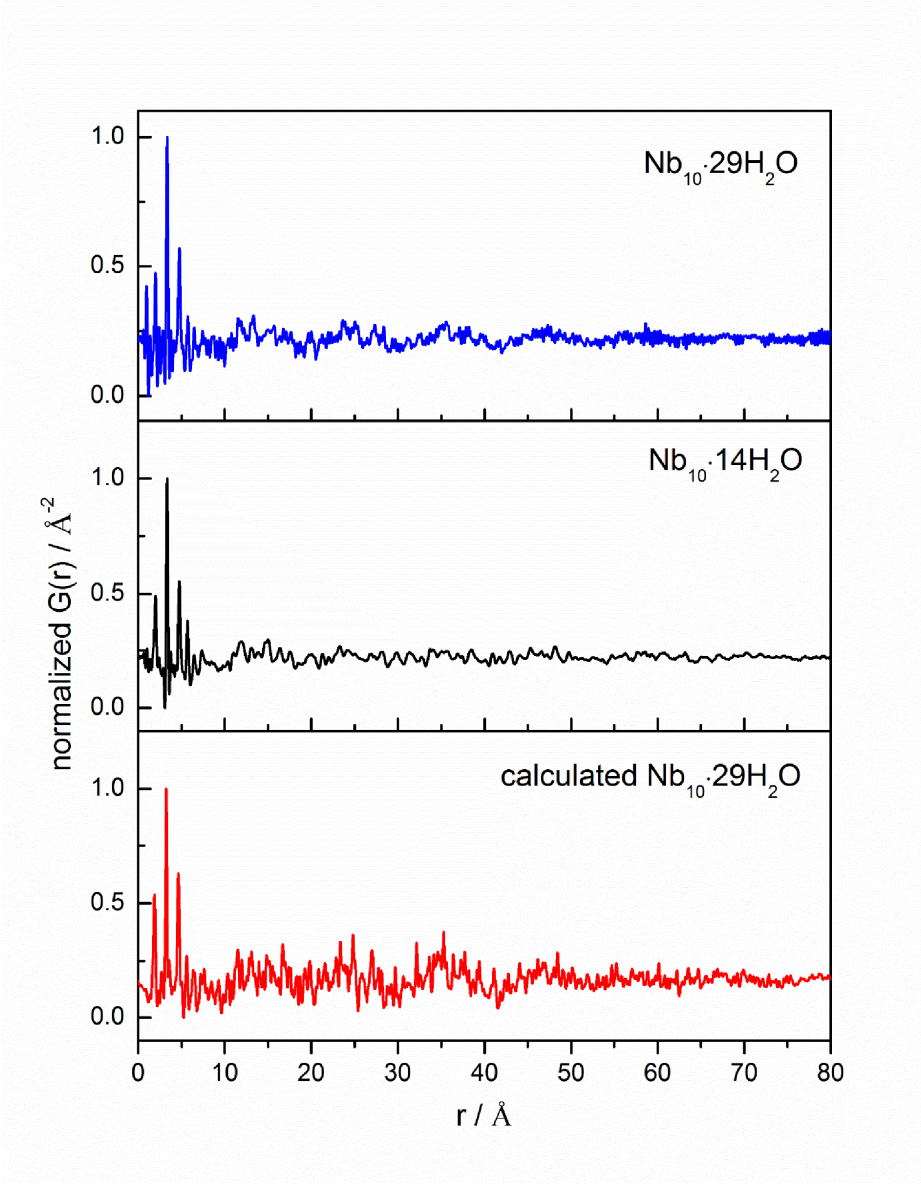

Figure S15. PDFs of the $Nb_{10}{\cdot}29H_2O$ (top) and $Nb_{10}{\cdot}14H_2O$ (middle) compared to the calculated (bottom).

18

References

[1] J. Niu, G. Wang, J. Zhao, Y. Sui, P. Ma, J. Wang, *Cryst. Growth Des.* **2011**, *11*, 1253.
[2] E. J. Graeber, B. Morosin, *Acta Crystallogr. B.* **1977**, 2137.
[3] M. Matsumoto, Y. Ozawa, A. Yagasaki, *Polyhedron* **2010**, 2196.
[4] I. Pérez-Toro, A. Domínguez-Martín, D. Choquesillo-Lazarte, E. Vílchez-Rodríguez, J. M. González-Pérez, A. Castiñeiras, J. Niclós-Gutiérrez, *J. Inorg. Biochem.* **2015**, *148*, 84.
[5] P. A. Tasker, L. Sklar, *J. Cryst. Mol. Struct.* **1975**, 329.
[6] N. S. A. Tajidi, A. Norbani, A. Zainudin, W. T. Kong, S. W. Ng, *Acta Crystallogr. E* **2010**, *66*, m889.
[7] N. S. A. Tajidi, N. Abdullah, Z. Arifin, *Acta Crystallogr. E* **2011**, *67*, m588-9.
[8] N. S. A. Tajidi, N. Abdullah, Z. Arifin, K. W. Tan, S. W. Ng, *Acta Crystallogr. E* **2010**, *66*, m888.
[9] A. Bondi, *J. Phys. Chem. A* **1964**, *68*, 441.
[10] N. S. A. Tajidi, N. Abdullah, Z. Arifin, K. W. Tan, S. W. Ng, *Acta Crystallogr. E* **2010**, *66*, m890.
[11] R. P. Bontchev, E. L. Venturini, M. Nyman, *Inorg. Chem.* **2007**, *46*, 4483.
[12] J. Niu, P. Ma, H. Niu, J. Li, J. Zhao, Y. Song, J. Wang, *Chem. Eur. J.* **2007**, *13*, 8739.
[13] J. Niu, X. Fu, J. Zhao, S. Li, P. Ma, J. Wang, *Cryst. Growth Des.* **2010**, *10*, 3110.
[14] J.-Q. Shen, Q. Wu, Y. Zhang, Z.-M. Zhang, Y.-G. Li, Y. Lu, E.-B. Wang, *Chem. Eur. J.* **2014**, *20*, 2840.
[15] P. Huang, C. Qin, X.-L. Wang, C.-Y. Sun, Y. Xing, H.-N. Wang, K.-Z. Shao, Z.-M. Su, *Dalton Trans.* **2012**, *41*, 6075.
[16] J.-Q. Shen, Y. Zhang, Z.-M. Zhang, Y.-G. Li, Y.-Q. Gao, E.-B. Wang, *Chem. Commun.* **2014**, *50*, 6017.
[17] J. Martín-Caballero, A. San José Wéry, S. Reinoso, B. Artetxe, L. San Felices, B. El Bakkali, G. Trautwein, J. Alcañiz-Monge, J. L. Vilas, J. M. Gutiérrez-Zorrilla, *Inorg. Chem.* **2016**, *55*, 4970.
[18] M. Bakaj, M. Zimmer, *J. Mol. Struct.* **1999**, *508*, 59.
[19] L. Infantes, J. Chisholm, S. Motherwell, *CrystEngComm* **2003**, *5*, 480.
[20] L. Infantes, S. Motherwell, *CrystEngComm* **2002**, *4*, 454.
[21] G. Diaz F., R.E. Clavijo C., M. M. Campos-Vallette, M. Saavedra S, S. Diez, R. Muñoz, *Vib. Spectrosc.* **1997**, *15*, 201.
[22] L. Shen, C.-H. Li, Y.-N. Chi, C.-W. Hu, *Inorg. Chem. Commun.* **2008**, *11*, 992.
[23] G. Socrates, *Infrared and Raman Characteristic Group Frequencies*, John Wiley@Sons LTD, Manchester, New York, Weinheim, Toronto, Brisbane, Singapore, **2001**.
[24] J.-H. Son, C. A. Ohlin, W. H. Casey, *Dalton Trans.* **2012**, *41*, 12674.
[25] G. Kortüm, W. Braun, G. Herzog, *Angew. Chem.* **1963**, *75*, 653.
[26] M. Boiocchi, A. Broglia, L. Fabbrizzi, N. Fusco, C. Mangano, *Can. J. Chem.* **2014**, *92*, 794.
[27] J. Černák, J. Kuchár, M. Stolárová, M. Kajňaková, M. Vavra, I. Potočňák, L. R. Falvello, M. Tomás, *Transit. Met. Chem.* **2010**, *35*, 737.

19

[28] A. Prevedello, I. Bazzan, N. Dalle Carbonare, A. Giuliani, S. Bhardwaj, C. Africh, C. Cepek, R. Argazzi, M. Bonchio, S. Caramori et al., *Chem. Asian J.* **2016**, *11*, 1281.
[29] H. Stephan, G. Geipel, D. Appelhans, G. Bernhard, D. Tabuani, H. Komber, B. Voit, *Tetrahedron Lett.* **2005**, *46*, 3209.

20

6.2 Publikationen, Manuskript und Tagungsbeiträge

Solvothermal synthesis to modify transition elements containing thiostannates, thioantimonates, and polyoxoniobates

J. Hilbert, C. Anderer, J. Dopta, C. Näther, W. Bensch;

DGKs Young crystallographers Lab Meeting, Darmstadt, **2015**.

Controlling crystallization of Polyoxoniobates

J. Dopta, C. Näther, W. Bensch;

19th International Symposium on the Reactivity of Solids, Bayreuth, **2018**.

Controlling Fast Nucleation and Crystallization of Two New Polyoxoniobates

J. Dopta, D.-C. Krause, C. Näther, W. Bensch;

Cryst. Growth. Des. **2018**, *18*, 4130 – 4139.

On the influence of the titanium source on the composition and structure of novel titanoniobates

J. Dopta, S. Grzanna, C. Näther, W. Bensch;

Dalton Trans. **2018**, *47*, 15103-15113.

Manuskript: Unveiling the Structural Changes Induced by Water Removal from a Water-rich Polyoxoniobate Using *in-situ* X-ray Powder Diffraction and Pair Distribution Function Analysis

J. Dopta, A.-L. Hansen, N. Pienack, L.M. Mahnke, H. Reinsch, M. Etter, C. Näther, W. Bensch;

Unveröffentlichtes Projekt, **2018**.

6.3 Proposal „ In situ XRD and PDF Investigations on Polyoxometalates: Reversible Water Uptake and Release”

In situ XRD and PDF Investigations on Polyoxometalates: Reversible Water Uptake and Release

Joanna Dopta, Anna-Lena Hansen, Dr. Nicole Pienack, Prof. Dr. Wolfgang Bensch

1. Aim of the proposed experiment and description of the scientific background

Polyoxometalates (POMs) are an outstanding class of materials with respect to their structural diversity and potential applications. They consist of oxoanions and are formed by group V and VI elements (V, Nb, Mo, W), which adopt variable geometries with oxygen. The self-assembly of the metal-oxygen-polyhedra leads to polynuclear cluster compounds with an enormous structural variety. While polyoxovanadates, -molybdates and -tungstates are most often in the focus of POM scientists, polyoxoniobates (PONbs) are less common due to the synthetic limitations related to the narrow pH working range of 10-12. In addition, the PONb chemistry still is dominated by the Lindqvist hexametalates. The high charge densities (which means the ratio between the polyoxoanion charge and the number of non-hydrogen atoms) of PONbs require charge compensation. Besides alkali metal and quaternary amine cations, transition metal (*TM*) complexes are suitable reagents to stabilize the high negative charge. Although research on transition metal substituted PONbs is in its early stage, most of the discovered compounds exhibit very interesting properties with respect to their photocatalytic activity for hydrogen evolution reaction or organic dye degradation.

2. Results of previous own work relating to this proposal

During the last few months, our group has made great success in solvothermal synthesis of PONbs using $[TM(\text{amine})_x]^{y+}$ complexes. In this context, we found a new compound $[TM(\text{amine})(H_2O)_2]\{[TM(\text{amine})]_2[Nb_{10}O_{28}]\} \cdot 27\ H_2O$. Interestingly, the PONb loses crystal water molecules, which are located between the $\{Nb_{10}O_{28}\}$ clusters (Fig. 1), under ambient conditions and retains its crystallinity. Time resolved X-ray diffraction experiments on samples prepared in capillaries showed that 1. two phases coexist: one containing crystal water and the “dry” phase (Fig. 2). The ratio between the water containing and the water free phase can be traced. 2. if the phase transition once started, it is finished in a very short time in the range of minutes. The loss of crystal water molecules obviously leads to a contraction of the unit cell as the corresponding Bragg peaks show a shift towards higher 2 theta angles, yet the exact structural changes are not understood.

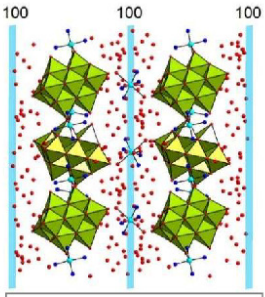

Fig. 1: Location of the crystal water molecules in $[TM(\text{amine})(H_2O)_2][[TM(\text{amine})]_2[Nb_{10}O_{28}]] \cdot 27\ H_2O$ along (100). Green polyhedra: NbO_6 units; turquoise spheres: TM, blue: N, red: oxygen

Fig. 2: Time resolved X-Ray diffraction patterns measured during the loss of crystal water molecules. Below: Waterfall plot. Right: Assignment of the lattice planes to the Bragg peaks.

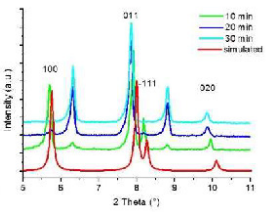

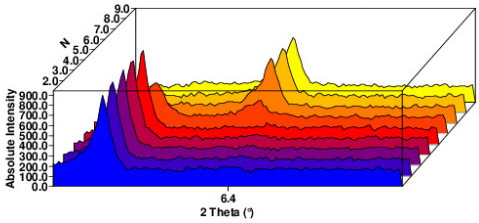

3. Description of the results expected and their scientific relevance

Once the reaction started, the loss of crystal water molecules is a very fast reaction. The in house powder X-ray diffraction (PXRD) experiments at room temperature show that an exposure time of less than two minutes (Fig. 2, right) is necessary. Within this limited time range, we are not able to cover a broader 2 theta range in house, required to gain insights into the changes of the whole structure. Using synchrotron radiation with better time resolution besides higher intensity could overcome this

problem. We expect to gain insights into the local structure and its change upon the loss of the crystal water molecules by considering the total scattering, e.g. analyzing the pair distribution function (PDF). As depicted in figure 1, the structure is built up by $\{Nb_{10}O_{28}\}$ clusters. We don't expect them to change their inner (short range) structure during water loss, but their intermolecular distances. Therefore, PDF analysis is the method of choice to understand and track these distances. Further, it is not clear if the water molecules, which were detected by single crystal X-ray analysis, occupy the same positions after the loss and the re-integration of water molecules into the crystal lattice. We expect combined PXRD and PDF investigations with synchrotron radiation to illuminate the processes during the reversible water uptake and release on the long and short range order. This study will give important insights into the influence of humidity of the sample environment and offer the possibility of "tuning" the water content for future applications. Additionally, we aim to understand the kinetics of this process. Therefore, we will perform time resolved studies and ambient and enhanced temperatures. Previous experiments showed that the solvent uptake of the "dry" phase is selective for water molecules; this means the material cannot adsorb, *e.g.* ethanol or methanol. Based on this property, the compound may be a promising material for industrial alcohol purification or be suitable as water sensor. PONbs could not only be applied as powerful catalysts, but also show antitumoral activity. Since active pharmaceutical ingredients are often hydrated materials, the knowledge about the dehydration pathways is essential to the research on pharmaceutical products. In conclusion, the simultaneous collection of PXRD and PDF data was not yet applied on PONbs, to the best of our knowledge, but this combination could be a novel approach for characterization and *in situ* studies of POMs.

4. Details of the proposed experiment at PETRA III

a) experimental method
- We request 6 shifts at beamline P02.1. In order to cover a sufficient Q-range suitable for PDF studies need a high energy beamline. Requested shifts in detail:

- 1 shift setup and calibration (measurement of empty capillaries and LaB6 standard material)
- 5 shifts temperature and time resolved measurements (room temperature, 60℃, 90℃)

Experiments will take place in open glass capillaries (1mm Ø), allowing the samples to dry and get remoistened with thin cannulas.

b) samples & safety related issues
- samples will be crystalline powders and the solvent is water. No additional safety cautions are required

c) specific technical requirements (if applicable)
- hot air blower, capillary spinner

5. Related own publications during the last 3 years

[1] M. Wendt, P. Polzin, J. van Leusen, C. Näther, P. Kögerler, W. Bensch, *In situ* ligand exchange-mediated 0D/1D transformation of a polyoxovanadate, *Dalton Trans.* **2017**, *46*, 1618 – 1623. DOI: 10.1039/C6DT04412C
[2] N. Pienack, L. Ruiz Arana, W. Bensch, H. Terraschke, *In-situ* studies on phase transitions of Tris(acetylacetonato)-aluminum(III) $Al(acac)_3$, *Crystals* **2016**, *6*, 157. DOI: 10.3390/cryst6120157
[3] M. Wendt, L.K. Mahnke, N. Heidenreich, W. Bensch, Nucleation and Crystal Growth of a $\{V_{14}Sb_8O_{42}\}$ Cluster from a $\{V_{15}Sb_6O_{42}\}$ Polyoxovanadate: *In-Situ* X-ray Diffraction Studies, *Eur. J. Inorg. Chem.* **2016**, 5393–5398. DOI: 10.1002/ejic.201601025
[4] M. Wendt, U. Warzok, C. Näther, J. van Leusen, P. Kögerler, C. A. Schalley, W. Bensch, Catalysis of "Outer-Phase" Oxygen Atom Exchange Reactions by Encapsulated "Inner-Phase" Water in $\{V_{15}Sb_6\}$-type Polyoxovanadates**,** *Chem. Sci.* **2016**, *7*, 2684–2694. DOI: 10.1039/C5SC04571A

6.3.1 Messzeiten an Synchrotronlichtquellen

19.-21.02.2017	Beamline I15, Diamond Light Source Oxfordshire
05.-07.04.2017	Beamline P02.1, DESY Hamburg
11.-13.12.2017	Beamline P02.1, DESY Hamburg

6.4 Eidesstattliche Erklärung

Hiermit versichere ich, Joanna Dopta, an Eides statt, dass ich die vorliegende Dissertation, abgesehen von der Beratung durch meinen Doktorvater Prof. Dr. W. Bensch, nach Inhalt und Form selbstständig und nur mit den angegebenen Hilfsmitteln verfasst habe. Weder ganz noch zum Teil wurde diese Arbeit an anderer Stelle im Rahmen eines Prüfungsverfahrens vorgelegt oder zur Veröffentlichung eingereicht.

Ich erkläre, dass ich die hier vorliegende Arbeit nach den Grundsätzen guter wissenschaftlicher Arbeit der Deutschen Forschungsgemeinschaft verfasst habe. Außerdem wurde mir bisher auch kein akademischer Grad entzogen.

Kiel, 17.12.2018 Joanna Dopta

6.5 Lebenslauf

PERSÖNLICHE DATEN

Name	Joanna Dopta
Geburtstag	14. Februar 1987
Geburtsort	Koscian (PL)
Staatangehörigkeit	Deutsch
Familienstand	Ledig

BERUFLICHER WERDEGANG

Seit 01/2013	Institut für anorganische Chemie, CAU Kiel
	Wissenschaftliche Mitarbeiterin
12/2012 04/2012-06/2012 02/2012	Institut für anorganische Chemie, CAU Kiel
	Wissenschaftliche Hilfskraft
08/2009-11/2008	Institut für physikalische Chemie, CAU Kiel
	Wissenschaftliche Hilfskraft
05/2008-08/2008 10/2008-12/2008	Institut für Pflanzenernährung, CAU Kiel
	Wissenschaftliche Hilfskraft

STUDIUM & SCHULE

10/2006-12/2012	Christian-Albrechts-Universität, Kiel
	Chemie (Diplom)
09/1997-07/2006	Hoffmann-von-Fallersleben, Gymnasium Lütjenburg
	Schülerin (Abitur)

6.6. Danksagung

Meinem Doktorvater Prof. Dr. Wolfgang Bensch danke ich für das spannende Thema, an welchem ich sehr gerne gearbeitet habe, für seine Geduld mit mir in der Zeit, in denen es keine zufriedenstellenden Ergebnisse gab und dafür, dass er mir immer mit Rat und Tat zur Seite stand.

Prof. Dr. Christian Näther danke ich für die zahlreichen Einkristallstrukturlösungen, die ihn oft viel Zeit und Nerven gekostet haben und seine Unterstützung bei den Publikationen.

Ein ganz besonderer Dank gilt Nicole Pienack, die mich inzwischen schon 10 Jahre im Studium und Promotion begleitet. Ich kann Dir nicht genug danken für Dein immer offenes Ohr, Deine vielen wissenschaftlichen Ratschläge und welchen fürs Leben, Süßigkeiten und Rescue-Tropfen in Notfällen, den Tritt in den Hintern zur richtigen Zeit, einfach für alles!

Vielen Dank an Frau Inke Jeß, die aus 1000 Kristallen meistens den richtigen findet, für ihre Engelsgeduld und ruhiges Händchen bei der Auswahl.

Der gesamten spektroskopischen Abteilung mit Frau Cornelissen, Frau Pehlke, Frau Pick und Tobias Engesser danke ich für die zahlreichen analytischen Messungen.

Vielen Dank auch an Steve Waitschat, Timo Rhauderwiek, Jannick Jacobsen und Jannik Benecke für die Sorptionsmessungen.

Anna-Lena Hansen und Martin Etter sowie Nicole, Lisa und Philipp danke ich für die Unterstützung beim Proposal und den Messzeiten, in denen wirklich schöne Ergebnisse entstanden sind. Anna danke ich besonders für ihre tatkräftige Unterstützung und ihren großen Anteil bei der PDF-Auswertung und der Erstellung des Manuskripts.

Bei Henning und Maren möchte ich mich herzlich dafür bedanken, dass sie mir in der Diplomarbeit und auch während der Promotion immer geholfen haben.

Ich danke der „alten“ Solvo-Truppe für die Hilfe und den Spaß in der ersten Zeit meiner Arbeit: Danke an Carolin für die Unterstützung, die aufbauenden Gespräche und wissenschaftlichen Diskussionen. Danke an Micha für seinen Humor, der mir die Zeit im Labor damals erheblich erleichtert hat und seine Hilfe bei den POMs. Danke auch an Jessica für ihre Ratschläge.

Auch dem „neuen“ Solvo-Team Lisa, Felix, Philipp, Dana und Assma möchte ich danken, und dabei natürlich besonders bei Lisa. Danke für die Raucherpausen, in denen wir oft über Chemie gesprochen haben und aus denen sich viele Ideen ergeben haben, Deine ständige Hilfsbereitschaft bei einfach allem, die astreinen TOC-Grafiken und kreativen Ideen aller Art.

Felix danke ich für die angeregten Gespräche über Gott, Politik und die Welt, die lockere Stimmung und sehr viele Lacher.
Den „Drei von der Tankstelle“ Philipp, Sebastian und Michael danke ich für eine denkwürdige Zugfahrt nach Dresden und zurück. Vielen Dank an meinen „Mitbewohner“ Sebastian sowie Philipp und Huayna für ihre mentale Unterstützung, gerade in der letzten Phase meiner Arbeit. Michael danke ich für seine Hilfe und Geduld bei der Katalyseanlage, und dass er mir diese Zuständigkeit abgenommen hat, ohne dass ich fragen musste.
Herzlichen Dank dem gesamten Arbeitskreis für die tolle gemeinsame Zeit und Hilfe aller Art, und besonders bei Tine für ihren Einsatz für uns Doktoranden und für das nette „Geschnatter“.
Unseren Sekretärinnen Lena Kunz, Britta Bahn und Cornelia Möller danke ich ganz herzlich für alles.
Großer Dank gilt auch meinen Bachelorstudenten und Praktikanten Aleksej, Alexander, Dana und Sven für die gute Zusammenarbeit.
Meinen ehemaligen Kommilitonen (sofern nicht schon erwähnt) Anne, Gernot, Melanie, Claudia und Kim danke ich für den Zusammenhalt und die schöne gemeinsame Zeit während des Studiums und der Promotion.
Ich danke Frau Andrea Heering, meiner ehemaligen Lehrerin, dafür, dass sie unglaublich viel Mühe und Geduld mit uns hatte und uns damals am meisten beigebracht hat, auch wenn wir das damals nicht angemessen zu schätzen gewusst haben.
Großer Dank auch an meine Schwiegereltern in spe Sabine und Ingwer für ihre Unterstützung und die aufmunternden Worte.
Ich danke auch meiner Mama Agata, die uns Kinder immer darin bestärkt hat, den Weg zu ergreifen, den wir wollten und sich selbst für uns zurückgestellt hat. Meinem Papa Volker danke ich dafür, dass er damals wie heute an mich geglaubt hat und sich durchgesetzt hat, dass ich auf Gymnasium gehe. Auch den besten Geschwistern der Welt Angelique und Hans möchte ich für alles danken.
Ich danke Jürn für seine immense Unterstützung und Geduld in den letzten 10 Jahren Studium und Promotion. Egal, welche Prüfung oder andere Aufgaben anstanden, Du hast immer an mich geglaubt, wenn ich Zweifel hatte und mich darin bestärkt, weiterzumachen. Dafür, dass Du immer die Ruhe bewahrt hast und mich gebremst hast, wenn meine Nerven mit mir durchgegangen sind, hast Du einen Orden verdient! Ohne Dich hätte ich das nicht geschafft. Danke für Deine Liebe und den Glauben an mich.

7. Literaturverzeichnis

[1] M. Nyman, *Dalton Trans.* **2011**, *40*, 8049.

[2] R. D. Shannon, *Acta Crystallogr. A.* **1976**, *32*, 751.

[3] M. Nyman, A. J. Celestian, J. B. Parise, G. P. Holland, T. M. Alam, *Inorg. Chem.* **2006**, *45*, 1043.

[4] G. J.-P. Deblonde, N. Delaunay, D. Lee, A. Chagnes, G. Cote, P. Gareil, *RSC Adv.* **2015**, *5*, 64119.

[5] D. J. Sures, S. A. Serapian, K. Kozma, P. I. Molina, C. Bo, M. Nyman, *Phys. Chem. Chem. Phys.* **2017**, *19*, 8715.

[6] E. Balogh, T. M. Anderson, J. R. Rustad, M. Nyman, W. H. Casey, *Inorg. Chem.* **2007**, *46*, 7032.

[7] M. R. Antonio, M. Nyman, T. M. Anderson, *Angew. Chem.* **2009**, *121*, 6252.

[8] C. M. Flynn, G. D. Stucky, *Inorg. Chem.* **1969**, 178.

[9] C. M. Flynn, G. D. Stucky, *Inorg. Chem.* **1968**, *8*, 332.

[10] H. Naruke, T. Yamase, *Acta Crystallogr. B.* **1996**, 2655.

[11] H. Naruke, T. Yamase, *J. Alloys Compd.* **1997**, *255*, 183.

[12] T. Ozeki, T. Yamase, H. Naruke, Y. Sasaki, *Inorg. Chem.* **1994**, *33*, 409.

[13] M. Nyman, F. Bonhomme, T. M. Alam, M. A. Rodriguez, B. R. Cherry, J. L. Krumhansl, T. M. Nenoff, A. M. Sattler, *Science* **2002**, *297*, 996.

[14] R. G. Finke, D. K. Lyon, K. Nomiya, T. J. R. Weakley, *Acta Crystallogr. C* **1990**, *46*, 1592.

[15] G.-S. Kim, H. Zeng, J. T. Rhule, I. A. Weinstock, C. L. Hill, *Chem. Commun.* **1999**, 1651.

[16] Richard G. Finke, Michael W. Droege, *J. Am. Chem. Soc.* **1984**, *106*, 7274.

[17] Ying-Jie Lu,†, Roger Lalancette,‡ and, and Robert H. Beer*,†, *Inorg. Chem.* **1996**, 2524.

[18] G. Guo, Y. Xu, J. Cao, C. Hu, *Chem. Commun.* **2011**, *47*, 9411.

[19] J.-H. Son, Ohlin, C. Andre, E. C. Larson, P. Yu, W. H. Casey, *Eur. J. Inorg. Chem.* **2013**, 1748.

[20] R. P. Bontchev, M. Nyman, *Angew. Chem., Int. Ed.* **2006**, *45*, 6670.

[21] J. Niu, P. Ma, H. Niu, J. Li, J. Zhao, Y. Song, J. Wang, *Chem. Eur. J.* **2007**, *13*, 8739.

[22] R. Tsunashima, D.-L. Long, H. N. Miras, D. Gabb, C. P. Pradeep, L. Cronin, *Angew. Chem.* **2010**, *122*, 117.

[23] H. Tan, W. Chen, D. Liu, Y. Li, E. Wang, *Inorg. Chem. Commun.* **2010**, *13*, 1354.

[24] P. Huang, C. Qin, Z.-M. Su, Y. Xing, X.-L. Wang, K.-Z. Shao, Y.-Q. Lan, E.-B. Wang, *J. Am. Chem. Soc.* **2012**, *134*, 14004.

[25] Y.-T. Zhang, C. Qin, X.-L. Wang, P. Huang, B.-Q. Song, K.-Z. Shao, Z.-M. Su, *Inorg. Chem.* **2015**, *54*, 11083.

[26] Z. Liang, D. Zhang, H. Wang, P. Ma, Z. Yang, J. Niu, J. Wang, *Dalton Trans.* **2016**, *45*, 16173.

[27] Z. Liang, K. Wang, D. Zhang, P. Ma, J. Niu, J. Wang, *Dalton Trans.* **2017**, *46*, 1368.

[28] M. Maekawa, Y. Ozawa, A. Yagasaki, *Inorg. Chem.* **2006**, *45*, 9608.

[29] L. Jin, Z.-K. Zhu, Y.-L. Wu, Y.-J. Qi, X.-X. Li, S.-T. Zheng, *Angew. Chem., Int. Ed.* **2017**, *56*, 16288.

[30] Z.-L. Wang, H.-Q. Tan, W.-L. Chen, Y.-G. Li, E.-B. Wang, *Dalton Trans.* **2012**, *41*, 9882.

[31] L. Jin, X.-X. Li, Y.-J. Qi, P.-P. Niu, S.-T. Zheng, *Angew. Chem.* **2016**, *128*, 13997.

[32] S. Chen, P. Ma, H. Luo, Y. Wang, J. Niu, J. Wang, *Chem. Commun.* **2017**, *53*, 3709.

[33] Y.-L. Wu, X.-X. Li, Y.-J. Qi, H. Yu, L. Jin, S.-T. Zheng, *Angew. Chem., Int. Ed.* **2018**, *57*, 8572.

[34] A. Müller, E. Beckmann, H. Bögge, M. Schmidtmann, A. Dress, *Angew. Chem. Int. Ed.* **2002**, *41*, 1162.

[35] E. J. Graeber, B. Morosin, *Acta Crystallogr. B.* **1977**, 2137.

[36] M. Nyman, L. J. Criscenti, F. Bonhomme, M. A. Rodriguez, R. T. Cygan, *J. Solid State Chem.* **2003**, *176*, 111.

[37] S. Chen, P. Ma, H. Luo, Y. Wang, J. Niu, J. Wang, *Chem. Commun.* **2017**, *53*, 3709.

[38] P. A. Abramov, A. T. Davletgildeeva, N. K. Moroz, N. B. Kompankov, B. Santiago-Schübel, M. N. Sokolov, *Inorg. Chem.* **2016**, *55*, 12807.

[39] J. Hu, Y. Wang, X. Zhang, Y. Chi, S. Yang, J. Li, C. Hu, *Inorg. Chem.* **2016**, *55*, 7501.

[40] D. Sures, M. Segado, C. Bo, M. Nyman, *J. Am. Chem. Soc.* **2018**, accepted.

[41] Y. Hou, L. N. Zakharov, M. Nyman, *J. Am. Chem. Soc.* **2013**, *135*, 16651.

[42] J.-H. Son, W. H. Casey, *Chem. Commun.* **2015**, *51*, 1436.

[43] F. Bonhomme, J. P. Larentzos, T. M. Alam, E. J. Maginn, M. Nyman, *Inorg. Chem.* **2005**, *44*, 1774.

[44] Abramov, P. A., A. T. Davletgildeeva, Sokolov, M. N., *J. Cluster Sci.* **2016**, *28*, 735.

[45] M. Nyman, F. Bonhomme, T. M. Alam, J. B. Parise, Vaughan, Gavin M. B., *Angew. Chem. Int. Ed.* **2004**, *43*, 2787.

[46] T. M. Anderson, S. G. Thoma, F. Bonhomme, M. A. Rodriguez, H. Park, J. B. Parise, T. M. Alam, J. P. Larentzos, M. Nyman, *Cryst. Growth Des.* **2007**, *7*, 719.

[47] M. Nyman, J. P. Larentzos, E. J. Maginn, M. E. Welk, D. Ingersoll, H. Park, J. B. Parise, I. Bull, F. Bonhomme, *Inorg. Chem.* **2007**, *46*, 2067.

[48] Z. Weng, Y. Ren, M. Gu, B. Yue, H. He, *Dalton Trans.* **2017**, *47*, 233.

[49] G.-S. Kim, H. Zheng, D. VanDerveer, C. L. Hill, *Angew. Chem. Int. Ed.* **1999**, *38*, 3205.

[50] J.-H. Son, C. A. Ohlin, R. L. Johnson, P. Yu, W. H. Casey, *Chem. Eur. J.* **2013**, *19*, 5191.

[51] Y. Zhang, J.-Q. Shen, L.-H. Zheng, Z.-M. Zhang, Y.-X. Li, E.-B. Wang, *Cryst. Growth Des.* **2014**, *14*, 110.

[52] Z.-Y. Zhang, J. Peng, Z.-Y. Shi, W.-L. Zhou, S. U. Khan, H.-S. Liu, *Chem. Commun.* **2015**, *51*, 3091.

[53] P.-H. Lin, H.-Y. Guo, X. Zhang, X.-B. Cui, Q.-S. Huo, J.-Q. Xu, *Inorg. Chem. Commun.* **2016**, *73*, 34.

[54] L. B. Fullmer, R. H. Mansergh, L. N. Zakharov, D. A. Keszler, M. Nyman, *Cryst. Growth Des.* **2015**, *15*, 3885.

[55] P. Huang, E.-L. Zhou, X.-L. Wang, C.-Y. Sun, H.-N. Wang, Y. Xing, K.-Z. Shao, Z.-M. Su, *CrystEngComm* **2014**, *16*, 9582.

[56] X. Zhang, S.-x. Liu, S.-j. Li, X.-n. Wang, H.-y. Jin, J.-l. Cui, Y.-w. Liu, C.-z. Liu, *Chem. J. Chinese U.* **2013**, *34*, 2046.

[57] N. Li, Y. Liu, Y. Lu, D. He, S. Liu, X. Wang, Y. Li, S. Liu, *New J. Chem.* **2016**, *40*, 2220.

[58] J.-Q. Shen, Q. Wu, Y. Zhang, Z.-M. Zhang, Y.-G. Li, Y. Lu, E.-B. Wang, *Chem. Eur. J.* **2014**, *20*, 2840.

[59] Q. Lan, Z.-M. Zhang, Y.-G. Li, E.-B. Wang, *RSC Adv.* **2015**, *5*, 44198.

[60] J.-Q. Shen, Y. Zhang, Z.-M. Zhang, Y.-G. Li, Y.-Q. Gao, E.-B. Wang, *Chem. Commun.* **2014**, *50*, 6017.

[61] J. Hu, Y. Xu, D. Zhang, B. Chen, Z. Lin, C. Hu, *Inorg. Chem.* **2017**, *56*, 10844.

[62] I. Lindqvist, *Ark. Kemi* **1953**, 247.

[63] F. J. Farrell, V. A. Maroni, T. G. Spiro, *Inorg. Chem.* **1969**, 2638.

[64] R. Mattes, H. Bierbüsse, J. Fuchs, *Z. Anorg. Allg. Chem.* **1971**, 230.

[65] A. Goiffon, B. Spinner, *Chim. Miner. Rev.* **1974**, *11*, 262.

[66] N. Etxebarria, L. A. Fernández, J. M. Madariaga, *J. Chem. Soc., Dalton Trans.* **1994**, 3055.

[67] G. Neumann, *Acta Chem. Scand.* **1964**, 278.

[68] M. Nyman, T. M. Alam, F. Bonhomme, M. A. Rodriguez, C. S. Frazer, M. E. Welk, *J Clust Sci* **2006**, *17*, 197.

[69] G. J.-P. Deblonde, A. Moncomble, G. Cote, S. Bélair, A. Chagnes, *RSC Adv.* **2015**, *5*, 7619.

[70] D. J. Sures, S. K. Sahu, P. I. Molina, A. Navrotsky, M. Nyman, *ChemistrySelect* **2016**, *1*, 1858.

[71] J. J. Borrás-Almenar, E. Coronado, A. Müller, M. T. Pope, *Polyoxometalate molecular science*. *Proceedings of the NATO Advanced Study Institute on Polyoxometalate Molecular Science, Tenerife, Spain, 25 August - 4 September 2001*, Kluwer, Dordrecht, **2003**.

[72] D. J. Sures, S. A. Serapian, K. Kozma, P. I. Molina, C. Bo, M. Nyman, *Phys. Chem. Chem. Phys.* **2017**, *19*, 8715.

[73] I. D. Brown, D. Altermatt, *Acta Crystallogr. B.* **1985**, *41*, 244.

[74] O´Keeffe, M., Brese, N. E., *J. Am. Chem. Soc.* **1991**, 3226.

[75] G. J.-P. Deblonde, C. Coelho-Diogo, A. Chagnes, G. Cote, M. E. Smith, J. V. Hanna, D. Iuga, C. Bonhomme, *Inorg. Chem.* **2016**, *55*, 5946.

[76] M. Aureliano, Ohlin, C. Andre, M. O. Vieira, M. P. M. Marques, W. H. Casey, L. A. E. Batista de Carvalho, *Dalton Trans.* **2016**, *45*, 7391.

[77] E. M. Villa, C. A. Ohlin, E. Balogh, T. M. Anderson, M. D. Nyman, W. H. Casey, *Angew. Chem.* **2008**, *120*, 4922.

[78] W. G. Klemperer, K. A. Marek, *Eur. J. Inorg. Chem.* **2013**, *2013*, 1762.

[79] E. M. Villa, C. A. Ohlin, J. R. Rustad, W. H. Casey, *J. Am. Chem. Soc.* **2009**, *131*, 16488.

[80] M. Matsumoto, Y. Ozawa, A. Yagasaki, *Polyhedron* **2010**, 2196.

[81] C. A. Ohlin, E. M. Villa, W. H. Casey, *Inorg. Chim. Acta* **2009**, *362*, 1391.

[82] L. Shen, C.-H. Li, Y.-N. Chi, C.-W. Hu, *Inorg. Chem. Commun.* **2008**, *11*, 992.

[83] J. Niu, G. Wang, J. Zhao, Y. Sui, P. Ma, J. Wang, *Cryst. Growth Des.* **2011**, *11*, 1253.

[84] C. A. Ohlin, E. M. Villa, J. C. Fettinger, W. H. Casey, *Angew. Chem.* **2008**, *120*, 5716.

[85] C. A. Ohlin, E. M. Villa, J. C. Fettinger, W. H. Casey, *Dalton Trans.* **2009**, 2677.

[86] E. M. Villa, C. A. Ohlin, W. H. Casey, *J. Am. Chem. Soc.* **2010**, *132*, 5264.

[87] Y.-T. Zhang, P. Huang, C. Qin, L.-K. Yan, B.-Q. Song, Z.-X. Yang, K.-Z. Shao, Z.-M. Su, *Dalton Trans.* **2014**, *43*, 9847.

[88] H. G. Becker, Berger, Werner, Domschke, G., *Organikum*. *Organisch-chemisches Grundpraktikum,* 21. Aufl., Wiley-VCH Verlag GmbH, Weinheim, New York, Chichester, Brisbane, Singapore, Toronto, **2001**.

[89] S. Hayashi, S. Yamazoe, K. Koyasu, T. Tsukuda, *RSC Adv.* **2016**, *6*, 16239.

[90] M. Nyman, C. R. Powers, F. Bonhomme, T. M. Alam, E. J. Maginn, D. T. Hobbs, *Chem. Mater.* **2008**, *20*, 2513.

[91] J. T. Rhule, C. L. Hill, D. A. Judd, R. F. Schinazi, *Chem. Rev.* **1998**, 327.

[92] J.-Y. Niu, G. Chen, J.-W. Zhao, P.-T. Ma, S.-Z. Li, J.-P. Wang, M.-X. Li, Y. Bai, B.-S. Ji, *Chem. Eur. J.* **2010**, *16*, 7082.

[93] Q. Geng, Q. Liu, P. Ma, J. Wang, J. Niu, *Dalton Trans.* **2014**, *43*, 9843.

[94] J.-Q. Shen, S. Yao, Z.-M. Zhang, H.-H. Wu, T.-Z. Zhang, E.-B. Wang, *Dalton Trans.* **2013**, *42*, 5812.

[95] J. Niu, F. Li, J. Zhao, P. Ma, D. Zhang, B. Bassil, U. Kortz, J. Wang, *Chem. Eur. J.* **2014**, *20*, 9852.

[96] Z. Zhang, Q. Lin, D. Kurunthu, T. Wu, F. Zuo, S.-T. Zheng, C. J. Bardeen, X. Bu, P. Feng, *J. Am. Chem. Soc.* **2011**, *133*, 6934.

[97] J.-H. Son, J. Wang, F. E. Osterloh, P. Yu, W. H. Casey, *Chem. Commun.* **2014**, *50*, 836.

[98] J.-H. Son, J. Wang, W. H. Casey, *Dalton Trans.* **2014**, *43*, 17928.

[99] Z. Liang, D. Zhang, Q. Liu, P. Ma, J. Niu, J. Wang, *Inorg. Chem. Commun.* **2015**, *54*, 19.

[100] H. Wang, Z. Liang, Q. Liu, D. Zhang, J. Wang, *Inorg. Chem. Commun.* **2015**, *61*, 157.

[101] M. Liu, H. Chen, H. Zhao, Y. He, Y. Li, R. Wang, L. Zhang, W. You, *Dalton Trans.* **2017**, *46*, 9407.

[102] P. Huang, C. Qin, X.-L. Wang, C.-Y. Sun, G.-S. Yang, K.-Z. Shao, Y.-Q. Jiao, K. Zhou, Z.-M. Su, *Chem. Commun.* **2012**, *48*, 103.

[103] X. Zhang, S.-x. Liu, S.-j. Li, Y.-H. Gao, X.-n. Wang, Q. Tang, Y.-w. Liu, *Eur. J. Inorg. Chem.* **2013**, *2013*, 1706.

[104] J. Niu, X. Fu, J. Zhao, S. Li, P. Ma, J. Wang, *Cryst. Growth Des.* **2010**, *10*, 3110.

[105] Y. Ye, C. Chen, H. Feng, J. Zhou, J. Ma, J. Chen, J. Yuan, L. Kong, Z. Qian, *OJIC* **2013**, *03*, 59.

[106] Abramov, P. A., C. Vicent, Kompankov, N. B., Gushchin, A. L., Sokolov, M. N., *Chem. Commun.* **2015**, *51*, 4021.

[107] P. A. Abramov, C. Vicent, N. B. Kompankov, A. L. Gushchin, M. N. Sokolov, *Eur. J. Inorg. Chem.* **2016**, 154.

[108] D. Zhang, S. Li, J. Wang, J. Niu, *Inorg. Chem. Commun.* **2012**, *17*, 75.

[109] Z. Liang, J. Sun, D. Zhang, P. Ma, C. Zhang, J. Niu, J. Wang, *Inorg. Chem.* **2017**, *56*, 10119.

[110] L. Shen, Y.-q. Xu, Y.-Z. Gao, F.-Y. Cui, C.-W. Hu, *J. Mol. Struct.* **2009**, *934*, 37.

[111] J.-H. Son, D.-H. Park, D. A. Keszler, W. H. Casey, *Chem. Eur. J.* **2015**, *21*, 6727.

[112] B.-X. Liu, Z.-W. Cai, T. Yang, X.-X. Li, G.-Y. Yang, S.-T. Zheng, *Inorg. Chem. Commun.* **2017**, *78*, 56.

[113] J. Hu, J. Dong, X. Huang, Y. Chi, Z. Lin, J. Li, S. Yang, H. Ma, C. Hu, *Dalton Trans.* **2017**, 8245.

[114] L. Li, Y. Niu, K. Dong, P. Ma, C. Zhang, J. Niu, J. Wang, *RSC Adv.* **2017**, *7*, 28696.

[115] a) M. K. Kinnan, W. R. Creasy, L. B. Fullmer, H. L. Schreuder-Gibson, M. Nyman, *Eur. J. Inorg. Chem.* **2014**, *2014*, 2361; b) A. L. Kaledin, D. M. Driscoll, D. Troya, D. L. Collins-Wildman, C. L. Hill, J. R. Morris, D. G. Musaev, *Chem. Sci.* **2018**, *9*, 2147.

[116] W. Guo, H. Lv, K. P. Sullivan, W. O. Gordon, A. Balboa, G. W. Wagner, D. G. Musaev, J. Bacsa, C. L. Hill, *Angew. Chem.* **2016**, *128*, 7529.

[117] Q. Gan, W. Shi, Y. Xing, Y. Hou, *Front. Chem.* **2018**, *6*, 7.

[118] G. Fraqueza, L. A. E. Batista de Carvalho, M. P. M. Marques, L. Maia, C. A. Ohlin, W. H. Casey, M. Aureliano, *Dalton Trans.* **2012**, *41*, 12749.

[119] G. Fraqueza, C. A. Ohlin, W. H. Casey, M. Aureliano, *J. Inorg. Biochem.* **2012**, *107*, 82.

[120] K. D. von Allmen, *Dissertation*, Universität Zürich, Zürich, **2016**.

[121] J. van Alphen, *Rec. trav. chim.* **1937**, *56*, 343.

[122] M. Bakaj, M. Zimmer, *J. Mol. Struct.* **1999**, *508*, 59.

[123] H. Stetter, K.-H. Mayer, *Chem. Ber.* **1961**, *94*.

[124] L. Fabbrizzi in *Macrocyclic and Supramolecular Chemistry*, S. 165–199.

[125] E. Kent Barefield, *Inorg. Chem.* **1972**, *11*, 2273.

[126] M. Filowitz, Ho, R. K. C., W. G. Klemperer, W. Shum, *Inorg. Chem.* **1979**, *18*, 93.

[127] J. Dopta, S. Grzanna, C. Näther, W. Bensch, *Dalton Trans.* **2018**, *47*, 15103.

[128] J. W. Steed, *Coord. Chem. Rev.* **2001**, *215*, 171.

[129] N. Pienack, W. Bensch, *Angew. Chem. Int. Ed.* **2011**, *50*, 2014.

[130] H. Terraschke, M. Rothe, P. Lindenberg, *Rev. Anal. Chem.* **2018**, *37*, 107.

[131] H. Terraschke, L. Ruiz Arana, P. Lindenberg, W. Bensch, *Analyst* **2016**, *141*, 2588.

[132] S. Lin, W. Liu, Y. Li, Q. Wu, E. Wang, Z. Zhang, *Dalton Trans.* **2010**, *39*, 1740.

[133] M. Zhang, A.-M. Zhang, X.-X. Wang, Q. Huang, X. Zhu, X.-L. Wang, L.-Z. Dong, S.-L. Li, Y.-Q. Lan, *J. Mater. Chem. A* **2018**, *6*, 8735.